NASA CR-72369
ADL C-69507

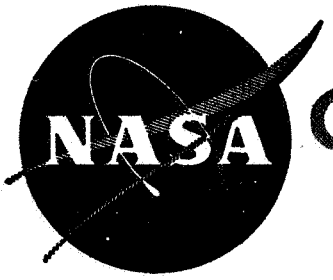

CONCEPTUAL DESIGN AND ANALYSIS OF SHADOW SHIELD SYSTEMS FOR THERMAL PROTECTION OF CRYOGENIC PROPELLANTS

by

F. GABRON and D. NATHANSON

prepared for

NATIONAL AERONAUTICS AND SPACE ADMINISTRATION

CONTRACT NAS 3-10292

Arthur D. Little, Inc.

NASA CR-72369

ADL C-69507

INTERIM REPORT

CONCEPTUAL DESIGN AND ANALYSIS OF SHADOW SHIELD SYSTEMS FOR THERMAL PROTECTION OF CRYOGENIC PROPELLANTS

by

F. Gabron and D. Nathanson

prepared for

NATIONAL AERONAUTICS AND SPACE ADMINISTRATION

1 July 1968

CONTRACT NAS 3-10292

NASA Lewis Research Center
Liquid Rocket Technology Branch
James R. Barber

ARTHUR D. LITTLE, INC.
20 Acorn Park
Cambridge, Mass. 02140

CONCEPTUAL DESIGN AND ANALYSIS OF SHADOW SHIELD SYSTEMS FOR THERMAL PROTECTION OF CRYOGENIC PROPELLANTS

by

F. Gabron and D. Nathanson

ABSTRACT

A study was made to determine the effectiveness of shadow shields for the long-term thermal protection of a spaceborne liquid-hydrogen storage vessel. A number of shadow shield conceptual designs were evaluated for an upper-stage configuration in which the shadow shields were located between a sun-oriented, 10-foot-diameter payload and a nine-foot-diameter liquid-hydrogen tank. The designs were evaluated on the basis of the system mass penalty (the mass of the shadow shields and payload support structure plus the mass of liquid hydrogen vaporization for a 10,000-hour mission) and inherent reliability.

TABLE OF CONTENTS

TABLE OF CONTENTS - Continued

TABLE OF CONTENTS - Continued

TABLE OF CONTENTS - Continued

ACKNOWLEDGMENTS

The suggestions, comments and technical direction provided by Mr. James Barber, who acted as Technical Monitor, and Mr. Richard Knoll of NASA Lewis Research Center are appreciated.

The technical staff at Arthur D. Little, Inc., who contributed to this Interim Report include:

Mr. F. Gabron - Program Manager

Mr. D. Nathanson - Task Leader, Conceptual Design and Analysis

Mr. B. Allen

Dr. D. Almgren

Mr. P. Athens

Mr. R. Breckenridge, Jr.

Dr. A. Germeles

Mr. J. McCullough

Mr. N. Memmo, Jr.

Mrs. R. Schiraldi

LIST OF FIGURES

LIST OF FIGURES - Continued

LIST OF FIGURES - Continued

LIST OF FIGURES - Continued

LIST OF TABLES

LIST OF APPENDICES

CONCEPTUAL DESIGN AND ANALYSIS OF SHADOW SHIELD SYSTEMS FOR THERMAL PROTECTION OF CRYOGENIC PROPELLANTS

by

F. Gabron and D. Nathanson

Arthur D. Little, Inc.

SUMMARY

Conceptual designs for six shadow shield systems used to reduce the heat flow (and resultant propellant vaporization) between a sun-oriented spacecraft payload and a liquid hydrogen (LH_2) tank were established. The shadow shield systems evaluated in this study comprised an open-truss structure for supporting the payload from the LH_2 tank and low-emittance shadow shields spaced between the payload and tank. An additional insulation system was selected to provide thermal protection for the LH_2 tank during ground-hold, ascent heating and "near-planet" (non-sun-oriented) phases of the mission.

The investigation was limited to the application of shadow shield concepts to a ten-foot-diameter payload and nine-foot-major-diameter oblate spheroid LH_2 tank with a propellant capacity of 1160 lb_m. The inter-planetary mission period during which the payload was oriented was taken to be 10,000 hours.

The shadow shield systems which were studied included:

a) Fixed support structures designed to withstand launch loads;

b) Space-erected structures designed to withstand orbital attitude-control forces; and

c) Space-erected shadow shields to provide additional compensation for solar-vector misalignment.

Following a preliminary investigation of LH_2 boil-off rates (due to heat flow via support conduction and thermal radiation via the shadow shields) and preliminary structural analyses, design layout drawings of six concepts were made. Optimization analyses were made to select a configuration for each concept which would result in a minimum stage mass penalty - where the mass penalty was defined as the mass of the LH_2 boil-off for a 10,000-hour mission plus the mass of the shadow

shields and support structure. The six designs were evaluated from considerations of mass penalty and inherent reliability.

The results of this study demonstrated that shadow shield systems with fixed payload support structures could be designed to have a small mass penalty and a small payload-to-tank spacing. The LH_2 boil-off mass for compact, fixed-structure concepts can be made small by: 1) using several low-emittance, low-conductance, circular shadow shields appropriately spaced between the payload and LH_2 tank to reduce the radiant heat flow to the LH_2 tank, and 2) properly selecting the configuration, materials and thermal control coatings for radiatively cooled structural supports to reduce the conductive heat flow to the LH_2 tank.

For the LH_2 tank and payload dimensions assumed for the study, a shadow shield system with a fixed payload support structure would have a solar-vector misalignment capability of approximately $\pm$ 5°, which is judged to be compatible with current guidance and control practice. Space-erected systems do not offer any appreciable reduction in mass penalty, and the added complexity and reduced reliability introduced by deployment mechanisms makes such systems unattractive for this specific application.

The results also showed that the LH_2 boil-off mass for a sun-oriented, 10,000-hour mission was small by comparison to the LH_2 boil-off during ascent and non-oriented phases of the mission.

1.0 INTRODUCTION

The long-term storage of cryogens in space has received a great deal of attention during the past decade, particularly with the advent of high specific-impulse, hydrogen-fueled, space propulsion methods. In general, a large effort has been devoted to the development of highly efficient multilayer insulations (MLI) as a means for minimizing the heat inleakage and resulting cryogenic propellant boil-off in the space environment. The use of MLI--applied directly to the outer surfaces of the cryogenic tankage--will be required for those missions where the vehicle is randomly oriented, especially in the vicinity of planets where the heat inputs from planet-emitted radiation, albedo and direct sunlight vary in time and direction over an orbit. However, the demonstrated reliability and capability of attitude control systems to accurately orient a spacecraft for long periods in deep-space missions, (e.g., Mariner IV which was sun-oriented, and more frequent use of high-altitude, sun-synchronous* earth orbits) have stimulated interest in shadow shielding techniques which rely upon directional effects to minimize the heat inputs from a payload or direct sunlight.

The objectives of the subject contract are to evaluate six shadow shield systems and to deliver to NASA LeRC two selected systems together with a cold-sink calorimeter. This effort consists of two basic tasks:

- Conceptual Design and Analytical Evaluation of Shadow Shield Systems
- Test Apparatus Design and Fabrication of Thermal Scale Models of Two Selected Systems

This Interim Report summarizes the work which has been accomplished in the conceptual design and evaluation of six concepts which utilize shadow shielding techniques to reduce the heat flow to an LH_2 tank comprising part of a solar-vector-oriented spacecraft. The evaluation is based on total system weight (defined as the weight of the shadow shield system plus the weight of vaporized propellant due to heat leaks for operational periods up to 10,000 hours) and the inherent reliability based on mechanical and operational complexity. The concepts evaluated in this study include:

- Space-Erectable Systems
- Ground-Erected (Fixed) Systems
- Systems which Provide for Solar-Vector Misalignment

---

* Typically, near-polar earth orbits where the period of nodal regression can be made equal to a year and the orbital plane thereby fixed with respect to the sun.

The vehicle chosen as a representative configuration for this study is ten feet in diameter with an 1160-pound capacity LH_2 tank suspended within the vehicle structure. The tank is a nine-foot-diameter oblate spheroid and weighs 200 pounds. The vehicle structure (between the LH_2 tank and payload) transmitting the thrust loads of lower stages and inertia loads of the LH_2 tank is an open-frame truss, and the shadow shields are placed between the payload and LH_2 tank.

The payload was assumed to be at a constant temperature of 520R (288K) with a mass of either 1500, 2500 or 4000 lbs.

In addition to the evaluation of the shadow shield concepts, this Interim Report contains a brief study and evaluation of insulation systems to be applied to the LH_2 tank for thermal protection during groundhold, ascent, and phases of the mission where the spacecraft receives radiation from planetary sources.

Following the selection of two of the concepts described herein by NASA LeRC, the design of the two selected systems will be scaled down, and the thermal performance of each evaluated under test conditions. The two systems will be fabricated, instrumented and delivered to NASA LeRC for testing.

2.0 BACKGROUND

The basic concept of utilizing shadow shields to protect payloads or cryogenic storage vessels has been discussed in the literature for a number of different missions including solar probes, lunar and planetary orbiters, etc. A considerable portion of the literature on shadow shield systems has been devoted to shadow shield systems which are used to intercept solar energy - the main source for extended duration interplanetary missions by use of space-erected (mechanical or inflatable) shadow shields. The shadow shields in such cases are located in front of the oriented payload to be protected so as to intercept the collimated solar energy and reradiate the major fraction of the intercepted energy to outer space. A space-erected solar shield was utilized on the recent Mariner Venus 67 spacecraft to minimize the effects of the change in solar intensity which occur in the Earth-Venus trajectory.

The present study is directed (by contract) to shadow shield systems for reducing the heat flow between a payload, whose temperature is controlled to a fixed level, and an LH_2 storage tank. In this situation, the stage is oriented so that the payload faces the sun and the shadow shields are interposed between the payload and the LH_2 storage vessel. The shadow shields are used to protect the LH_2 tank from thermal radiation emanating from the payload and the payload in effect thus becomes the shadow shield which intercepts the incident solar energy.

The concept of shadow shielding an LH_2 tank from payload radiation in the manner described above was discussed by Knoll and Oglebay

(1963).* This preliminary analytical study showed that a few spaced shadow shields of low emittance could be used to eliminate any heat leakage by radiation from a room-temperature payload to an LH_2 tank. The advantages of using shadow shield systems as opposed to the use of multilayer insulations and the problem and application areas for lightweight thermal protection systems were discussed.

A more recent publication by Knoll, et al (1966) presents the results of a combined analytical and experimental study of the effectiveness of multiple, flat-plate shadow shields. Tests were made on a shadow shield system using a 12.75-inch-diameter LN_2 tank as a calorimeter and a heater plate (to simulate a payload) whose temperature could be controlled up to approximately 800R. The test results agreed reasonably well with analytical predictions, and provided an indication of the thermal interaction between the shadow shields and their supporting structure. The results of preliminary design studies for a shadow-shielded, 7000-lb., hydrogen-oxygen stage having a mission duration of 200 days were also presented. In this study a sun-oriented payload was maintained at 530R and there was a 1-foot spacing between the payload and LH_2 tank. The results showed that the LH_2 boil-off due to support conduction could be appreciable and indicated the need for additional work to reduce that component of system mass penalty. It was also concluded that shadow shield systems offer potential weight savings for the storage of cryogens during long-term missions, in comparison to systems where the vehicle is oriented and multilayer insulation ("super insulation") is used for thermal protection.

The work presented herein is an extension of the work presented by Knoll, et al (1966). Considerable effort was devoted to a detailed optimization study of flight-type thermal protection systems which included the following important variables:

- Tank-to-Payload Spacing Dimensions
- Shadow Shield System Characteristics
  - Surface Optical Properties
  - Number of Shields
  - Location and Attachment
  - Shape
- Structural Supports
  - Materials
  - Configuration
  - Surface Optical Properties
  - Improved Cooling Methods

---

* Cited references are listed in Section 13.1.

- Space-Erected Systems to Provide Solar Misalignment Capability and Minimum LH_2 Boil-off
- Ground-Hold and Orbital Insulation

3.0 CONCEPTUAL DESIGN OF SHADOW SHIELD SYSTEMS

3.1 Introduction

An analysis of chemical upper stages for scientific missions was presented by the Advanced Development and Evaluation Division of NASA LeRC (1965). A number of configurations utilizing hydrogen fuel that could be introduced into the present family of NASA launch vehicles (i.e., Atlas-Centaur and Saturn IB-Centaur launch vehicles) to provide increased capacity and capability for advanced, high-energy NASA missions were studied. The performance of small, high-energy kick-stage configurations is critically dependent on the mass of insulation and boil-off of the LH_2 fuel during the mission. These configurations are, furthermore, rather ideally suited to the use of shadow shield systems for thermally protecting the LH_2 storage vessel.

The general arrangement of component systems for an LH_2 fueled upper stage is presented in Figure 1. The drawing does not include the necessary thermal protection system for the LH_2 tank. The major components consist of the payload structurally connected to an LH_2 propellant tank, oxidant tanks, propulsion components, etc. With this general arrangement of the payload and LH_2 tank, the shadow shield concept could be used to protect the LH_2 tank assuming that an attitude control system was provided to continuously orient the payload to the sun. The shroud surrounding the LH_2 tank and payload would be jettisoned during the initial stage of the interplanetary transfer orbit. With an open-truss structure connecting the LH_2 tank to the payload, multiple shadow shields could be interposed between the payload and tankage to minimize the boil-off of LH_2 propellant.

It is within this basic class of upper-stage configurations that the study reported herein was directed. The system requirements included the provisions of a support structure between the payload and the LH_2 tank to withstand launch loads, a thermal protection system for ground-hold and planetary operations, and a system of shadow shields between the payload and LH_2 tank to minimize radiative transfer during a coast mission up to 10,000 hours. The study was limited by contract definition to a payload having a constant temperature of 520°R. The payload mass was varied parametrically in the study to include masses of 1500, 2500 and 4000 lbs. The LH_2 tank was taken to be a 9-foot-diameter oblate spheroid made of aluminum, weighing a maximum of 200 lbs., with an 1160-lb. LH_2 capacity.

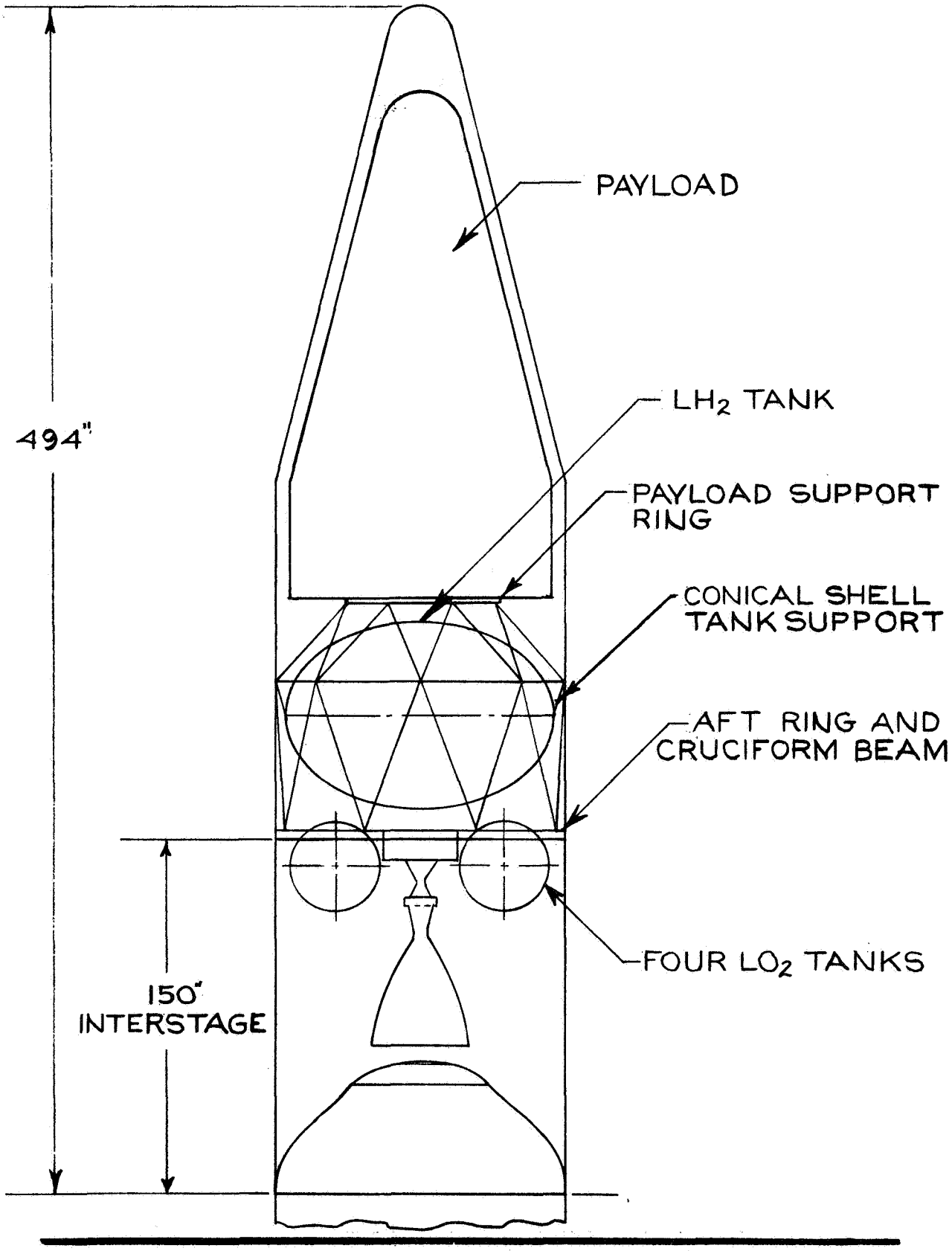

FIGURE 1 - TYPICAL UPPER STAGE CONFIGURATION

3.2 Program Plan

The plan of approach was to first complete conceptual designs of six realistic flight-type shadow shield systems. Each system was analyzed with respect to both thermal and structural characteristics by digital computer techniques, and the temperature distributions in shields and supports and the LH_2 boil-off for each of the six concepts were predicted. Finally, a detailed evaluation of the conceptual designs was made establishing the merit of the conceptual designs by providing a rating of:

1) Total system mass--the mass of the shadow shield system including supports between the payload and the LH_2 tank plus the LH_2 boil-off, due to heat leak through the system for times up to 10,000 hours.

2) Mechanical and operation complexity (inherent reliability).

The details of the approach presented in graphical form are shown in Figure 2.

This work was made up of three major phases as indicated in the diagram. The first phase involved a preliminary selection of a number of basic concepts which seemed suitable for application in shadow shield systems. The selection included concepts for fixed launch support structures, space-erected structures, various shadow shield geometries, space-erected shields and methods of cooling the structure to reduce boil-off losses from conduction. Concepts were also considered and outlined for supporting the LH_2 tank, distributing loads uniformly about the tank structure, and for providing a thermal protection system for ground-hold and planetary operations.

The second phase involved parametric studies of shadow shields and payload support structures assuming "no thermal interactions" so that the significant design parameters of each could be characterized independently. The results of this study indicated the shield configuration at each L/D (the ratio of payload-tank spacing to the payload diameter) resulting in the minimum value of the shield mass plus the LH_2 boil-off and, depending upon the structural material and whether the structure was fixed or space-erected, the optimum configuration and geometry of the structural supports as a function of L/D.

The third and final phase consisted of combining the two separate analyses to obtain a measure of minimum total mass (structure plus boil-off) as a function of L/D and to select and design shadow shield systems for final evaluation. Each concept was thermally analyzed in detail considering the effects of thermal interactions, ground-hold and orbital thermal protection, etc.; the overall masses of the systems were summarized; and systems evaluations were made on the basis of mass and inherent reliability.

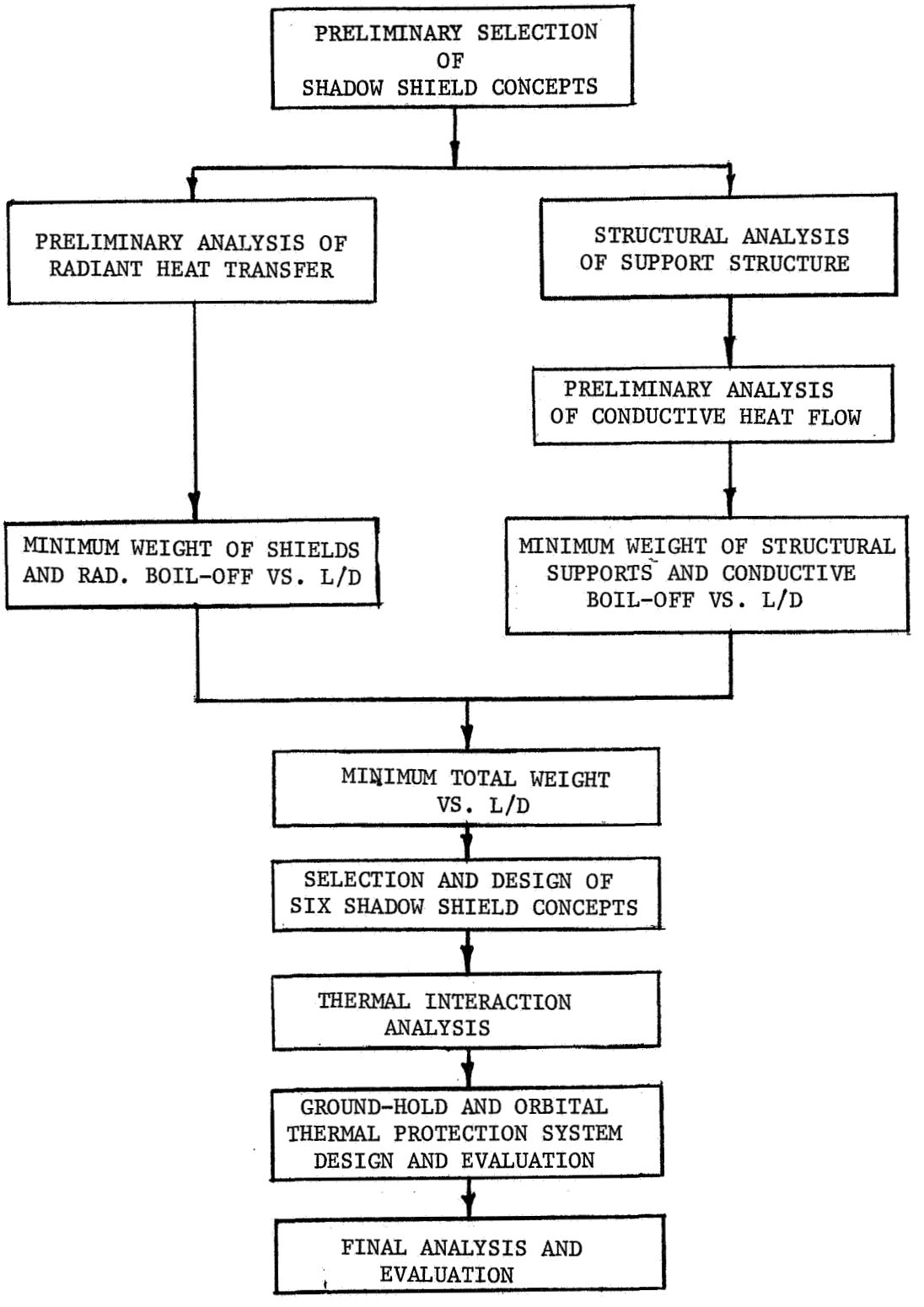

FIGURE 2 PROGRAM PLAN - CONCEPTUAL DESIGN AND EVALUATION OF SHADOW SHIELD SYSTEMS

* L/D is the ratio of the spacing between the LH_2 tank and payload divided by the diameter.

3.3 Preliminary Concepts

The following discussion briefly outlines various basic concepts which were suitable for shadow shield systems including various concepts for reducing heat leak due to conduction heat transfer in the structural supports. The system concepts fall into two general categories:

1) Fixed launch support structure with fixed shields.

2) Fixed launch support structure with space-erected shields, and space-erected structures.

3.3.1 Fixed Structure and Fixed Shields

A typical shadow shield concept with a fixed launch support structure is shown in Figure 3. The payload support structure consists of a simple truss framework arranged symmetrically in cylindrical fashion between the payload and the LH_2 tank. The elements of the truss are tubular in geometry and of equal length. A tank support system provides a transition between the payload support structure and the LH_2 tank and serves to distribute the loads uniformly over the circumference of the tank. The 9-foot-diameter oblate spheroid tank and the tank support contain an integrated insulation system to provide for ground-hold and orbital thermal protection. The angle θ defines the allowable misalignment in pointing angle for the fixed structure. The angle is only a function of the spacing ratio for the fixed-diameter payload and tank considered in this study.

The system mass of a shadow-shielded design includes the following components:

1) Mass of the shield system.

2) Mass of the payload support structure.

3) LH_2 boil-off mass due to radiant transfer.

4) LH_2 boil-off mass due to conduction between the payload and LH_2 tank.

In designing a fixed-structure system, it is desirable to minimize the sum of the above four components and, at the same time, maintain a payload-to-tank spacing which is as short as possible to reduce the length and mass associated with the shroud enclosing the upper stage.

The mass of the shadow shield system is related to the number, shape and material used in fabrication. The mass of the structure is related to the truss arrangement, payload mass, tank-to-payload spacing and the support material properties. The mass of the

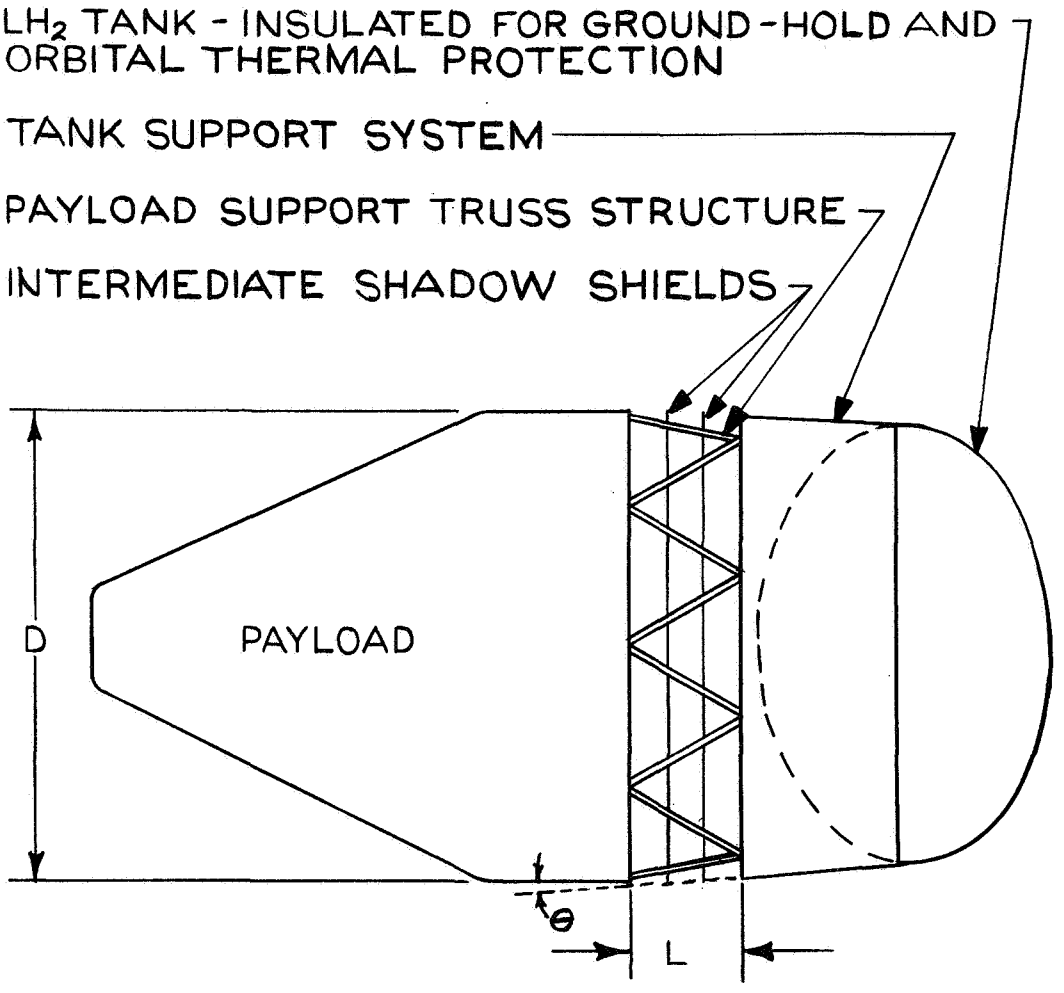

FIGURE 3 - FIXED LAUNCH SUPPORT STRUCTURE CONCEPT

LH_2 boil-off due to radiant transfer from the payload is determined by:

- Overall spacing ratio between the LH_2 tank and payload
- Number of shadow shields
- Shape of shadow shields
- Spatial distribution of the shields between the tank and payload
- Emittance properties
- Reflectance characteristics
- Effectiveness of the ground-hold and orbital insulation

Finally, the mass of LH_2 boil-off due to conduction via the support structure depends on the structural arrangement (number of truss members, diameter, wall thickness, etc.), spacing ratio, thermal conductivity, and the surface thermal/optical properties.

Investigations of the fixed-structure concept included the use of different shield shapes and arrangements as shown in Figure 4. The relative effectiveness of such shapes was evaluated in a preliminary analysis to be described in Section 4.2.2.

In a fixed-support structure, the LH_2 boil-off due to conduction along the supports can be considerable, because of the required wall thickness to withstand the launch loads. Several methods of cooling the structure temperatures and reducing the conduction boil-off mass are illustrated in Figure 5. Concept (a) illustrates a typical pattern of thermal-control coatings which provides radiation cooling. The surface near the periphery of the shadow shield (facing space) has a high-emittance coating to allow the support to radiatively dissipate heat, while the portion facing the interior of the shadow shield system has a low-absorptance coating to minimize radiative interactions with the shadow shields and the payload.

The support for Concept (b), in addition to similar thermal-control pattern, has a pant-leg radiator heat stationed to the support at some location, x, and extends over the remaining portion of the support. The inner surface of the radiator and the support area it encloses have low-emittance surfaces to minimize radiative heat exchange between the radiator and the cooler portion of the support. The high thermal conductance radiator or fin cools the support by dissipating heat to space from a high-emittance surface, and can reduce the temperature gradient at the base of the support (near the LH_2 tank). The

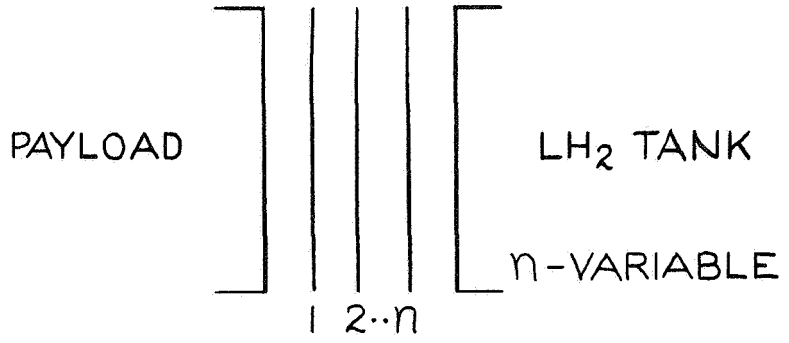

a) MULTIPLE FLAT SHIELDS

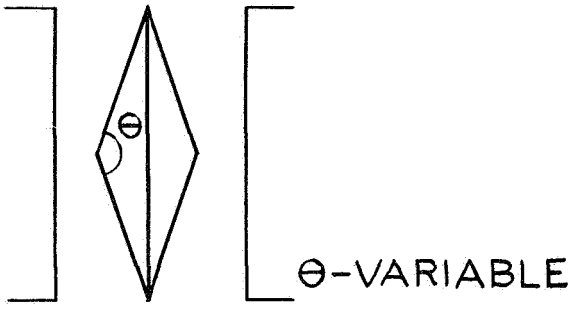

b) CONICAL SHIELDS

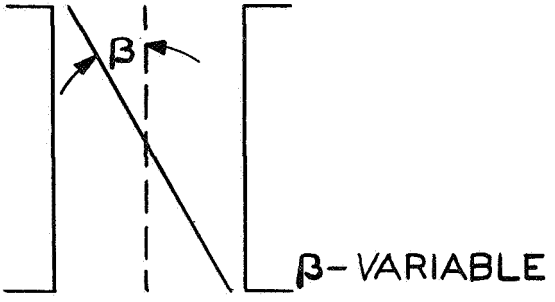

c) ELLIPTICAL DISK-TYPE SLANTED SHIELDS

FIGURE 4 - SHADOW SHIELD CONCEPTS

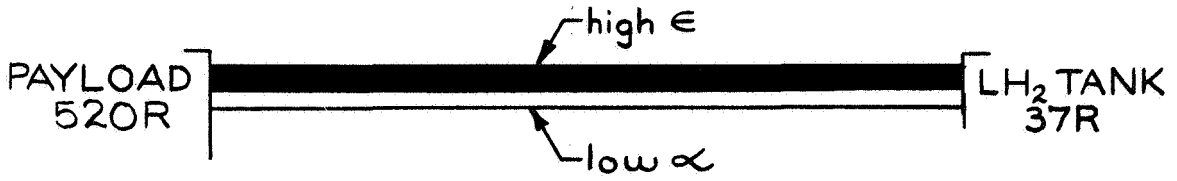

a) RADIATIVELY COOLED SUPPORTS

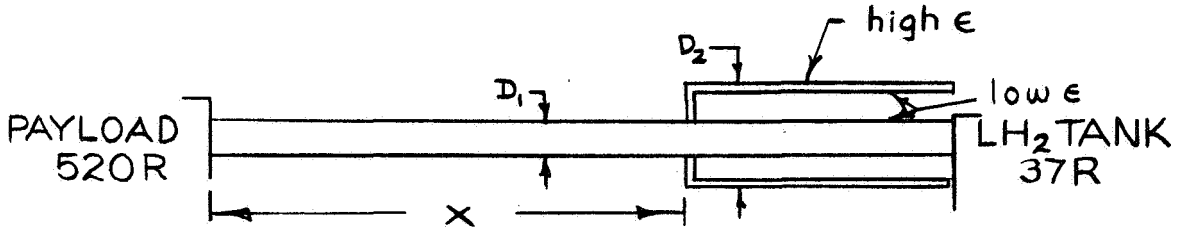

b) SUPPORTS WITH PANT LEG RADIATORS

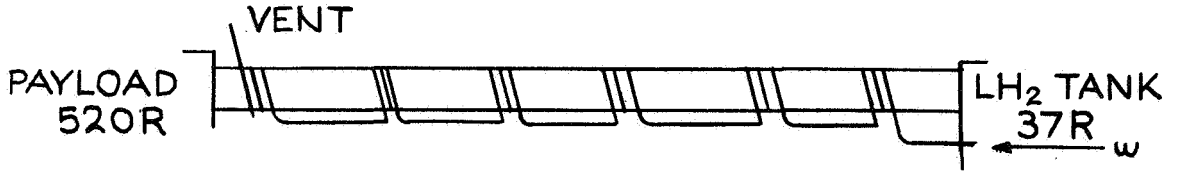

c) VAPOR-COOLED SUPPORTS

FIGURE 5- COOLING CONCEPTS TO REDUCE LH_2 BOIL-OFF DUE TO CONDUCTION EFFECTS

effectiveness of this concept in reducing the LH_2 boil-off from conduction depends upon location of the radiator, the ratio of diameters D_2/D_1, and the thermal-control pattern on the support and radiator.

Concept (c) shows a structural support cooled using the sensible enthalpy of the LH_2 boil-off which results from the radiation and conduction heat flow to the LH_2 tank. A vapor-coolant line is bonded to the support at a number of locations so that the venting gaseous hydrogen will cool the support structure and thereby reduce the conductive heat flow at the tank end.

A number of the important variables and design options available to minimize the heat leak and system mass have been discussed. From these considerations, it can thus be seen that the number of variables is large and that a truly optimum design of minimum system mass would be essentially impossible to define if the interactions of all variables were to be considered simultaneously. This is the reason why a number of the important variables were screened and optimized independently to arrive at near-optimum configurations.

It will be demonstrated by the results of analyses described in following sections that it is not difficult to design a system with essentially no LH_2 boil-off due to radiation and that the shield mass will be small. Furthermore, it will be shown that the mass of the ground-hold and orbital insulation and the LH_2 boil-off during ascent and orbital operation play an important role in determining the overall system mass.

It should be noted that a cylindrical tank support was designed to distribute the loads from the open-truss structure around the periphery of the LH_2 tank. This structure was designed to be insulated for minimizing the ground-hold heat leak. This cylindrical tank support is common to all of the concepts to be discussed.

3.3.2 Space-Erected Concepts

Figure 6 illustrates a shadow shield concept with a fixed-payload support structure and part of the shadow shield system space erected. In this case, two flat, circular shields are used with multiple annular shields which are deployed in space to compensate for vehicle misalignment with the solar vector. The forward surface of the space-erected shield on the payload has a coating with a low solar absorptance-to-emittance ratio to minimize solar heat input to the system. The degree to which solar misalignment can be accommodated depends on the shield diameters as deployed. During launch, the shields are folded within the shroud and restrained. After the shroud is jettisoned, a pyrotechnic or other suitable device is used to deploy the annular deployable shields.

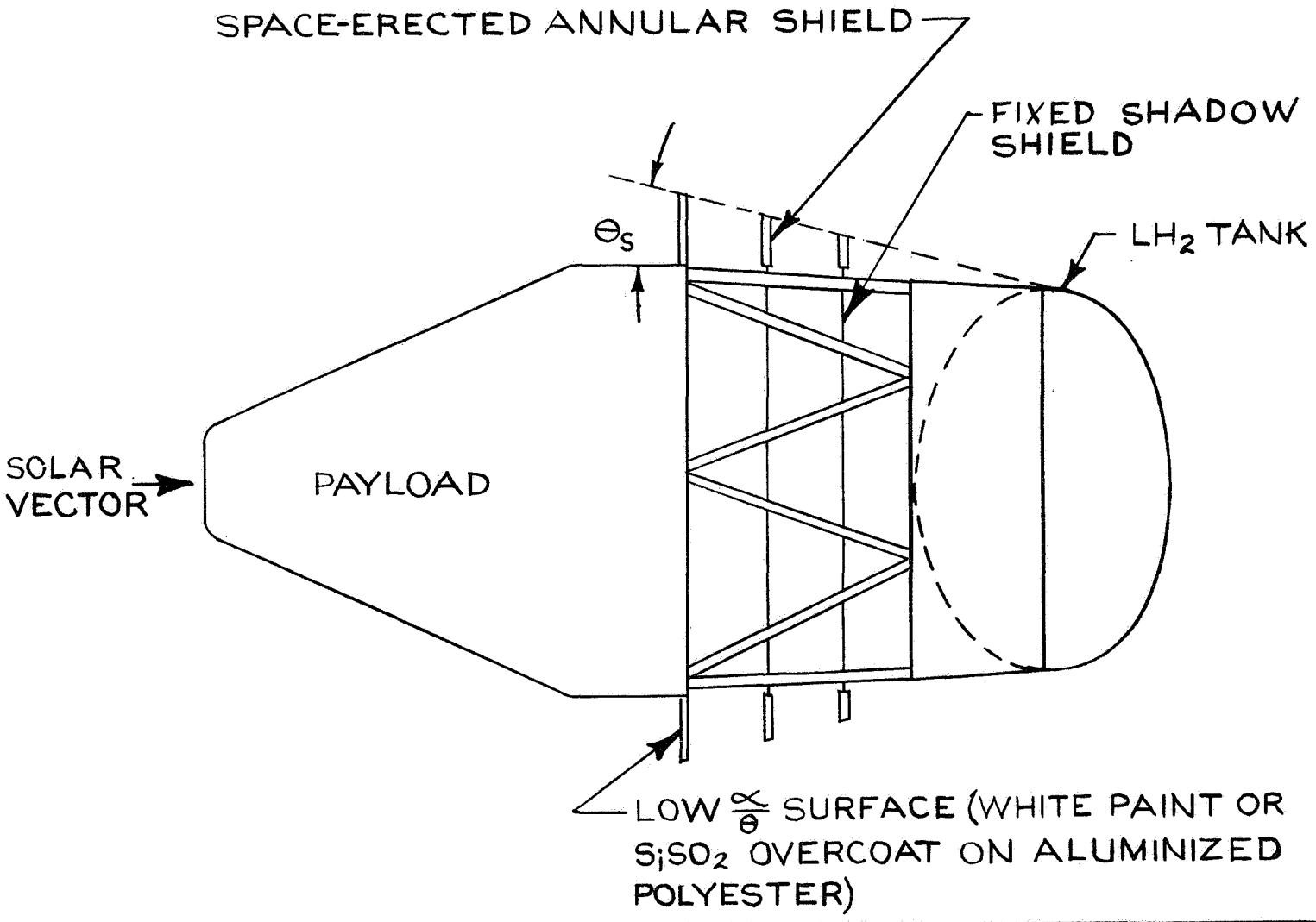

FIGURE 6 - CONCEPT WITH COMPENSATION FOR SOLAR VECTOR MISALIGNMENT

The thermal considerations in this case are similar to those previously described for a fixed structure.

A structure which is deployed in space has the advantage of not having to withstand the launch loads and would instead be subject to the considerably lower maneuvering loads during the coast mission. As a result, the structure can be composed of lightweight, low thermal conductance members which can reduce the mass of the structure and the conduction heat flow. Since the deployed length does not affect the length of the shroud, a large payload-tank spacing can be utilized to minimize radiant heat transfer with a small number of lightweight, space-erected shadow shields. The savings in structure and shield masses, however, must be traded-off against the mass and operational complexity of the actuation systems required for deployment.

One concept for an erectile structure includes hinging lightweight tubular "A" frames from the payload and LH_2 tank, as shown in Figure 7. These frames would be joined at their apexes by a hinge so that they can be swung outward and eventually back against the circumference of the LH_2 tank during retraction. When deployed, this structure consists of a series of "X" members spaced around the circumference of the shadow shields. Figure 7 shows the "A" frame concept in the deployed and stowed configuration. The actuation system for this structure has been omitted for clarity but would consist of a powered winch which would simultaneously wind and unwind actuation cables attached to the apexes of all the "A" frames which have hinged connections at the payload and tank support system. In this manner all "A" frames move simultaneously to prevent cocking, and the system always has sufficient rigidity so that the attitude control system could be actuated during structure deployment, if necessary.

An extendible structure made by using many "STEM" elements in parallel, spaced around the spacecraft circumference is shown schematically in Figure 8. A "STEM" is a storable, tubular, extendible member made up of a preformed thin metal tape which is wound on a drum during storage. When the tape is unwound from the drum, it assumes thin-wall tubular shape. This system would be actuated by a central power source which would be connected to all the "STEM" winding drums. In this way, all "STEM" elements, like the "A"-frame elements, would deploy and retract simultaneously to prevent cocking.

A third concept for a space-erected structure is presented in Figure 9. The elements are composed of stepped-diameter, thin-wall tubes which nest inside one another when the structure is retracted. The actuation system would consist of a central-powered winch which would simultaneously wind and unwind cables which would extend or retract all tubes.

A detailed analysis of the structural characteristics and the mass of the structure for these three preliminary concepts will be presented in Section 5.3.

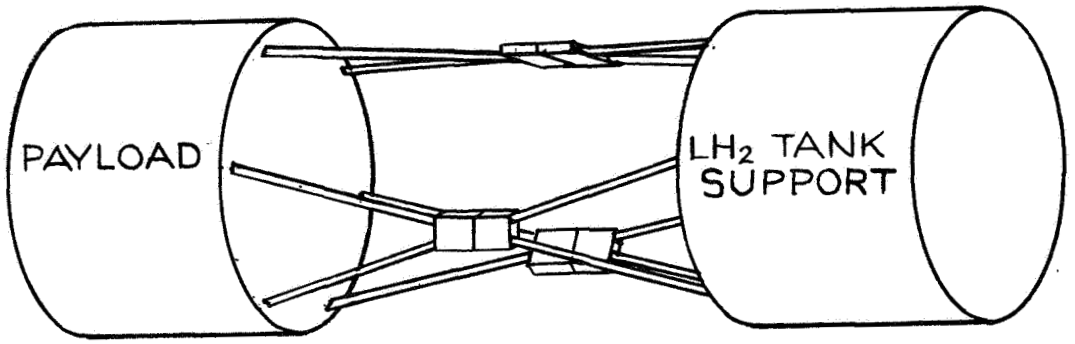

ERECTED STRUCTURE

RETRACTION STEPS

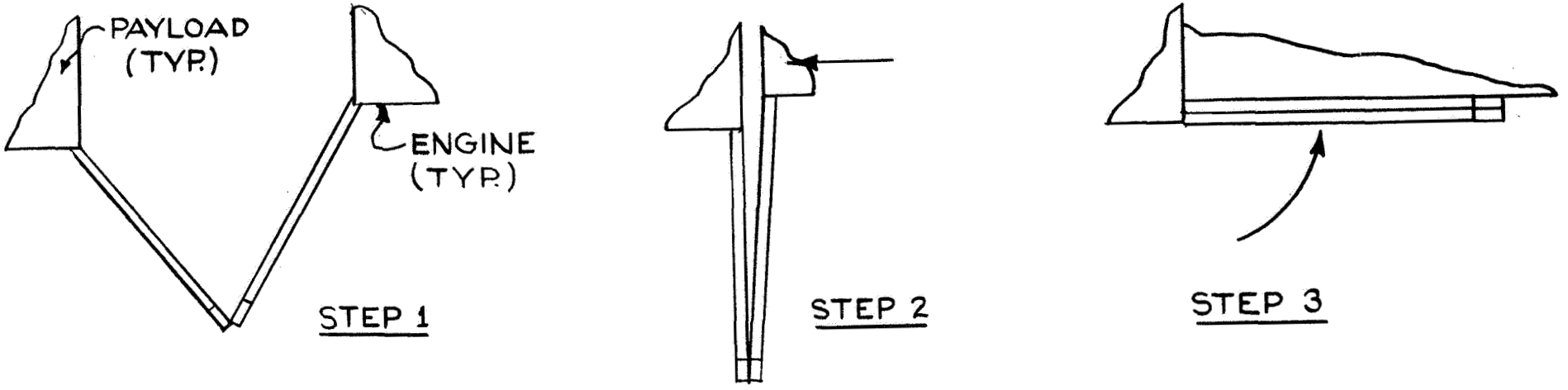

FIGURE 7 "A"-FRAME ERECTILE STRUCTURE

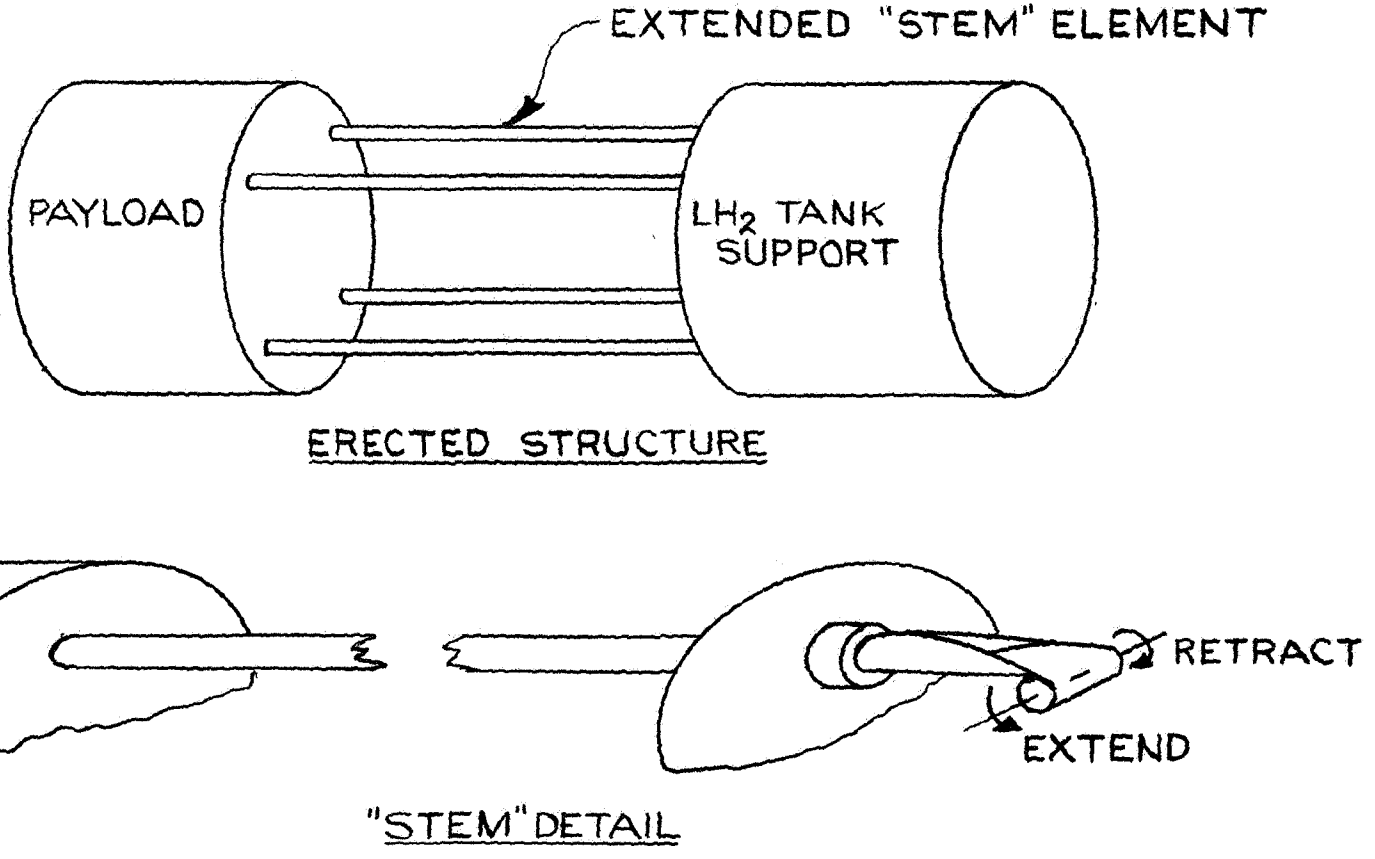

FIGURE 8 - "STEM" ERECTILE STRUCTURE

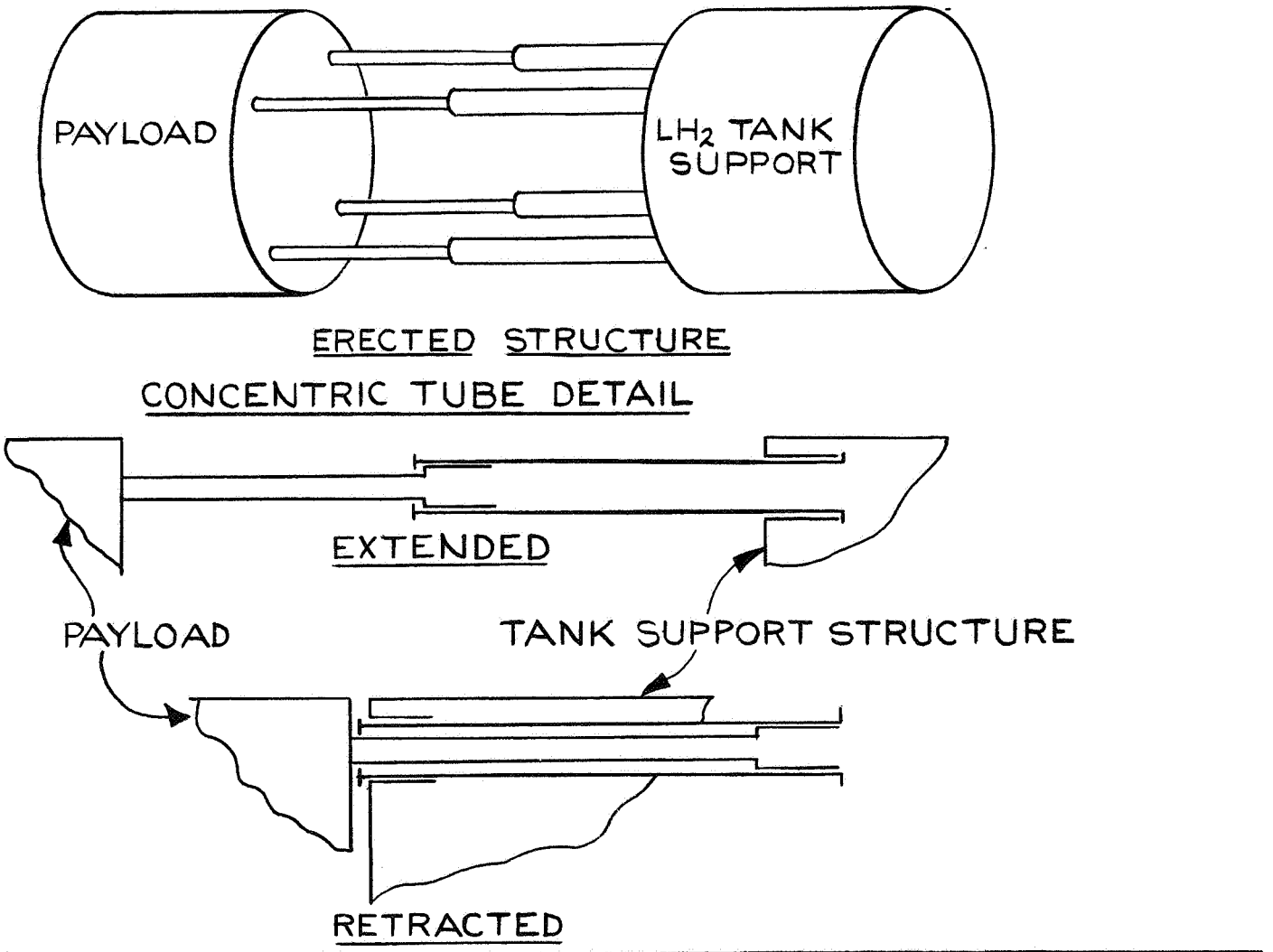

FIGURE 9 - CONCENTRIC TUBE ERECTABLE STRUCTURE

4.0 RADIANT HEAT TRANSFER IN SHADOW SHIELD SYSTEMS

4.1 Introduction

The following discussion describes the thermal analysis of a thermal protection system composed of shadow shields--situated between a sun-oriented payload and a shadowed LH_2 tank--to intercept, reflect and reject the radiant heat flux emanating from the payload. This analysis consisted of two phases: 1) a preliminary analytical analysis, and 2) a detailed parametric study using digital computer techniques.

In the preliminary analysis, simplified mathematical models were used to investigate the effects of shield shape and spacial distribution of shields between the payload and the LH_2 tank. The results of this analysis, presented in Section 4.2, served as a preliminary guide for the initial design of shadow shield systems and aided in defining the requirements of a radiant heat transfer computer program, which was developed as a part of this work. In Section 4.2 reference is also made to studies performed at NASA Lewis Research Center investigating the effects of shield spacing.

The use of a computer program developed for evaluating the radiant transfer in shadow shield systems as a function of L/D, number of intermediate shadow shields between the payload and LH_2 tank, shield material and surface optical characteristics (specular or diffuse reflections) is discussed in Section 4.3. The computed data are presented in a general format so their use is not limited to a particular payload diameter or mission time. Detailed data obtained from computer analyses which were utilized to determine near-optimum arrangements of shadow shields for a 10-foot-diameter payload and a 10,000-hour coast mission are presented in Section 7.2.1. The shadow shield optimization was based on the mass of the shields including supports and attachments, and the LH_2 boil-off due to radiation.

4.2 Simplified Analysis

A number of studies have been reported which relate the performance of shadow shield systems to the emittance, the number of equally spaced shields and the spacing between a high-temperature source and a low-temperature sink. In many cases, the physical model consisted of a circular source and sink of some diameter, and intermediate shields of the same diameter with a uniform temperature distribution, a uniform radiosity distribution and surfaces with a diffuse emittance and reflectance. The data resulting from these studies indicated that the heat flux absorbed by the low-temperature sink was a strong function of the number of equally spaced shields, the temperature of the source, the overall spacing between the source and sink, and the surface emittance of the shields.

Complex mathematical models and computer programs are required for a detailed study to predict the performance of practical shadow shield systems, i.e., systems with lightweight, low-emittance shields of finite thermal conductance, where the effects of non-uniform distributions of radiosity, the optical characteristics (diffuse or specular) and thermal interactions between shields and supports are important.

Prior to the development of the computer programs used in the detailed analysis of the shadow shield systems, a simplified analysis was initiated to examine the influence of the spacial distribution of shadow shields and shield shape, and to guide the preliminary selection of conceptual designs. This simplified analysis was based on a system comprising a high-temperature source at a temperature of 520R (the payload) and a low-temperature sink at 0°R (simulating the LH_2 tank). For these simplified analyses, the circular surfaces of the payload, the LH_2 tank and the intermediate shadow shields were taken to be isothermal discs with a uniform distribution of radiosity.

4.2.1 Shield Shape

It is of interest to determine whether or not shield shape may be an important factor in reducing the heat flux absorbed by the cold sink. Shaped shadow shields which are space-erected in front of a space vehicle to shield the vehicle from sunlight have been studied, and the results have been presented in the literature. In the subject study, however, the shadow shields must be placed between the payload and LH_2 tank; any additional spacing required to provide clearance for spherical, conical or other shapes of shadow shields can result in a large mass penalty because of the additional mass of the structure designed to support the payload and the additional mass of the interstage structure.

The thermal performance for a double conical shadow shield centrally located between a 520R source and a 0°R cold sink with an L/D of unity is compared to the thermal performance for a circular shield in Figure 10. It is assumed that all surfaces are diffuse, have an emittance of 0.03, and that the double conical shield is formed from two radiatively coupled shields with uniform radiosity and infinite radial conductance (i.e., the shields are isothermal). At $\theta = 180°$ the two shields become flat, circular discs centrally located between the source and sink; at $\theta = 90°$ the double cone just touches the source and sink. In Figure 10 the heat flow per unit area to the 0°R sink for conical shields normalized to the heat flow for two circular shields is plotted versus the conical apex angle. Figure 10 shows that the minimum heat flux occurs at $\theta = 90°$. The percentage reduction in heat flux for the conical shields compared to flat, circular, closely spaced shields is less than 20%. At smaller L/D ratios the advantages of a conical shield are further reduced. (It can be noted that if the heat flow per

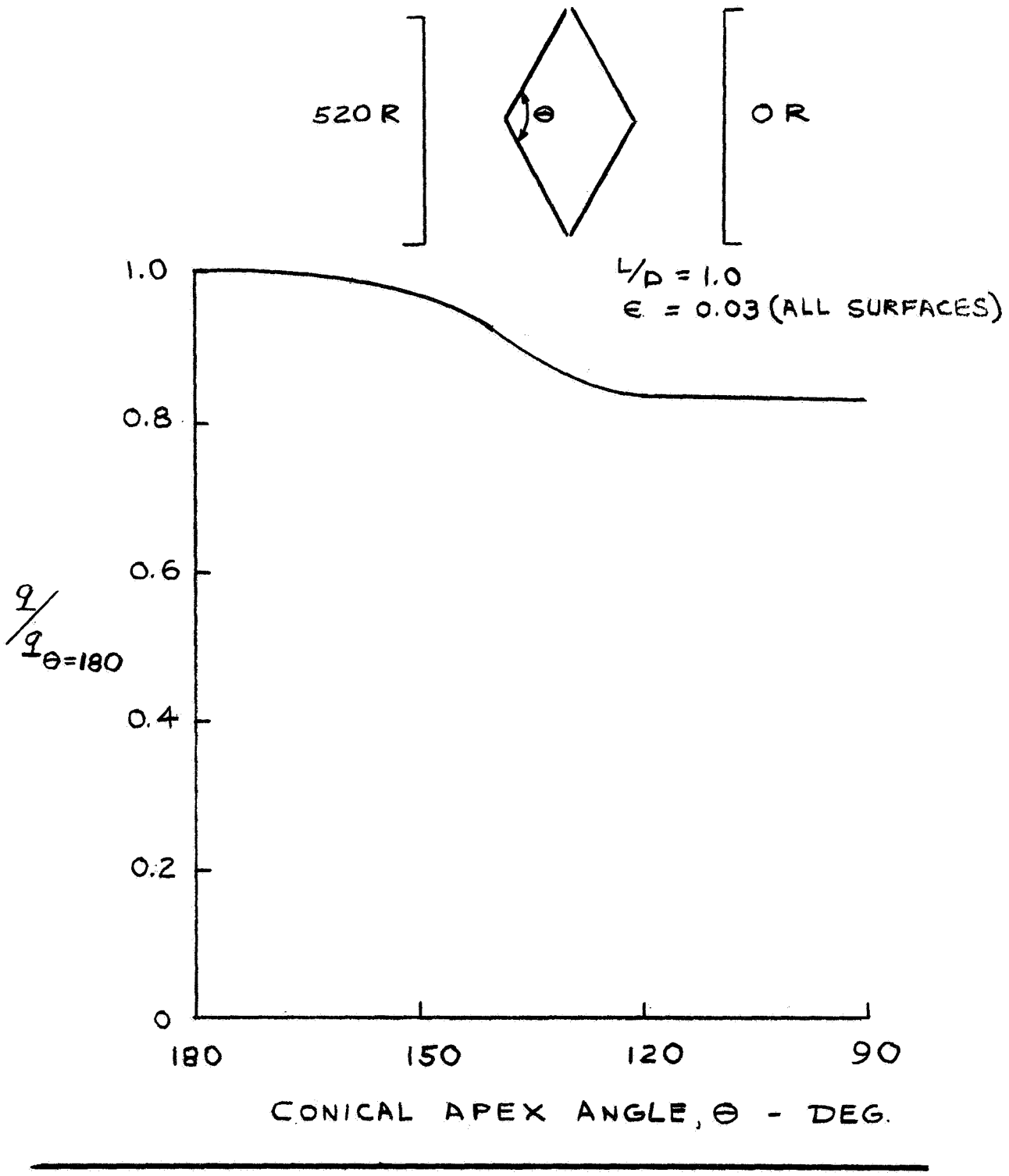

FIGURE 10 COMPARISON OF HEAT FLUXES FOR A CONICAL AND CIRCULAR SHIELD CENTRALLY LOCATED BETWEEN SOURCE AND SINK

unit area for the two conical shields was normalized to the heat flow for a single circular shield, centrally located between the source and sink, the normalized heat flow would vary between 0.51 at $\theta = 180°$ to 0.42 at $\theta = 90°$.)

A similar calculation was performed for a single slanted shield centrally located between the source and sink with an L/D of unity. The surfaces are all assumed to be diffuse and have an emittance of 0.03. The ratio of the heat flux to the 0°R sink for a slanted shield to the heat flux for a circular shield is plotted against the slant angle, β, in Figure 11, for a shield with uniform radiosity and infinite conductance. The slant angle is measured from a plane parallel to the source and sink; thus at $\beta = 0$ degrees, the shield is circular and parallel to the source and sink. The results obtained with this simple model show that the heat flux actually increases slightly as the shield is slanted.

For the present application we did not believe that a refined, detailed analysis (accounting for non-uniform radiosity distributions, finite thermal conductance, specular-reflectance characteristics, etc.) was required to eliminate the consideration of shaped shadow shields. Although a detailed analysis of specularly reflecting shaped shields might show that the heat flux computed using the diffuse assumption is conservative, (i.e., higher than that computed for specular surfaces), the use of conical or slanted shields will increase the payload-to-tank spacing required. The increased spacing will result in a higher structural mass required to support the LH_2 tank during launch and a higher mass associated with the longer interstage shroud used to protect the system during launch. Flat shadow shields offer the advantages that they are lightweight, simple to support, and can be positioned between a closely spaced payload and LH_2 tank. The final design concepts to be described will illustrate that the use of a few flat, parallel, low-emittance shields will effectively reduce the radiative component of heat transfer to a negligible value (for a 10,000-hour mission) with an extremely small shield weight penalty.

A conical shield shape would be feasible in concepts with space-erected structures where the spacing ratio in a deployed configuration is large and the structure is lightweight, since it does not withstand launch loads. However, our preliminary calculations indicated that, at large spacing ratios, the LH_2 boil-off (for a 10,000-hour mission) could be made negligible with a single, flat, low-emittance shield.

4.2.2 Shield Location and Number of Shields

The simplified mathematical models (uniform radiosity, isothermal shields with diffuse emittance and reflectance) were also used to examine the influence of shield location in a system with one or more shields. Results of preliminary studies made at NASA Lewis

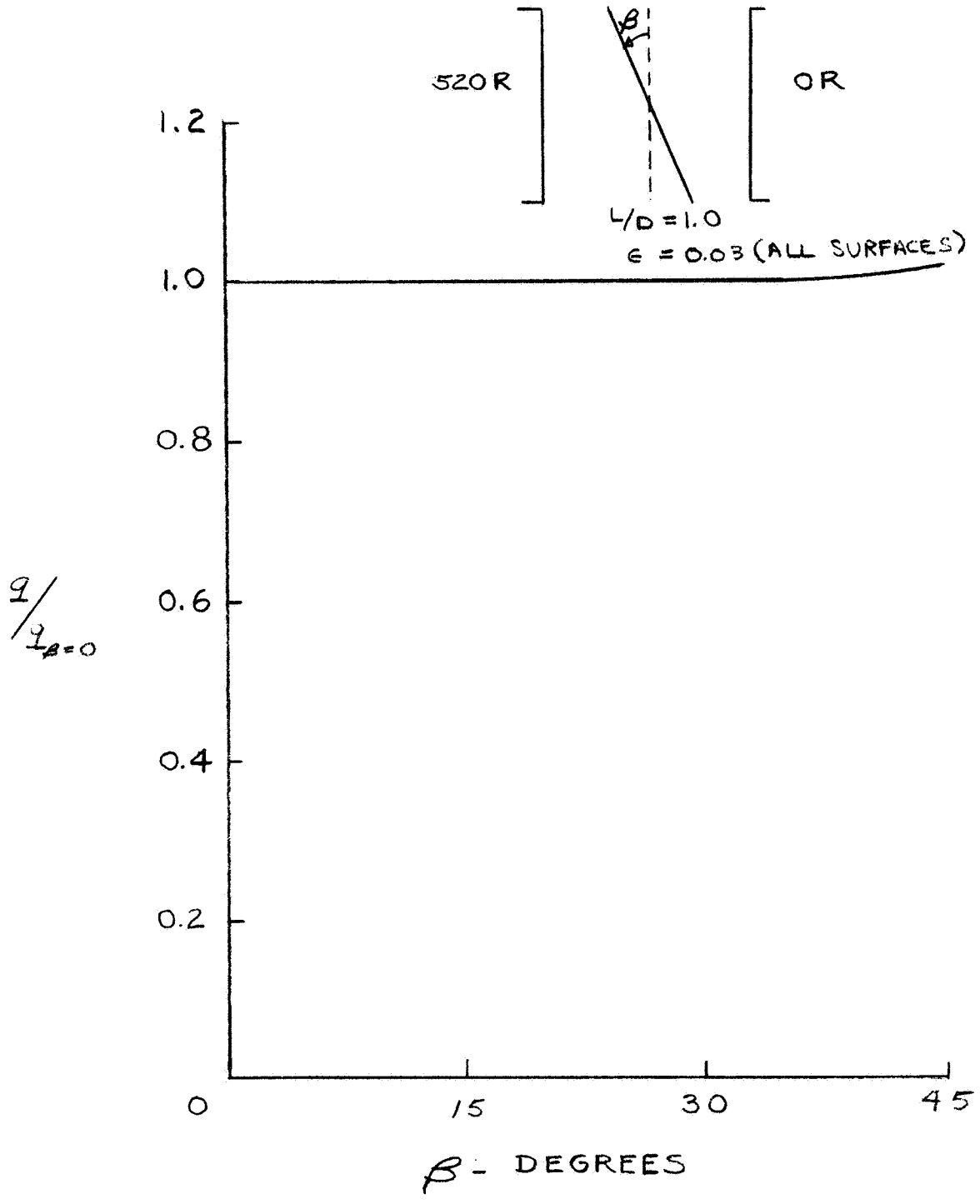

FIGURE 11 COMPARISON OF HEAT FLUXES FOR A SLANTED AND CIRCULAR SHIELD CENTRALLY LOCATED BETWEEN SOURCE AND SINK

Research Center for more refined models will also be presented in the discussion.

In conceptually designing near optimum shadow shield systems from an overall mass standpoint, one of the important geometrical variables is the spacing between the payload and the LH_2 tank. For example, in designing fixed structures the mass of the structure and the LH_2 boil-off from conduction are dependent upon length (as well as material, configuration, etc.). Likewise, the payload-tank spacing plays an important role in evaluating the trade-offs between the number of shields, shield mass and the LH_2 boil-off due to radiant heat transfer. In addition, the spacial distribution of the shields between the payload and tank can be important. The effect of spacial distribution is rather complex since the optimum spacing (spacing for minimum heat transfer), like the overall mass of shadow shields, depends upon the payload-tank spacing, shield emittance and number of shields.

The results of various calculations of the effects of shield spacing are presented below. It was not possible to generalize or determine an optimum arrangement for all values of L/D, emittance and number of shields. However, many of the results indicated that systems with evenly spaced shields were optimum from the standpoint of minimizing radiant heat leak or were not significantly different from the optimum arrangement. In the detailed computer studies (Section 4.3) where the L/D, the number of shields and the emittance were parametrically varied for shields with specular and diffuse reflectances, the shields were taken as equally spaced.

The first results presented are those obtained for a simplified model (uniform radiosity, infinite conductance shields). Figure 12 presents the relationship between the heat flux absorbed by the 0°R sink and shield location for a system with one intermediate shield and a spacing ratio, L/D, of 1.0. The normalized heat flux absorbed at the 0-degree sink is q/A, the temperature of the source is T_o, and the emittance of the surfaces of the source, shield and sink is ε_s. The heat flux is minimized when the shield is centrally located between the payload and sink (X/L = 0.5) when the surfaces are black (ε_s = 1) and also when the emittances of the surfaces are 0.05. Also, in both cases the absorbed heat flux is symmetrical about the central position. The maximum variation in heat flux between the worst location (near the source or the sink) and the best location (central position) is approximately 18% for black surfaces, while there is an order of magnitude variation when ε_s is 0.05.

For systems with more than one intermediate shield, the relationship between shield location and heat flux has been shown to depend on the radial thermal conductance, the emittances of the source, sink and shield, the assumptions relating to the distribution of radiosity, and the spacing between the source and sink. The effect of shield location on the heat flux for a two-shield system is shown in Figure 13 for L/D ratios of 0.1 and 0.5. The physical model here

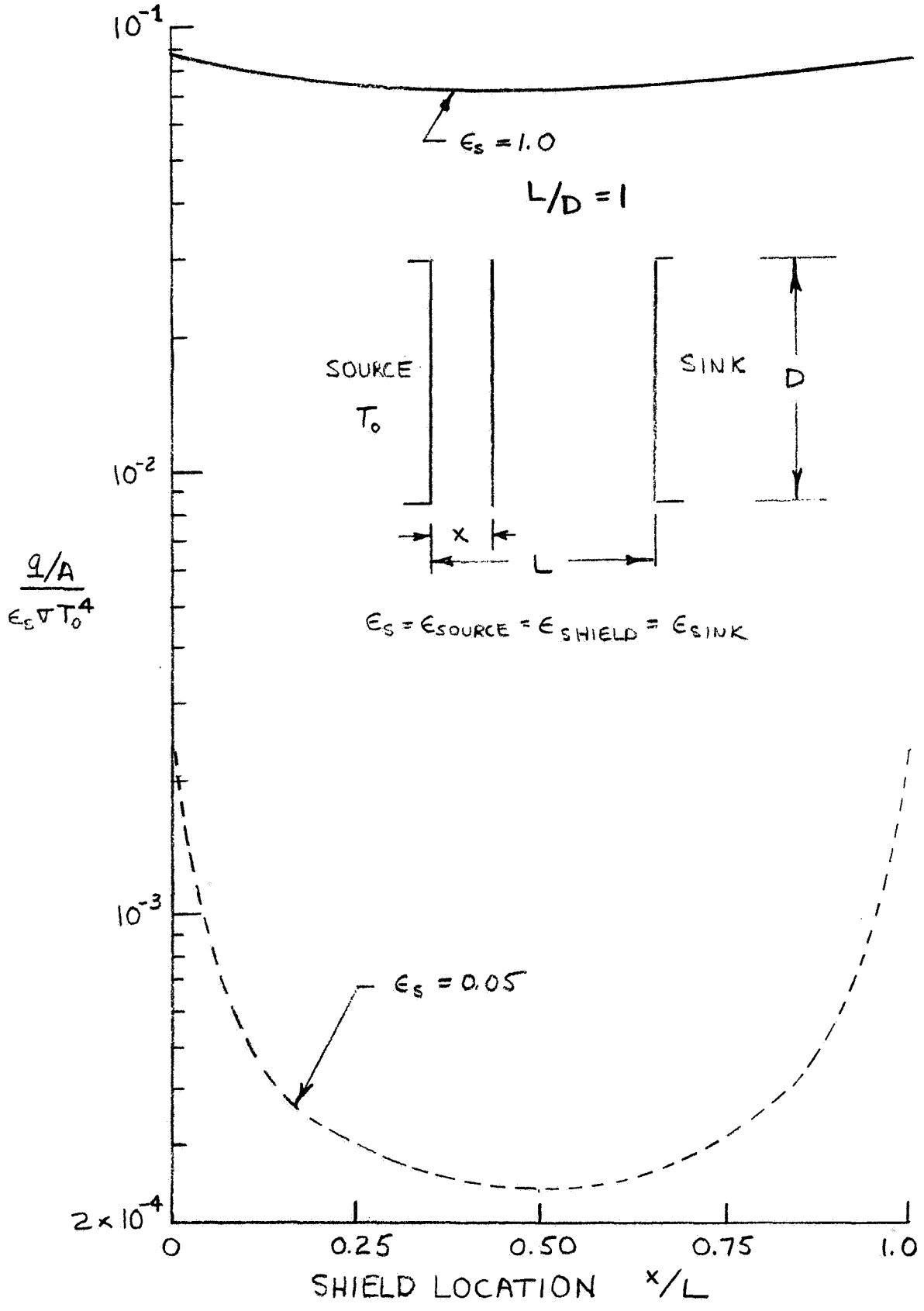

FIGURE 12 - EFFECT OF SHIELD LOCATION ON HEAT FLUX FOR ONE SHIELD

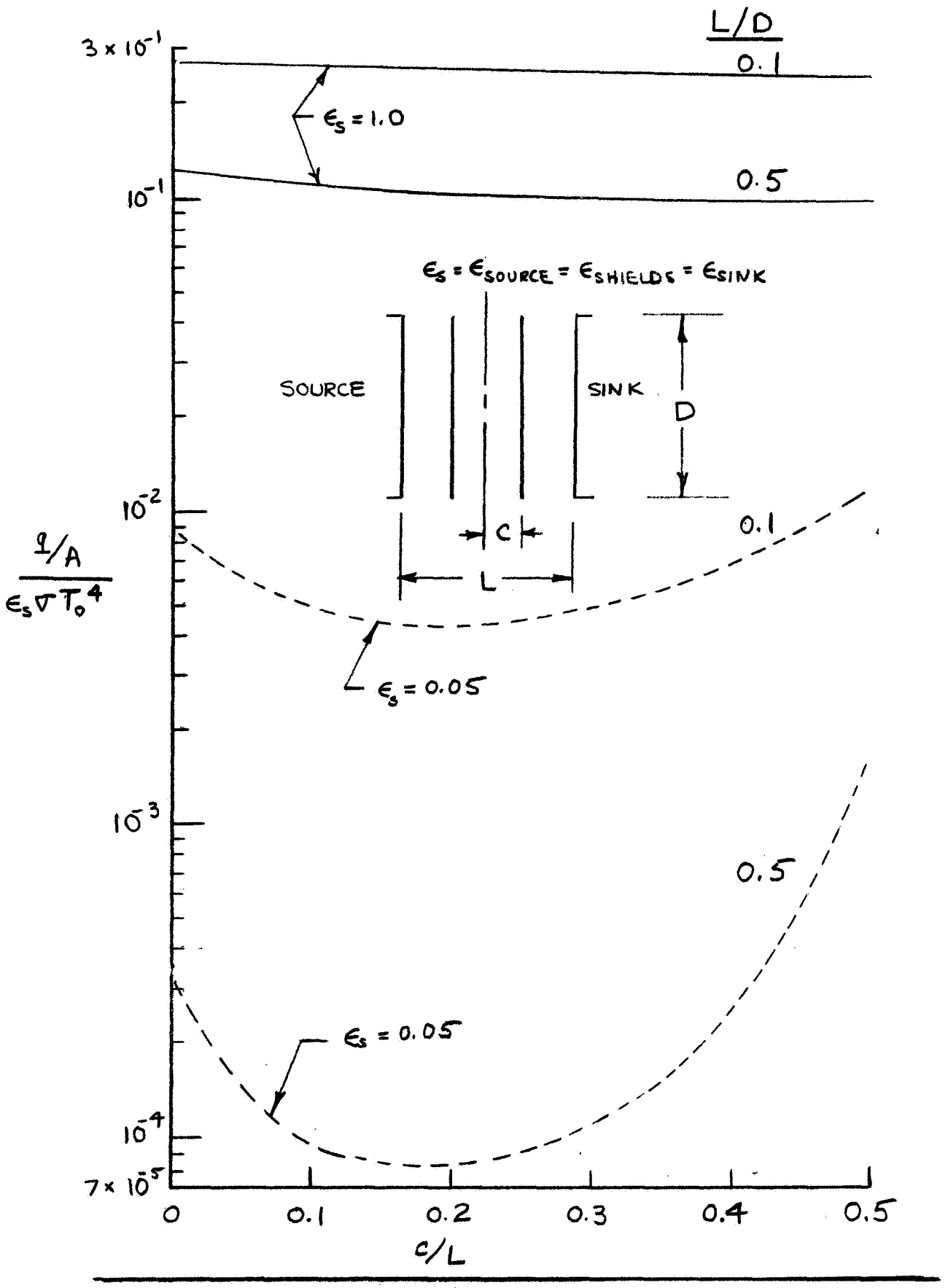

FIGURE 13 - THE EFFECT OF SPACING ON HEAT FLUX FOR A TWO SHIELD SYSTEM ARRANGED SYMMETRICALLY ABOUT THE CENTER

consists of two intermediate shields with uniform radiosity and infinite radial conductance, symmetrically positioned about a plane centrally located between the source and sink; ε_s is the emittance of the surfaces of the source, intermediate shields and sink. The non-dimensional heat flux is shown as a function of C/L, the ratio of the distance of each shield from the central position to the total spacing.

For black surfaces the minimum heat flux occurs when C/L is near 0.5, where one shield is adjacent to the source and one shield is adjacent to the sink. However, the magnitude of the heat flux is relatively insensitive to the intermediate spacing between the two shields. The variation between the minimum heat flux and the heat flux when the shields are equally spaced (C/L = 0.167) is approximately 5% when L/D is 0.1 and 8% when L/D = 0.5.

For low-emittance shields (ε = 0.05), the heat flux is near minimum when the shields are equally spaced. It can be seen from Figure 13 that the heat flux substantially increases when the intermediate spacing between the two shields is decreased or increased.

The following discussion relates to the effect of varying the spacial distribution of shields for a physical model where the radiosity is non-uniform and the shields are assumed to have a zero thermal conductance. The low-emittance (ε = 0.05) shields are diffusely reflecting and are positioned symmetrically about a plane centrally located between the source and sink. Data for the heat flux to a 0°R sink and the equivalent boil-off of LH_2 (10-foot-diameter LH_2 tank for 10,000 hours) for shadow shield systems comprising two and three intermediate shadow shields are presented in the following table.*

	Equal Spacing		Spacing for Minimum Heat Flux		$\frac{(q/A)_{equal}}{q/A \text{ min.}}$
	q/A (Btu/hr-ft^2)	W_{LH_2} (**) (lb_m)	q/A (Btu/hr-ft^2)	W_{LH_2} (**) (lb_m)	
L/D = 0.1,* ε = 0.05					
2 intermediate shields	0.125	504.7	0.106	428.0	1.2
3 intermediate shields	0.0783	316.2	0.0426	172.0	1.8
L/D = 0.5,* ε = 0.05					
2 intermediate shields	8.77×10^{-4}	3.5	8.77×10^{-4}	3.5	1.0
3 intermediate shields	1.41×10^{-4}	0.6	1.41×10^{-4}	0.6	1.0

* ε = 0.05 for all surfaces

(**) = Equivalent mass of LH_2 boil-off for a 10-foot-diameter payload at 520R for 10,000 hrs.

* The calculations are taken from preliminary work at NASA Lewis Research Center by Robert J. Boyle and Richard H. Knoll (Personal communication, 16 May 1968).

For two intermediate shields at an L/D of 0.1, the minimum boil-off occurs with one shield adjacent to the payload (source) and one shield near the LH_2 tank (sink). The boil-off with this arrangement is approximately 16% lower than the boil-off with equally spaced shields. For three shields at an L/D of 0.1, the minimum boil-off occurs with one shield centrally located, one shield adjacent to the payload and one shield adjacent to the LH_2 tank. The boil-off with this arrangement is approximately 45% lower than the boil-off with equally spaced shields. It may be noted that in both cases these systems with small L/D would not be practical because of the relatively high boil-off rate.

At L/D ratios of 0.5, it can be seen from the previous table that the minimum boil-off occurs with the shields equally spaced for either two or three shields. Because of the increased spacing ratio, the boil-off for either two or three shields is considerably lower than for an L/D of 0.1. It is also interesting to note that at L/D ratios of 0.5, the effect of shield spacing is more important, on a relative basis, than at L/D ratios of 0.1. This effect is illustrated in the following tabulation which shows the relationship between the highest and lowest heat flux, when the shield spacing is varied maintaining symmetry about the central plane.

	$\frac{(q/A)_{max}}{(q/A)_{min}}$
L/D = 0.1 ε = 0.05	
2 intermediate shields	1.4
3 intermediate shields	2.7
L/D = 0.5 ε = 0.05	
2 intermediate shields	20
3 intermediate shields	23

In conclusion, for several low-emittance, diffuse shields at small overall spacing ratios (L/D = 0.1), the effect of shield location may be important from the standpoint of the absolute value of the boil-off rate, since the boil-off rate is large. The minimum boil-off occurs at non-equal spacings, but the relative variations in boil-off rate resulting from variations in the shield locations are not large (the ratio of maximum to minimum boil-off rate is less than a factor of 3). At larger overall spacing ratios (L/D = 0.5), the boil-off rate is considerably reduced, the effect of shield spacing is important on a relative basis (the ratio of maximum to minimum boil-off rate is approximately 20), and equally spaced shields result in near minimum boil-off rates. It should be noted that the above conclusions apply to diffuse shields positioned symmetrically about a plane centrally located between the source and sink. Additional work would be required to investigate other non-symmetrical shield arrangements.

There are a number of other factors which may influence the optimization of shield location. They include:

1) Non-diffuse properties of shield coatings with low emittance.

2) Temperature dependence of emittance.

3) Geometry of the source and sink.

However, in the final selection of a near-optimum concept for a shadow shield system one must consider the optimization of the system mass which would include the mass of LH_2 boil-off due to both radiative transport and conduction via the support structure, the mass of the shields and the mass of the support structure. The necessity for optimizing the location of the shields will depend on whether or not the boil-off component due to radiation significantly influences the overall system mass penalty.

4.2.3 Shield Emittance

A simplified analysis may also be utilized to illustrate the effect of using low-emittance shield surfaces on the magnitude of the heat flux absorbed by the LH_2 tank.

Consider, for example, a single shadow shield having an emittance ε_s on both sides, centrally located between the payload and LH_2 tank. The surfaces of the payload and LH_2 tank facing the central shadow shield also have an emittance ε_s and are maintained at temperatures of 520R and 37R, respectively. By making the assumption that the distribution of radiosity is uniform over all surfaces and that the surfaces emit and reflect diffusely, the heat flux absorbed by the LH_2 tank may be obtained by a direct solution of the heat-balance equations for each surface.

The results of a hand calculation of the absorbed heat flux for this simple model are presented in the following tabulation for surface emittances of 1.0 and 0.03 and several spacing ratios. (The choice of an emittance of 0.03 is based on a typical value for vacuum-deposited metal coatings. Typical room-temperature emittance values for coatings deposited on polyester films range from 0.015 for silicon monoxide-protected silver films to 0.025 for aluminum films. Data on such materials will be presented in Section 4.3.5 of this report.)

Radiant Heat Flux Absorbed by a 37R Sink
with One Central Shadow Shield-Source Temperature 520R

	Absorbed Heat Flux $\frac{Btu}{hr\ ft^2}$	
L/D	$\varepsilon_s = 1.0$	$\varepsilon_s = 0.03$
0	62.6	9.6×10^{-1}
0.25	40.0	5.7×10^{-3}
0.50	23.3	1.4×10^{-3}
1.0	9.1	2.4×10^{-4}
2.0	1.8	negative

These results illustrate the reduction in heat flux which can be obtained by use of low-emittance surfaces which are spaced apart. Reducing the emittance from 1.0 to 0.03 reduces the heat flux by about four orders of magnitude for spacing ratios (L/D) of 0.25 or greater.

This simplified example was chosen to merely indicate the potential of using spaced, low-emittance shield systems for heat flux reduction; and further discussion of the heat fluxes calculated for "real" systems where simplifying assumptions are deleted will follow in Section 4.3.

4.2.4 Preliminary Estimate of Radiant Heat Transfer in a Shadow Shield System

Because of the importance of the relative magnitudes of structural mass, shield mass and the LH_2 boil-off in a typical system, it is important to give the reader a preliminary indication of the magnitude of the LH_2 boil-off resulting from the radiant transfer. The table below illustrates the magnitude of the LH_2 boil-off resulting from radiant transfer between a 520R source and the 1160-pound-capacity LH_2 tank for a mission period of 10,000 hours. These approximate calculations are based on a model which assumes all surfaces to be diffuse with a total hemispherical emittance of 0.03 and the radiosity to be radially uniform. Two intermediate shadow shields are assumed to be equally spaced between the LH_2 tank and payload.

L/D	LH_2 Boil-off in 10,000 Hours
0.15	20.7 lb_m
0.25	1.7
0.50	-0.1

It can be seen that the magnitude of the propellant loss is extremely small even for a spacing ratio of 0.15. For a 10-foot payload the distance between the tank and payload would be 18 inches. At L/D ratios approaching 0.5, the heat flux is negative indicating that the temperature of the shield closest to the LH_2 tank is depressed far enough so that the net heat flow is from the LH_2 tank to outer space.

These estimates are, of course, crude because of the nature of the approximations in the mathematical model. Nonetheless, they indicate that the component of LH_2 boil-off due to radiant transfer can be made extremely small even for small spacing ratios with only a few low-emittance shields.

4.2.5 Conclusions

As a result of these preliminary studies, it is concluded that:

1) Flat, parallel, circular shadow shields of low emittance will provide the necessary reduction in radiant heat flux.

2) Large spacing ratios L/D > .25 and large numbers of low-emittance shields n > 3 will not be necessary to reduce the LH_2 boil-off due to radiation to less than 1% per year. (This may be considered as a very low loss in current cryogenic technology.)

3) Optimizing the shield shape is not particularly attractive in view of conclusion 1) and the fabrication and support mass considerations associated with complex shield shapes.

4) When diffuse shadow shields are positioned <u>symmetrically</u> about the central position between the payload and LH_2 tank, the effect of shield location is important in determining radiant heat flux.

   a) For several low-emittance shields ($\varepsilon < 0.05$) at small overall spacing ratios (L/D = 0.1), the effect of shield location may be important from the standpoint of the absolute value of the boil-off rate, since the boil-off rate is large. The minimum boil-off occurs at non-equal spacings, but the relative variations in boil-off resulting from variations in shield location are not large.

b) For several low-emittance shields and large overall spacings (L/D = 0.5), the heat flux can be made small, near-minimum boil-off rates result when the shields are equally spaced, and the effect of shield location is important on a relative basis.

Additional work would be required to investigate the effects of non-symmetrical shield arrangements and non-diffuse properties of "real" materials. Thus, it is difficult to conclude what the optimum arrangement of real shields might be. For the purpose of this work, equal spacings are used although it is realized that the location of the shields may have a significant effect on radiant heat transfer rates (a contributing factor to the overall mass penalty) for some shadow shield configurations.

4.3 Computer Analysis of Radiant Heat Transfer

4.3.1 Computer Program

Finite-difference techniques were used to formulate and analyze thermal models for shadow shield systems with radial distributions of radiosity and temperature and with surfaces that were assumed to have either diffuse or specular reflectance characteristics. Considerable labor is required in formulating models (computing interchange factors, setting up heat-balance equations, etc.) so that the temperature distributions can be solved numerically on a computer. For instance, a practical shadow shield system might be composed of lightweight, low thermal-conductance, shadow shields. In this case, the distribution of radiosity determines the temperature distributions; and there may be large radial temperature gradients. Therefore, the thermal model requires a large number of geometric subdivisions (annular sections) on the shields to accurately describe their temperature distributions. To set up a single problem, each shadow shield must be geometrically subdivided; the radiation interchange factors (including reflections) must be computed; and the heat-balance equations for each node must be written as input data to a computer program which solves for the temperature distributions by numerical techniques. The rate of heat transfer to the LH_2 tank is computed from the resultant shield temperature distributions and the radiation interchange factors. It is evident from these considerations that considerable labor is required to execute a detailed study, involving many parametric studies, to classify the thermal performance and obtain near-optimum configurations for practical shadow shield systems.

A computer program was developed to automate the thermal analysis calculations and allow the large number of required study cases to be analyzed efficiently.

The general thermal model of the shadow shield system for the parametric computer studies is shown schematically in Figure 14 with a description of the terms which make up the input data. A circular disc at 520R is used to simulate the payload, a disc at 37R to simulate the LH_2 tank; and there is an arbitrary number of intermediate shadow shields situated between the payload and LH_2 tank. This mathematical model is conservative in that it assumes that the last shield is at LH_2 temperature and that the heat absorbed by the 37R shield is transferred to the LH_2. Actually, in the final analysis of practical systems, there will be insulation for ground-hold and orbital thermal protection between this last shield and the LH_2 tank. When the shadow shield systems for final evaluation were designed on the basis of several parametric studies of shields and structure configurations, and the ground-hold and orbital insulation systems were defined from other considerations, the temperature distributions in all the shields (including the last shield) and the radiant heat leak to the LH_2 tank were computed accounting for the effects of the insulation system and thermal interactions with the support structure.

A simplified flow chart, shown in Figure 15, lists in sequence the basic operation of the computer program. The input data consists of the following:

1) A title card (for reference).

2) A data card indicating the number of spacings and the number of radial subdivisions on each shield.

3) A card with the emittance, which is assumed to be identical for all surfaces.

4) A card listing consecutively the spacings between shields (beginning with the shield near the simulated payload and ending with the spacing between the last intermediate shield and the simulated hydrogen tank).

5) A card listing the outer radii of the annular subdivisions (beginning with the outermost and ending with the innermost).

6) A control card with coded instructions for the subroutine which numerically solves the heat-balance equations.

Given the above input data, the computer:

1) Subdivides the shields and numerically codes the subdivisions consecutively, beginning with the outermost subdivision on the payload and ending with the innermost subdivision on the shield on the propellant tank.

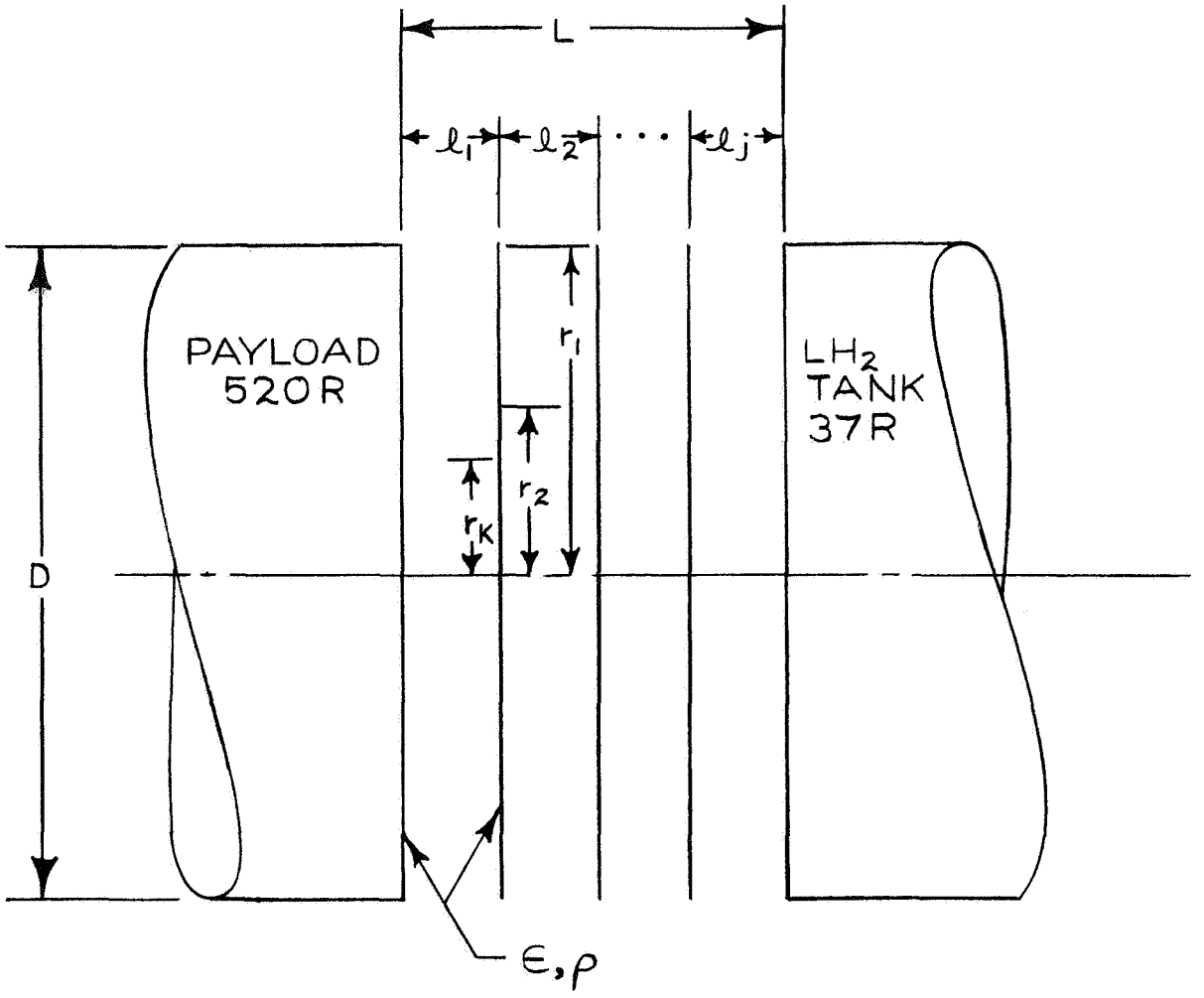

J = NO. OF SPACINGS (EQUALS n+1, WHERE n = NO. OF INTERMEDIATE SHADOW SHIELDS)

K = NO. OF ANNULAR SUBDIVISIONS OF EACH SHIELD

r_K = OUTERMOST RADIUS OF K^{th} ANNULAR SUBDIVISION

ϵ = EMITTANCE (DIFFUSE)

ρ = REFLECTANCE (SPECULAR OR DIFFUSE)

} SAME FOR ALL SURFACES

FIGURE 14 - MATHEMATICAL MODEL OF SHADOW SHIELDS FOR COMPUTER ANALYSIS

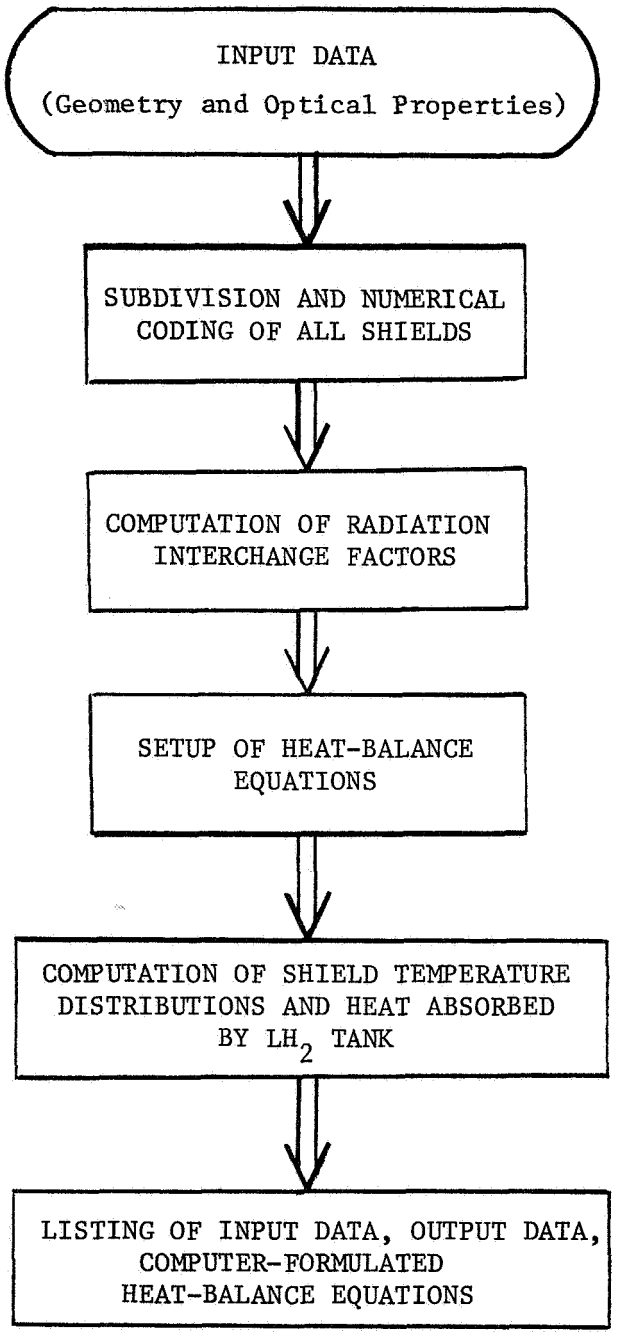

FIGURE 15 SIMPLIFIED FLOW CHART OF RADIANT HEAT TRANSFER COMPUTER PROGRAM

2) Computes the radiation interchange factors for a system of surfaces with a diffuse emittance and either a diffuse or specular reflectance (for the specularly reflecting surface, it was assumed that the reflectance was independent of angle).

3) Sets up the heat-balance equations in a data format compatible with a subroutine which numerically solves for the temperature distributions.

4) Computes the temperature distribution, radiant heat absorbed by the propellant tank, and the propellant boil-off due to radiation during a 10,000-hour mission.

5) Lists the input data, the temperature distributions in all shields, computed heat flow and boil-off, and the heat-balance equations.

A number of options are provided in the computer program to provide flexibility in calculating the thermal performance of shadow shield configurations. For example, there is the option of utilizing a data insertion and correction routine which automatically inserts data into the computer-formulated, heat-balance equations before the temperature distributions are computed. This option is useful for studying the effect of shield conductance, interactions between support structure and shields, heat leaks with ground-hold and orbital insulation on the LH_2 tank, etc. In accounting for shield conductance effects, input data describing the conductance couplings between annular zones (typically three data cards for each zone) are combined with the basic input data described above. After the heat-balance equations are formulated by the computer for non-conducting shields, the new card images describing the conductance couplings are automatically inserted in the appropriate locations to modify the heat-balance equations and the shield temperature distributions and heat flux to the LH_2 tank are computed.

A typical computer output data sheet in shown in Table I. For each problem, the input data, computed temperatures, and resultant heat leaks are listed, including the total number of radial subdivisions on each disc (K) and the outer radius of each subdivision (measured in feet). The computed temperatures are listed for the K subdivisions of the 520R disc (T_1 through T_K, inclusive), the intermediate shield (T_{K+1} through T_{2K}) and the 37R disc (T_{2K+1} through T_{3K}). For the intermediate shields, T_{K+1} is the outermost radial subdivision and T_{2K} the innermost.

The first two rows of data under the heading "temperatures" are associated with the computer program and do not relate

TABLE I TYPICAL COMPUTER OUTPUT DATA SHEET FOR RADIANT HEAT TRANSFER PROGRAM

ADL APPLIED THERMODYNAMICS GROUP
SHADOW SHIELD CONCEPTUAL DESIGN AND ANALYSIS

SPECULAR REFLECTION R19A NONUNI RAD ZERO COND 1SHD 9SUB L/D=.3

I N P U T D A T A

PAYLOAD TEMP.= 520R, PROPELLANT TANK TEMP.= 37R, EMITTANCE= .0300

SHIELD DIAM.= 10.0000FT., L/D= .3000, NUMBER OF SHIELDS= 1, NUMBER OF RADIAL SUBDIVISIONS= 9

SHIELD SPACING(S)= 1.500E+00 1.500E+00

RADII = 5.000E+00 4.713E+00 4.408E+00 4.081E+00 3.726E+00 3.332E+00 2.886E+00 2.356E+00

RADII = 1.666E+00

T E M P E R A T U R E S (DEG. R)

REL= 1.40 TOL= 9.0E-04 DT= 1.0 WF= 1 PF= 10 TIMX= 1.0 TB= 300.0 SIZE= 27 ALPHA= 1.00

TI = 1.00 EP = 5.01300000E+03 ES =-4.59448E-01 EIN = 0. NI= 0

1 520.00 2 520.00 3 520.00 4 520.00 5 520.00 6 520.00 7 520.00 8 520.00 9 520.00 10 199.07

11 203.57 12 207.76 13 211.42 14 214.52 15 217.22 16 219.50 17 221.61 18 223.48 19 37.00 20 37.00

21 37.00 22 37.00 23 37.00 24 37.00 25 37.00 26 37.00 27 37.00

R E S U L T S

THE NET HEAT LEAK TO THE HYDROGEN TANK IS 4.5976255E-01 BTU/HR.

THE BOIL OFF OF HYDROGEN FOR 10,000 HOURS IS 2.3638177E+01 LBM.

ELAPSED TIME IN TTA SOLUTION = 1.300SECONDS

to output data. For a general problem, the heat-balance equations alone would require the preparation of $4nK^2$ input data cards (n = number of shields, K = number of radial subdivisions) if the problem was formulated by hand--instead of about six when the heat-balance equations are prepared by computer. Thus, for the problem shown in Table I, with a single intermediate shield, the computer set up the equivalent of 900 data cards before the numerical solution of the shield temperatures. This problem required approximately 60 seconds of computer time (CDC 6400) to read in the data, solve for the interchange factors and set up the heat-balance equations; about 1.3 seconds was required to solve the heat-balance equations. This computer time increases if the number of shields or the number of radial subdivisions increases, or if the shields have a finite conductance.

In summary, the computer program developed for the shadow shield analysis has the capability of studying a wide range of cases efficiently and minimizes time-consuming manual operations associated with setting up the heat-balance equations.

4.3.2 Distribution of Radiosity

The analytical techniques described previously in Section 4.2 were used to evaluate the radiant heat transfer to cold sink for a thermal model consisting of diffusely emitting and reflecting shields with a uniform distribution of radiosity and with a uniform temperature distribution (infinite-conductance). This simplified model (used to obtain the data in Figures 10 to 13) is convenient for preliminary studies because solutions can be obtained by hand calculations.

Generally, the distribution of radiosity along the radius of a shadow shield will be non-uniform, even when an infinite thermal conductance is assumed. Moreover, the conductance of a shield material will actually be finite and possibly quite small. Therefore, a more realistic thermal model is required.

For illustration, the heat fluxes computed using uniform radiosity, infinite conductance and non-uniform radiosity, zero conductance thermal models are presented in Table II for a typical example. From the comparison, it is obvious that the simplified model cannot be used for accurate predictions of heat flux for non-conducting diffusely reflecting shields and that in the analysis of practical shadow shield systems (lightweight, low radial conductance shields), any detailed analysis should allow for non-uniform radiosity distributions where the L/D is small, but finite. At large spacing ratios, the radiosity becomes uniform radially and the conductance of the shield does not affect the accuracy of the heat flow calculation.

TABLE II

COMPARISON OF THERMAL MODELS OF RADIANT HEAT TRANSFER IN SHADOW SHIELD SYSTEMS

HEAT FLUX ABSORBED BY 37R SINK FROM A 520R PAYLOAD ($BTU/HR\ FT^2$)

L/D	UNIFORM RADIOSITY INFINITE CONDUCTANCE	NON-UNIFORM RADIOSITY ZERO CONDUCTANCE	% DIFFERENCE
0.10	5.1×10^{-3}	2.6×10^{-2}	+409
0.25	4.2×10^{-4}	1.4×10^{-3}	+221
0.50	-2.0×10^{-5}	3.0×10^{-5}	+250
1.00	-9.0×10^{-5}	-9.0×10^{-5}	0

Two equally spaced shields.
$\varepsilon = 0.03$ for all surfaces including LH_2 tank and payload.
Diffuse reflection characteristics.

4.3.3 Shield Thermal Conductance

The thermal conductance of a shield is dependent upon its material (thermal conductivity) and its thickness. For lightweight, low thermal conductance shadow shields, the distribution of radiosity is the principal driving force for determining the temperature distribution in the shields. There can be large radial temperature gradients across the shield because the annuli located near the center of the shield are more strongly coupled to the neighboring shields than the annuli at the extremities of the shield. For given surface properties, the temperature gradients are a function of the payload-tank spacing and the number of shields. Since the radiosity distribution becomes smoothed on the lower-temperature shields near the LH_2 tank, the temperature gradients are largest for the shield near the warm payload and are smallest on the shield near the LH_2 tank. Highly conductive shields can further smooth radial temperature gradients, reduce the incident radiosity on the LH_2 tank and, consequently, reduce the propellant boil-off. On the other hand, to be of benefit, the reduction in heat flow must exceed the mass penalty associated with the high-conductance shield material, especially in a multi-shield system.

A comparison of the performance of a typical shadow shield configuration with a low-conductance, lightweight shield material and a higher-conductance, higher-weight material is presented in Table III. The system consists of two equally spaced shields with a diffuse emittance of 0.03 and a diffuse reflectance of 0.97. The L/D was taken to be 0.25.

The aluminized, polyester shields consist of a nylon fabric reinforcement laminated between two layers of 1/2-mil polyester film. The outermost surfaces of the film are coated with vacuum-deposited aluminum (or gold) to have an emittance of 0.03 at room temperature.

The comparison reveals the following results:

1) The difference in heat leak obtained considering non-conducting shields and shields composed of aluminized polyester film with a nylon fabric reinforcement is quite small. (The heat flow with non-conducting shields is about 2% higher.)

2) The use of high-conductance shields, compared to the polyester shields, introduces a mass penalty significantly larger than the reduction in LH_2 boil-off. In fact, the mass of the shield material, alone, exceeds the combined mass of the boil-off and shield material for the low-conductance system.

TABLE III

EFFECT OF SHIELD THERMAL CONDUCTANCE

ON RADIANT HEAT LEAK AND SYSTEM MASS

Payload temp.: 520R
LH_2 tank temp.: 37R

		Non-Conducting Shields	Aluminized Polyester with Nylon Fabric Reinforcement	10-mil Aluminum
Kδ	$\frac{BTU}{HR\ °R}$	0	2.9×10^{-5}	8.3×10^{-2}
1) Radial ΔT				
1st Intermediate Shield	°R	75.2	73.0	7.5
2nd Intermediate Shield	°R	45.7	40.4	0.5
2) Radiant Heat Flow Absorbed by Hydrogen Tank	$\frac{BTU}{HR}$	0.10616	0.10552	0.08201
3) Hydrogen Boil-off during 10,000-hour Mission	LBS.	5.5	5.4	4.2
4) Shadow Shield Mass (less supports)	LBS.	-	3.4	21.7
System Mass: (3) + (4) (less supports)	LBS.	5.5	8.8	25.9

3) Shield materials with intermediate masses and conductances do not appear promising, because in a system with low heat leak, even a material with a high conductance reduces the long-term boil-off by less than two pounds.

Since studies made by use of the computer analysis demonstrated that the LH_2 boil-off radiant heat leaks in typical shield configurations (low L/D, small number of shields) with low-conductance shields can be made a relatively small fraction of the total system mass, the non-conducting shields' assumption was used in preliminary trade-off studies.

It will also be shown in a following section that the temperature distributions in shields with specularly reflecting surfaces are more uniform than when the surfaces are considered to reflect diffusely. Therefore, conductance effects are less significant when the shields are assumed to have a specular reflectance characteristic.

4.3.4 Number of Radial Subdivisions Required

The accuracy of finite-difference techniques in thermal problems involving radiation transfer is related to the size of the geometrical subdivisions of the object being analyzed. A procedure for insuring that the number of subdivisions is sufficiently large to accurately predict temperature distributions is to successively increase the number of subdivisions until a further increase does not affect the temperature predictions within engineering accuracy. Detailed studies of the radial temperature distributions in shadow shields showed that the temperature gradients are largest at the outer radius.

In analyzing the radiant transfer in shadow shields, the circular shields were subdivided into annular zones of equal area. Since the linear dimension across each zone decreased as a function of distance from the center, the smallest zones were located in the region of the largest temperature gradients, thereby improving the accuracy of the calculation.

A number of computer runs were made during the preliminary analysis to determine the number of subdivisions required to accurately describe the temperature distributions and obtain accurate predictions of radiant heat leak and LH_2 boil-off. Some of the results are illustrated in Figure 16, which shows the computed radiant heat transfer to the LH_2 tank plotted as a function of the reciprocal of the number of subdivisions. It was desired to determine the number of subdivisions which would allow accurate thermal predictions and, at the same time, not be so large as to exceed computer-storage capacity or require large amounts of computer time to set up and solve the heat-balance equations. These studies showed that for spacing ratios as low

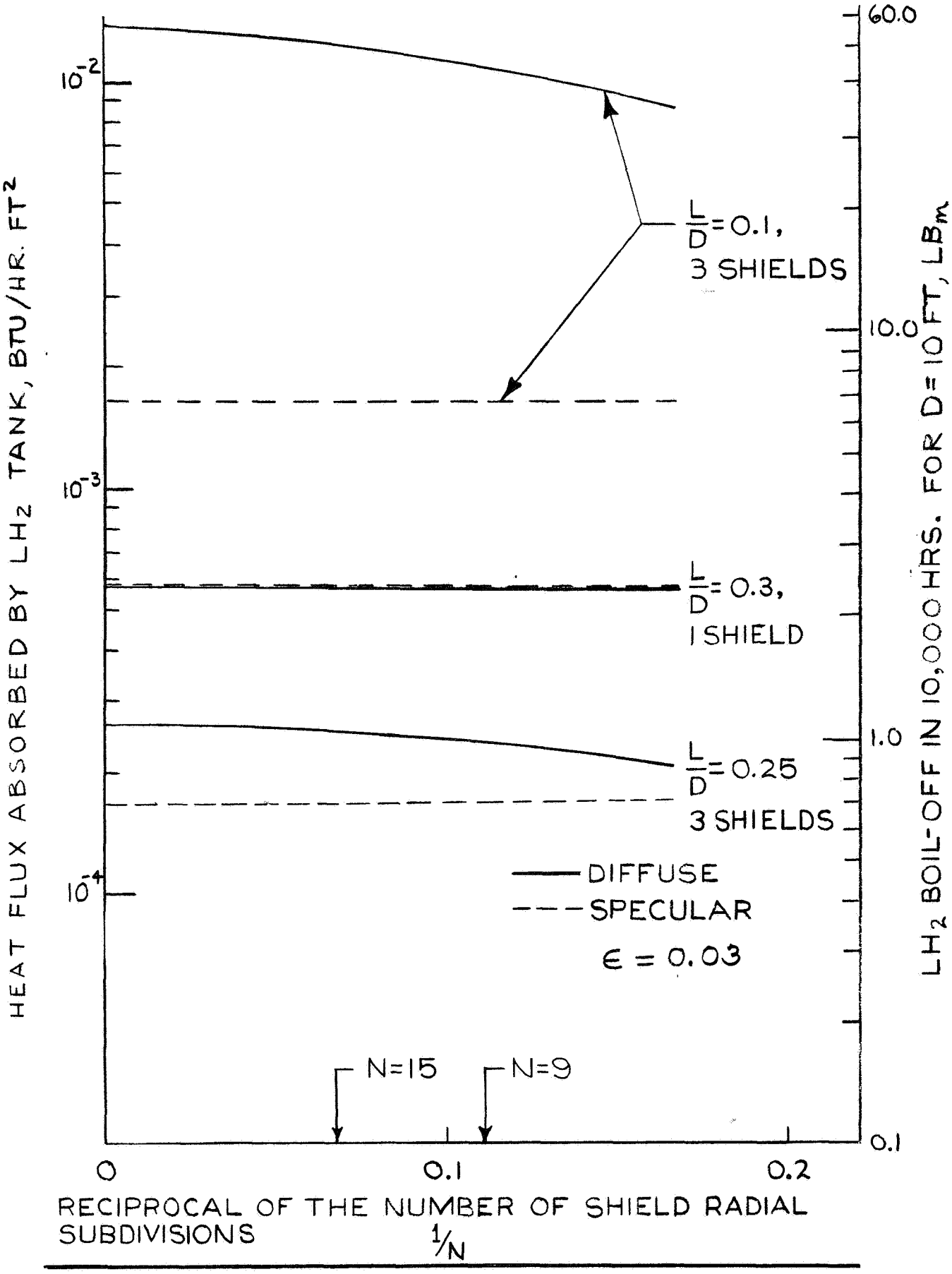

FIGURE 16 - EFFECT OF NUMBER OF RADIAL SUB-DIVISIONS ON LH_2 BOIL-OFF

as 0.25 and as many as 3 equally spaced, diffusely reflecting shields, 15 radial subdivisions were sufficient to compute heat fluxes within engineering accuracy. When the shield surfaces were assumed to have specular reflectances, the computed heat leak was not sensitive to the number of subdivisions. Therefore, shields were subdivided into 9 equal areas for calculations in which the surfaces were assumed to reflect specularly.

4.3.5 Reflection Characteristics, Number of Shields, and Spacing Ratio

The radiant heat transfer computer program was set up to analyze shadow shields that emit diffusely and reflect diffusely or specularly. A surface that reflects diffusely is characterized by having the intensity of reflected radiation from an incident ray uniformly distributed in all directions. With a surface having isotropic, specular-reflection characteristics, the reflected ray leaves the surface in the same plane as the incident ray at an angle equal to the angle of incidence. The further assumption was made that the reflectance was independent of angle of incidence.*

Figure 17 illustrates the effects of the reflection characteristics on the radial temperature distribution in a single, non-conducting shield centrally located between the payload and the LH_2 tank. All surfaces were assumed to have a total hemispherical emittance of 0.03. For the spacing ratios considered, the following observations can be made:

1) The temperature distribution is more uniform in shields having a specular reflectance; diffusely reflecting shields have larger temperature gradients at the edges.

2) For $L/D \leq 0.25$, the mean temperature of the diffusely reflecting shield exceeds that of the specular shield. The opposite is true at $L/D = 0.5$.

---

* An ADL company-funded effort is currently being undertaken to set up a computer program to account for the variation of reflectance with angle. This work was not completed in time for including the results in this Interim Report. This program uses the Monte Carlo technique for computing radiant interchange factors with surfaces having arbitrary reflection characteristics.

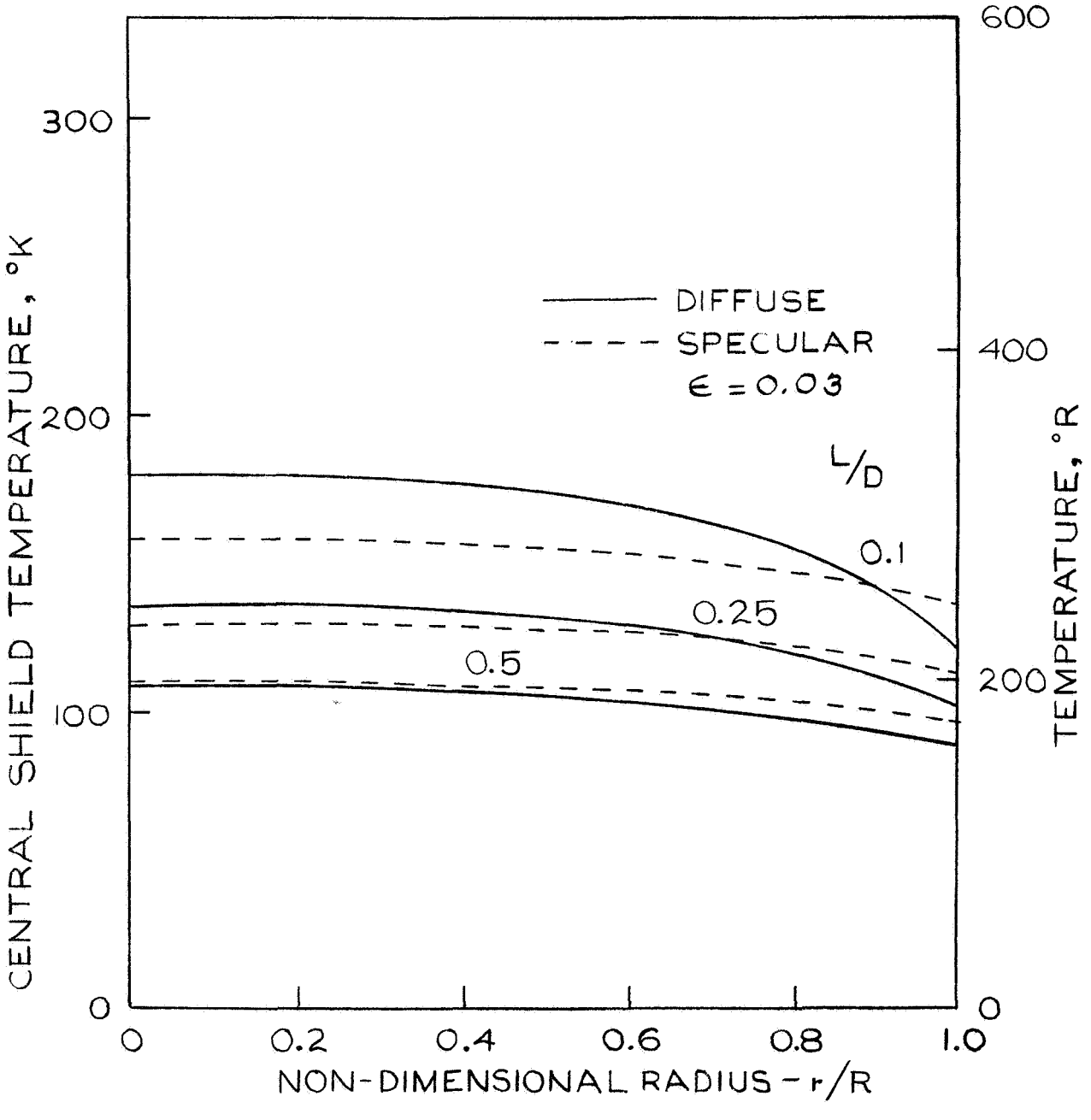

FIGURE 17- RADIAL TEMPERATURE DISTRIBUTIONS FOR DIFFUSELY AND SPECULARLY REFLECTING SHIELDS

Figure 18 shows generalized plots of the heat flux absorbed by the LH_2 tank as a function of spacing ratio, the reflection characteristics and number of equally spaced intermediate shields for a 520R payload temperature and a 37R LH_2 tank temperature. The total hemispherical emittance is 0.03 for all surfaces including the tank and payload. The shields are taken to be non-conducting.

With regard to the reflection characteristics, the results show that for "closed" systems (spacings between shields less than 0.1 or 0.2 diameters) the assumption of a diffuse reflectance is conservative (i.e., a higher heat flux is predicted than for specular reflectance characteristics). The opposite is true for open systems, when the spacing between shields is greater than 0.2 diameters. When the spacing between shields is approximately 0.15 diameters, the assumption of specular or diffuse-reflection characteristics does not influence the absorbed heat flux calculation.

A similar effect was noted by Viskanta et al (1967) in a study of radiant heat exchange between two parallel rectangular surfaces. In this work, the radiant interchange factors between two surfaces of equal emittance were calculated by Monte Carlo techniques for a number of mathematical models relating to the surface reflectance characteristics. The reflectance models which were studied include directionally independent reflectance properties and directionally dependent properties. The results show that for low-emittance surfaces with spacing ratios comparable to those used in this work the assumption of either directionally independent diffuse or specular-reflection characteristics provides an upper bound on the radiant transfer between a source and sink when the radiosity distribution is non-uniform. In our computer calculations, the heat leak was calculated for both directionally independent specular and diffuse-reflectance characteristics; and the mass estimates of LH_2 boil-off were made on the basis of the highest calculated value.

The results of Viskanta's calculations for the radiant interchange between two parallel surfaces having a length-to-width ratio (L/N) = 0.5, total hemispherical emittances of 0.1, and various spacing ratios (H/W), where H is the distance between the source and sink at temperatures T_1 and T_2, will serve to illustrate the effects of various reflectance models. A table giving the overall absorption factors (script F_{12}) which are proportional to the heat flux absorbed by the sink is presented below for five different models. The models are:

D^*CP - Diffuse, constant (directionally independent) properties, uniform radiosity.

DCP - Diffuse, constant properties, non-uniform radiosity.

SCP - Diffuse emission, constant property specular reflection non-uniform radiosity.

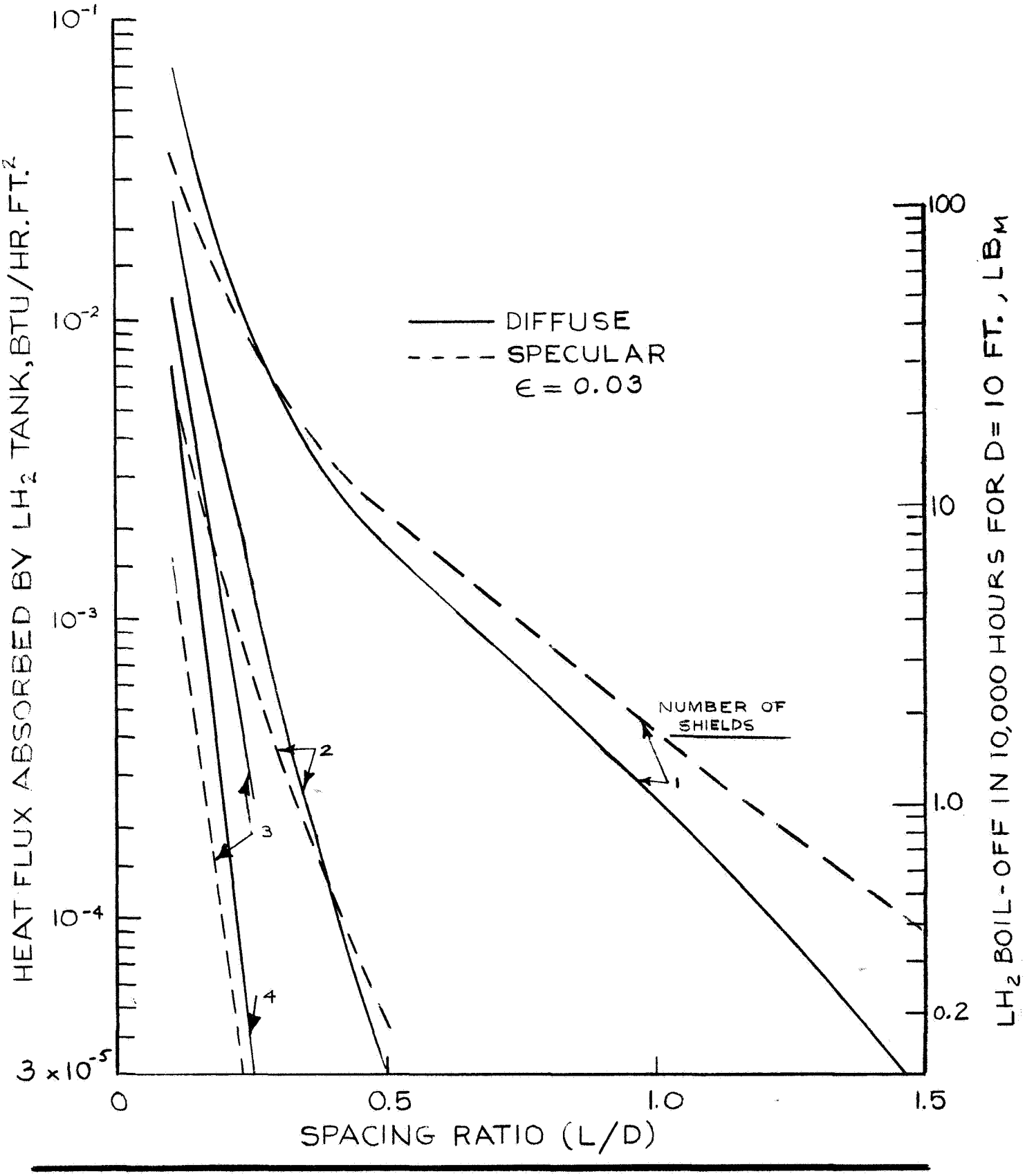

FIGURE 18 - EFFECT OF SPACING RATIO AND NUMBER OF EQUALLY SPACED SHIELDS ON RADIANT HEAT FLOW

SDP - Directional emission, specular reflection with directional properties given by Fresnel's equations.

BP - Directional emission and bidirectional reflection.

Overall Absorption Factors (Script F_{12}) for Heat Flow to a Sink at T_2 from a Source at T_1 ($\varepsilon = 0.1$, $L/W = 0.5$)

Spacing Ratio (H/W)	Reflectance Model				
	D^*CP	DCP	SCP	SDP	BP
0.5	0.031	0.031	0.037 (max.)	0.024	0.021
0.25	0.064	0.069	0.075 (max.)	0.056	0.046
0.05	0.220	0.258 (max.)	0.238	0.206	0.174
0.025	0.310	0.363 (max.)	0.326	0.300	0.264

From this tabulation it can be seen that either the diffuse or specular constant property models - such as used in the computer program described in this report - give the maximum heat flux to the heat sink. At small spacing ratios, the diffuse model is conservative; and at large spacing ratios, the specular model is conservative. This observation is in agreement with the data presented in Figure 18 for the specular and diffuse constant property models of equal-diameter circular surfaces.

It is significant to note that Viskanta's results indicate that the constant property (directionally independent) models are not conservative when the surface emittances are above 0.50. In practical shadow shield systems, it is anticipated that surface emittances will always be an order of magnitude less than 0.5. Therefore, we conclude that the computer model used in this study will give conservative estimates of the heat flux to the LH_2 tank. Furthermore, the uncertainties in the shield emittance will provide uncertainties in the calculated heat fluxes larger than those associated with the detailed characteristics of the surface reflectance properties.

The computed results presented in Figure 18 also show that the radiant heat leak to the LH_2 tank with a low-emittance shield system is strongly dependent upon the number of shadow shields and the payload-tank spacing. For one shield, changing the spacing

ratio from 0.25 to 0.50 reduces the heat leak by a factor of 5. For a system with a spacing ratio of 0.25 and one intermediate shield, each additional shadow shield reduces the heat leak by an order of magnitude.

Although this preliminary analysis is somewhat conservative because it assumes an uninsulated LH_2 tank is exposed to the shadow shield system, it is interesting to note that the following shadow shield configurations would limit the LH_2 boil-off due to radiation from the payload to 10 lbs. (an equivalent heat flux of 2.5 x 10^{-3} Btu/HR FT^2) during a coast mission of 10,000 hours:

Spacing Ratio L/D	Number of Non-Conducting Shadow Shields (ϵ = 0.03)
0.15	3
0.20	2
0.50	1

The information contained in Figure 18 characterizes shadow shield systems for a wide range of conditions that could exist in shadow shield systems with fixed or space-erected structures. In a later section of this report, these characteristics will be used to optimize the shield systems from a minimum-mass standpoint considering the trade-offs between shield mass and LH_2 boil-off.

4.3.6 Surface Emittance

The results of a simplified analysis have shown that the total hemispherical emittance of the shadow shields will be an important variable in minimizing the heat flux to the LH_2 tank. Considerable work has been done in minimizing the emittance of thin (1/4-mil) polyester films metallized by vacuum-deposition techniques. To achieve low-emittance surfaces, it is necessary to vacuum deposit highly conductive metals of high purity, at low pressures, with fast deposition rates, on a clean film. Importantly, the metal coating must be sufficiently thick to provide a low emittance.

Ruccia, et al (1966) presented results of measurements of the total hemispherical emittance of various aluminum, gold, silver and copper coatings on 1/4-mil polyester film. The effects of environmental conditions (relative humidity, salt air and CO_2) on the emittance were also studied. The results of this work showed that aluminized polyester films with emittances of 0.022 and gold films with emittances of 0.017 are available commercially. Such surfaces, particularly gold coatings, do not appear to be degraded appreciably by exposure to humidity, salt air and CO_2 environments. In the present application, it is expected that any shadow shield system associated

with a scientific payload and LH_2 tank enclosed in an interstage shroud will not be subjected to environments as damaging as the environments described previously.

However, in order to allow for degradation of the surface emittance, all of the calculations of radiant heat transfer have been based on a minimum value of the emittance of 0.03 which would provide for approximately a 50% increase in emittance.

Figure 19 illustrates the effect of shield emittance on radiant heat flux to an LH_2 tank for a shield system comprising two non-conducting, equally spaced shadow shields. A shield at 520R located at the payload and a shield at 37R at the LH_2 were also assumed to have the same emittance as the two central shields.

From Figure 19 it may be seen that the heat flux is a strong function of the assumed value of the emittance. A 50% degradation (increase) in emittance will increase the heat flux to the LH_2 tank by a factor of about 4 for low-emittance surfaces.

In these calculations it was assumed that the emittance was independent of temperature, and the analyses were based on emittances' values greater than 0.03 which would apply to room-temperature measurements of degraded coated films. The shields' temperatures in shadow shield systems fall well below room temperature. Both theoretical considerations and measurements indicate that a decrease in temperature reduces the emittance. Therefore, calculations made with the emittance independent of temperature and equal to room-temperature values will be conservative with respect to the boil-off of LH_2.

5.0 STRUCTURAL ANALYSIS

5.1 General

There were two separate analyses made for fixed and space-erected structures since the former must transmit the thrust loads of the lower stages and the inertia loads of the LH_2 tank to the payload, while the latter is subjected to maneuvering loads in space when the structure is deployed. The structural analyses were based upon the following launch load information as defined by contract:

1) Launch loads

(a)	Longitudinal:	+ 5.7g maximum
(b)	Lateral:	0.3g maximum occurs when longitudinal acceleration is 2.5g
(c)	Vibration:	6g vibratory longitudinal load between 20 and 150 cps. This can occur when longitudinal load is 2.5g or less.

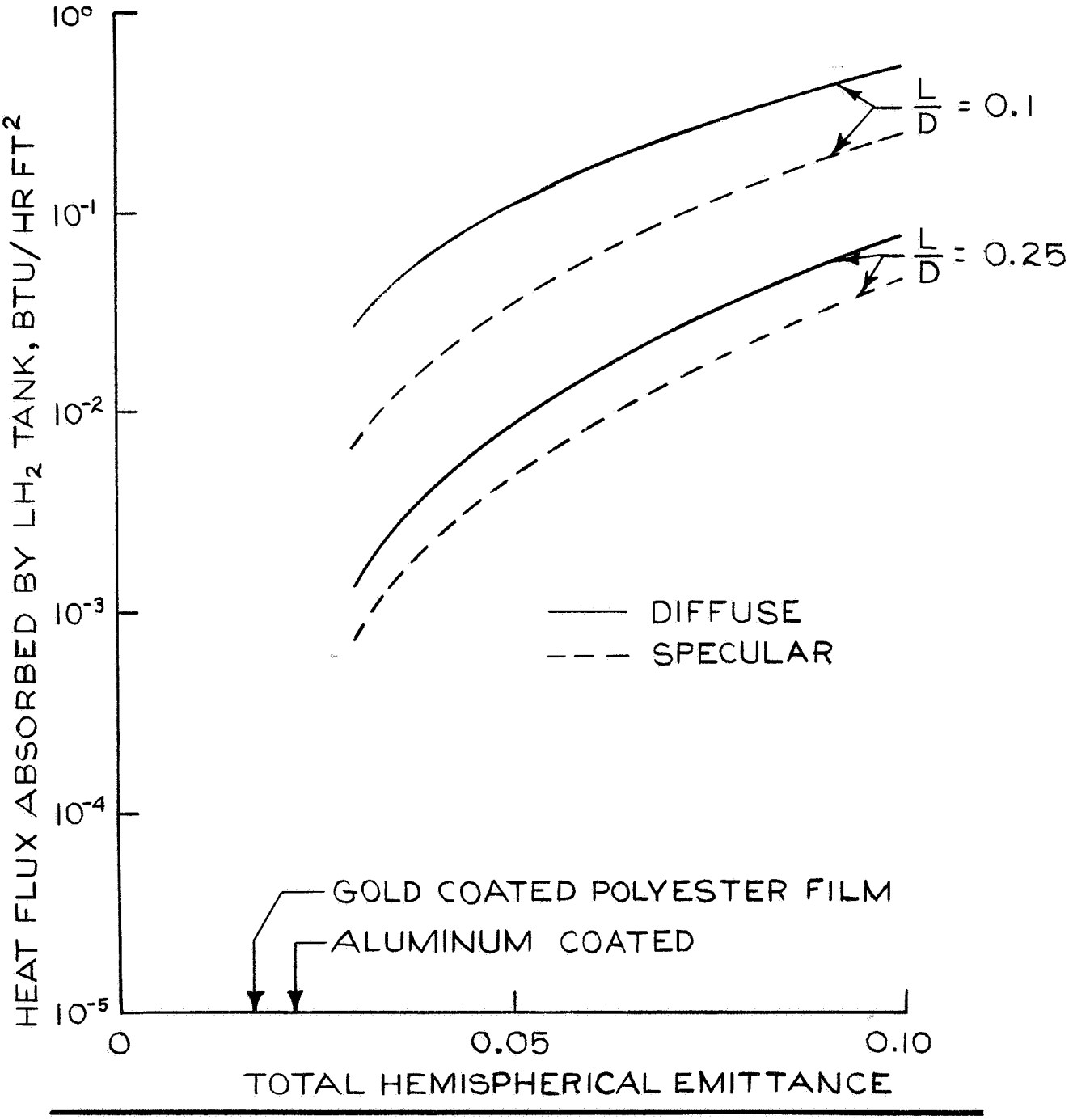

FIGURE 19 - EFFECT OF SURFACE EMITTANCE ON RADIANT HEAT FLUX

2) Loads during space maneuvering (lateral): 10^{-3}g.

5.2 Design of Fixed Structures

Following a preliminary study, the configuration chosen for the fixed structural system consisted of a simple Warren-truss framework arranged in a cylindrical fashion to forward and aft-ring girders. This open configuration allows the shadow shields to radiate effectively from the thermal standpoint, while providing an efficient structure, and it has the additional feature that all of the connecting truss members are of equal length. This characteristic is important because no differential thermal strains will be introduced at the truss joints as the entire structural system is cooled to the space thermal environment.

With the major loadings on the truss being compressive, buckling criteria are of particular importance in the design. Consequently, a tubular cross section was chosen for the strut members to maximize the stiffness-to-mass ratio.

With the general configuration and cross-sectional geometry chosen, the remaining design parameters include the support material, payload mass, number and length of the supports, and the tube wall thickness. The overall diameter of the truss was taken equal to the maximum allowed value of 120 inches as limited by the shroud structure.

In the following sections, the pertinent design equations are discussed; and the manner in which the optimization of the design was programmed is described.

5.2.1 Structural Load Criteria

As a result of communications between the contractor and technical personnel of NASA-Lewis Research Center (c.f. Shaker (1967)), the following ground rules were established to define the design loads for fixed structures.

1) The input launch loadings specified in the Scope of Work, Exhibit A, of the subject contract were not to be applied to the kick-stage structure as input loadings, but rather were the loads on the various components resulting from the launch. These specified loadings, therefore, would be utilized as inputs in the design of smaller components incorporated or attached to the principal massive elements. Electronic packages or control assemblies attached to the payload, for example, would be designed on the basis of the specified loads.

2) The structural loads for the design of the kick-stage structure are based on the analyses presented by Staley and Leondis (1967). This report, prepared for NASA LeRC, considered the static and dynamic loadings on each of the important mass components of the kick stage for each of the transient loading conditions during the mission. The inertial loadings were tabulated in terms of design limit accelerations, for each of the loading conditions for two truss configurations and two payload masses.

3) Of more importance was the calculation of the maximum loads imposed on the truss itself by the mass components. These components were determined by Staley (1967) on the basis of assumptions relating the phasing of the inertial loads of the various masses. These truss loads depend upon the payload mass and also upon the particular location of the truss point at which the loads are calculated. A typical configuration of a kick-stage assembly taken from this reference is shown in Figure 20. The loadings were taken at the aft truss ring, between the LOX and LH_2 masses, assuming that this was the location of the connection of the kick stage with the nose fairing.

4) Maximum truss loadings were calculated using the load factors given by Staley (1967) for the particular set of payload masses used in this study. These calculated loads were used in designing the shadow shield structures.

The kick-stage assembly masses were divided into the following items by Staley (1967).

1.	Payload	- 3000 lb and 300 lb
2.	Payload ring and equipment	- 436 lb
3.	Forward ring and equipment	- 174 lb
4.	LH_2 and structure	- 1390 lb
5.	Aft ring and support beams	- 290 lb
6.	LOX and structure	- 6130 lb
7.	Engine and structure	- 380 lb

The total mass of the assembly was assumed to be 8800 lb_m plus the payload. The connection to the nose fairing was assumed to be the aft ring. Thus, the payload LH_2 tank, and intermediate structure would be loading the truss at that connection during acceleration phases

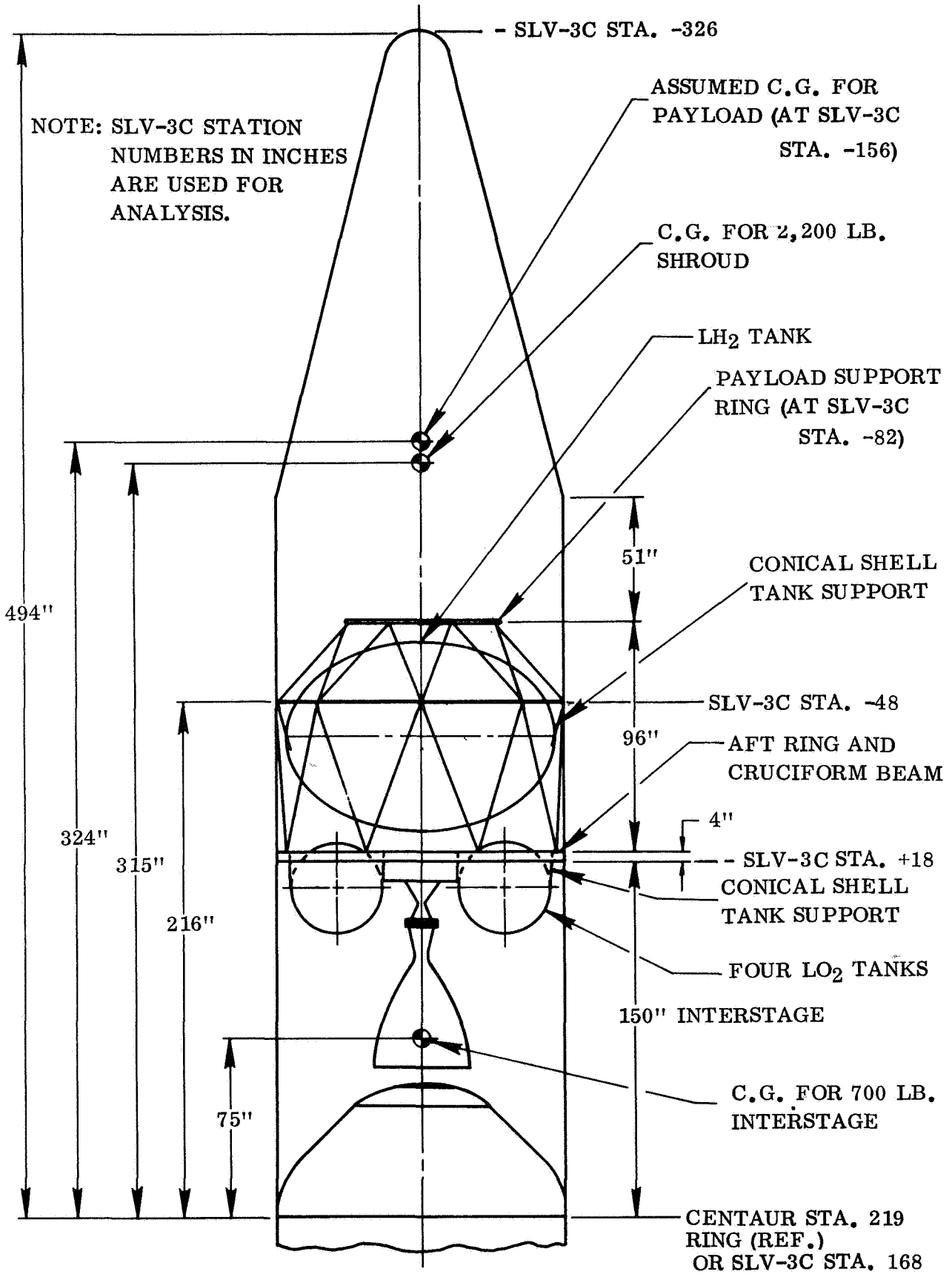

Figure 20 Cryogenic Kick Stage Configuration for Use With Centaur (From Staley and Leondis (1967))

of the mission. Dynamic models for longitudinal and lateral motions were defined by Staley (1967) for the entire missile, so that the maximum acceleration in both the longitudinal and lateral directions could be calculated for each of the missile conditions. These values together with the geometric and elastic properties of the various elements of the system were then used to establish the truss loads in terms of axial loadings, shear loadings, and bending moments.

Following this procedure for the set of payload masses used in this study we assumed:

1) The structural masses are similar to those given by Staley (1967).

2) The geometric and elastic properties of the structures are similar so that bending moments, shears, and axial loads are proportional to those presented by Staley (1967).

3) The attenuation of the environmental inputs was assumed to be inversely proportional to the square root of the mass.

4) For the fixed structure connecting the payload and the conical shell tank support, the loads were assumed to be the same as those applied to the lower truss extending from the conical shell tank support to the aft ring. (This is a conservative assumption since this condition would only develop if the payload and LH_2 tank were inertially out of phase during either the launch or maximum booster acceleration conditions.)

This procedure resulted in the truss loads tabulated below for the most critical loading conditions.

TRUSS LOADS FOR FIXED SHADOW SHIELD STRUCTURES

Condition	Payload Mass	Truss Loads (Lbs.) Axial	Shear	Bending Moment (in-lbs)
Launch	1,500	7,530	4,420	630,000
	2,500	9,270	5,430	770,000
	4,000	12,420	7,300	1,040,000
Maximum Booster Acceleration	1,500	21,490	1,370	113,000
	2,500	27,470	1,740	145,000
	4,000	36,360	2,310	192,000

In each of these cases, the total load includes a static component and an RMS summation of the random components.

The total axial load on any given support member of a truss depends on the number of supports and the spacing of the forward and aft rings. In any case, the maximum axial loading will be due to the tabulated axial load and the bending moment in accordance with the relation,

$$F_{max} = \frac{L}{n} + \frac{A}{n}\left(\frac{Mr}{I}\right)$$

where F_{max} = max. strut load

L = total axial load

n = number of struts

M = bending moment

r = radius of truss

I = effective cross-sectional moment of inertia of truss

A = total cross-sectional area of struts

For $n = 12$, $I = 0.58\ Ar^2$

For $n = 16$, $I =$ (minimum $\doteq 0.6\ Ar^2$

For $n = 24$, $I =$ (minimum $\doteq 0.62\ Ar^2$

For $n = \infty$, $I = 0.5\ Ar^2$

The value of I for a given radius and total cross-sectional area is insensitive to the number of struts. The maximum strut load is therefore given by,

$$F_{max} \doteq \frac{1}{n}\left[L + \frac{M}{0.6r}\right]$$

and for r = 60 inches,

$$nF_{max} \doteq L + 0.028M$$

The total effective axial loading due to the axial load and the bending moment is tabulated below.

EFFECTIVE AXIAL LOADS FOR A SUPPORT

CONDITION	PAYLOAD MASS (lb_m)	LOAD (lb)
Launch	1,500	25,100
	2,500	31,000
	4,000	41,700
Max. Booster Accel.	1,500	24,700
	2,500	31,600
	4,000	41,800

The loading on the individual struts of the truss will be produced by the effective axial load and by the shear load. For a strut inclined at an angle θ with the axial direction, the strut loading due to the effective axial load is given by

$$F_{sa} = F_{max}/\cos\theta$$

and the strut loading due to shear loads is

$$F_{ss} = S_e/\sin\theta$$

where S_e is the effective shear load on a single truss. Since the individual members of the truss are not equally effective in resisting the shear load, the value of S_e is not the total shear load divided by n. For a planar Warren truss, for example, shear loads would produce tensile forces in half of the members and compressive forces in the remaining half. For a circular truss arrangement, it has been qualitatively estimated that the equivalent of about one-half of the compressively loaded members are fully loaded. It has been assumed, consequently, that the shear loading can be distributed among one-fourth of the truss members.

On this assumption, the total strut load is given by

$$F_t = F_{max}/\cos\theta + S_e/\sin\theta$$

$$= \frac{1}{n}\left[(L + 0.028M)/\cos\theta + 4S/\sin\theta\right]$$

where S is the total shear load.

The truss members were designed on the basis of the maximum strut loads, in accordance with conventional structural design techniques for stress, stability, and local buckling.

5.2.2 Design Analysis

The individual truss members must be designed to withstand the stress limitations due to the axial compression forces, and the stability limitations imposed by local (symmetric) buckling and by column (unsymmetric) buckling action. The axial stress is limited by the requirement that

$$\frac{F_t}{A/n} \leq \sigma_a$$

where σ_a is the maximum allowable value of stress for the specific material. F_t, A, and n are as defined in Section 5.2.1. A factor of safety of 1.4 on ultimate strength or 1.2 on yield strength, whichever resulted in the lower value, was used to determine the value of σ_a.

The column buckling criterion is governed by relations originally formulated by Euler in terms of critical loads. In terms of critical stress for a thin-walled tube, the resultant equation is

$$\sigma_{c.b.} = K_c \frac{\pi^2 E}{8} \left(\frac{d^2}{\ell^2}\right) = K_c \frac{\pi^2 E}{8} \cos^2\theta \left(\frac{d^2}{L^2}\right)$$

where L = axial length of truss

ℓ = length of truss member = $L/\cos\theta$

θ = angle between truss member and axial direction

K_c = constant dependent upon end conditions of column

E = modulus of elasticity of material

Since, in all cases, the maximum stress is not allowed to exceed the yield strength of the material (allowable stress cannot exceed yield strength/1.2), the value of the modulus of elasticity may be taken as the elastic (i.e., initial) value. The value of the constant K_c is equal to one for a column member having hinged or round ends and is equal to four for a column with fixed or built-in ends. Clearly, the case of truss members falls between these end conditions, since a considerable amount of restraint against rotation is provided by the socket supports attaching the truss struts to the ring members. For purposes of this study, a value of $K_c = 2$ was chosen as a reasonable estimate of the influence of the strut end supports. Accordingly, the resulting column buckling stress relation became

$$\sigma_{c.b.} = \frac{\pi^2 E}{4} \cos^2\theta \frac{d^2}{L^2}$$

For local buckling of unstiffened cylindrical tubes, the classical small deflection theories lead to the relation

$$\sigma_{\ell.b.} = K E \frac{t}{d}$$

where $\sigma_{\ell.b.}$ = critical buckling stress

t = tube wall thickness

d = tube diameter

and

$$K = \frac{2}{\sqrt{3(1-\mu^2)}}$$

where μ = Poisson's ratio

The value of E is, again, taken as the initial (elastic) value.

For most materials, $\mu = 0.3$, given $K = 1.2$. Extensive series of experiments on thin-walled cylinders have shown that the

experimental value obtained for the constant K is generally lower than the theoretical value of 1.2, and also that it decreases with increasing values of d/t. Much of this is due to fabrication imperfections and loading dissymmetries. For the range of tube geometries to be investigated in this study, a value of 0.6 for the buckling stress coefficient K appeared reasonable. The local buckling stress criterion for the strut members was defined, therefore, as

$$\sigma_{\ell.b.} = 0.6E \frac{t}{d}$$

For a truss system design, therefore, the maximum stress in the tubular struts will be defined by the smaller of the three stress criteria developed for axial compression, local buckling, and column buckling. To illustrate the procedure for designing the supports of fixed structures, the solution to an example problem is described below.

5.2.3 Illustrative Example

5.2.3.1 Statement of Problem

For a titanium fixed structure of the following configuration, determine the governing stress criterion and compute the wall thickness and mass of the supports. The overall diameter of the truss, D, is 120 in.; the axial length, L, is 60 in.; and there are 12 supports, each 3 in. in diameter. For this problem, ρ = 0.16 lb_m/in^3, E = 16 x 10^6 psi, and σ_a = 93,000 psi (based on σ_{ult} = 130,000 psi and a safety factor of 1.4).

5.2.3.2 Solution

The first step in determining the minimum stress or the governing stress criterion is the calculation of the allowable stress in column buckling from the following expression:

$$\sigma_{cb} = \frac{\pi^2 E \cos^2\theta}{4} \frac{d^2}{L^2}$$

where $\theta = \text{Arctan} \frac{\pi D}{nL} = 27.7°$

thus $\sigma_{cb} = 77{,}000$ psi

Since $\sigma_a > \sigma_{cb}$, at this stage of the solution $\sigma_{cb} = \sigma_{min}$ and column buckling governs the truss design. The total cross-sectional area of all the supports, A, and the wall thickness of each support, t, can be computed as follows:

$$A = \frac{n F_t}{\sigma_{min}} = 1.43 \text{ in}^2$$

where $$n F_t = \left[\frac{F_{max}}{\cos\theta} + \frac{4 S}{\sin\theta}\right]$$

$$= \frac{41,700}{0.885} + \frac{4(7300)}{0.465} = 110,000 \text{ psi}$$

and $$t^* = \frac{A}{n\pi d} = 0.0126 \text{ in}$$

Using the above value for thickness, the allowable stress to resist local buckling can be computed as follows:

$$\sigma_{\ell b} = 0.6 E \frac{t}{d} = 40,500 \text{ psi}$$

If $\sigma_{\ell b}$ was greater than σ_{min}, A and t computed above would specify the design; and column buckling would be the governing stress criterion. However, since $\sigma_{cb} > \sigma_{\ell b}$, the local buckling criterion governs the design of the supports in this sample case.

The wall thickness required to satisfy the governing local buckling criterion can be determined from the following equation (which can be derived from the simultaneous solution of $A = n F_t/\sigma_{\ell b}$, $t = A/n\pi d$, and $\sigma_{\ell b} = 0.6 Et/d$):

$$t = \sqrt{\frac{F_t}{(\pi)(0.6)E}} = 0.0175 \text{ in}$$

Finally, $\sigma_{\ell b}$ and the total mass of the supports, M, can be computed from:

$$\sigma_{\ell b} = 0.6 \frac{Et}{d} = 56,000 \text{ psi}$$

$$M = \frac{\rho n \pi d t L}{\cos\theta} = 21.1 \text{ lb}_m.$$

5.2.4 Parametric Studies

In general, different optimal configurations are expected for different payload masses and for the various truss materials. Although the calculations required in any particular case are simple and straightforward, the number of system parameters and the range of values of these parameters which required investigation suggested that the most expedient manner to effect these optimizations would be by programming the design process for automatic computation. The discussion of this procedure is given below.

---

* For the purpose of this illustrative example, we assume that the strut is a thin-wall tube and that the cross-sectional area is πdt.

Parametric studies of fixed structures (and space-erected structures) were made using the following five materials which are commonly used in aerospace applications:

1) Fiber glass - Material E-1, YM-31A glass roving, cross plied at 57° and 303° with 80 plies.

2) Titanium - Alloy 6Al-4V

3) Stainless steel - 301 Extra Full Hard

4) Aluminum - Alloy 7075-T6

5) Beryllium - Commercially pure, 1 to 2% BeO

The mechanical properties and densities of these materials are summarized in Table IV. The allowable stress was taken as the lower value obtained using a factor of safety of 1.4 on ultimate strength or 1.2 on yield strength. However, the allowable stress for the fiber glass material was based on a factor of safety of 2.0 due to considerations of fatigue strength.

Conceptually, the combination of the mass of the supports making up a Warren truss plus the LH_2 boil-off (heat leak) due to conduction down the structure is related to the specific stiffness (modulus-to-density ratio (E/ρ)) and the ratio of E/k, where k is the thermal conductivity, when the supports are sized on the basis of stability. Similarly, when a structure is designed for an axial stress criterion, its mass is related to the specific stress (σ/ρ) and the σ/k ratios for the materials. A measure of the four property ratios is given for the five materials at a reference temperature of 520°R in Table V. This tabulation illustrates the wide range of materials properties represented by the selection. For example, on the basis of this simple comparison, fiber glass appears suitable as a structural material because of its high E/k and σ/k ratios. On the other hand, specific stiffness is less than one-tenth that of beryllium, which is not as attractive as fiber glass from thermal considerations.

A comprehensive structural and thermal analysis was used to determine the relative magnitudes of the mass of the supports and the LH_2 boil-off penalties associated with fixed structures for a given mission period. The temperature dependence of thermal conductivity with support temperature was included in the heat flow analysis.

A diagram illustrating the methods which were used to calculate the required mass of the support truss and the resulting LH_2 boil-off mass due to support conduction is shown in Figure 21. The diagram illustrates how the structural analysis was combined with a thermal analysis to determine the most promising structural materials and configurations. The operational descriptions enclosed by the dotted

TABLE IV

MECHANICAL PROPERTIES OF STRUCTURAL MATERIALS

Material	Modulus of Elasticity (E) 10^6 PSI	Density (ρ) LBM/in^3	Ultimate Stress (σ_{ULT}) 10^3 PSI	Yield Stress (σ_Y) 10^3 PSI	Allowable Stress (σ_{ALL}) 10^3 PSI	Reference*
Fiber glass	4.0	.075	100	100	50	18
Titanium	16.0	0.16	130	125	93	17
Stainless steel	28.0	.29	225	192	160	16
Aluminum	10.5	0.10	79	70	57	16
Beryllium	44.2	0.067	78	60	50	19

* Numbers relate to references listed in Section 13.2.

TABLE V

COMPARISON OF STRUCTURAL MATERIALS AT 520R

REFERENCED TO ALUMINUM ALLOY

Material	$\frac{E/\rho}{(E/\rho)}$	$\frac{E/k}{(E/k)}$	$\frac{\sigma/\rho}{(\sigma/\rho)}$	$\frac{\sigma/k}{(\sigma/k)}$
1) Fiber glass reinforced plastic	0.5	70.0	2.3	350.0
2) Titanium (6Al-4V)	1.0	18.0	1.2	25.0
3) Stainless steel (301)	0.9	11.0	1.2	18.0
4) Aluminum (7075-T6)	1.0	1.0	1.0	1.0
5) Beryllium	6.5	2.5	1.8	1.0

E = Modulus of elasticity (psi)

ρ = Density (lbm/in^3)

k = Thermal conductivity (BTU/HR FT °R)

σ = Ultimate stress (psi)

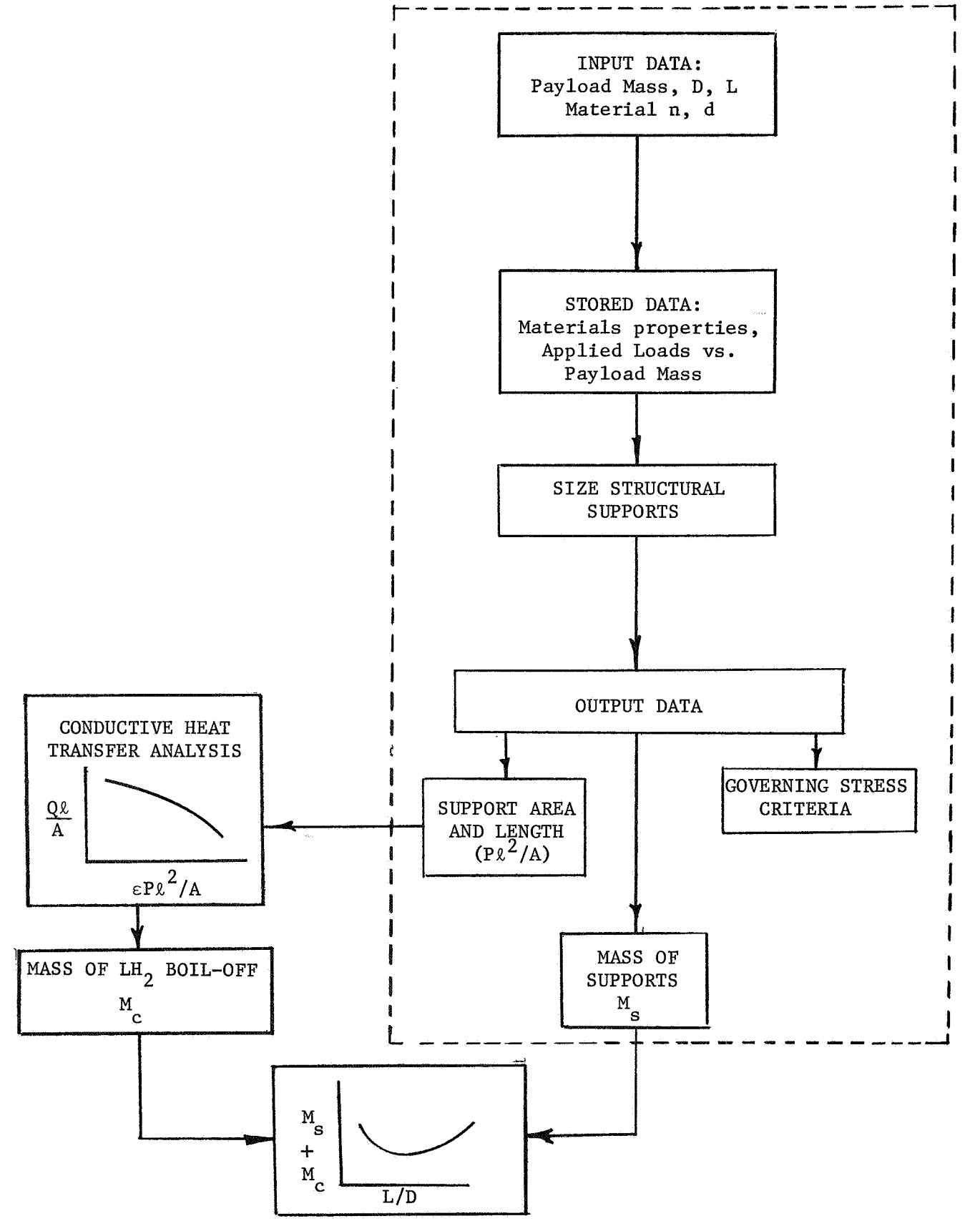

FIGURE 21 PARAMETRIC STUDIES OF FIXED STRUCTURES

n = number of supports
d = diameter
P = perimeter
A = cross-sectional area
ℓ = total length

lines were executed using a computer program which was used to determine the governing stress criteria, and evaluate the support geometry and the mass of the truss members given the material and the structural configuration as input data.

A typical output data sheet from the Structural Analysis Computer program is presented in Table VI. The input data for the problem, shown in the left column, results from the specification of the following information on a single data card:

- Material code number and name
- Payload diameter
- Payload - tank spacing
- Number of supports
- Support diameter
- Code number for payload mass

The material properties and axial and shear forces are stored as part of the program and are called according to the code numbers for the material and payload mass specified on the data card. All the parameters and properties used in the computation are printed as "input data" as a check on the consistency of the data specification. The central column contains the output data and the governing stress criterion, which determines the cross-sectional area (and wall thickness) required to support the launch loads. The last column contains three additional terms which provide checks on the computation and a geometrical parameter which is used in conjunction with the preliminary analysis of conduction heat transfer (Section 6.0). Trade-off studies using the results of the structural analysis and the conduction heat transfer analysis are presented in Section 7.0.

5.2.5 Sample Calculations

Figure 22 shows the computed masses of truss members as a function of L/D and material properties for a typical configuration consisting of 12 tubular supports, 3 inches in diameter, and a payload mass of 4000 lbs. For spacing ratios between 0.1 and 0.4, the masses of the supports were of the same order of magnitude for all materials and ranged from 5 to 25 lb_m. The stress criteria which were found to govern the wall thickness of the supports are also indicated in Figure 22. The governing criteria for the fiber glass, titanium, and stainless steel structures were local or column buckling, while the aluminum and beryllium structures were sized on an axial stress criterion. Since, in general, the physical masses of the supports were relatively similar for all the materials, it was not possible to disqualify any of the five selected materials for use in fixed structures on structural considerations alone.

TABLE VI TYPICAL OUTPUT DATA SHEET FOR TRUSS DESIGN COMPUTER PROGRAM

WARREN RING TRUSS DESIGN

INPUT DATA	OUTPUT DATA	
PAYLOAD WT. = 4000. LBS.	SUPPORT LENGTH = 33.63 IN.	SIGMC = 139602. PSI
PAYLOAD DIA. = 120. IN.	WALL THICKNESS = 0.014456 IN.	SIGMB = 69390. PSI
L / D = 0.2000	AREA = 0.09017 SQ. IN.	SIGMA = 69391. PSI
NO. OF SUPPORTS = 16		P*SL**2/A = 6568. FT.
SUPPORT DIAMETER = 2.000 IN.	THE DESIGN IS BASED ON	
SUPPORT MATERIAL = TITANIUM	LOCAL BUCKLING CRITERIA	
DENSITY = 0.160 LB/CU IN		
E = 0.160E 08 PSI	TOTAL SUPPORT WT. IS 7.764 LBS.	
ALLOW. AXIAL STRESS = 93000. PSI		
AXIAL FORCE = 41700. LBS.		
SHEAR FORCE = 7300. LBS.		

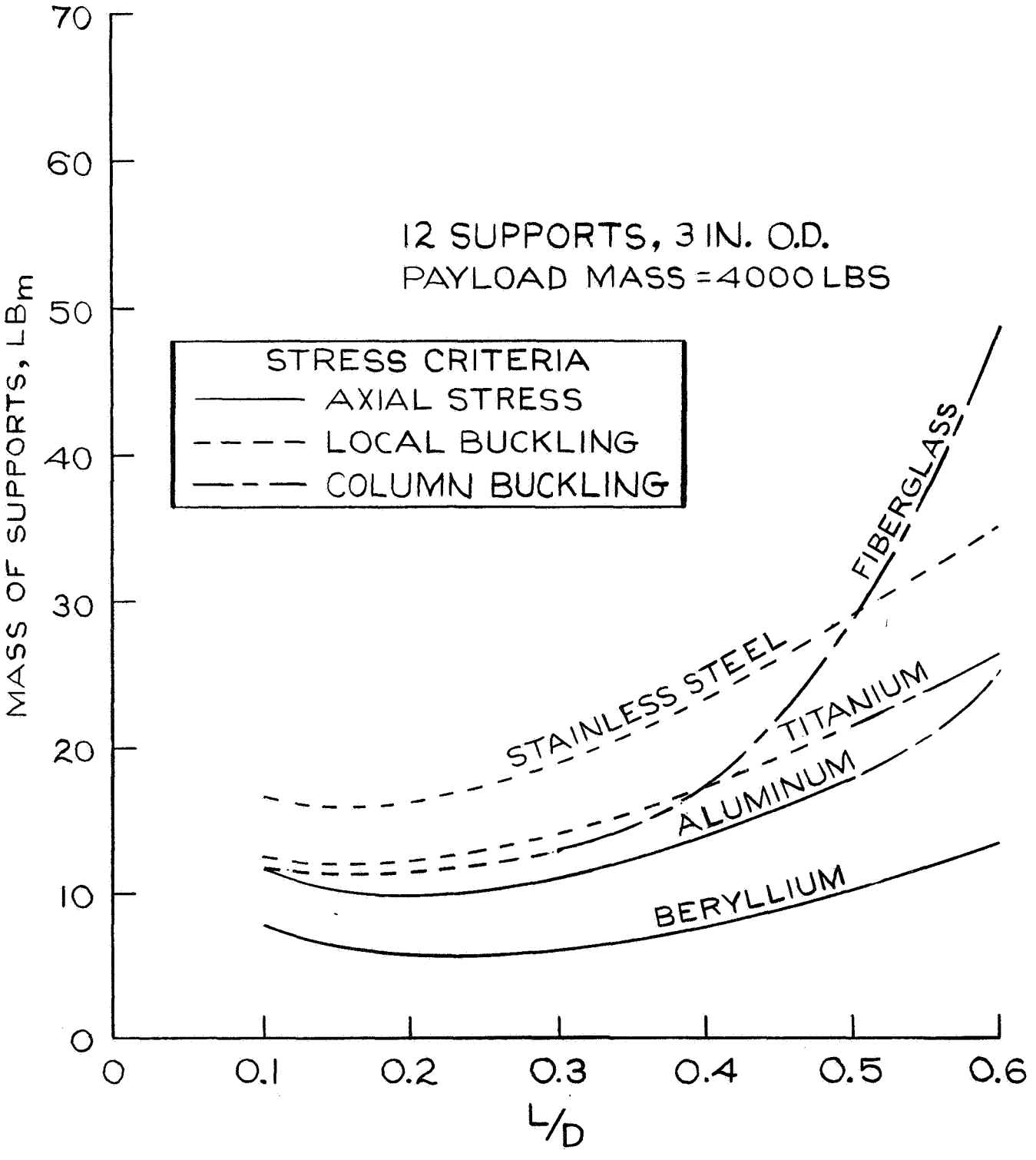

FIGURE 22 - MASS OF SUPPORTS VS. L/D FOR A TYPICAL WARREN-TRUSS STRUCTURE

5.3 Design of Space-Erected Structures

5.3.1 Introduction

During launch, the payload and the LH_2 tank support are locked, and the retracted structures do not provide any supporting function. After deployment in space, the erected structures, connecting the payload and the LH_2 tank, will only be subjected to small accelerations associated with attitude control. The following assumptions were made in the design analysis of space-erected structures.

1) The erected structure interconnects and supports the payload and a kick-stage engine system of mass 4000 lb_m and 8724 lb_m, respectively. Each mass is uniformly distributed in a 10-foot-diameter configuration.

2) The attitude control system is capable of exerting sufficient force to the vehicle to cause accelerations of $10^{-3}g$ in roll, pitch and yaw. These forces are assumed to be exerted by control nozzles located on the payload.

The mathematical model of the kick stage and intermediate, erected structure was represented by a two-mass system connected by a structure of length, L, and with a spring constant, k. This system will have three natural modes of vibration - a torsional mode with the masses rotating in opposite directions and twisting the structure, a lateral deflection mode bending the structure as the masses move laterally in phase, and an axial deflection mode with the masses moving axially in phase opposition to alternately compress and extend the structure. Any or all of these natural vibration modes could be excited when a control torque was applied to one of the system masses. Obviously, if the erected structure were very flexible, it would develop large deflections when the control system was actuated. These large deflections could continually exert disturbing forces on the controlled mass and, therefore, require the attitude control system to function continuously.

For example, if a maneuvering torque was exerted on the payload to rotate it for star-orienting purposes and the structure was flexible, the payload could be driven to its final orientation before the uncontrolled mass reacted. The subsequent twisting of the structure would then exert torques on both masses causing them to rotate and the control system would then be required to stabilize the payload against the continually varying torque exerted on it by the torsionally deformed structure and engine mass. In the absence of any structural damping in the erected structure, the attitude control system would be operating continuously which might require large amounts of attitude control gas.

By making the erected structure as stiff as possible within a reasonable total mass, it would approach a rigid body system which could be easily controlled in attitude. In effect, when the oscillation amplitude of the payload is within the control limits of the attitude control system, no position error is sensed; and the system will behave like a rigid body. Of course, some damping would be present in the structure which would cause oscillations to disappear after a finite time. Since a space-erected structure should have low mass and a high stiffness in all directions when erected, it is generally desirable for a space-erected structure to have a high stiffness-to-mass ratio.

5.3.2 Design Analysis

Consider a mathematical model, consisting of the payload mass M_1 with moment of inertia I_1, the kick-stage engine and propellant mass M_2 with moment of inertia I_2, and the torsional spring constant k of the connecting structure. The following equation of motion describes the angle of twist of the structure when the attitude control torque is constant and damping is neglected:

$$\frac{I_1 I_2}{I_1 + I_2} \ddot{\psi} + k \psi = \frac{I_2}{I_1 + I_2} T_o$$

where ψ = angle of twist

T_o = attitude control torque

This equation can be solved to yield the following expressions for the maximum angle of twist and the natural circular frequency.

$$\psi_{max} = \frac{2 I_2 T_o}{k(I_1 + I_2)}$$

$$\omega_n = \sqrt{\frac{k(I_1 + I_2)}{I_1 I_2}}$$

Thus, if a steady control torque T_o is applied to the payload, M_1, the system will oscillate at its natural circular frequency, ω_n, with a maximum twist angle of ψ_{max}. Note that the absolute angular excursions of the separate masses would be less than ψ_{max} because one point along the structure tends to remain fixed in space.

If a torque reversal to stop the spacecraft roll should occur at the worst time, i.e., when the reversed torque and the structural twist act together to accelerate M_1, the frequency of oscillation will remain the same but the amplitude will increase in accordance with the following equation:

$$\psi_{max} = \frac{4 I_2 T_o}{k(I_1 + I_2)}$$

Since the torque exerted on the structure is equal to its angular deflection times its spring constant:

$$T_{s(max)} = \psi_{max} k$$

$$T_{s(max)} = 4T_o \left(\frac{I_2}{I_1 + I_2} \right)$$

Since this relation defines the maximum torque on the erected structure in terms of known quantities, it serves as a quantitative criterion for designing these structures. The mathematical analysis used to evaluate the element geometry of "A"-frame "STEM," and concentric tube structures and the resulting torsional spring constants is described in the following paragraphs. Thereafter, the performance of the structures will be compared from the standpoints specific stiffness and inherent reliability. This preliminary comparison served to illustrate the advantages and trade-offs of the systems to aid in the selection of concepts for final evaluation, which is described in Section 7.0.

5.3.2.1 "A"-Frame Erectile Structures

An "A"-frame structure is a frame consisting of two structural elements joined together at one end and hinged to the payload or engine at the other. The elements were considered two-force members (all loads are coaxial with the element) with an included apex angle of 2β. A load F acting in the plane of the "A" frame at the apex but perpendicular to its axis of symmetry would, therefore, produce a load f in the elements:

$$f = \frac{F}{2\sin\beta}$$

The erected structure was assumed to consist of six "A" frames (3 frames hinged from the payload and tank supports, respectively), equally spaced around the circumference of a 10-foot-diameter vehicle at 60° intervals. Therefore, a torque T_s exerted on this structure would cause the following loads in the elements:

$$f = \frac{T_s}{3(5\cos 30°)(2\sin\beta)}$$

Using the previously derived equation for the torque, and substituting I_1 and I_2, the maximum moment of inertia of the payload and the moment of inertia of the engine, respectively:

$$T_s = 2.75\, T_o$$

Since the maximum roll acceleration of the vehicle at its periphery is 10^{-3} g, the torque required to produce this acceleration, assuming a rigid vehicle, is 31.8 lbf.ft. In view of the fact that the number of torque reversals and their timing is unknown, T_o was arbitrarily multiplied by 1.22:

$$T_s = 1.22(2.75)\ T_o = 107 \text{ lbf. ft.}$$

The load on the elements comprising the "A" frame can be either tensile or compressive; however, in this case only the latter is significant from a sizing standpoint. Using thin-walled tubing for the "A"-frame elements, the critical stresses associated with local and column buckling can be determined as a function of the following variables:

- modulus of elasticity
- tube wall thickness
- tube diameter
- Poisson's ratio
- length of the tube

Thus, for a given material and total length of the "A"-frame system, one can determine the minimum wall thickness and tube diameter required. The mass of the "A"-frame structure can thus be determined.

The transverse spring constant K of the basic frame (in the plane of the elements perpendicular to the axis of symmetry) is given by the equation:

$$K = 2k \sin^2\beta$$

where k is the axial spring constant of the individual elements.

Since there are three "A" frames connected to each part of the spacecraft (in parallel) and these in turn are connected together (in series), the torsional spring constant for the whole structure can be shown to be:

$$K_t = \frac{3}{2}\frac{(4.33)^2\pi}{10}\left[\frac{t \cdot d \cdot E}{\left(\frac{1}{4} + \left\{\frac{L}{D}\right\}^2\right)^{3/2}}\right]$$

where t = wall thickness (in)

d = tube diameter (in)

E = modulus of elasticity (psi)

L/D = spacing ratio

K_t = torsional spring constant (lbf/in)

5.3.2.2 "STEM" Erectile Structure

A "STEM" erectile structure would consist of a parallel array of "STEM" elements whose ends are built into the payload and engine portions of the vehicle. For each "STEM" element of diameter d, length L, and wall thickness t, the lateral spring constant at the end is:

$$k = \frac{24EI}{L^3}$$

where the moment of inertia is given by Rimrott (1965)

$$I = 0.535\, d^3\, t$$

For an array of "STEM" elements arranged in parallel around the vehicle circumference, the system torsional spring constant is:

$$K_t = 1810\, \frac{ENd^3t}{L^3}$$

The total mass for such a system would be:

$$M = \pi NdLt\rho$$

where N = number of tubes

ρ = density

The lateral load-carrying ability of such an element is limited by local buckling so that in this particular case a conservative estimate of the system torsional capacity is:

$$T_s = 2.06\, \frac{ENdt^2}{L}^*$$

These three equations are not enough to completely define a structure, but they can provide information on the ratio of $\left(\frac{K_t}{M}\right)$ which it is desirable to maximize. For example, at a given spacing ratio (L/D), the spring constant K_t per unit mass is given by the equation

$$\frac{K_t}{M} = \frac{1810}{\pi}\left(\frac{E}{\rho}\right)\frac{d^2}{L^4}$$

In other words, the best material is the one with the highest specific modulus of elasticity and the optimum size is represented by the maximum possible diameter and the shortest length. For a space vehicle diameter of 120" assumed in this study,

---

* (c.f. Rimrott (1965))

the maximum allowable structural element diameter is about 4 inches; therefore, if d is set equal to 4 inches and D = 120", the following equations apply

$$\frac{K_t}{M} = \frac{1810\ (4)^2}{\pi\ (120)^4} \frac{E}{\rho (L/D)^4}$$

and

$$\frac{ENt^2}{L} = 12.97$$

This equation determines the allowable element configuration (wall thickness and number of elements) based upon buckling criteria.

Note that these last two equations do not define specific structural configurations, but rather a family of configurations which have identical Nt^2 products and $\frac{K_t}{M}$ values.

The total structural mass for this system would consist of the mass of the "STEM" tubes plus the mass of the end fittings, guide bushings, and winding drum.

5.3.2.3 Concentric Tube Erectile Structures

A concentric tube erectile structure would be very similar to a "STEM" structure since it would consist of multiple circular elements acting in parallel which are built into the payload and engine portions of the space vehicle. For estimating purposes, the sliding joints of this structure will be considered solid so that the elements can be treated as single, thin-wall tubes extending from the payload to the engine.

The derivation of equations for this structure is almost identical to that for the "STEM" structure. The final for the torsional spring constant is

$$\frac{K_t}{M} = 3.24 \times 10^{-5} \frac{E}{\rho} \frac{1}{\left(\frac{L}{D}\right)^4}$$

based on the assumption that the tube diameter is 4" and the payload diameter is 120".

The allowable element configuration would be governed by the equation

$$\frac{ENt^2}{L} = 10.20$$

Here again, we are not defining a specific structural configuration only a family of configurations of identical Nt^2 products and $\frac{K_t}{M}$ values.

The mass includes only the tube mass and not the fittings which would be required at the ends of all the tubes to provide solid joints.

5.3.3 Comparison of Erectile Concepts on the Basis of Mass, Stiffness and Reliability Potential

It has previously been mentioned that it is desirable for an erectile structure to have a high torsional stiffness-to-mass ratio. A stiff structure would react as a rigid body during attitude-control maneuvers and, therefore, could be positioned with conventional control systems, while a flexible structure would be difficult to control. Since it is also desirable to make the erectile structure (as well as the entire shadow-shield system) as light as possible, the three concepts ("A" frame, "STEM" and Concentric Tubes) were initially compared on the basis of specific torsional stiffness versus extended length (payload-tank spacing).

The five materials considered in the evaluation of fixed structures were also considered in this analysis. Fiber glass was not considered for the concentric tube and "STEM" structures due to physical limitations.

The ratios of torsional spring constant to the mass of the tubes (or elements) for each system are presented in Figure 23 as a function of the spacing ratio in the deployed configurations. The mass M does not include end fittings, actuation systems, etc. It was assumed that all systems would require an equal mass of end fittings and essentially the same actuation system; therefore, the additional mass was not considered in the comparison. For the "A" frame system, beryllium yielded the best performance over the entire range of spacing ratios and exceeded the best performance of the other two systems. For each system, the curves representing the best and worst materials are shown. The intermediate ranking materials were eliminated for clarity.

From Figure 23, it is clear that at L/D ratios in excess of 0.25, "A" frame structures fabricated from any of the five materials has a significantly better stiffness-to-mass ratio than the best-performing other structures. In fact, at spacing ratios greater than 1.0, the specific stiffness of the best "A" frame system is two orders of magnitude greater than that of the next best system.

The concepts which will be considered in the final analysis and evaluation will be compared on the basis of mass and inherent reliability. Therefore, some preliminary comments will be made concerning the reliability potential of the three space-erected structures:

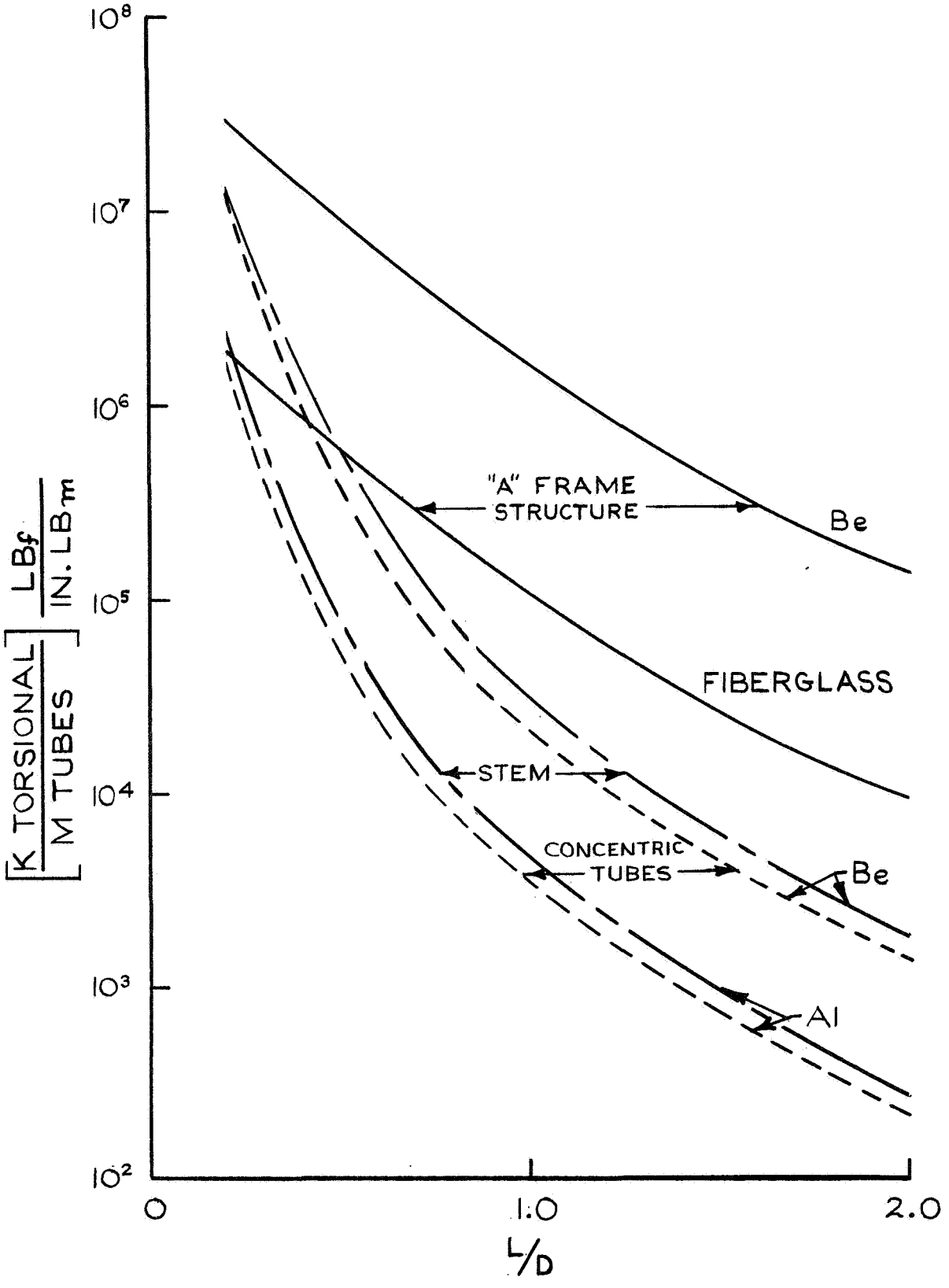

FIGURE 23 - TORSIONAL STIFFNESS TO MASS RATIO VS. L/D FOR VARIOUS ERECTILE CONCEPTS

1) Coefficients of friction are somewhat unpredictable; and, when closely contacting surfaces rub in a vacuum, there is the possibility of cold welding. In this regard, the concentric tube and "STEM" concepts have more rubbing contacting area than the "A" frame system and would require special attention in the design and material specification of the contacting parts. On the other hand, the rotating joints of the "A" frame system could be easily designed using standard spacecraft hardware components.

2) The concentric-tube structure requires that slip joints be made with tapers or closely fitting cylindrical surfaces so that the structure is rigid when fully extended. Extension of the structure and locking of these rigid joints may not be a problem, but reliably unlocking these joints after exposure to the space environment and a complicated load history may require extensive design work and experimental verification.

In summary, on the basis of torsional stiffness per unit mass and reliability potential, the "A" frame system appears more promising than the other two concepts. Additional parametric studies were made with the "A" frame system to determine the optimum structural material and L/D considering mass and thermal performance. This work will be discussed in Section 7.0.

5.4 Stress Levels and Natural Frequency of Shadow Shields

The circular, 120"-dia. shadow shields which are assumed to comprise a three-layer composite of polyester film, rip-stop nylon cloth, and polyester film are supported at their periphery. During launch the static accelerations and vibratory inputs from the support structure produce stresses in the circular diaphragms. The purpose of this section is to present the results of estimates of the natural frequencies and the maximum stresses in the shields during launch.

The following launch loadings apply:

- Static acceleration - 5.7 g (max)
- Vibratory inputs - 6 g at 20-150 HZ at 2.5 g acceleration

The shield materials and the weight per unit area comprising the shield are as follows:

Material	Thickness (mils)	W/A (oz/yd^2)
polyester film	.5	1.0
rip-stop nylon	2.0	1.1
polyester film	.5	1.0
	3.0	3.1

For a composite consisting of one layer of 1/2-mil polyester film and the 1.1 oz/yd^2 rip-stop nylon, the breaking strength is approximately 55 lbs/inch of width. The corresponding tensile stress is 22,000 psi. If the elongation at break is taken to be 0.2, the modulus of elasticity for large strains will be 110,000 psi. It may be noted that the construction of the composite is not balanced since the polyester film is capable of greater elongation at breakage (70-100%) than the fabric. Thus at the break point the load will be transferred to the polyester film.

For the three-layer composite, the average breaking stress will be 20-25,000 psi and the modulus for small strains will be about 250,000 psi.

During static acceleration the maximum stress will occur in the center of the diaphragm, and the stress is given by the following formula:

$$\sigma_{max} = 0.423 \sqrt[3]{\frac{E w^2 a^2}{t^2}}$$

where E - modulus of elasticity = 250,000 psi

w - effective mass per unit area = $.85 \times 10^{-3}$ psi @ 5.7 g

a - radius = 60.0 in

t - thickness = 3×10^{-3} in

The resulting stress for 5.7 g's is

$$\sigma_{max} = 177 \text{ psi}$$

Thus the static loading is small by comparison to the breaking strength, and the use of a modulus based on small strains is appropriate. A stress of 177 psi corresponds to a tensile force of 0.53 lbs/inch compared to the tensile force at break of 55 lbs/inch.

Under the vibratory input, the static acceleration is 2.5 g and the corresponding stress is 135 psi.

It may be noted that uncertainties in the value of the modulus for small strains of a factor of two will change the stress level by a factor of only 1.25.

The maximum deflection during static acceleration is given by the formula

$$y = 0.662\, a \sqrt[3]{\frac{wa}{Et}}$$

At 5.7 g acceleration the corresponding deflection is

$$y = 2.3 \text{ inches}$$

Therefore, from considerations of static accelerations it is concluded that the stress levels in the shields are essentially negligible; however, provisions must be made to allow for static deflections of several inches. Furthermore, such low stress levels will produce only small loads at the periphery; and the attachment of the shield to the shield rim by a multiplicity of grommets will not be a significant problem.

The natural frequency f of a circular diaphragm disturbed at its circumference is given by the formula

$$f = \frac{1}{2\pi} A \sqrt{\frac{T}{\mu a^2}}$$

where T - tension (lbs/inch)

μ - mass/unit area (lb sec^2/in^3)

a - radius

A - constant = 2.4 for 1st mode

If it is assumed that the shield is assembled with a small initial tension of 300 psi (1 lb/inch of width), the fundamental natural frequency is

$$f_1 = 10.3 \text{ HZ}$$

which is below the range of input frequencies. By comparison, if the shield was tensioned to the breaking strength

$$f_1 = 76.1 \text{ HZ}$$

The limiting case of failure by vibratory acceleration would occur with a stress of 22,000 psi corresponding to a tensile force of 55 lbs/inch. In this case the required acceleration would be in excess of 1000 g's. It is highly improbable that amplification factors at resonance could produce such accelerations because of internal damping and the damping provided by the air mass within the interstage.

During the launch environment the shield material will be heated from the interstage by aerodynamic heating effects. If the polyester film is not preshrunk, heating will cause an initial shrinkage of approximately 1.2% for a 30-minute exposure at 300°F. Using a modulus of elasticity of 250,000 psi for small strains, the resulting additional stress would be 3000 psi which would be small by comparison to the average allowable stress of about 22,000 psi. In an actual assembly the polyester film could be preshrunk before lamination. The temperature rise during ascent would then tend to cause a slight decrease in the initial tension in the shield; however, the expansion of the aluminum shield rim would tend to increase the tension. The maximum shield stress due to thermal effects would occur if the expansion of the shield material were neglected. Using a temperature rise of 250F for the aluminum shield rim during ascent, the tensile stress in the shield material would be 457 psi or a tensile force of 1.4 lbs/inch of width. This is, again, a small force compared to the breaking force of 55 lbs/inch. Furthermore, the low stress levels will not appreciably alter the natural frequency of the shields, since the natural frequency is proportional to the square root of the tension.

During sun-oriented operation, the shields will cool down to cryogenic temperatures. The maximum stress in the shield material due to thermal contraction to temperatures below 140°R will be approximately 440 psi - a tensile force of only 1.3 lbs/inch of width - which is small with respect to the allowable stress levels.

6.0 CONDUCTIVE HEAT TRANSFER

6.1 General

The propellant boil-off due to conduction heat transfer can be large or unimportant depending upon the mechanical and thermal properties of the structural materials. Procedures for determining the size and mass of fixed and space-erected structures have been described previously.

Now it will be shown how the propellant loss by conduction (conduction boil-off) was obtained given the geometrical, material and emittance properties of the structural elements.

A preliminary conductive heat transfer analysis was used to obtain a family of generalized curves relating the conductive heat transfer to the LH_2 tank to the surface radiative properties, geometry and material properties. Since the support structures are made up of tubular elements symmetrically placed in cylindrical fashion between the payload and LH_2 tank, a mathematical model was formulated for one element.

6.2 Mathematical Model

Figure 24 illustrates the mathematical model used to analyze and predict the conductive heat flow to the LH_2 tank via the support structure. The model consists of a single tubular support with a one-dimensional temperature distribution, two fixed boundary temperatures and a 0°R environment. The temperature of the support at the connection to the payload ($x = \ell$) was specified at 520R. The end connected to the tank support ($x = 0$) was assumed to be at 37R, although its temperature will actually be somewhat higher depending upon the material and dimensions of the tank support system. (The design of the tank support was later specified on the basis of structural considerations, mass and ground-hold requirements. The thermal resistance of the tank support was considered in the final detailed analysis when the temperature distributions and heat flow in the structure were evaluated for the six shadow shield concepts.)

The notation for the pertinent variables is also indicated in Figure 24. The temperature dependence of thermal conductivity was quite important in this preliminary evaluation since the support temperatures range from 520R near the payload to cryogenic temperatures near the connections to the payload. Data for thermal conductivity, covering a range of temperatures from 37R to 540R (20 to 300K) was accumulated from a number of references and expressed in a 4th-order polynomial equation for use in the thermal analysis. The polynomial expressions shown graphically in Figure 25 were obtained using a "least squares" curve fitting technique. The values described by the equations were generally within 5% of the measured data.

6.3 Thermal Analysis

The differential equation for the steady heat flow in the radiating and conducting support illustrated in Figure 24 is given by Equation (6-1):

$$\frac{d}{dx}\left[k(T)A\,\frac{dT(x)}{dx}\right] - \varepsilon P\sigma T(x)^4 = 0 \qquad (6\text{-}1)$$

The boundary conditions at $x = 0$ and $x = \ell$, and the heat flow to the LH_2 tank, Q, are given by:

$$T(x = 0) = T_1 = 37R \qquad (6\text{-}2a)$$

$$T(x = \ell) = T_2 = 520R \qquad (6\text{-}2b)$$

$$Q = Q(x = 0) = \left[k(T)\,A\,\frac{dT(x)}{dx}\right]_{x = 0} \qquad (6\text{-}3)$$

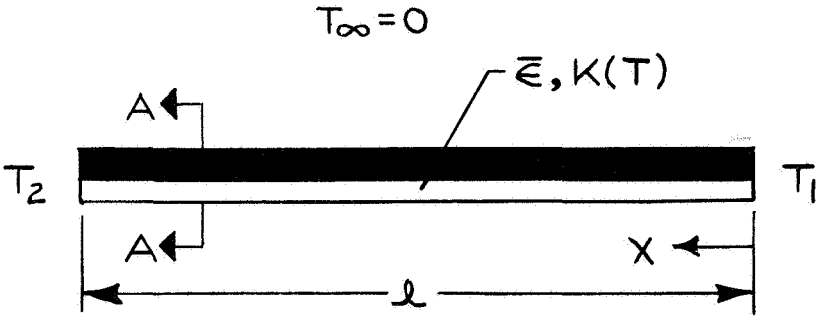

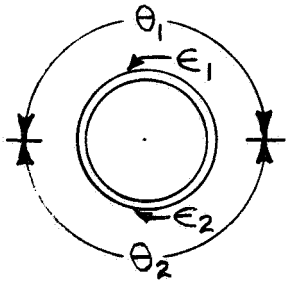

SECTION A-A

$\bar{\epsilon}$ = EFFECTIVE EMITTANCE = $\frac{\epsilon_1\theta_1 + \epsilon_2\theta_2}{2\pi}$

d = DIAMETER

K(T) = THERMAL CONDUCTIVITY, A FUNCTION OF TEMPERATURE

A = CROSS SECTIONAL AREA

P = PERIMETER

L = TOTAL LENGTH

FIGURE 24 - THERMAL MODEL FOR PRELIMINARY ANALYSIS OF CONDUCTION HEAT FLOW

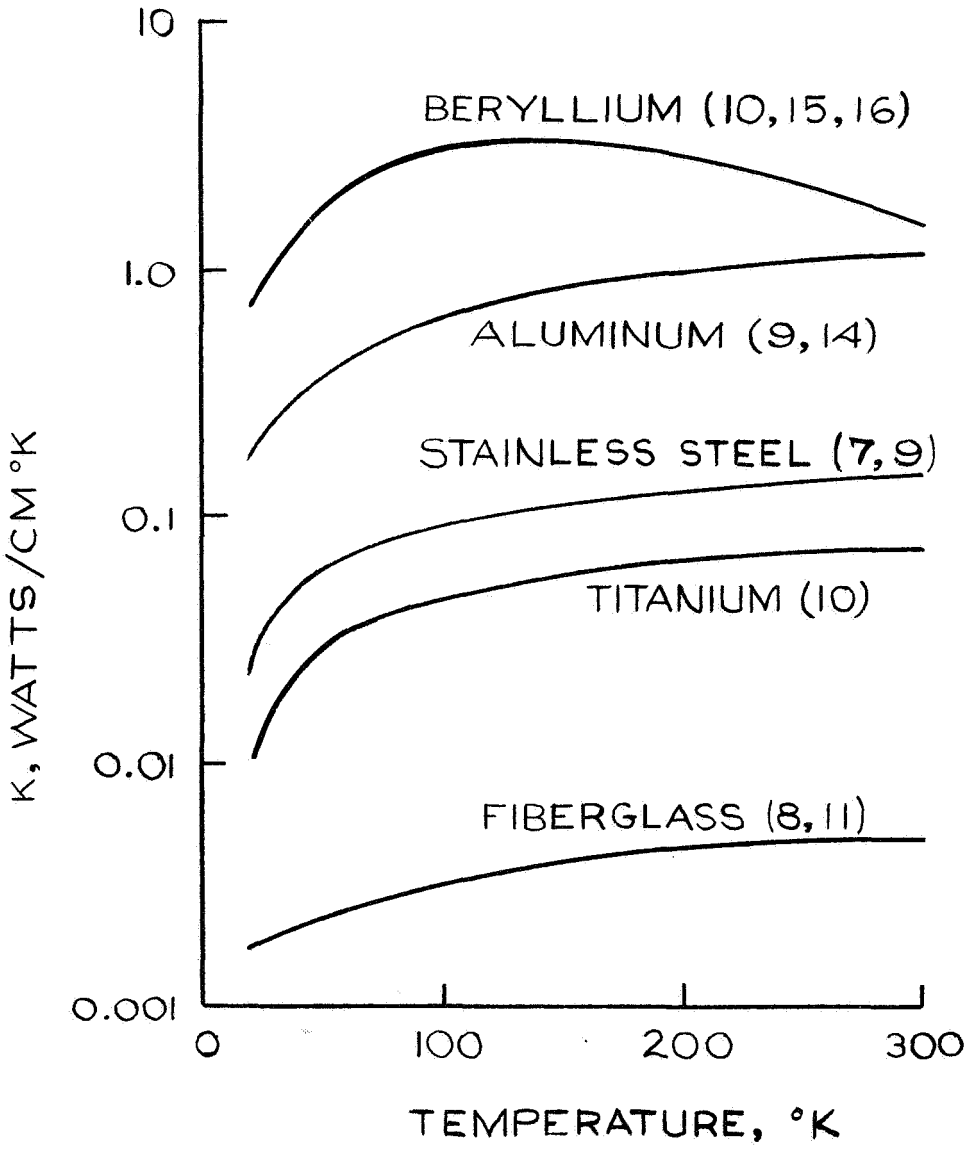

FIGURE 25- THERMAL CONDUCTIVITY VS. TEMPERATURE FOR STRUCTURAL MATERIALS -4th ORDER POLYNOMIAL CURVE - FIT TO EXPERIMENTAL DATA

1. Numbers in parentheses relate to references listed in Section 13.2.
2. The conductivity curve for aluminum is for alloy 2024-T4. Other materials are described in Section 5.2.2.

It is convenient to generalize these equations by introducing the following dimensionless variables:

$$\xi = \frac{x}{\ell}$$

$$\Theta = \frac{T(x)}{T_1}$$

$$C(\Theta) = \frac{k(T_1\Theta)}{k_1} \text{ where } k_1 = k\ (T_1)$$

Consequently, Equations (1), (2) and (3) may be rewritten as follows:

$$\frac{d}{d\xi}\ \beta(\xi) - \alpha\left[\Theta\ (\xi)\right]^4 = 0 \qquad (6\text{-}4)$$

$$\Theta(0) = 1 \qquad (6\text{-}5a)$$

$$\Theta(1) = \frac{T_2}{T_1} \qquad (6\text{-}5b)$$

and

$$\frac{Q\ell}{kAT_1} = \beta(0) \qquad (6\text{-}6)$$

where $$\beta(\xi) = C(\Theta)\ \frac{d\Theta(\xi)}{d\xi}$$

and $$\alpha = \frac{\varepsilon P \ell^2 \sigma T_1^{\ 3}}{k_1 A}$$

Due to the non-linearity of the differential equations (and the dependence of thermal conductivity on temperature), the solution to Equation (6-4) cannot be obtained by direct integration. The procedures used to obtain generalized solutions for the conductive heat leak to the LH_2 tank are outlined below.

The boundary-value problem was changed to an "initial-value" problem by specifying the dimensionless temperature and the dimensionless heat flow at x = 0. By defining an integration step in space and using a forward integration by Gill's fourth-order Runge-Kutta Method, the dimensionless temperature and heat flow were successively computed along the entire support up to and including the opposite boundary

at $\xi = 1$. The temperature at $\xi = 1$ is known and can be compared with the computed value for an arbitrary value of $\beta(0)$. An iterative procedure was employed where $\beta(0)$ was parametrically varied to obtain the value of $\beta(0)$ which gives the correct value of $\theta(1)$. Considerable effort was required to generate curves for one material with α as a variable and to repeat the process for each remaining material where the conductivity equation $C(\theta)$ is different. However, this procedure is more efficient in time and computer cost than the impossible task of formulating large numbers of finite-difference mathematical models for the geometries obtained from the structural analysis. The procedure yields generalized solutions for each material, accurately accounts for the temperature dependence of thermal conductivity, and provides a convenient means of performing optimizing and trade-off studies considering the mass of the structural supports and the long-term LH_2 boil-off due to conduction effects. After a brief description of the curve-generation procedures, the generalized curves used for the trade-off studies and a typical example will be presented.

Figure 26 shows a schematic flow chart of the manual and digital computer operations that were used to obtain generalized solutions for the conductive heat flow to the LH_2 tank as a function of geometry and material properties.

The procedure for calculating the conductive heat flow to the LH_2 tank is detailed below:

a) The conductivity for a particular material can be stored as a constant, a tabular value or an equation. In these calculations the conductivity vs. temperature relation was expressed as a fourth-order polynomial.

b) $\theta(0) = 1$ specifies the temperature of the conducting support at the propellant tank. For a specified value of α, $\beta(0)$ is parametrically varied.

c) The computer program is used to calculate the temperature at the payload, $\theta(1)$ for each value of $\beta(0)$.

and

d) Plotting these values as shown in "d" determines the value of $\beta(0)$. The procedure is repeated for a number of α's which cover a wide range of support geometries obtained from the structural analysis.

e) A family of curves for the parameter α are cross-plotted to obtain the generalized dimensionless plot of $\beta(0)$

and

f) vs. α for a particular material. The curves of $\beta(0)$ vs. α are replotted as shown in (f). Here, the parameter $\frac{Q\ell}{A}$ is plotted vs. the parameter $\varepsilon P\ell^2/A$ for different materials with the end temperatures of the support fixed at 520 and 37R, respectively. The variables are:

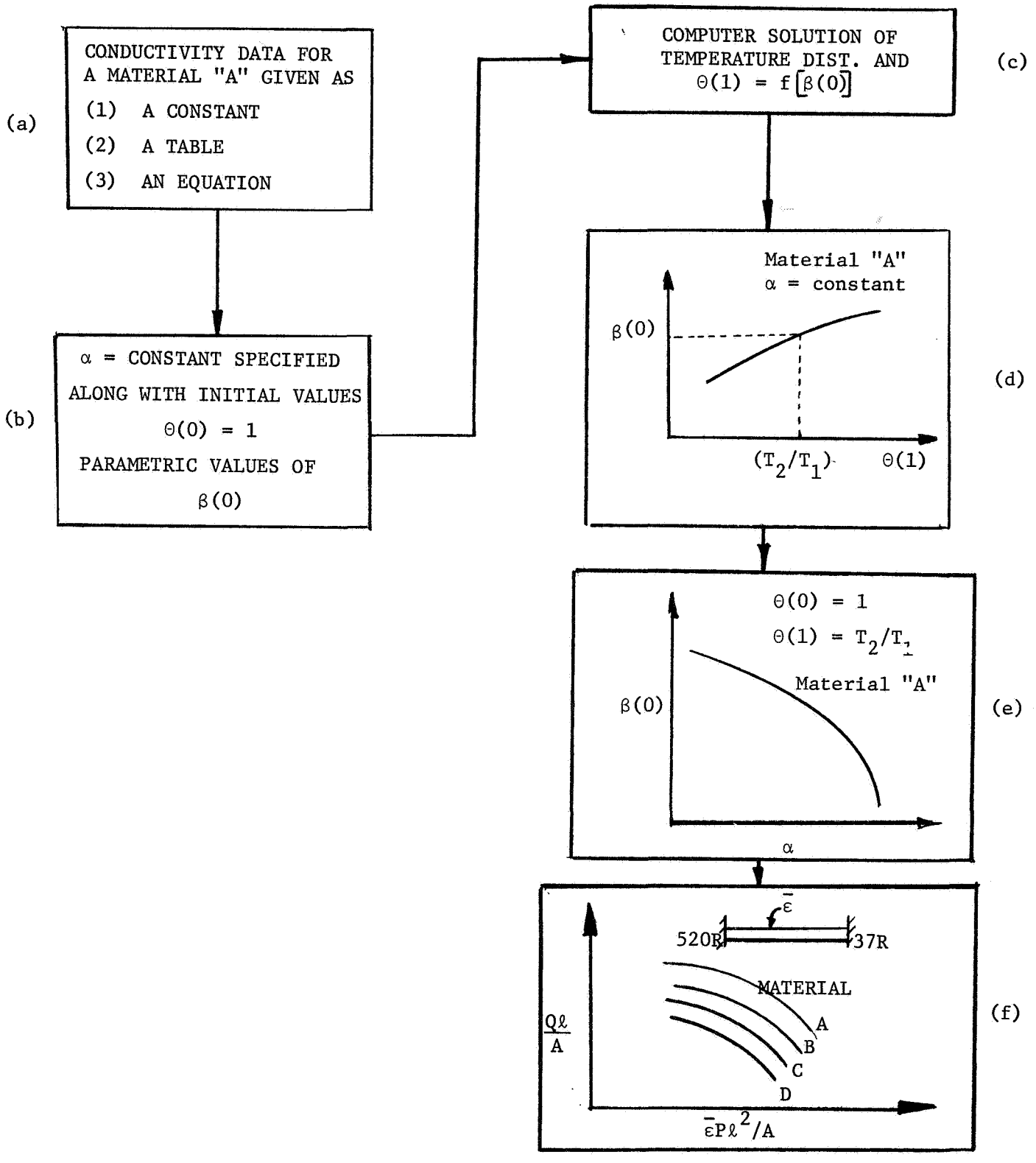

FIGURE 26 SCHEMATIC FLOW CHART OF PRELIMINARY CONDUCTIVE HEAT FLOW ANALYSIS

Q - heat flow to the LH_2 tank (Btu/hr)

ℓ - length of support (ft)

A - cross-sectional area of support (ft^2)

ε - support emittance

P - support perimeter (ft)

Thus, given the material, and the dimensions of the support and its emittance, the heat flow to the LH_2 tank is determined.

6.4 Generalized Results

Figure 27 shows a summary of the generalized plots, obtained using the procedures described above, for the five materials considered in the design of fixed and space-erected structures. The value of $\frac{\bar{\varepsilon} P \ell^2}{A}$ is determined from the effective surface emittance of the support structure and the geometry specified from the structural analysis, for a given loading condition and payload mass. Using these curves, the LH_2 boil-off due to conduction can then be evaluated from the equation:

$$W_c = \frac{nQt}{h_{fg}}$$

where n - the number of supports in the structure

Q - the heat flow to the LH_2 tank for each support (Btu/hr) obtained from Figure 27

h_{fg} - the heat of vaporization of LH_2 (Btu/lb_m)

and t - the mission time (hours)

Parametric studies, comparing the sum of the mass of the structure (radiating structural supports) plus the LH_2 boil-off due to conduction in 10,000 hours demonstrated that fiber glass and titanium were the most promising materials for fixed structures, due to thermal considerations. Also, by comparing the conduction heat leaks in radiating supports with those of insulated ($\bar{\varepsilon} = 0$), it was shown that radiating supports are very effective in minimizing the heat flow to the LH_2 tank for low thermal conductance supports.

These two points can be illustrated by referring to the previous example cited in Section 5.2 where a Warren truss having 12 supports, 3 inches in diameter, was used to support the payload. For a payload mass of 4000 lb_m, the mass of the 12 supports required to support the launch loads were shown to be less than 24 lbs. for payload-tank spacings between 0.1 to 0.4.

The LH_2 boil-off due to support conduction for this structure is presented in Figure 28. The heat flows were obtained using the

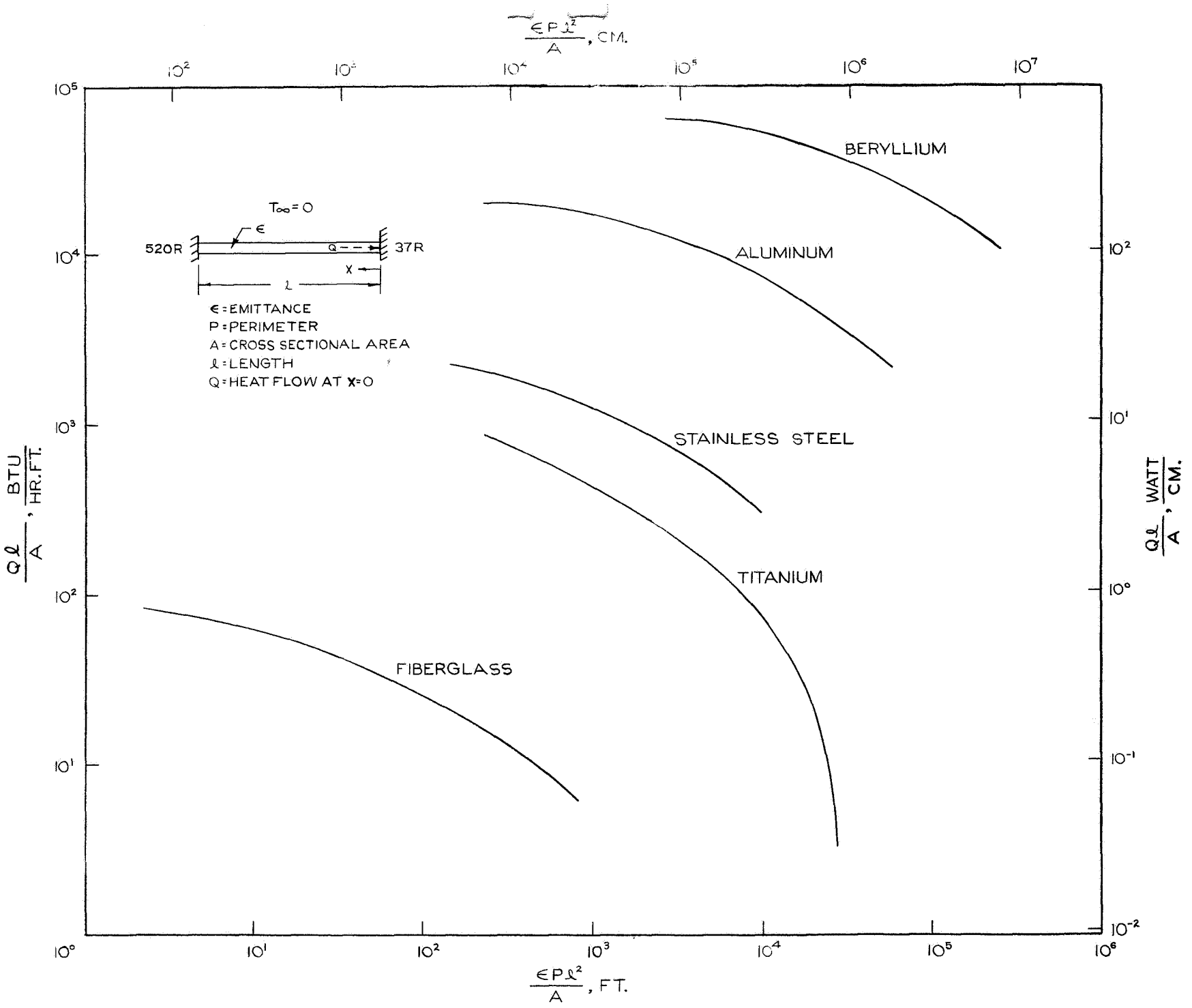

FIGURE 27 - GENERALIZED RESULTS FROM
CONDUCTIVE HEAT FLOW ANALYSIS

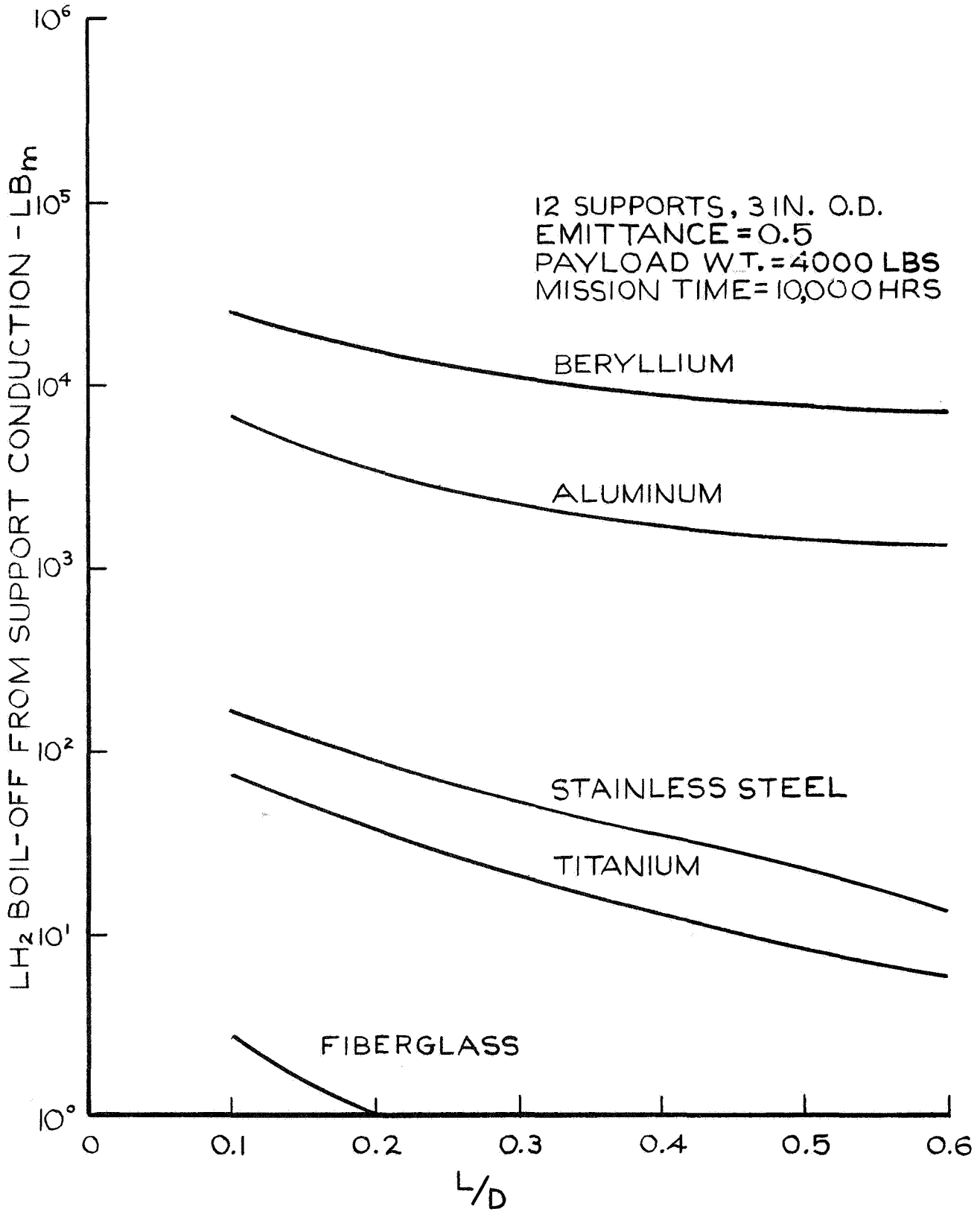

FIGURE 28 - LH_2 BOIL-OFF FROM SUPPORTS VS. L/D FOR A TYPICAL WARREN TRUSS STRUCTURE

geometries calculated from the structural analysis. The effective emittance was taken to be 0.5, and the heat leak was calculated for a mission time of 10,000 hours. The results for the LH_2 boil-off due to conduction showed that:

1) The LH_2 boil-off for a fixed fiber glass structure is very small. In this example, the boil-off is negligible at spacing ratios above 0.2.

2) The LH_2 boil-off for a fixed titanium structure is relatively large at very low spacing ratios, but is acceptable (less than 25 lbs.) at spacing ratios near 0.25 or larger.

3) The thermal performance of a fixed stainless steel structure is comparable but higher than a titanium structure.

4) Aluminum and beryllium are unsuitable as materials for fixed structures because of the large LH_2 boil-off rate for a long-term mission.

It is of interest to compare the effectiveness of radiation-cooled supports to insulated supports. We define the effectiveness as:

$$E = 1 - \frac{q_r}{q_i}$$

where q_r - heat flow to the LH_2 tank for a radiating support

q_i - heat flow to the LH_2 tank for an insulated support ($\varepsilon = 0$)

The effectiveness of radiation-cooled supports is shown in Table VII for a typical structural arrangement sized to support a payload mass of 4000 lb_m at a spacing ratio L/D = 0.2. It can be seen that the effectiveness is extremely high for low-conductance support materials. For a fiber glass structure, the heat leak to the LH_2 tank for a radiating support of $\varepsilon = 0.5$ is only 2% of that for an insulated support. For materials of high thermal conductivity radiation cooling is relatively unimportant.

The advantages of using a low-conductance structural material are two-fold: (1) as the conductance decreases, the maximum possible heat leak (when $\varepsilon = 0$) decreases, and (2) as the conductance decreases the effectiveness increases.

Vapor-cooling concepts can also be considered as a method to reduce conductive heat transfer in support structures. In such concepts the sensible enthalpy of the boil-off gas is used to cool the support.

TABLE VII

EFFECTIVENESS OF RADIATION-COOLED SUPPORTS

Support Structure: Warren ring truss with 12 supports, 3 inches in diam. L/D = 0.2
Payload mass = 4000 lbs.
Mission time = 10,000 hrs.

Support Material	$\bar{k}^*$ $\left(\frac{BTU}{hr ft °R}\right)$	A $\left(in^2\right)$	LH_2 Boil-off (lb_m)		Effectiveness E
			Insulated Supports $\varepsilon = 0$	Uninsulated Supports $\varepsilon = 0.5$	
Fiberglass	0.22	0.320	43.6	0.8	.98
Titanium	3.17	0.160	319.4	37.5	.88
Stainless Steel	6.36	0.121	484.8	80.5	.83
Aluminum	47.60	0.204	6,109.5	3,321.8	.46
Beryllium	150.00	0.176	16,623.9	14,226.2	.14

* $\bar{k} = \frac{1}{483} \int_{37}^{520} k(T)\,dT$

and is shown only to compare the relative magnitudes of the thermal conductivities. The variation of thermal conductivity with temperature, k(T), was used to compute the values of boil-off.

A simplified analysis used to determine the effectiveness of using the sensible enthalpy of the LH_2 boil-off to cool an insulated support is presented in Appendix I. The analysis assumed infinite thermal coupling between the support and GH_2 coolant gas. The maximum effectiveness of vapor cooling was calculated to be approximately 0.68. Therefore, in the fixed structure previously described radiation cooling is more effective than vapor cooling of either titanium or fiber glass supports. The effectiveness of vapor cooling in reducing the heat leak in radiating supports will be presented in a following section of this report.

7.0 SELECTION OF CONCEPTUAL DESIGNS

7.1 General

The results of the structural analysis and the preliminary analysis of heat flow via radiation and conduction for "no" interactions between the shields and support structure were used to determine the "near-optimum" (based on system mass) configurations for the final analysis. The selection of payload-tank spacings for various concepts was made by combining the results of two separate studies which were used to determine: 1) the minimum mass of the structure plus conduction boil-off vs. L/D for fixed and space-erected structures of various materials and geometries, and 2) the minimum mass of shields plus radiation boil-off vs. L/D for shadow shield configurations.

The fixed structures were optimized using fiber glass and titanium Warren-truss structures, since these proved to be the most promising materials from the system mass standpoint (especially from considerations of LH_2 boil-off due to conduction effects). A system with a space-erected structure was optimized considering an "A"-frame concept since a preliminary analysis showed this to be more promising than "STEM" or concentric tube concepts on the basis of torsional stiffness-to-mass ratio and reliability potential.

The optimization of the fixed and space-erected structures was made using the maximum payload mass (4000 lb_m) and an effective surface emittance of 0.5 for the truss supports. In the following discussions, the boil-off of LH_2 will be presented for various numbers of "intermediate" shadow shields. It is assumed for practical reasons that there will be two additional shields, one located at the payload attach ring and one at the tank. Thus, the total number of shields is N + 2 where N is the number of intermediate shields. In addition, the shield at the payload was assumed to be in contact with the payload and to have a uniform temperature of 520R. This conservative assumption was used throughout this study. The following sections outline the methods used to select conceptual designs and contain a detailed description of the six concepts selected for final evaluation.

7.2 Systems with Fixed Structures

7.2.1 Shield Mass and Boil-off Mass due to Radiation

The results of the preliminary analysis of radiant heat flow were combined with mass estimates of shield systems to project system masses (LH_2 boil-off mass plus shield mass) as a function of L/D ratio according to the following equation:

$$W_s = A + (B)\ N + \frac{Q_r\ t}{h_{fg}}$$

where W_s - system mass (shields plus LH_2 boil-off) (lb_m)

A - 5.2 = mass of the shields on the payload and tank support (lb_m)

N - number of intermediate shadow shields

Q_r - radiant heat flow to the LH_2 tank, a function of L/D, N, and surface optical properties (Btu/hr)

t - mission time (hours)

h_{fg} - latent heat of vaporization of LH_2 (Btu/lb_m)

B - 5 = unit mass of an intermediate shield (includes shield material, support ring, etc.) (lb_m)

The mass of the shadow shields were estimated for shields comprising two layers of 1/2-mil aluminized polyester film with a nylon fabric reinforcement sandwiched between the polyester films. The shield mass also includes the support rings used to pretension the shields, grommets and lacing, etc.

The sum of the LH_2 boil-off mass and shield mass was calculated as a function of L/D and N - the number of intermediate shields - for both diffusely and specularly reflecting shields of 0.03 emittance. The system mass corresponding to the higher of the two computed boil-off rates is plotted in Figure 29.

For systems of two or more intermediate shields, the "diffuse" values exceeded the "specular" values until the computed boil-off mass for both cases was a small fraction of a pound. For a single intermediate shield system and spacing ratios greater than 0.3, the specular values were about one or two pounds greater than the diffuse values.

It is interesting to note (from the flat portions of the curves) that the shield mass is the major component of the system mass for systems of two or more shields at spacing ratios greater than 0.4. Furthermore, although a three-shield system is more efficient thermally than a two-shield system at any spacing ratio, the overall

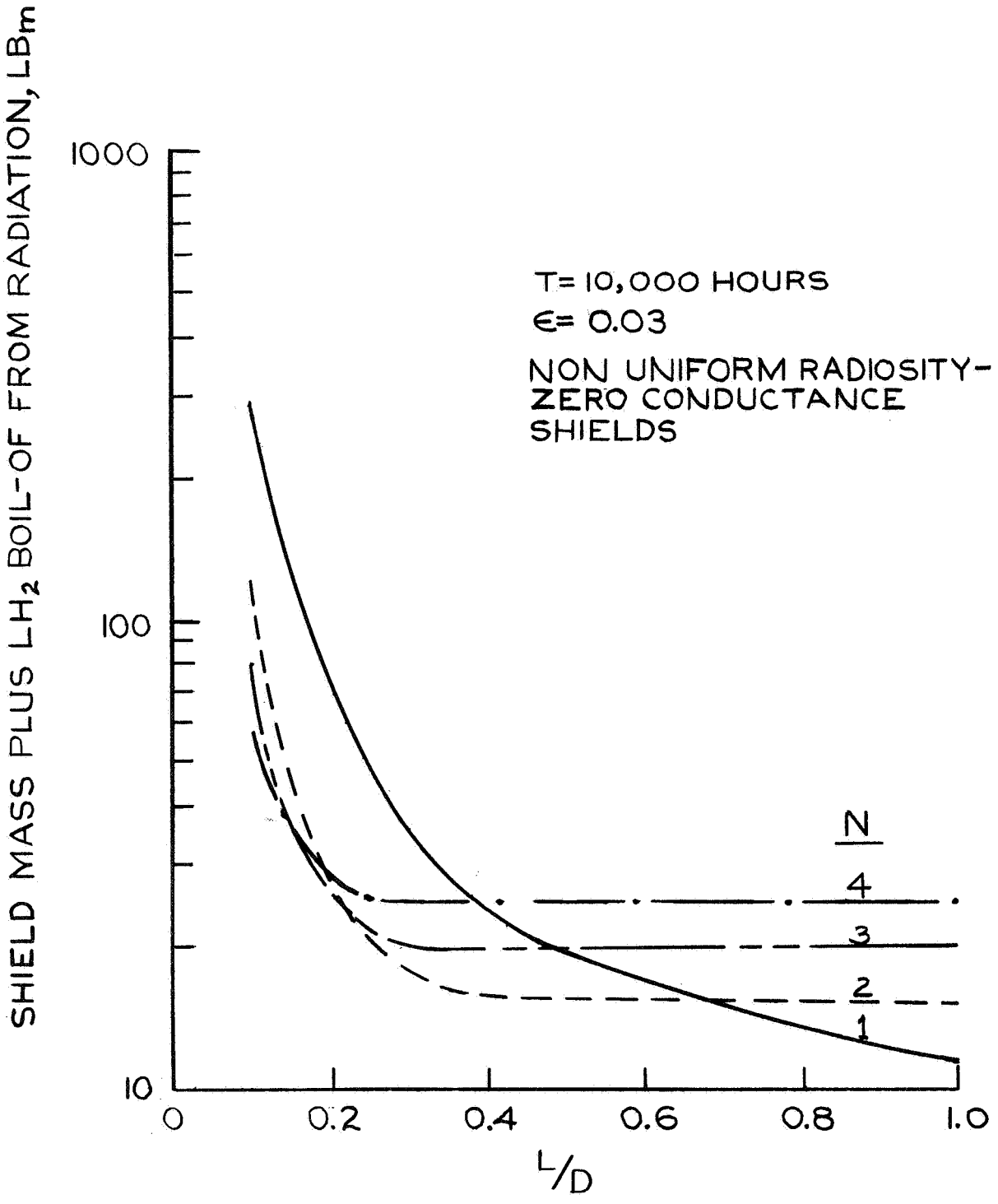

FIGURE 29 - SHIELD MASS PLUS RADIATION BOIL-OFF VS. L/D FOR VARIOUS SHADOW SHIELD SYSTEMS

mass of the two-shield system is lower for spacing ratios greater than 0.2 because the boil-off mass is small compared to the shield mass.

The table below lists the systems which have the lowest overall masses at various spacing ratios.

L/D	Optimum Number of Intermediate Shields
0.10 to 0.15	4
0.15 to 0.20	3
0.20 to 0.70	2
> 0.70	1

The systems for final evaluation were selected using the minimum value of mass on Figure 29 at each L/D and the results from analyses of the structural mass and the LH_2 boil-off due to conduction in the supports. When approximately the same total system mass existed for two systems (of different numbers of shields) at a given spacing ratio, the system with the lower value of shield mass was chosen, since the consideration of ground-hold and orbital insulation will further reduce the heat flow.

Although the calculations of radiant heat flow have been made with a somewhat conservative model, the results do indicate that lightweight shadow shield systems for reducing boil-off due to radiant heat leaks can be obtained for a large range of spacing ratios.

7.2.2 Support Mass and Boil-off Mass due to Conduction

Parametric studies were also conducted for fiber glass and titanium fixed structures to optimize the sum of the mass of the supports plus the LH_2 boil-off due to conduction heat transfer. The system mass in this case is:

$$W_{sr} = \rho n A \ell + \frac{n\, Q_c\, t}{h_{fg}} \qquad (1)$$

where ρ - material density (lb_m/ft^3)

n - number of supports

A - cross-sectional area of each support (ft^2)

ℓ - length of each support (ft)

Q_c - conduction heat flow to the LH_2 tank from each support

Figure 30 shows the combined structural mass for a number of fiber glass trusses as a function of L/D. In the case of fiber glass, almost all the mass is due to the supports - the boil-off mass reached a maximum of 2 lbs. at low spacing ratios for a 10,000-hour

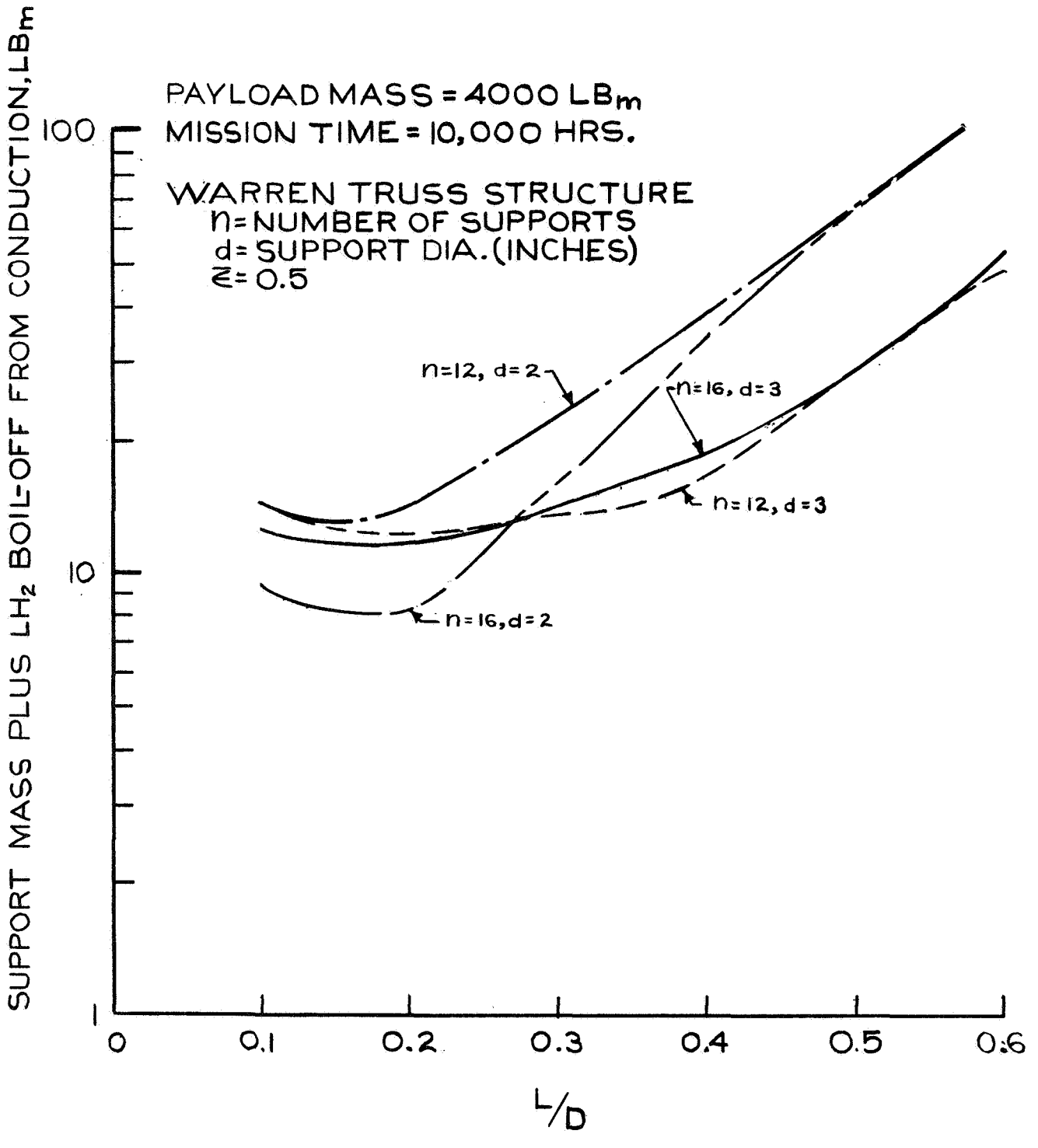

FIGURE 30 - SUPPORT MASS PLUS LH_2 BOIL-OFF FROM CONDUCTION VS. L/D FOR FIBERGLASS FIXED STRUCTURES

mission. Fiber glass is quite attractive from a mass standpoint for consideration in fixed structures, where a short payload-tank spacing is desirable. The support plus conduction boil-off masses for the designs shown are less than 10 lbs. for spacing ratios between 0.1 and 0.25 and less than 30 lbs. up to a spacing ratio of 0.5. As shown in Figure 31, the trade-offs at low spacing ratios were more sensitive for titanium trusses because of the stronger influence of the conduction boil-off. The mass penalties of titanium structures exceed those of fiber glass at low spacing ratios. However, they can be considered for fixed structures since the support mass plus LH_2 boil-off is approximately 30 lb_m at spacing ratios between 0.25 and 0.60.

7.2.3 Optimization of Concepts with Fixed Structures

Figures 32 and 33 present a measure of total system mass vs. L/D for systems with fixed structures of fiber glass and titanium, respectively, and also illustrate the magnitudes of the various components making up the system mass.

The minimum system masses for systems with a fiber glass structure occurred at spacing ratios between 0.2 and 0.4. The system mass increased below 0.2 because of the increase in the radiation boil-off at low spacing ratios, and increased above 0.4 because the structure mass rapidly increases due to satisfying the structural criteria for column stability.

Fiber glass structures for conceptual designs were selected with a spacing ratio as low as 0.15 because the system mass in this region will be reduced by an improved radiation boil-off when ground-hold and orbital insulations are included in the final analysis.

The system mass vs. L/D with a titanium structure, illustrated in Figure 33, shows a gradual decrease with increasing spacing ratio, reaching a minimum near L/D = 0.3, and remaining relatively constant up to L/D = 0.6. Systems with titanium-fixed structures were chosen with a spacing ratio of 0.25 since it was desired to minimize the payload-tank spacing, and it was expected that the thermal resistance of the tank support would reduce the conduction boil-off.

7.3 Space-Erected Systems

Three concepts for space-erected structures were evaluated structurally in a previous section. This evaluation showed that the "A"-frame concept was more promising than the "STEM" or concentric tube concepts from the standpoints of torsional stiffness-to-mass ratio and reliability potential. This section deals with the considerations in optimizing a system with an "A"-frame structure and determining the payload-tank spacing in the deployed configuration.

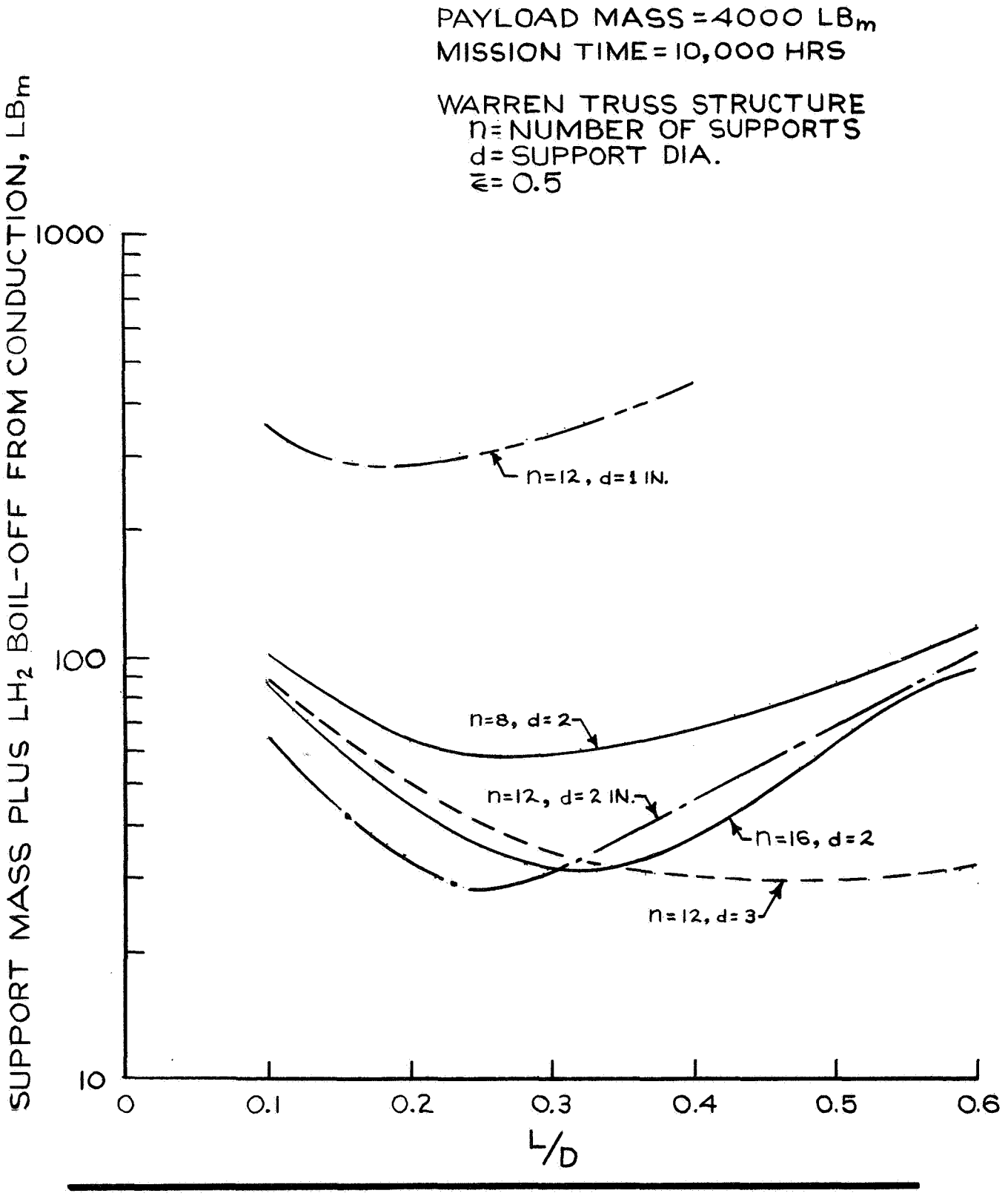

FIGURE 31 - SUPPORT MASS PLUS LH_2 BOIL-OFF FROM CONDUCTION VS. L/D FOR FIXED TITANIUM STRUCTURES

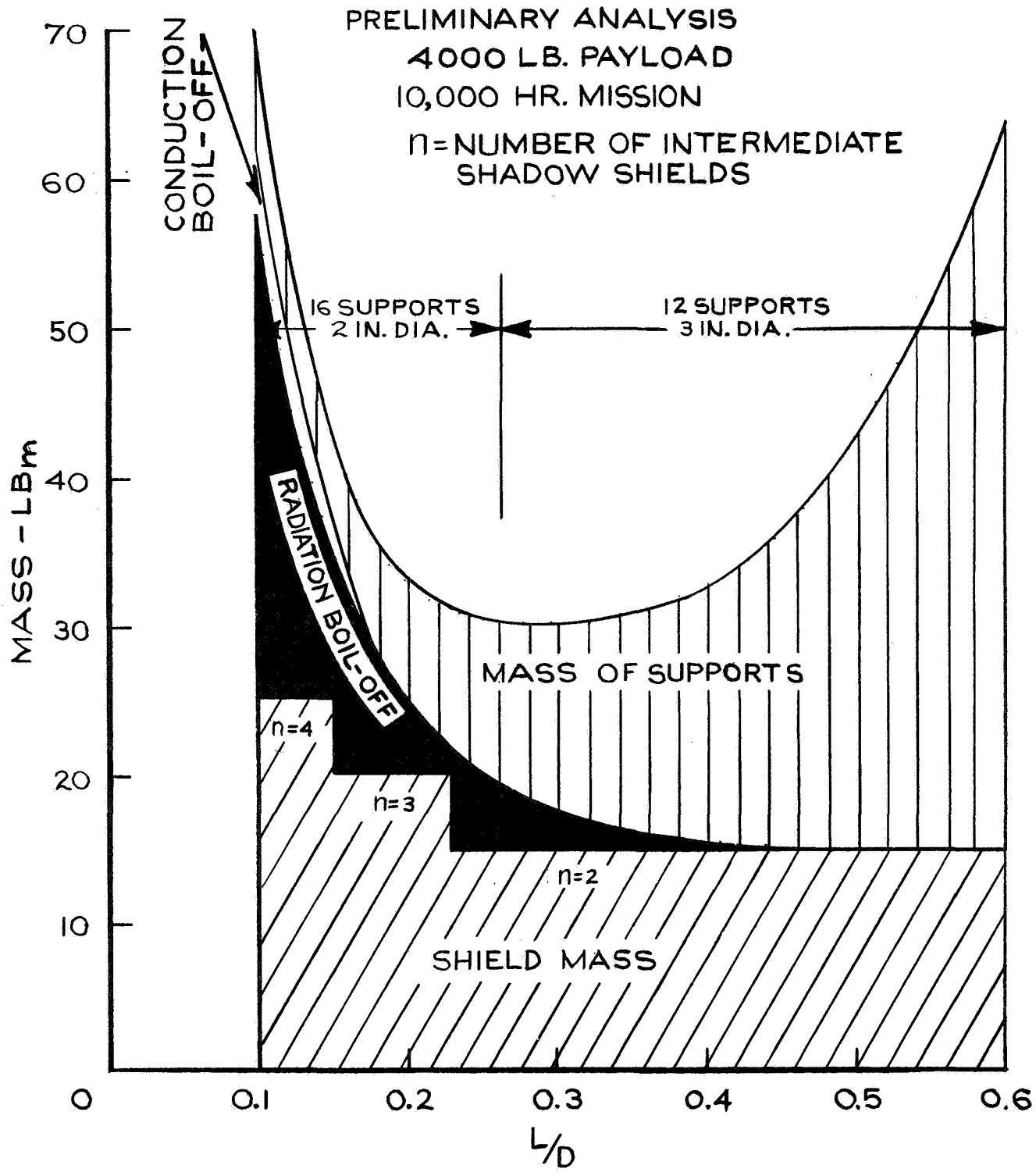

FIGURE 32- OPTIMIZATION OF SHADOW SHIELD SYSTEMS WITH FIXED FIBERGLASS STRUCTURES

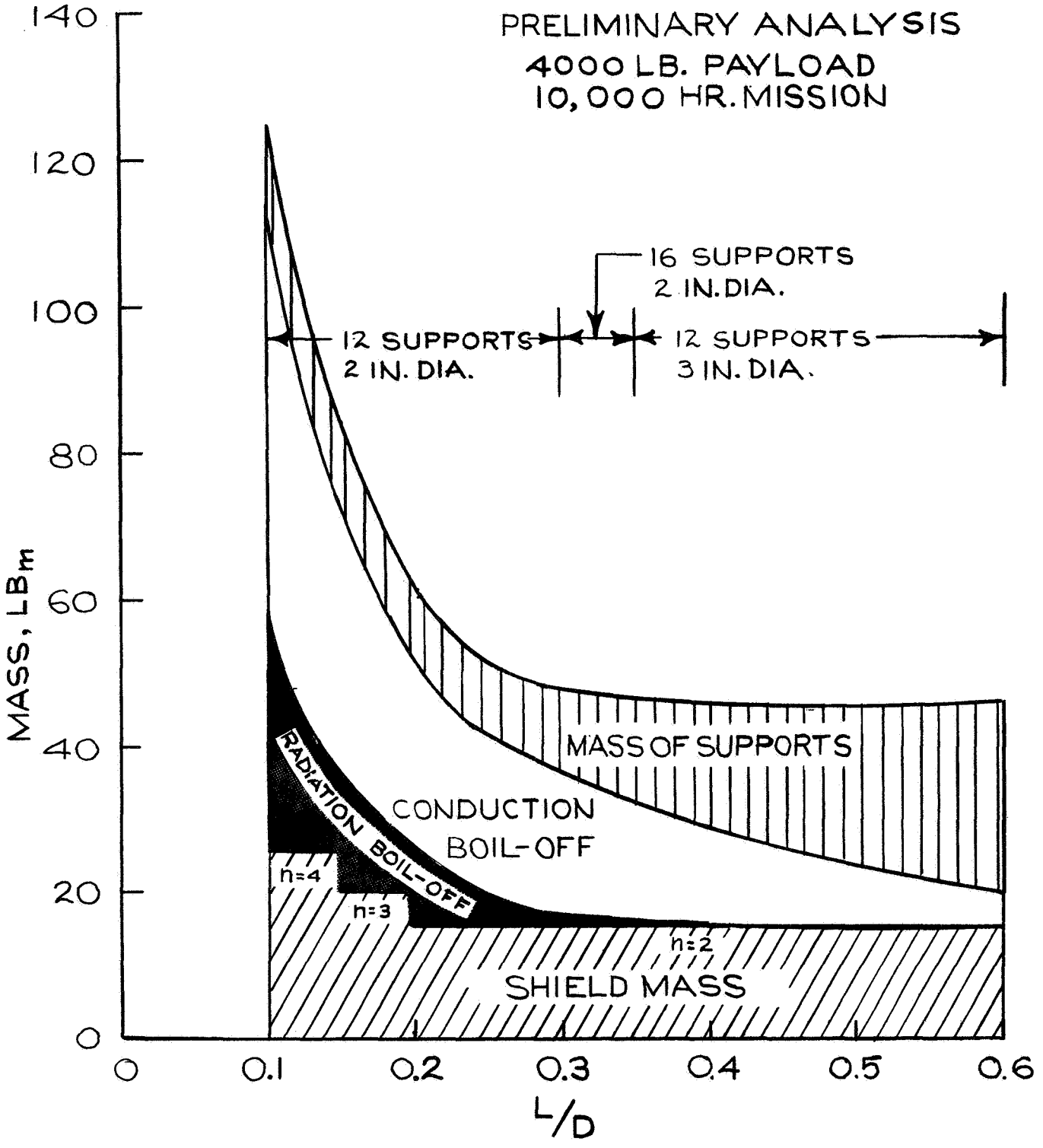

FIGURE 33 - OPTIMIZATION OF SHADOW SHIELD SYSTEMS WITH FIXED TITANIUM STRUCTURES

First, a comparison of the sum of the mass of the supports plus the conduction boil-off was made for the five structural materials considered for "A"-frame structures. Figure 34 illustrates that titanium is most suitable from the overall mass standpoint, although stainless steel and fiber glass structures exhibit nearly the same performance. The mass of the supports alone was approximately the same for all the materials, running from 7 lbs. at a spacing ratio of 0.1 to approximately 20 lbs. at a spacing ratio of 2.0. The higher system mass of the aluminum and beryllium "A"-frame structures was due to considerations of conduction heat transfer.

A measure of the total mass of a shadow shield system with an "A"-frame erectile structure is shown in Figure 35 as a function of L/D and the number of intermediate shadow shields. The total mass is relatively constant for spacing ratios beyond 0.5 so that the selection of a payload-tank spacing was not critical from the standpoint of mass, nor was it important from the standpoint of minimizing the shroud length, since this structure is erected in space.

A concept was chosen with an L/D of 1.0, since in this range only one shadow shield is required. The use of a single intermediate shield simplifies the mechanical operation of the system and improves reliability.

7.4 Selected Concepts for Final Evaluation

7.4.1 General Discussion

The following discussion describes the configuration of a typical cryogenic upper stage and the application of shadow shield concepts for long-term thermal protection. A typical kick stage which might be used in conjunction with an Atlas-Centaur or Saturn IB - Centaur launch vehicle is presented in Figure 36. The kick stage shown consists of a shadow-shielded LH_2 tank, insulated for ground-hold and orbital thermal protection, a payload support structure, and another structure supporting the LH_2 tank, oxidant tanks, etc. The study of shadow shield concepts included the design, analysis and evaluation of systems comprising:

- Payload support structure (fixed or space-erected)
- Ground-hold and orbital thermal protection system
- Shadow shields located between the sun-oriented payload and the LH_2 tank

The thermal analysis of shadow shield systems was restricted by contract to considerations of the heat transfer from the

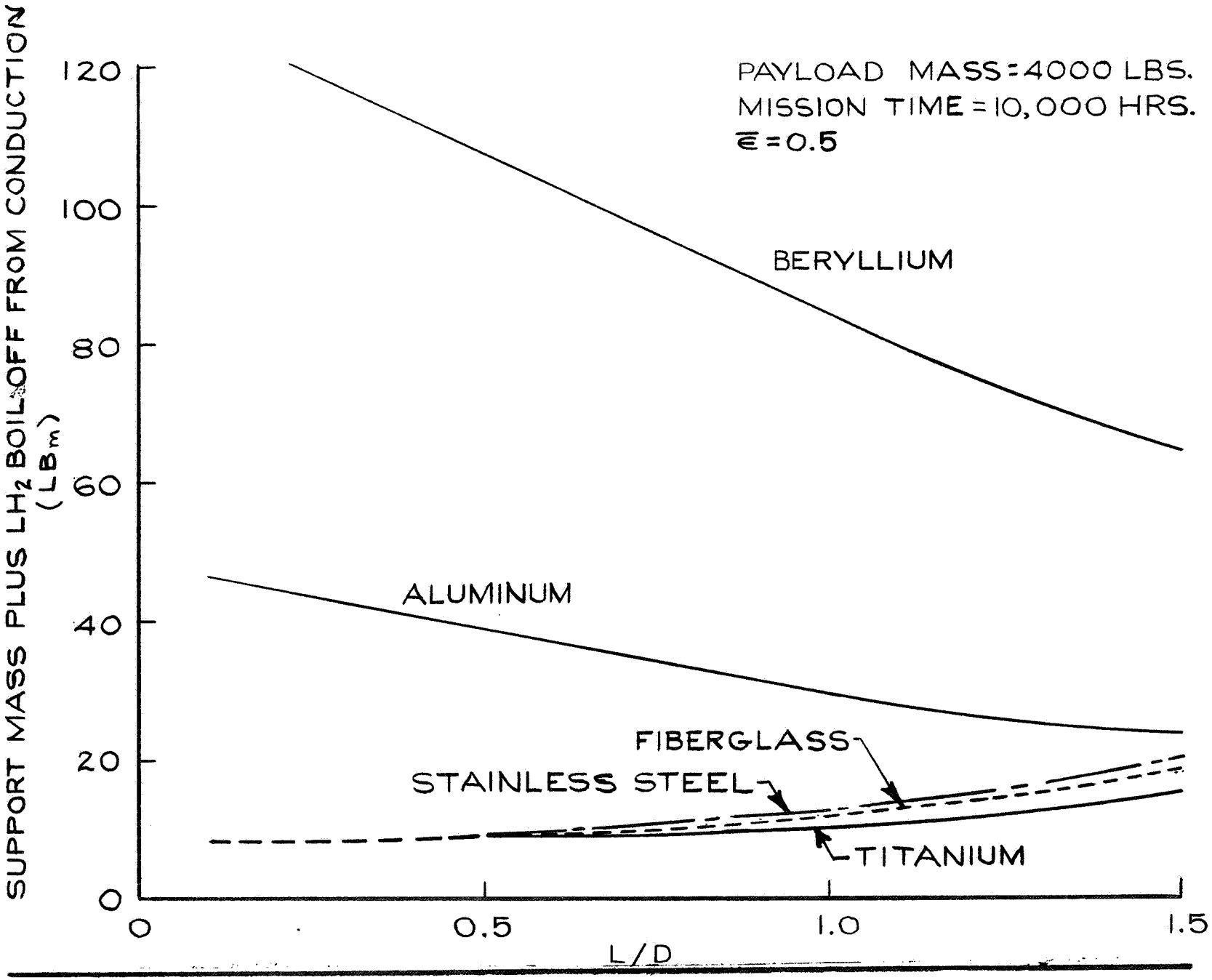

FIGURE 34 - SUPPORT MASS PLUS LH_2 BOIL-OFF FROM CONDUCTION VS. L/D FOR "A"-FRAME ERECTILE STRUCTURES OF VARIOUS MATERIALS

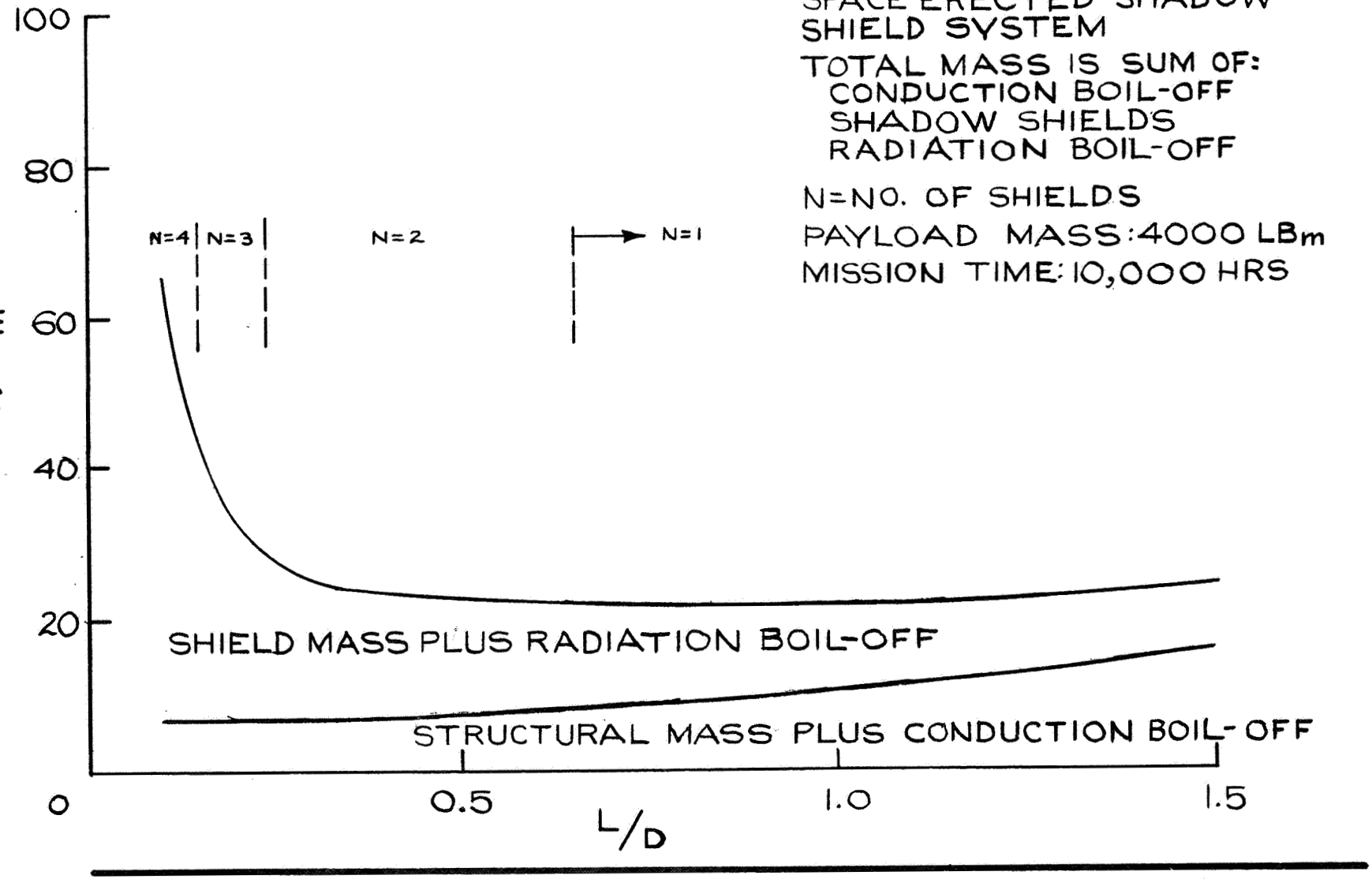

FIGURE 35 – OPTIMIZATION OF A SHADOW SHIELD SYSTEM WITH AN "A"-FRAME ERECTABLE STRUCTURE

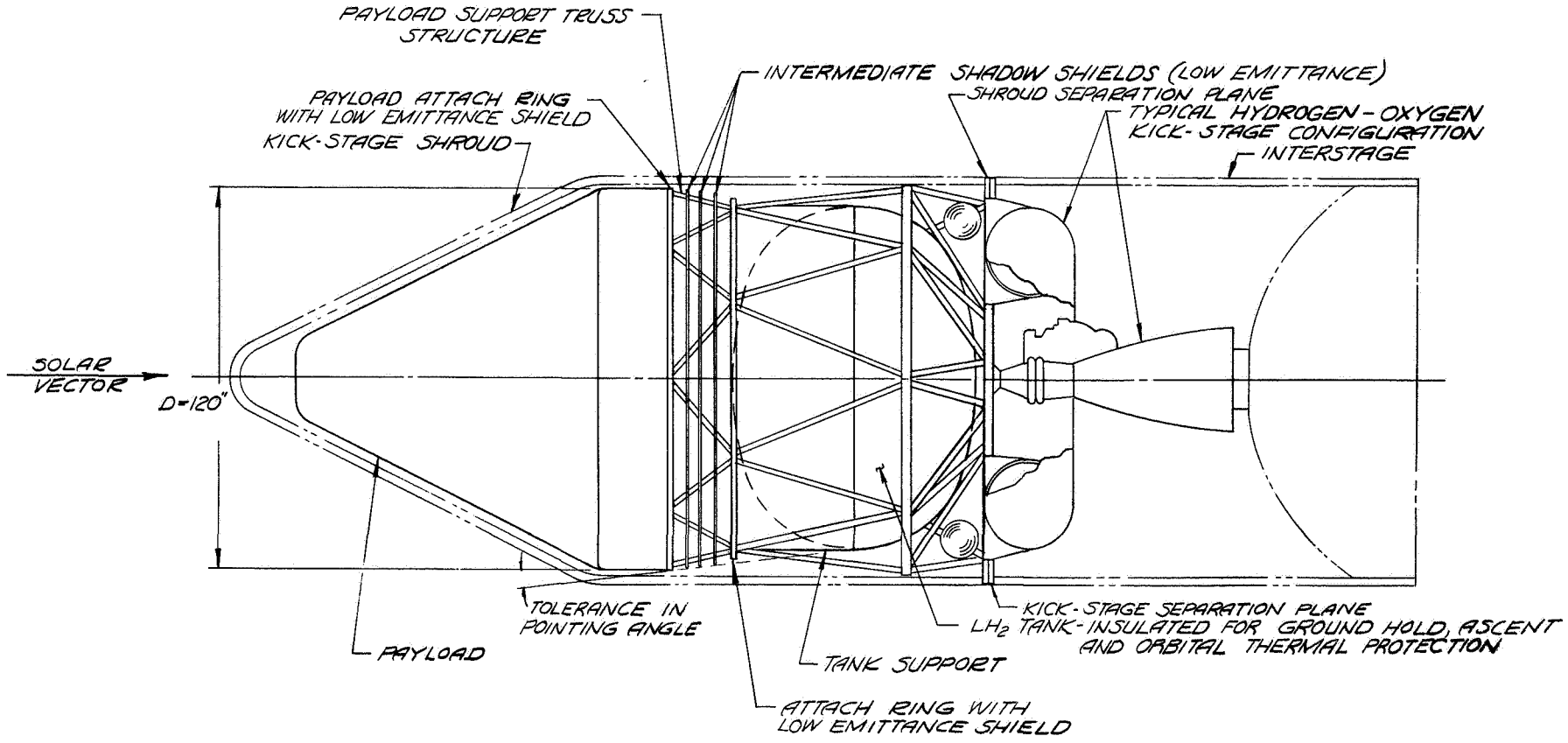

FIGURE-36
SHADOW-SHIELDED LH_2 TANK
WITH TYPICAL "KICK-STAGE" CONFIGURATION

payload to the LH_2 tank by conduction heat transfer along the structure and radiation transfer through the shadow shield system. The effects of other structures required to support the engine, LOX tanks, etc., were not considered in the analyses and design calculations presented in this report.

For the "fixed-structure" shadow shield configurations applied to a 10'-diameter payload and 9'-diameter LH_2 tank, there exists an allowable tolerance in pointing angle. This angle is defined by the intersection of the solar vector and a line connecting the extremities of the payload and LH_2 tank, and the angle is a function of the spacing ratio. The present study was restricted to the analysis of shadow shield systems where the attitude control system was assumed capable of maintaining the payload orientation within this allowable angle thus preventing solar energy from falling on the shields or LH_2 tank. It will be shown that a 10' payload and 9' tank provide considerable latitude in the allowable pointing error for the reasonably small payload-to-tank spacing ratios used in the final design concepts.

A misalignment from the solar vector within the noted tolerance in pointing angle does not, however, preclude solar radiation from being absorbed by the kick-stage structure supporting the engine, etc., and being transmitted to the LH_2 tank by conduction. The actual allowable error for any kick stage will depend upon the detailed configuration of the oxidant tanks, location and diameters of the aft ring and supports. In general, these structures could be suitably arranged behind the LH_2 tank to prevent solar radiation from directly impinging on their surfaces.

The shadow shield concepts which were selected for final analysis and evaluation are described in the following paragraphs. A breakdown of the masses of the shadow shield assemblies and the payload support structures for each concept is presented in Section 12.0.

The tank support, connecting the payload support structure and the LH_2 tank, and the ground-hold and orbital insulation systems are common to all the shadow shield concepts and will be discussed in detail in Sections 8.0 and 9.0, respectively.

7.4.2 Concept 1 - Fixed Fiber Glass Structure, Fixed Shields

The general arrangement of Concept 1 is shown in Figure 37. The LH_2 tank is spaced 18 inches from the payload by a "fixed" Warren truss structure composed of 16 fiber glass tubular supports 2" OD by .030" wall. In this concept, and in the following concepts, a low-density foam insulation (foam-in-place) is used inside the structural supports to eliminate radiant transfer from the payload to the LH_2 tank via reflections within the tubes.

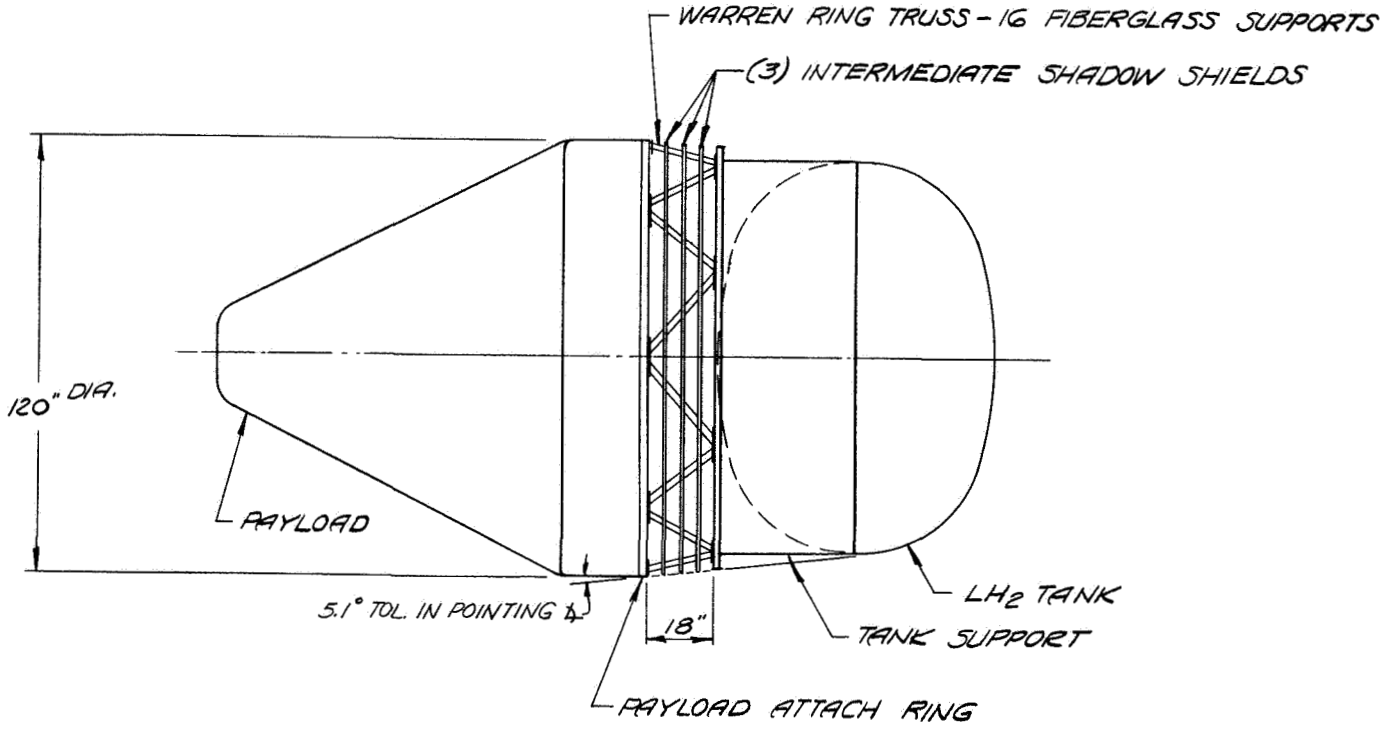

FIGURE-37
CONCEPT-1
FIXED STRUCTURE, FIXED SHADOW SHIELDS
$L/D = 0.15$

The LH_2 tank is shielded from the payload by five low-emittance shields, including three equally spaced intermediate shadow shields, a shield on the payload support ring and a shield near the LH_2 tank attached to the cylindrical side of the tank support. A ground-hold and orbital insulation system is provided on the LH_2 tank.

A detailed view of the shadow shields and structural interface is shown in Figure 38. Each intermediate shadow shield consists of a single low-emittance assembly. The shield material shown is composed of two layers of 0.5-mil aluminized polyester film bonded to a nylon fabric (120 x 120 count, ripstop weave).* The edges of the shield are reinforced by an overlap area, and the shield is tensioned and laced to any angular-type support ring. The support rings are rigidly mounted to each structural support by bolted connections to a fiber glass mounting bracket attached to the supports. Therefore, each shadow shield is connected to the support structure at 16 locations. The cutaway areas of the shields are reinforced and covered by a "boot" to prevent stray radiation from the payload from reaching the lower temperature shields.

Figure 38 also illustrates the manner in which the structural supports are mounted to the attach ring on the conical tank support. (The arrangement is similar at the interface between the structural supports and the payload.) Near the end connections, the wall thickness of the supports is increased and flanges are provided for interconnection. A split ring is used to mount the supports to the attach ring.

The tubular supports are selectively coated with thermal control coatings to improve the thermal performance of the shadow shield system. The preliminary analysis of conduction heat transfer in support structures demonstrated that radiation cooling significantly reduced the LH_2 boil-off due to conduction heat transfer. The portion of the support surface viewing outer space has a high-emittance coating (black paint) to enhance the loss of heat by radiation, and that portion directly viewing the shields, (i.e., directed towards the center of the shadow shield system) has a low-emittance coating to minimize radiative coupling with the payload and the shadow shields.

The structural supports of the shadow shield concepts are assumed to be coated with "black" paint ($\varepsilon \doteq 0.95$) over approximately 50% of their circumference and coated to have a low emittance ($\varepsilon \doteq 0.03$) over the remainder. Thus, the average emittance is approximately 0.5.

---

* This material is similar in construction to GT-76, a laminate manufactured by G. T. Schjeldahl Co., Northfield, Minn. The GT-76 laminate is composed of one layer of 0.5-mil aluminized polyester film bonded to a nylon fabric.

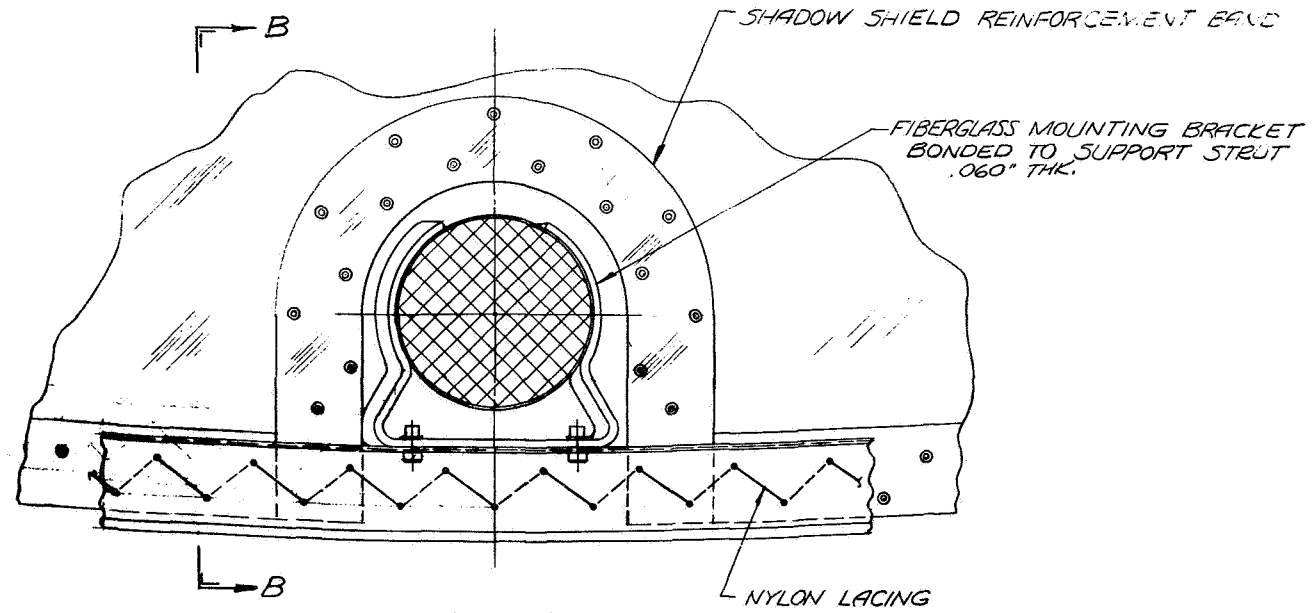

PLAN A-A
(WITHOUT BOOT)

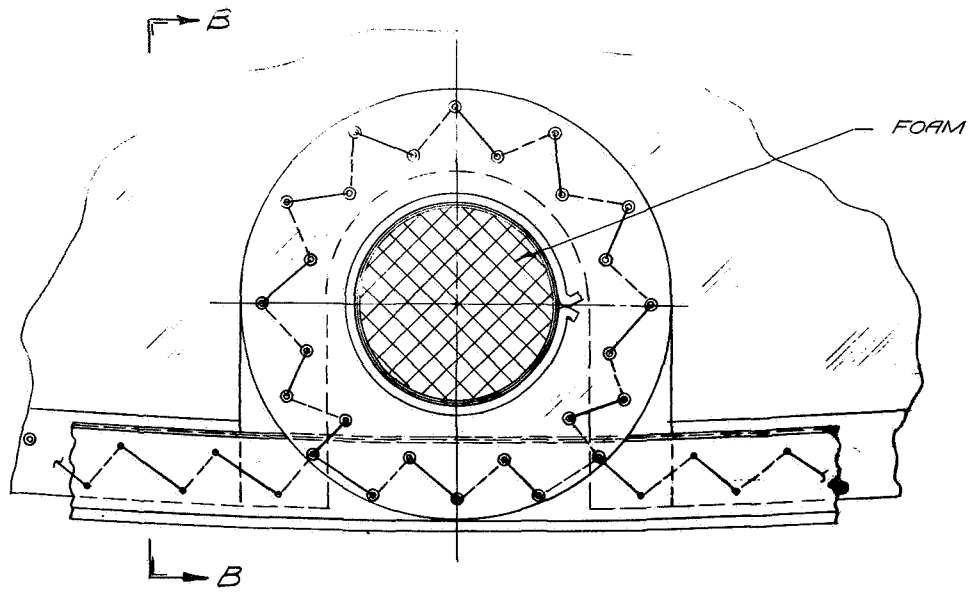

PLAN A-A
(WITH BOOT)

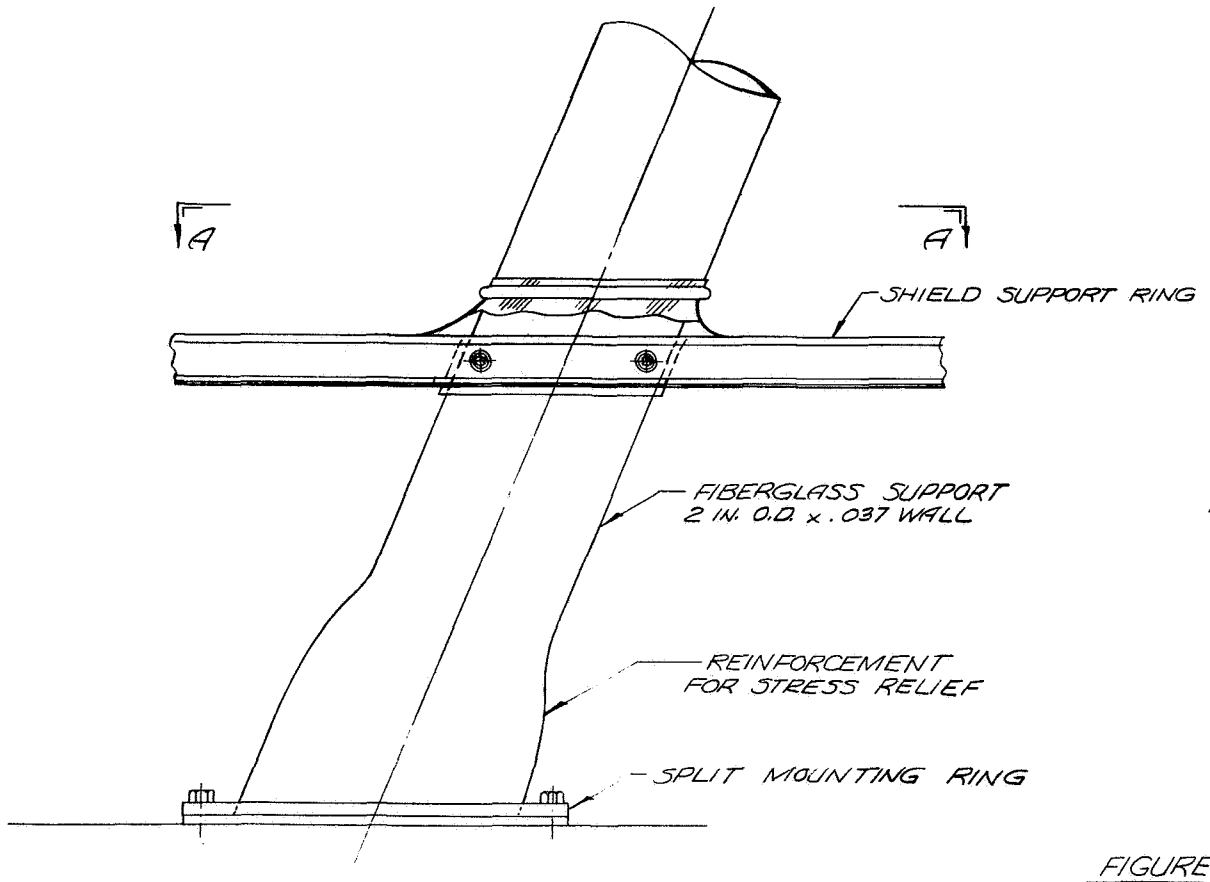

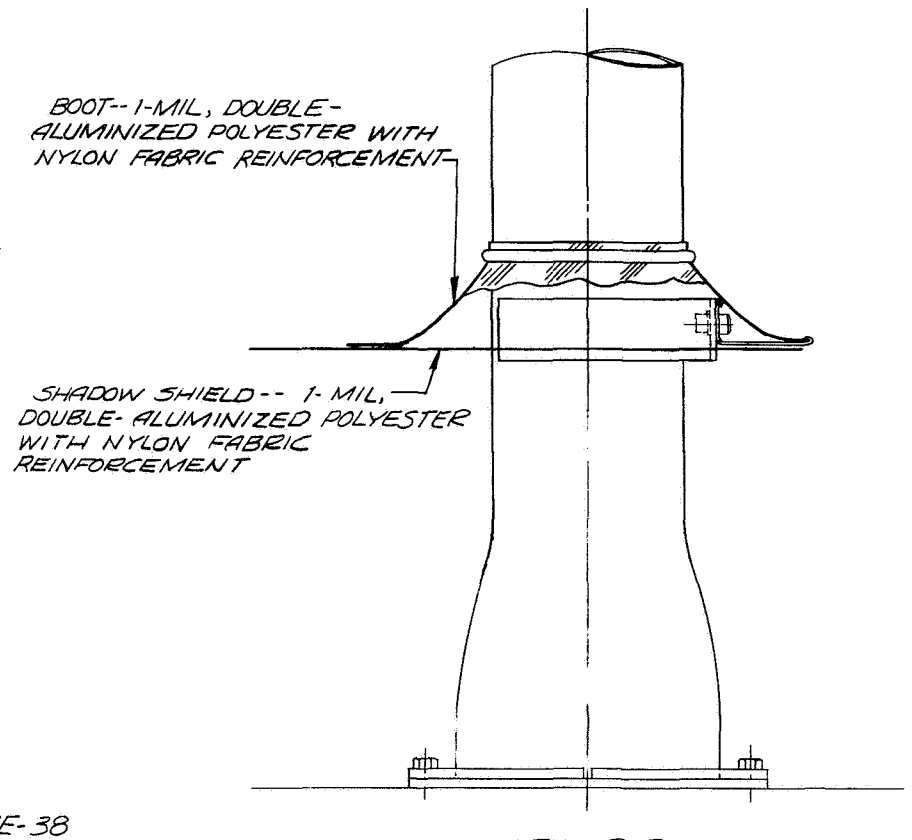

VIEW B-B

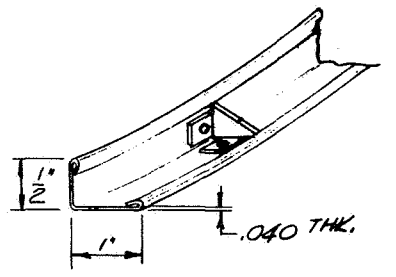

TYPICAL SECTION
SHIELD SUPPORT RING

FIGURE-38
SHADOW SHIELD AND STRUCTURE MOUNTING DETAIL - CONCEPT - 1

7.4.3 Concept 2 - Fixed Titanium Structure, Fixed Shields

Figure 39 illustrates the assembly of a shadow shield concept with a fixed titanium structure and a tank-spacing distance of 30 inches (or a spacing ratio of 0.25). The fixed structure is a Warren truss with 12 titanium supports, 2" OD x .017" wall. The assembly details of the shadow shields are similar to that of Concept 1, except that the support-shield mounting brackets are made of titanium. A detail of the end connections for the structure is shown in Figure 41.

In this concept 4 shadow shields (single sheets) are utilized. Two of the four shields are equally spaced between the LH_2 tank and payload, and the other two shields are located in the plane of the payload attach ring and the tank support ring, respectively.

This concept is similar to Concept 1. The only differences are in the number of shields, payload-tank spacing, and the size and materials used in the support structure.

7.4.4 Concept 3 - Fixed Titanium Structure with Vapor-Cooled Supports, Fixed Shields

A fixed structure with vapor-cooled supports is illustrated in Figures 40 and 41. In this concept the titanium structure is radiatively cooled and, in addition, the gaseous H_2 vapor venting from the storage tank (due to radiation and conduction heat transfer) is also used to cool the supports. A 1/8" OD tubing line is attached to the structural supports to provide an effective method for transfer of heat from the supports to the resulting boil-off vapor.

This concept is similar to Concept 2 (same structure, shield configuration, etc.) except for the addition of the vapor-cooling line. This concept was selected for analysis because of the inherent potential of vapor cooling to reduce conductive heat flow.

7.4.5 Concept 4 - Fixed Titanium Supports with Pant-Leg Radiators, Fixed Shields

A concept for passively cooling the structural supports by use of additional radiating surface is shown in Figures 42 and 43. "Pant-leg" radiators are attached to the structural supports near the second shadow shield and extend along the remaining portion of the support to the attach ring on the structural support. The pant-leg radiator is fabricated from 8-mil aluminum in order to provide an effective extended surface radiator. The external surface of the radiator has a thermal control pattern identical to the structural supports - an average emittance of 0.5. However, the entire inner surface of the radiator and the external surface of the support structure enclosed by the radiator have low-emittance surfaces to reduce radiation transfer between the radiator and the support.

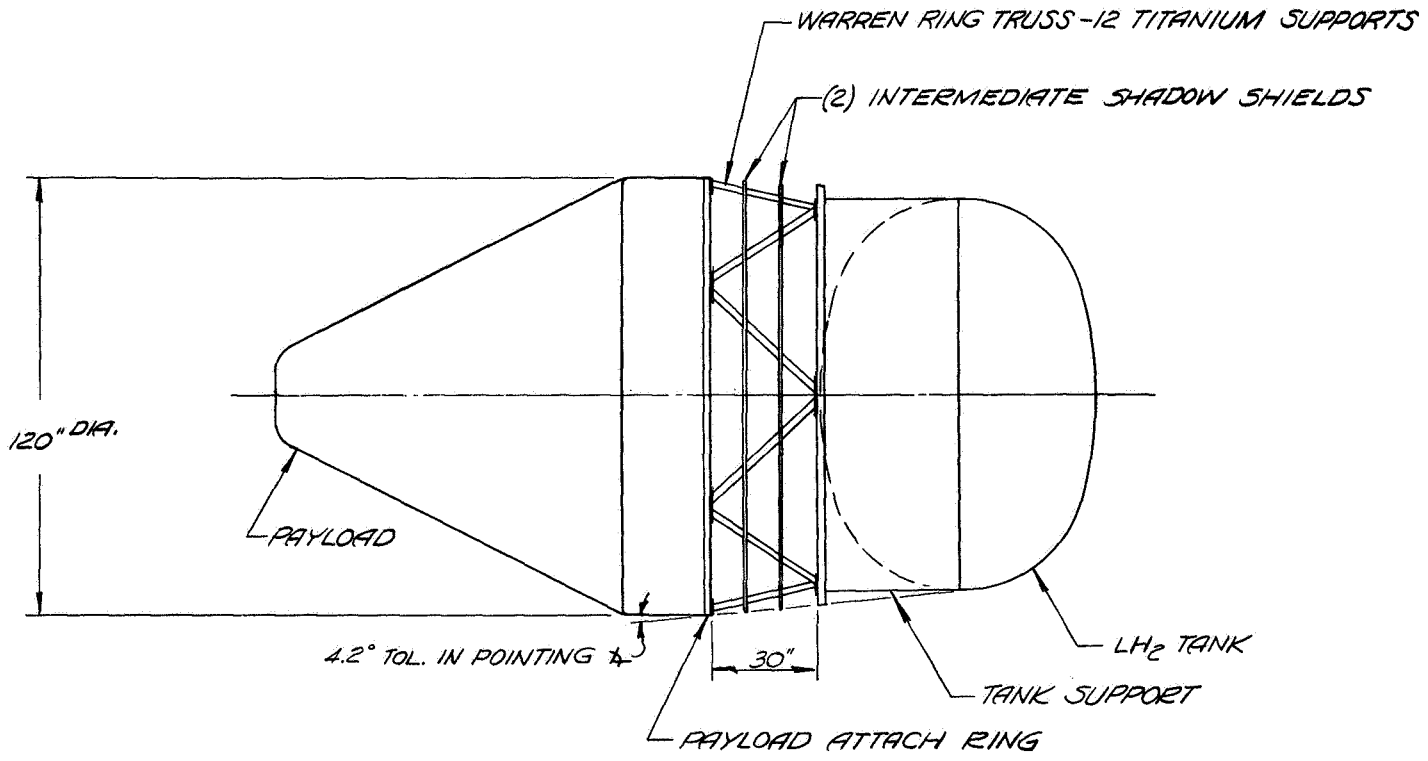

FIGURE-39
CONCEPT - 2
FIXED STRUCTURE, FIXED SHADOW SHIELDS
$L/D = 0.25$

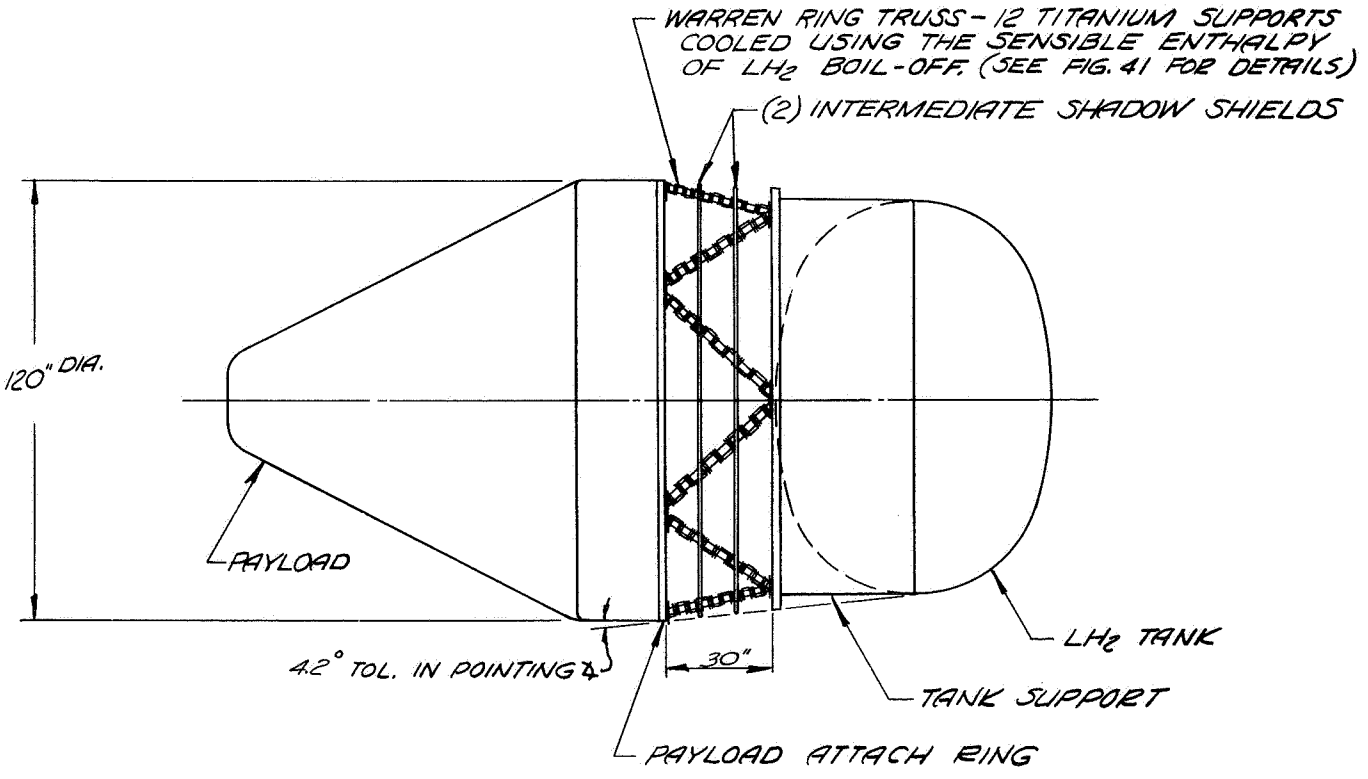

FIGURE-40
CONCEPT - 3
FIXED VAPOR-COOLED STRUCTURE, FIXED SHADOW SHIELDS
$L/D = 0.25$

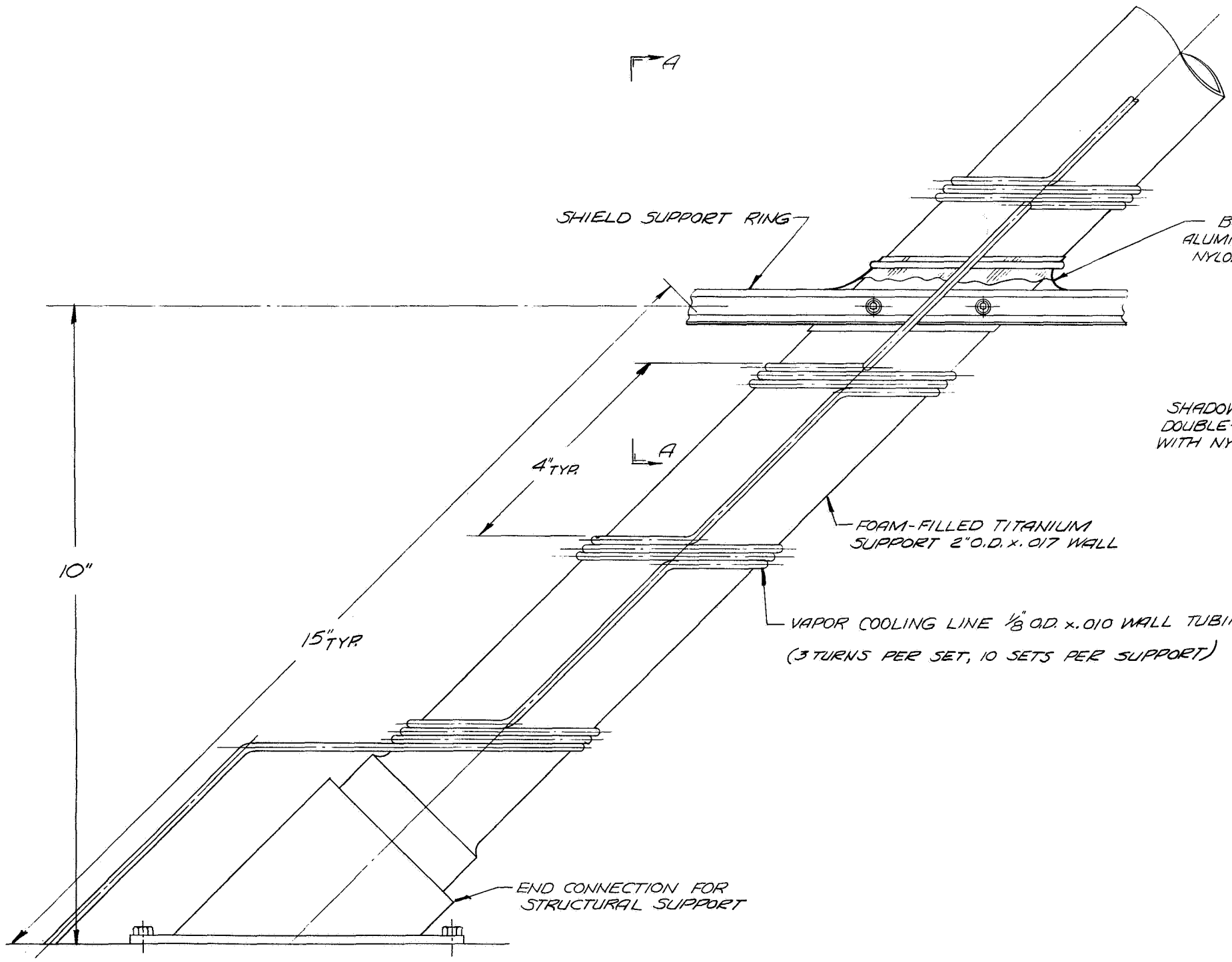

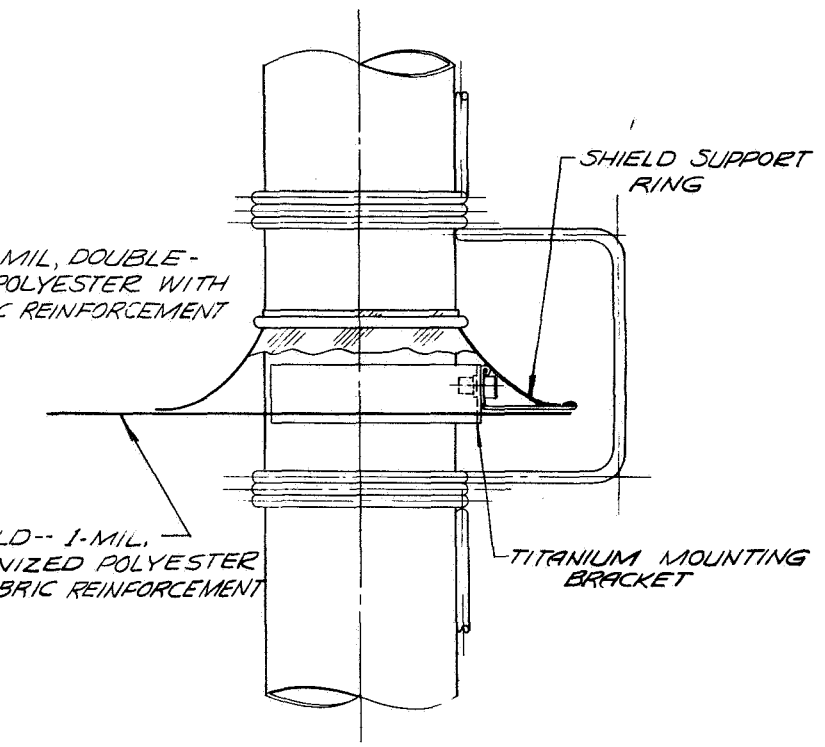

VIEW A-A

FIGURE-41
VAPOR-COOLED STRUCTURAL SUPPORT - CONCEPT-3

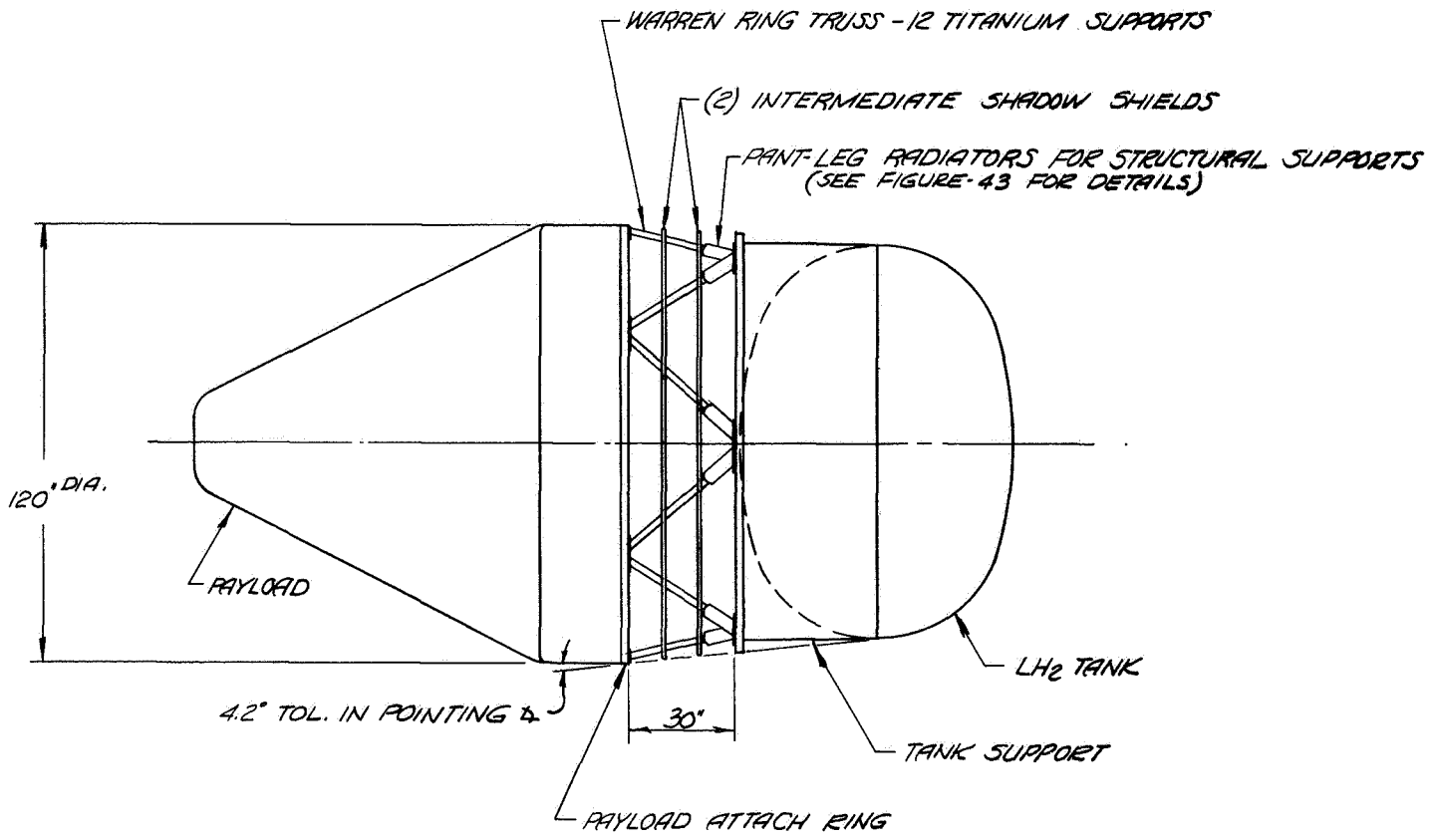

FIGURE-42
CONCEPT-4
FIXED STRUCTURE WITH PANT-LEG RADIATORS, FIXED SHADOW SHIELDS
L/D = 0.25

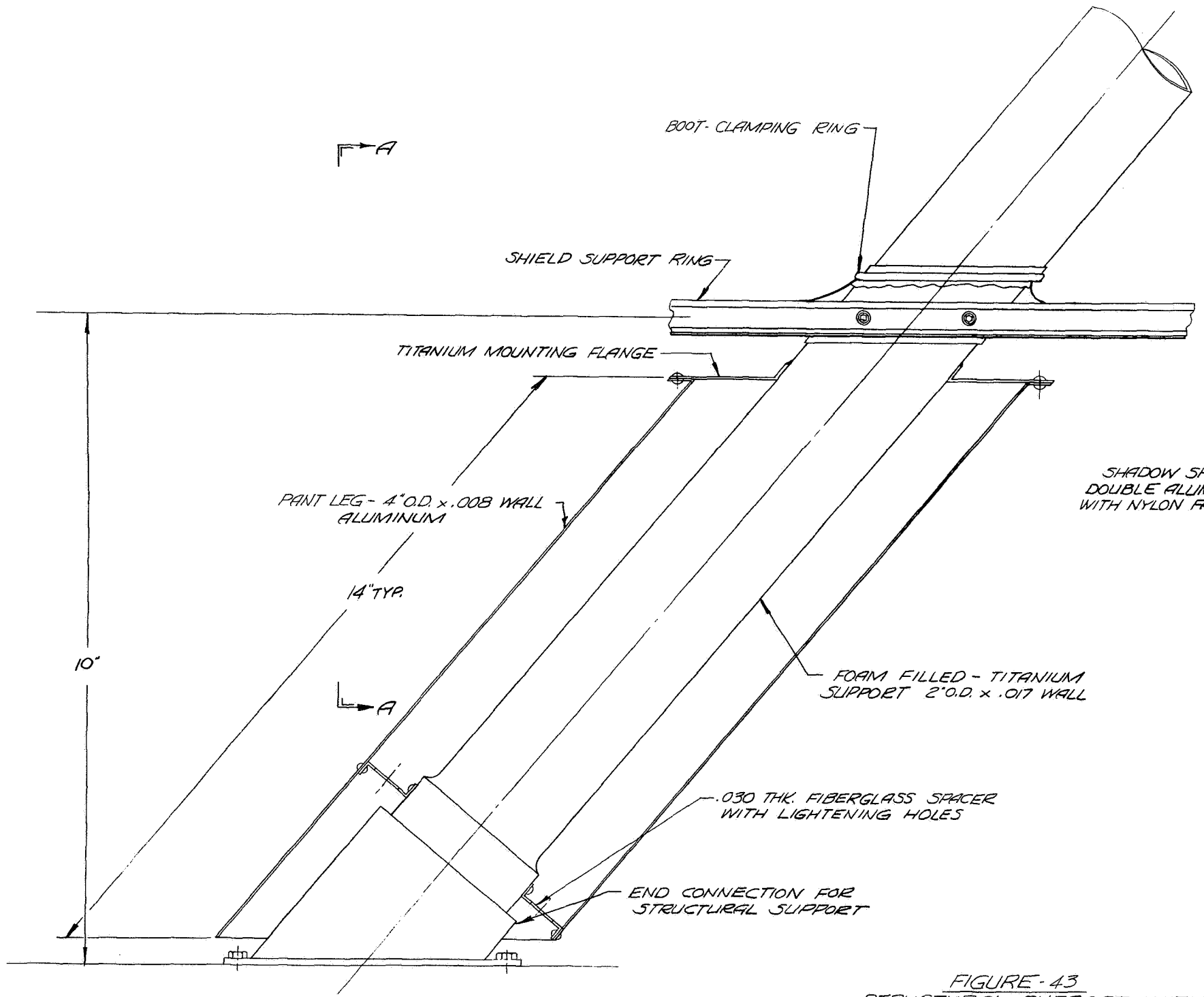

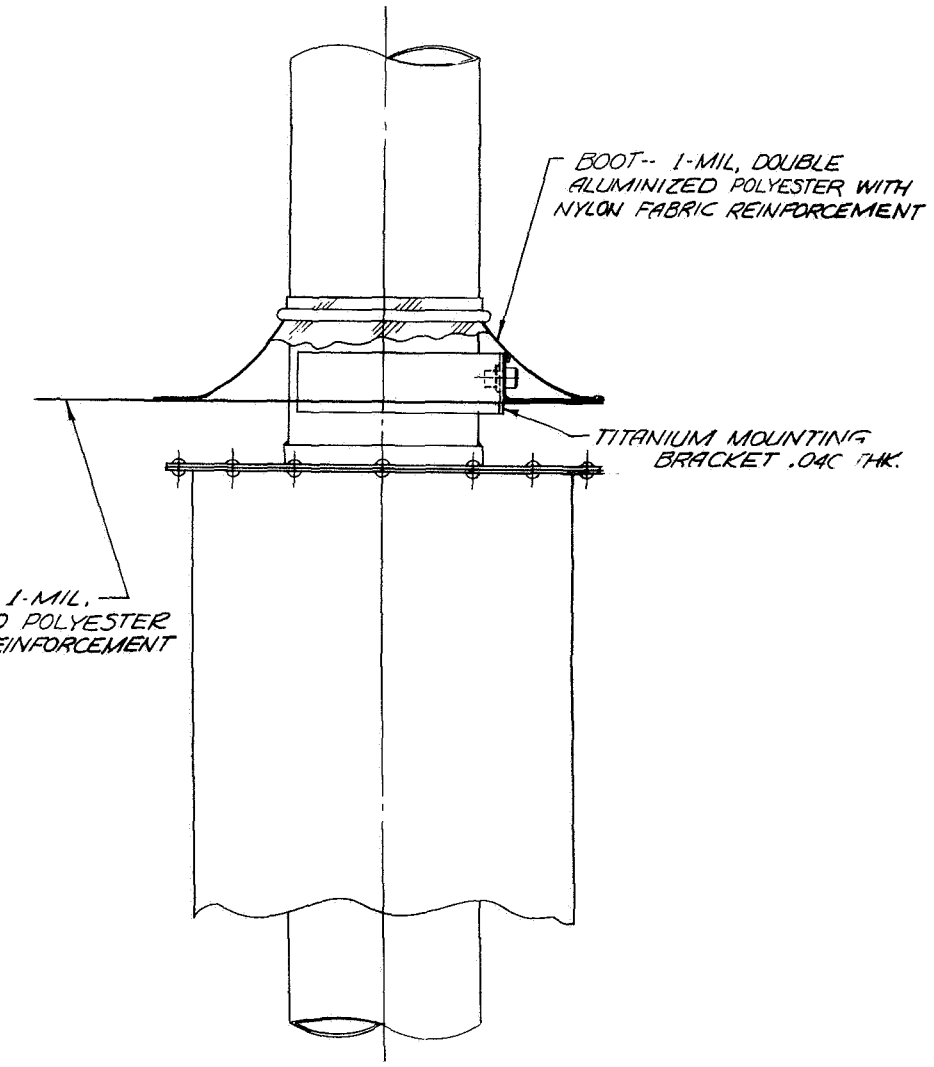

VIEW A-A

FIGURE-43
STRUCTURAL SUPPORT WITH PANT-LEG RADIATOR-CONCEPT-4

The principle of operation of the pant-leg radiator is to remove heat from the supports by radiation at a high temperature, depress the temperature at the support-radiator interface and lower the conduction heat transfer at end of the support. The location of the support-radiator interface is important since the total surface area of the radiator depends on the location and the structural support is not permitted to radiate heat to space from the low-emittance portion covered by the radiator. If it is too close to the high-temperature portion of the support near the payload, although the temperature at that location may be lowered, the resultant heat leak along the remaining shielded portion may exceed that when there is no radiator and the entire support is permitted to radiate. On the other hand, if it is placed too near the LH_2 tank end, the area of the radiator will be reduced; and the emitted power at the low temperature may be insignificant.

The following tabulation illustrates the relationship between the LH_2 boil-off from conduction along the support structure and the location of a pant-leg radiator for an example where the diameters, wall thicknesses and thermal control coatings of the structural supports and pant-leg radiators are the same as those described above for Concept 4. For this example, thermal interactions between the structure and shadow shields are neglected; x is the location of the radiator-support connection, measured axially from the payload; L is the payload-tank spacing; m_p is the LH_2 boil-off from conduction for a structure with a pant-leg radiator; and m_r is the LH_2 boil-off from conduction for the same structure without pant-legs and an effective emittance of 0.5 along the entire length of the supports.

x/L	m_p/m_r
0.2	1.20
0.4	0.94
0.6	0.87
0.8	0.88
1.0	1.00

The location of the pant-leg radiator in Figure 43, at an x/ℓ of approximately 0.7, was based on this analysis.

7.4.6 Concept 5 - Fixed Fiber Glass Structure, Fixed Shields with Space-Erected Shields to Compensate for Solar Vector Misalignment

Figure 44 shows a shadow shield system with a fixed structure and provisions for increasing the tolerance in pointing angle over what is provided by the geometry of the payload and LH_2 tank. The compensation for solar-vector misalignment is accomplished by space-erected annular shields mounted at the periphery of the payload and the

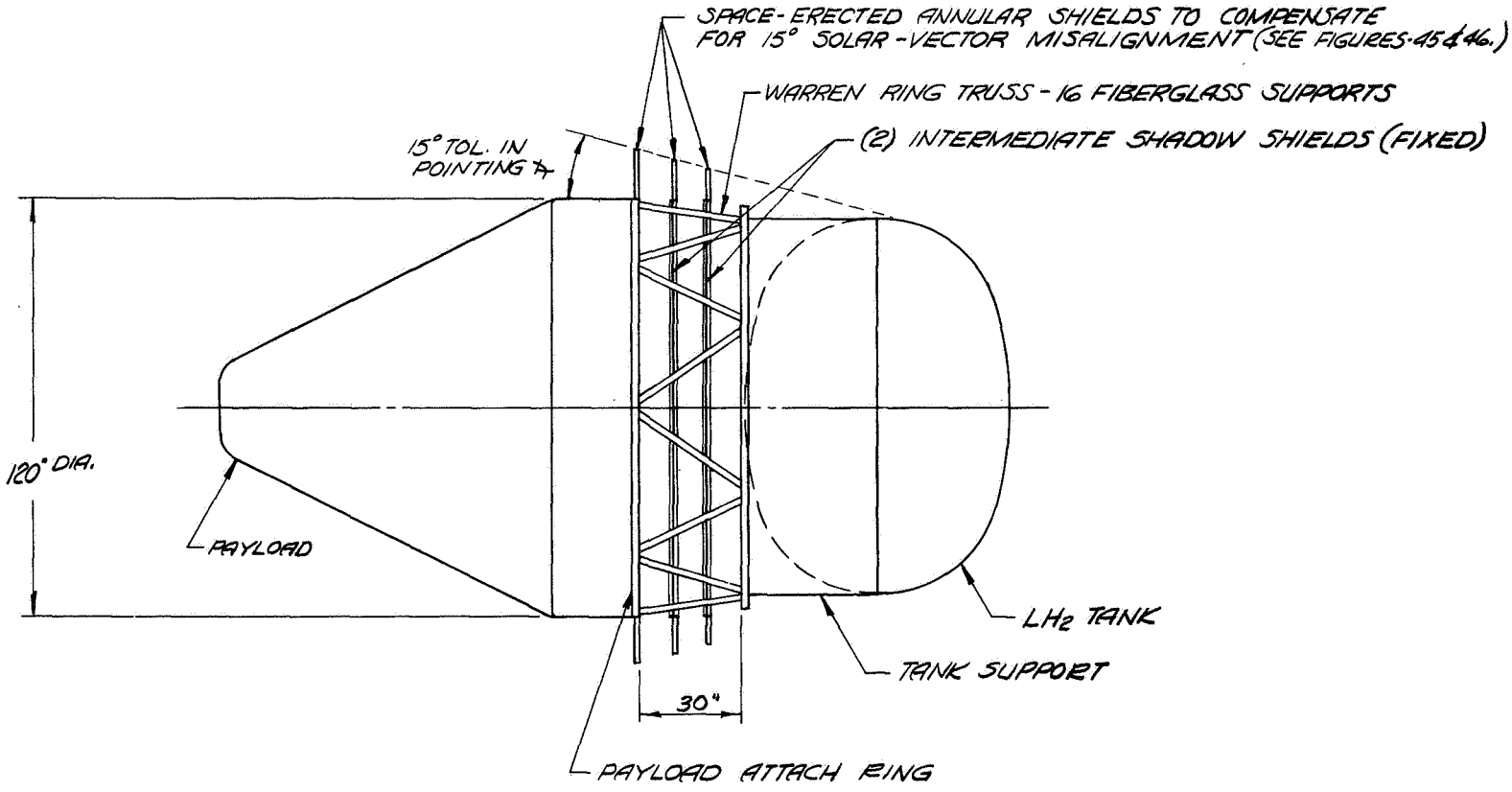

FIGURE-44
CONCEPT-5
FIXED STRUCTURE, FIXED SHIELDS, SPACE-ERECTED ANNULAR SHIELDS FOR 15° SOLAR-VECTOR MISALIGNMENT
L/D= 0.25

ARTHUR D. LITTLE INC

two intermediate shadow shields, as shown in Figure 45. For the intermediate shields, a hoop or shield support structure is mounted to the structural supports to provide a peripheral band for supporting the annular shields when they are stowed, and also to support the deployment arm and the central fixed shadow shields. The hoop consists of two formed angles which clamp the inner diameter of the annular shields during assembly. After the hoop is bolted to the mounting brackets on the structure, the central shield would be stretched and locked in place. The annular shield on the payload would be attached directly to the payload attach ring and would not require a separate hoop structure.

The annular shield is stowed by making multiple alternating folds tangential to the circumference of the hoop, forming pleats which contain spring-like deployment arms, and restraining the assembly by a plastic band around the periphery of the shield hoop. As shown in Figure 46, when the release mechanism (pyrotechnic squib or other device) is actuated, the restraining band parts, allowing the stowed shields to unfold under the action of the deployment arms.

The space-erected shield configuration shown for Concept 5 increases the tolerance in pointing angle from 4.2 to 15 degrees. However, a similar stowing and deployment arrangement would be required for space-erected shields of any diameter to provide additional solar misalignment capability. A study of the weight breakdown of space-erected annular shields showed that the shield mass was small with respect to the mass required for a structure suitable for stowing and deploying the shields. In other words, there is a fixed mass penalty associated with space-erecting annular shields; and the total mass of the erected-shield system is nearly independent of the unfolded diameter of the annular shields, and, therefore, the misalignment capability. However, increasing the diameter of the annular space-erected shields does reduce the effectiveness of radiation cooling the support structure.

Since the annular erected shield located at the payload end of the shadow shield system is directly illuminated by sunlight, provisions must be made to minimize its temperature. The temperature of this shield will be determined by the solar absorptance-to-emittance ratio of the surface viewing the sun as well as the radiant thermal interactions with the payload. For this study, the shield temperature was taken to be 520R - a temperature level which would be easily achieved with a "white" (low α_s/ε) surface coating.

7.4.7 Concept 6 - Space-Erected Structure, Space-Erected Shield

A shadow shield system with a titanium "A"-frame erectible structure is shown in the deployed configuration in Figure 47. The payload-to-tank spacing when deployed is 120 inches (L/D = 1). This

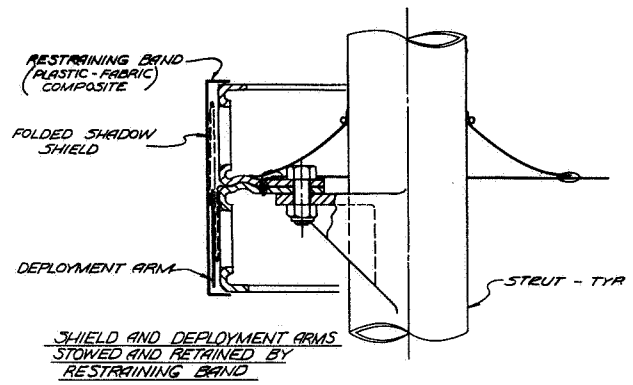

SHIELD AND DEPLOYMENT ARMS STOWED AND RETAINED BY RESTRAINING BAND

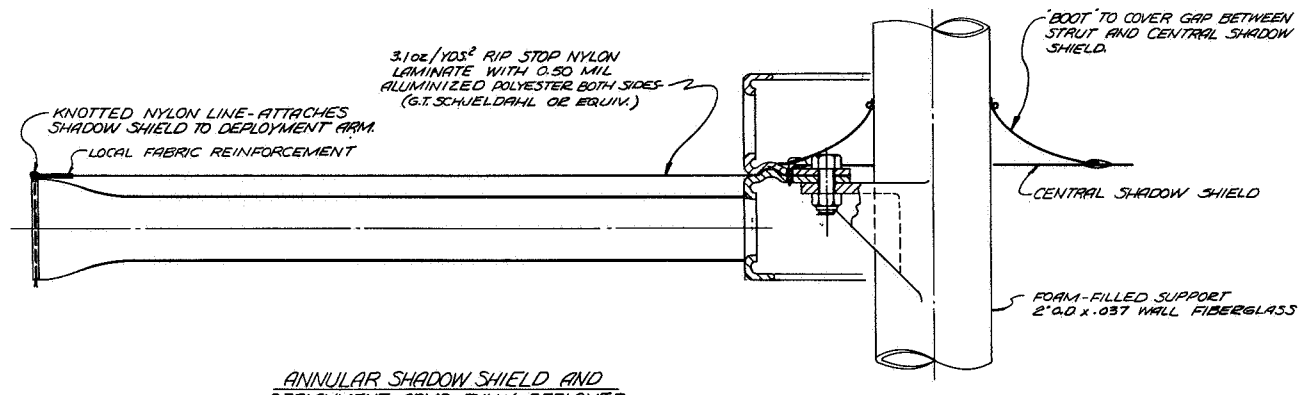

ANNULAR SHADOW SHIELD AND DEPLOYMENT ARMS - FULLY DEPLOYED

SECT. B-B
SCALE - FULL

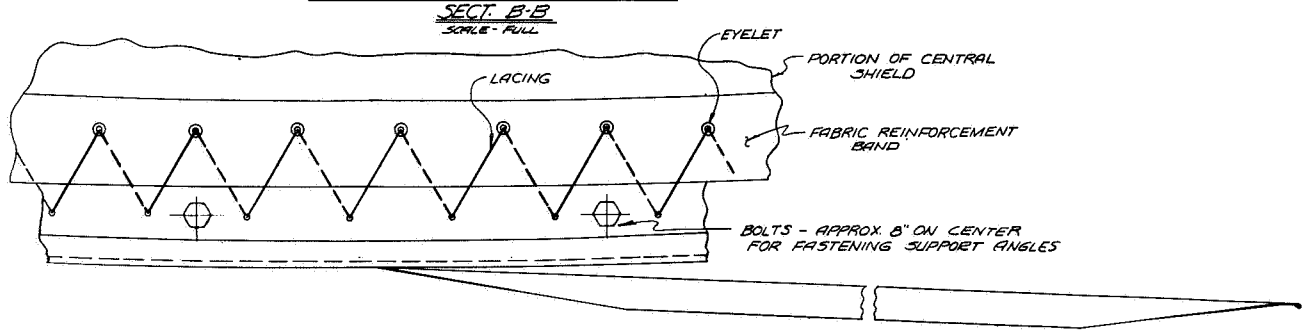

TOP VIEW (C-C)

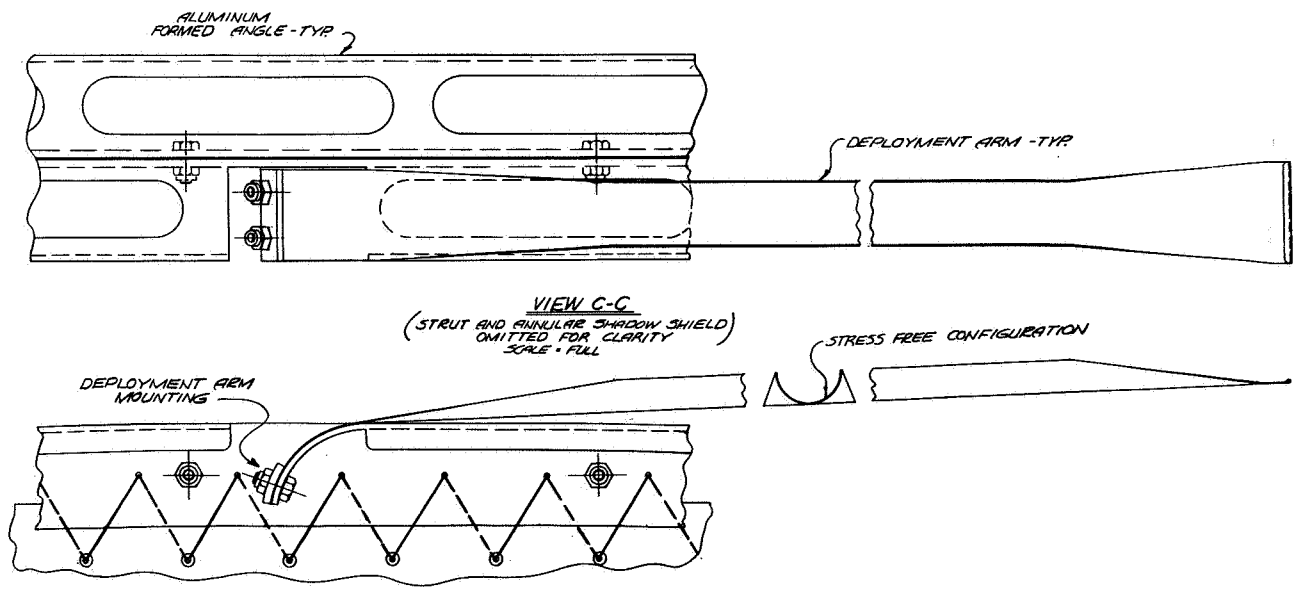

VIEW C-C
(STRUT AND ANNULAR SHADOW SHIELD OMITTED FOR CLARITY)
SCALE - FULL

BOTTOM VIEW (C-C)

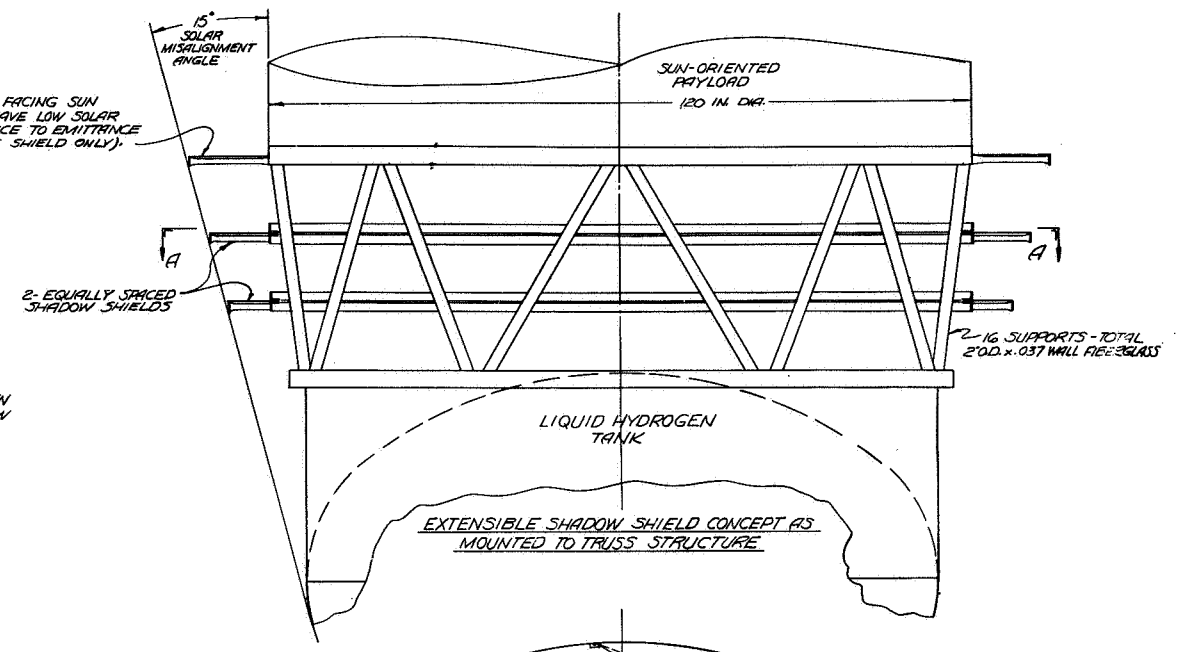

EXTENSIBLE SHADOW SHIELD CONCEPT AS MOUNTED TO TRUSS STRUCTURE

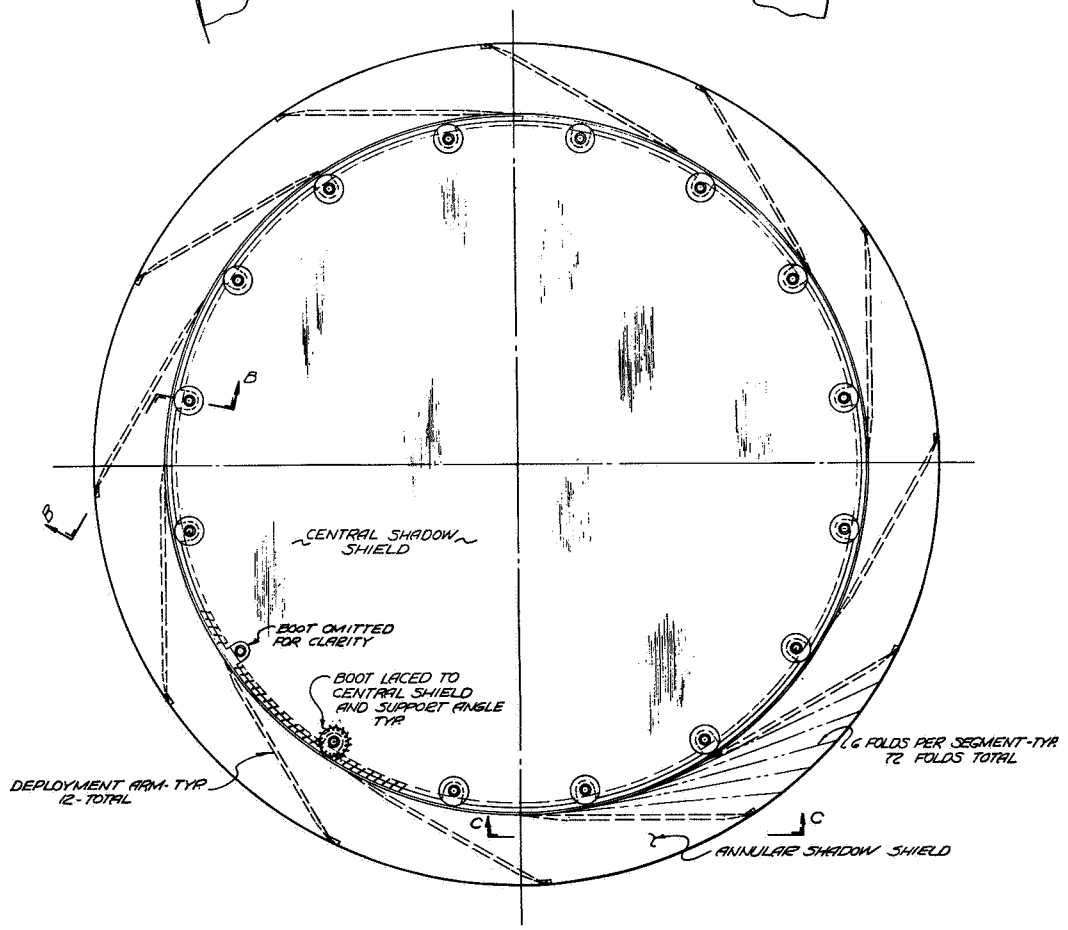

PLAN A-A
DEPLOYED ANNULAR SHIELD

Figure 45 Truss Mounting Concept for Annular Shadow Shield Detail - Concept 5

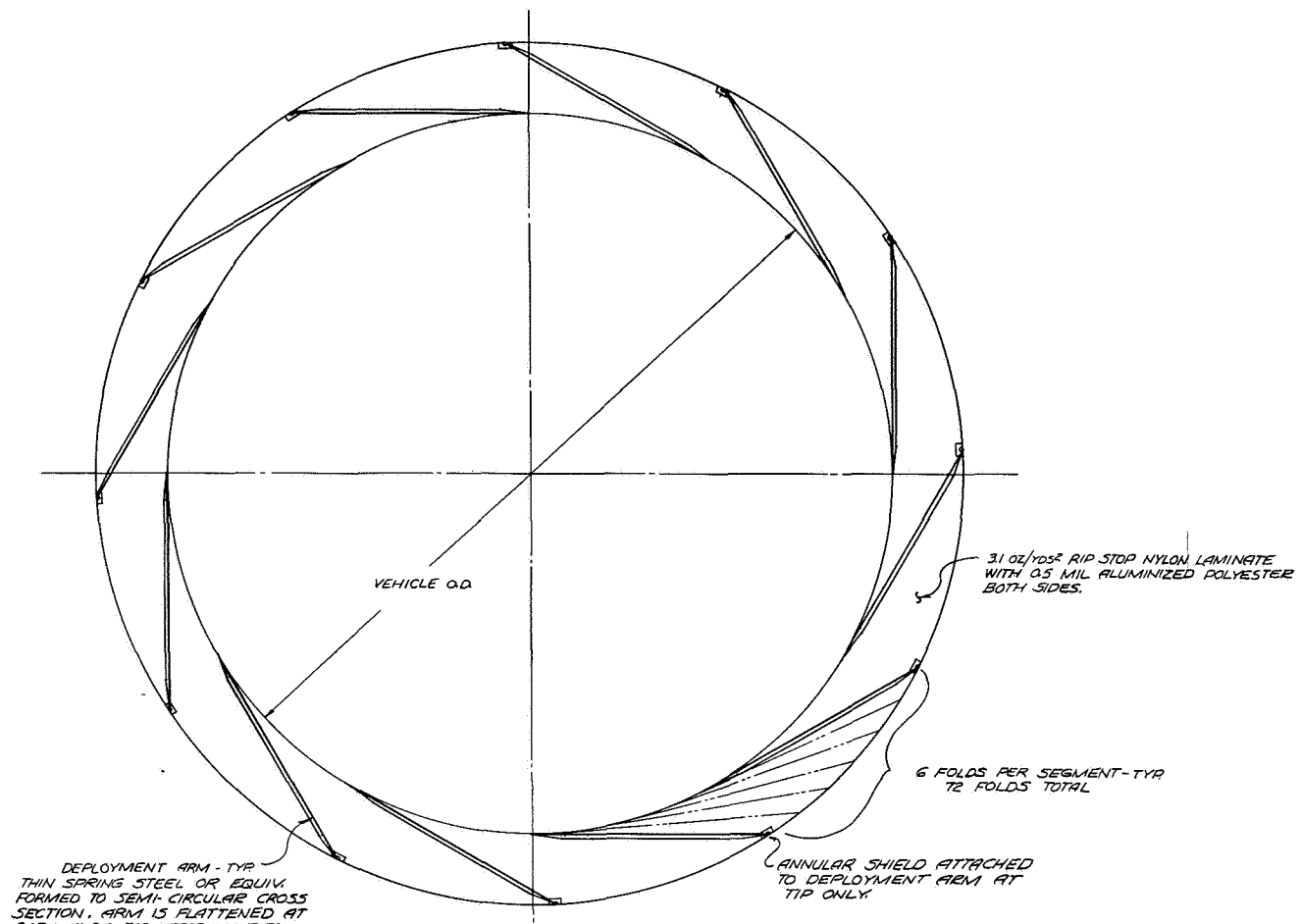

PLAN VIEW
DEPLOYED ANNULAR SHIELD

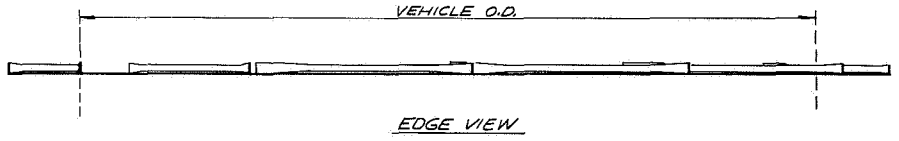

EDGE VIEW

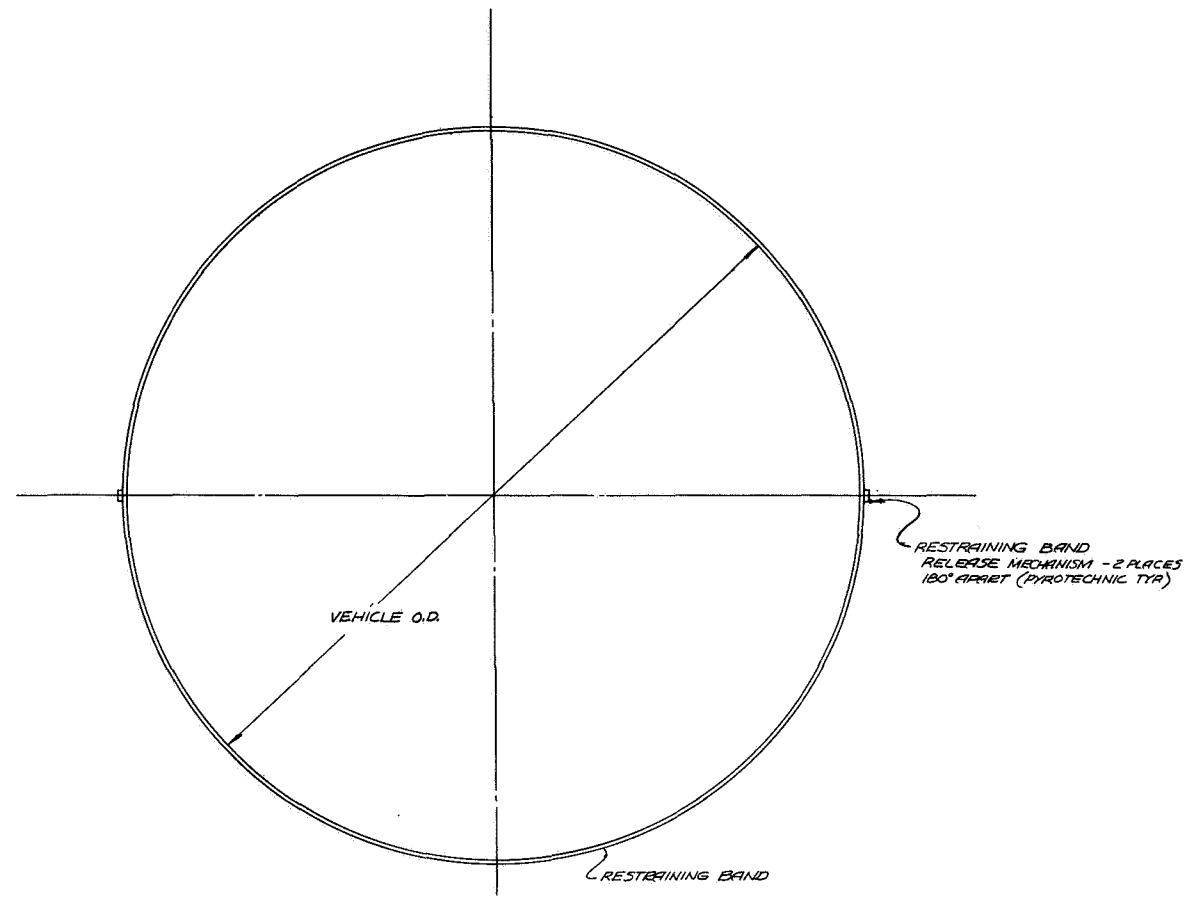

PLAN VIEW
STOWED ANNULAR SHIELD

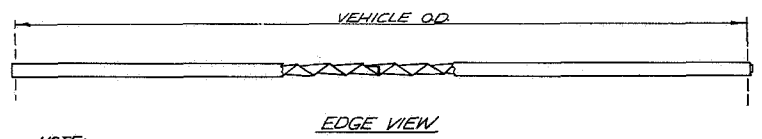

EDGE VIEW

NOTE:
DEPLOYMENT ARMS ARE FLATTENED AND FOLDED ALONG WITH ANNULAR SHIELD. THE WHOLE ASSEMBLY IS THEN HELD IN PLACE WITH A RESTRAINING BAND.

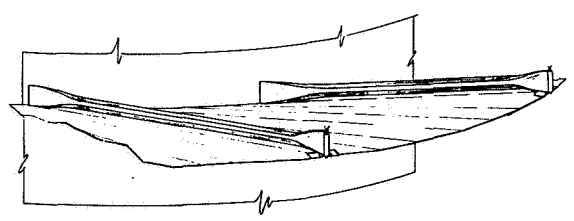

ANNULAR SHIELD DEPLOYED

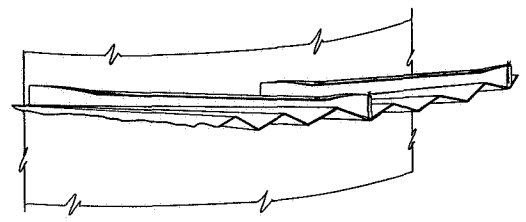

ANNULAR SHIELD PARTIALLY FOLDED

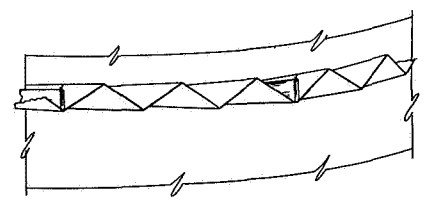

ANNULAR SHIELD COMPLETLY FOLDED

Figure 46 Annular Shadow Shield Concept - Space Erectable

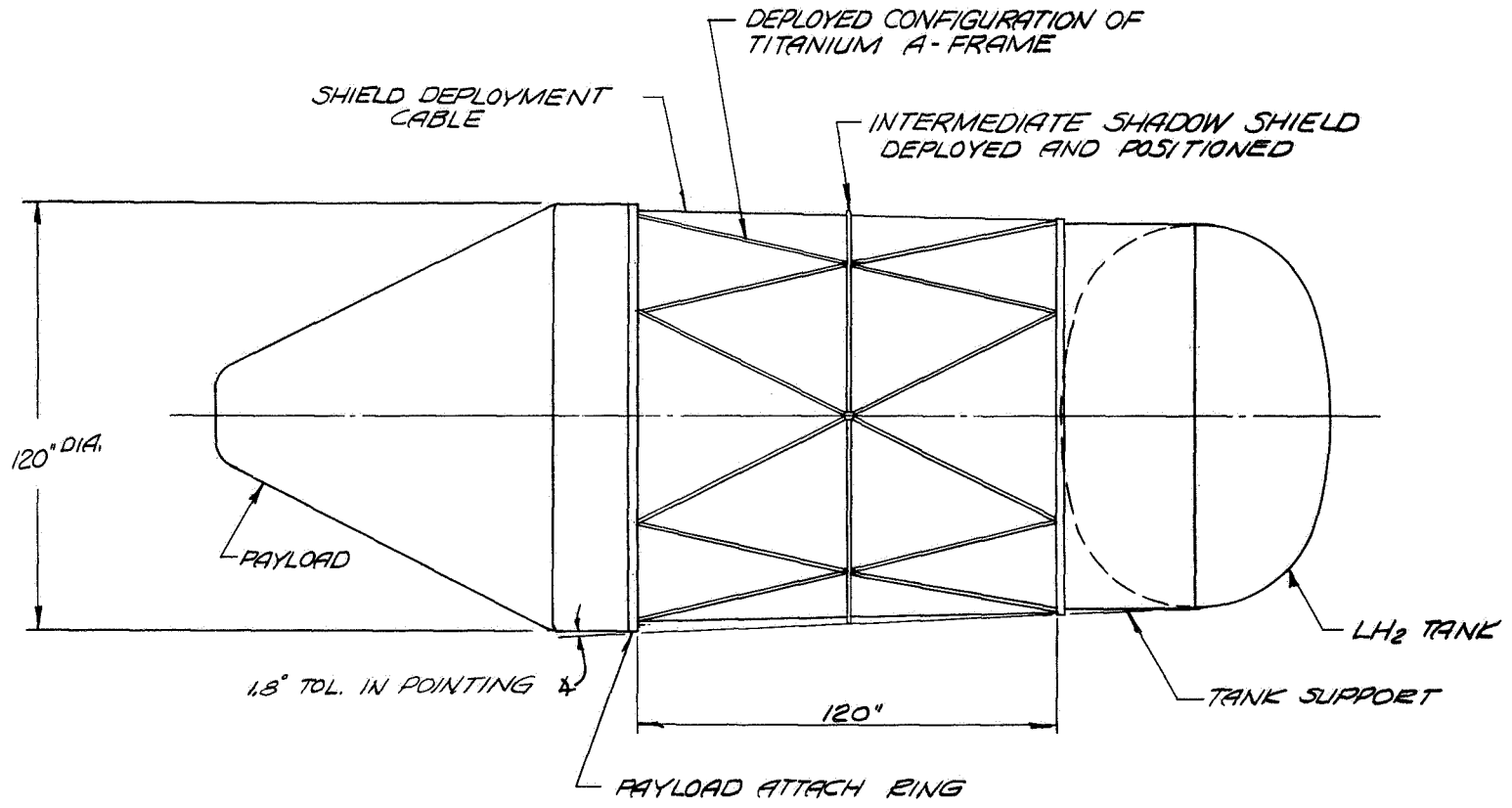

FIGURE-47
CONCEPT-6
SPACE-ERECTED STRUCTURE AND SHIELD

spacing was selected from the preliminary analysis which showed that the system mass was optimized near L/D ratios of 1.0 where only one intermediate shield was required to minimize the radiation boil-off. Because of the large spacing, the 1.8 degree tolerance in pointing angle is lower than the other concepts.

This concept utilizes three shadow shields with one centrally located shadow shield deployed during the deployment of the "A"-frame structure. The deployment sequence is illustrated in Figure 48, and some of the details of the system are shown in Figure 49.

In this configuration, the LH_2 tank is positioned against the payload attach ring during launch with the intermediate shadow shield stowed between the LH_2 tank and payload. The launch loads are transferred to the payload via the cylindrical tank support. After deployment, the loads on the "A"-frame structure are produced by the 10^{-3} g accelerations due to attitude control.

The "A"-frame structure consists of 12 titanium tubes which make up 3 hinged "X" members in the deployed configuration. A powered winch and cable system attached to the apexes of all the "A" frames is used to deploy and retract the system. The "A" frames have hinged connections at the payload and tank support and are actuated simultaneously to prevent cocking. The structure has sufficient rigidity so that the attitude control system could be actuated during deployment, if necessary.

At the termination of the coast phase, the system would be retracted; and the thrust loads of the "kick-stage" engine would be transmitted to the payload via the cylindrical tank support.

This conceptual design allows for a relatively small tolerance in pointing angle because of the large spacing. However, as shown in Figure 35, the overall mass of a space-erected system is not sensitive to the payload-tank spacing so the following measures could be taken to increase the tolerance in pointing angle, if required:

1) The payload-tank spacing could be reduced to about 30 inches with a small increase in radiation boil-off if an additional shadow shield was utilized. The present design could also be used with a commensurate increase in LH_2 boil-off due to radiation.

2) Provisions could be made for additional solar-vector misalignment capability by deploying annular shields similar to those described for Concept 5 at the expense of an additional complication in deployment.

REVISIONS				
ZONE	LTR	DESCRIPTION	DATE	APPROVED

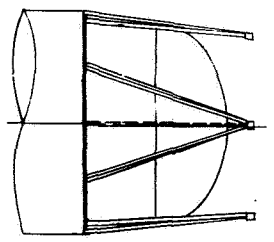

STEP-1 STOWED CONFIGURATION

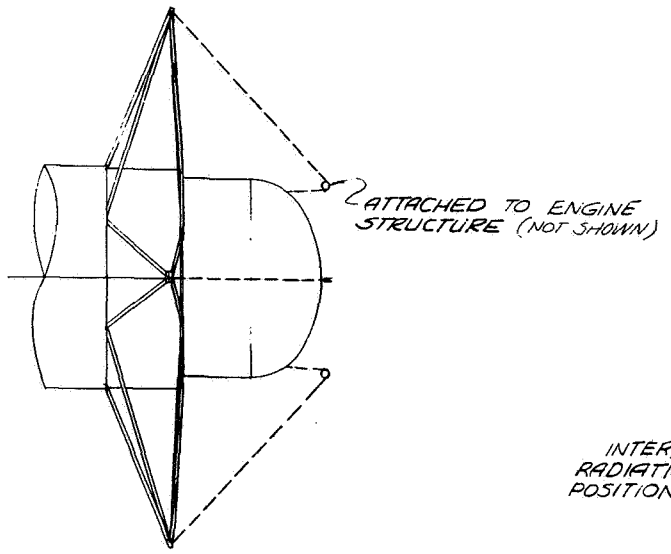

STEP-2 PARTIAL DEPLOYMENT OF "A" FRAMES

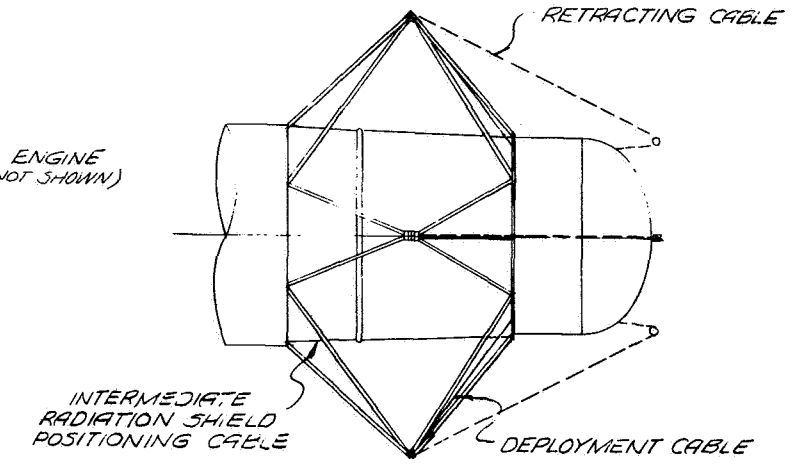

STEP-3 INTERMEDIATE RADIATION SHIELD DEPLOYED

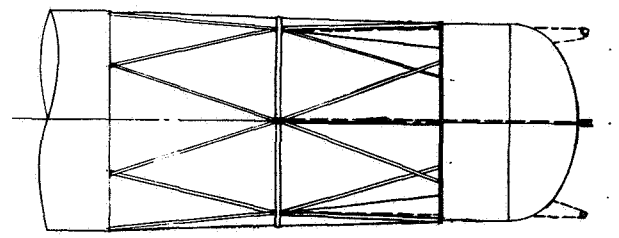

STEP-4 DEPLOYED CONFIGURATION INTERMEDIATE RADIATION SHIELD DEPLOYED AND POSITIONED

ITEM NO	QTY REQ	PART OR IDENTIFYING NO.	NOMENCLATURE OR DESCRIPTION	MATERIAL

LIST OF PARTS

UNLESS OTHERWISE SPECIFIED	
DIMENSIONS ARE IN INCHES	
TOLERANCES: DECIMAL .XX=±.010 .XXX=±.005	FRACTIONAL ±1/64 ANGULAR ±1°
FINISHED SURFACES BREAK SHARP CORNERS	RMS R
DO NOT SCALE THIS DRAWING	
NEXT ASSY	USED ON
APPLICATION	
MATERIAL	
CASE	69507-1
ISSUE DATE:	
DRAWN NAM	9-25-67
CHECKED	
APPROVED	

Arthur D. Little, Inc.
CAMBRIDGE, MASSACHUSETTS 02140

FIGURE 48
DEPLOYMENT SEQUENCE OF AN "A" FRAME EXTENSIBLE STRUCTURE

SIZE	CODE IDENT NO.		
D		3782-004	

SCALE 1/4"=1" SHEET

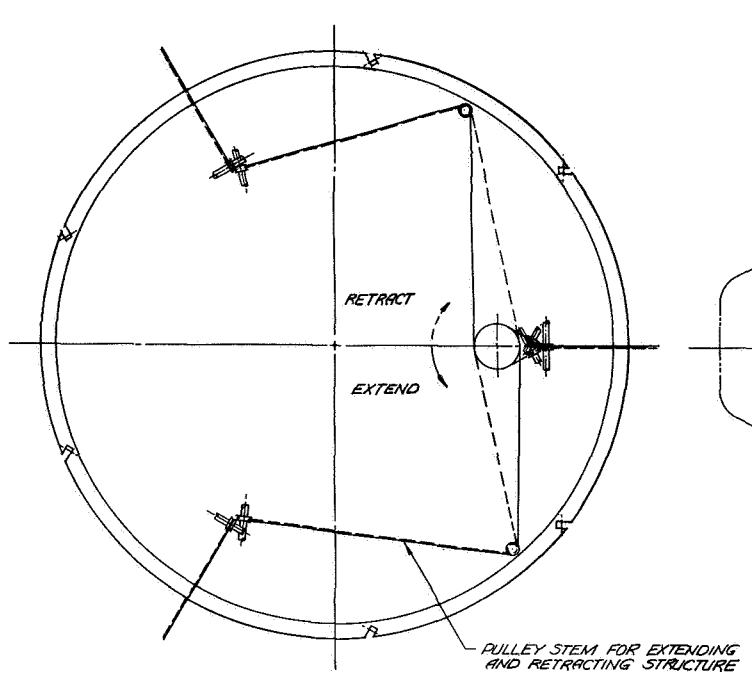

SECT. A-A

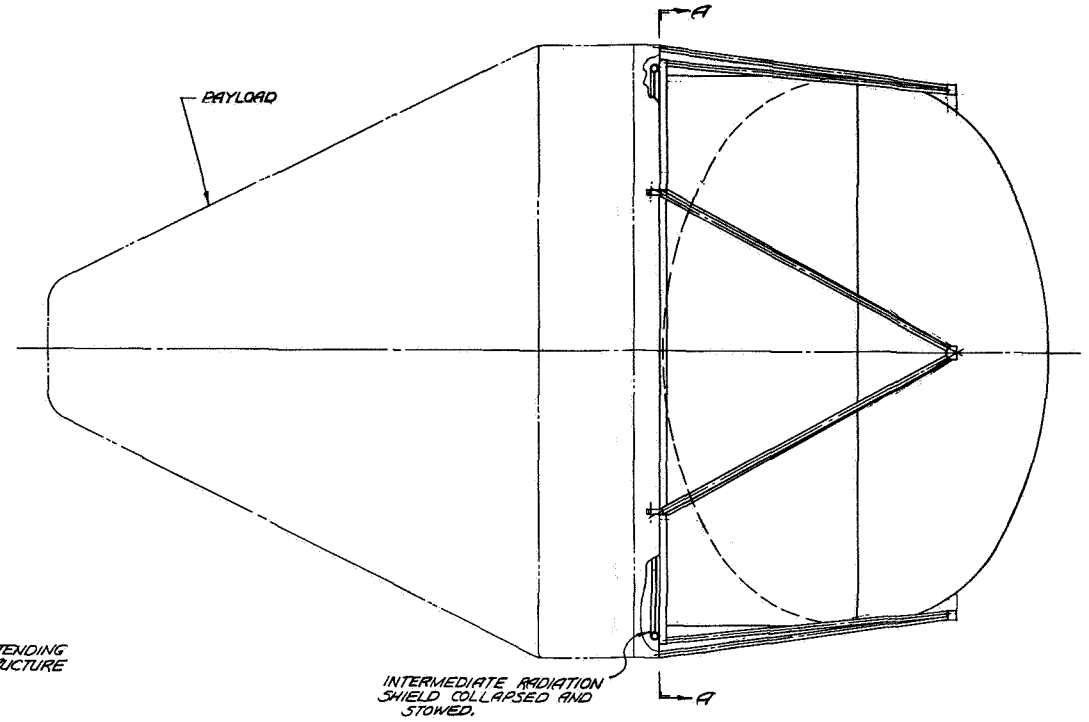

SYSTEM STOWED

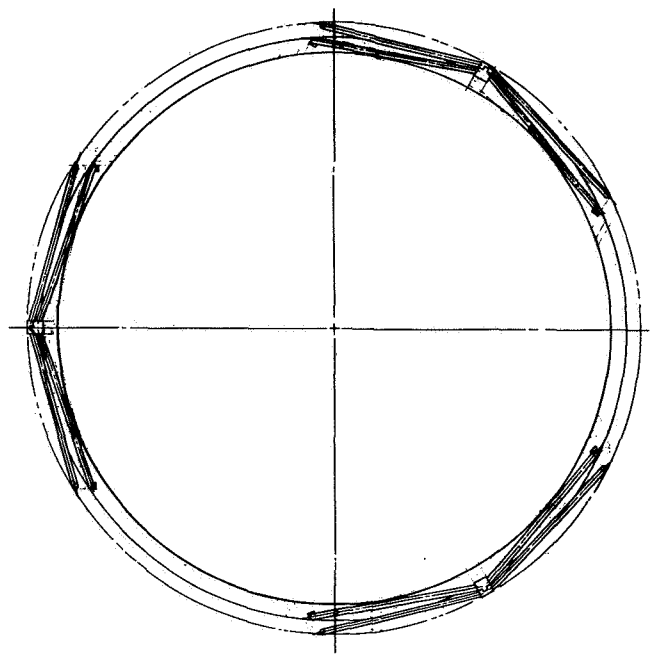

END VIEW

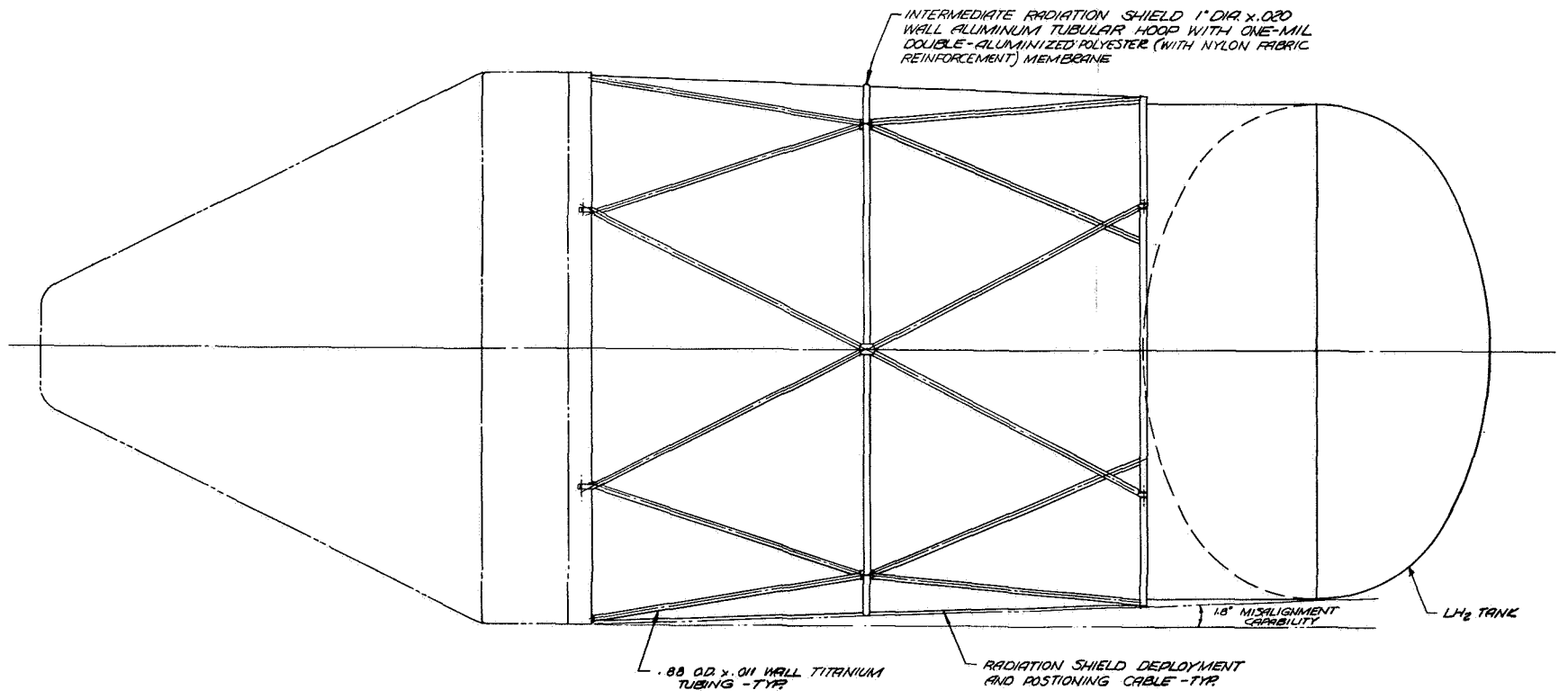

SYSTEM DEPLOYED

Figure 49 "A"-Frame Space-Erected Extensible Structure - Concept 6

7.4.8 Alternative Concepts

The general configurations of five concepts with fixed structures have been described in the previous paragraphs. Numerous combinations and alternative concepts based on these five configurations may also be considered.

The conceptual design of the shields was based on the use of single-sheeted, reinforced polyester shields coated to have a low emittance. It is also possible to consider the use of double-sheeted shields as discussed by Knoll, et al (1966). In this configuration, a single circumferential support ring could be used to support two closely spaced shields each having low-emittance surfaces. The number of reflective surfaces per shield support assembly would be increased from two to four, thereby reducing the radiant component of heat flux at the expense of adding additional shield material mass. Although the use of closely spaced shields is not efficient from a thermal standpoint, the use of the double-sheeted shield may provide some measure of protection to exposed low-emittance surfaces which could possibly be contaminated during launch or by prelaunch handling, etc. With this concept, the two interior low-emittance surfaces would not be directly exposed to the environment. Thus, the double-sheeted system could improve the reliability of the system. The additional mass penalty would primarily be associated with the mass of the additional shield material.

The projected performance (system mass) of a double-sheeted system will be compared with a single-sheeted shield system for a fixed structure, similar to that used in Concept 1, in Section 12 of this report.

8.0 TANK SUPPORT SYSTEM

8.1 Introduction

The support system for the hydrogen tank must support the tank while providing sufficient thermal isolation from the rest of the vehicle structure during ground-hold, ascent, and orbital maneuvers. Because the mass of the LH_2 tank support system is common to all shadow shield concepts, and, therefore, its mass would not alter the relative ranking of the various shadow shield systems, a simplified structural and mass analysis was undertaken in this study. However, the structural support was designed in sufficient detail so that a reasonable estimate of its mass could be made. A primary objective in the design of this lightweight structure is to distribute the loads around the periphery of the LH_2 tank while providing an acceptable ground-hold and orbital heat leak. In addition, the design concept is based on a configuration to which ground-hold and multilayer insulation can be easily and effectively applied.

The sections which follow describe the support system and its imposed loads, the selection of the support concept used, and the two critical elements in this system, the aluminum tank skirt and the fiber glass support cylinder.

8.2 Selection of Support Concept

The support system may be considered as composed of two primary elements: 1) structural elements on the tank and main vehicle which are designed from mechanical considerations alone, and 2) a thermal isolator which provides a barrier to heat flow in addition to transmitting loads from the tank structure to the main vehicle structure. Starting with these considerations, all support systems may be classified as one of two general types: 1) a continuous support system in which all the loads from the tank to the main structure of the vehicle are carried through a continuous shell, made of a good thermal insulator, or 2) a point support system in which the loads are collected at a number of points around the circumference of the tank shell by structure on the tank, transferred to the main structure of the vehicle and then redistributed around the circumference by structure on the main vehicle. In both systems the supports must be of relatively low thermal conductance to minimize the heat flow to the LH_2 tank during ground-hold and space operation; they also must be insulated to prevent excessive heat flow to the LH_2 tank during orbital operation where the vehicle is not sun-oriented.

Although the total structural mass associated with either a continuous or point support system may not be significantly different (c.f., Sterbentz and Baxter (1963)), the continuous support system has the following advantages:

1) The application of effective ground-hold and multilayer insulation is more easily accomplished with a continuous support.

2) The design of a continuous support system is inherently more simple.

3) A continuous support system possesses better dynamic characteristics and is structurally more redundant.

4) For this application a continuous support design is common to both space-erected and ground-erected shadow-shielded tankage.

For these reasons a cylindrical, continuous, tank support system was chosen for this investigation. In order to achieve the objective of comparing the relative mass penalties of both space-erected and ground-erected shadow shield systems, the tank support concept selected was designed for use with either system.

8.3 Description of Support System

The tank support system comprising a cylindrical skirt designed to withstand the thrust loads associated with the mass of the LH_2 and tankage is shown in Figure 50. This configuration allows the launch loads associated with the payload mass to be transmitted directly to the boost vehicle. Because the temperature gradients between the LH_2 tank and room-temperature are taken in the cylindrical tank support, no thermal stresses are introduced in the main payload support truss structure during the launch environment.

As shown in Figure 50, the tank support consists of cylindrical aluminum and FRP* sections. The attach ring which joins the continuous tank support to the shadow shield truss structure is terminated at the tangent point of the top of the tank itself. The choice of this termination point was based on using the same tank support system for both ground-erected systems (similar to the fixed open-truss structure shown in Figure 50) and space-erected systems where no open-truss structure is required. In the final comparison of the system masses for the various concepts selected for study, the mass of the tank support system itself was therefore a constant. Several design options for the choice of the skirt length are available. For example, in a fixed structure the length of the skirt could be shortened and the tubular truss structure lengthened. In this case the mass of the skirt would decrease and the thermal conductance of the skirt would increase. Correspondingly, the mass of the tubular structure would increase and the LH_2 boil-off due to conductive heat flow via the supports would be altered. A reduction in the skirt length would also provide a more "open" system from the radiation standpoint which would have a smaller radiative heat leak for the same spacing between the tank and payload.

The support point on the tank is at the horizontal center line, where a .030"-thick cylindrical aluminum skirt is welded to the tank. The thickness of the tank wall is increased at this point as required to minimize stresses at the attachment point. A 0.060"-thick fiber glass support cylinder connects this aluminum skirt to the main structure of the vehicle at the tank attachment ring. This cylinder, riveted to mating structure at both ends, is built up from a number of curved panels, and is reinforced with fiber glass doublers and riveted at the longitudinal seams. The tank attachment ring is a round tube to which connections from various other elements are made. The attachment for the liquid-hydrogen tank is a continuous angle welded to the tube around its entire circumference. The fiber glass support is riveted to the lip of this angle around the entire circumference. Box sections are welded to the attachment ring at points where the struts on the truss intersect it, and provide the dual function of local stiffening of the truss structure and ring plus providing flat surfaces for bolting the struts to the ring. A continuous angle is welded to the top of the tubular attachment ring around its entire circumference. This angle is contoured around the inside of the truss attachment points

---

* FRP (fiber glass reinforced plastic)

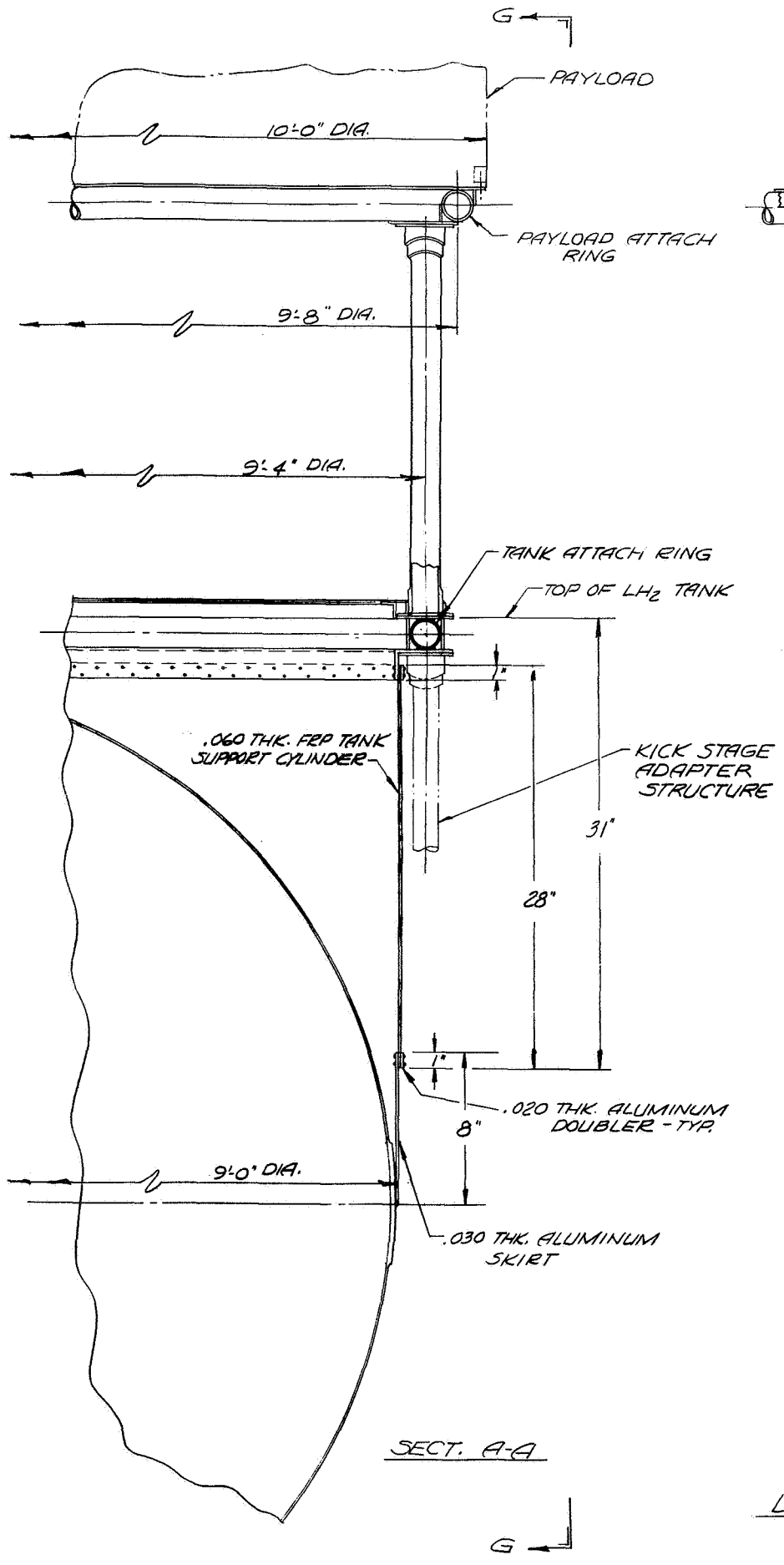

SECT. A-A

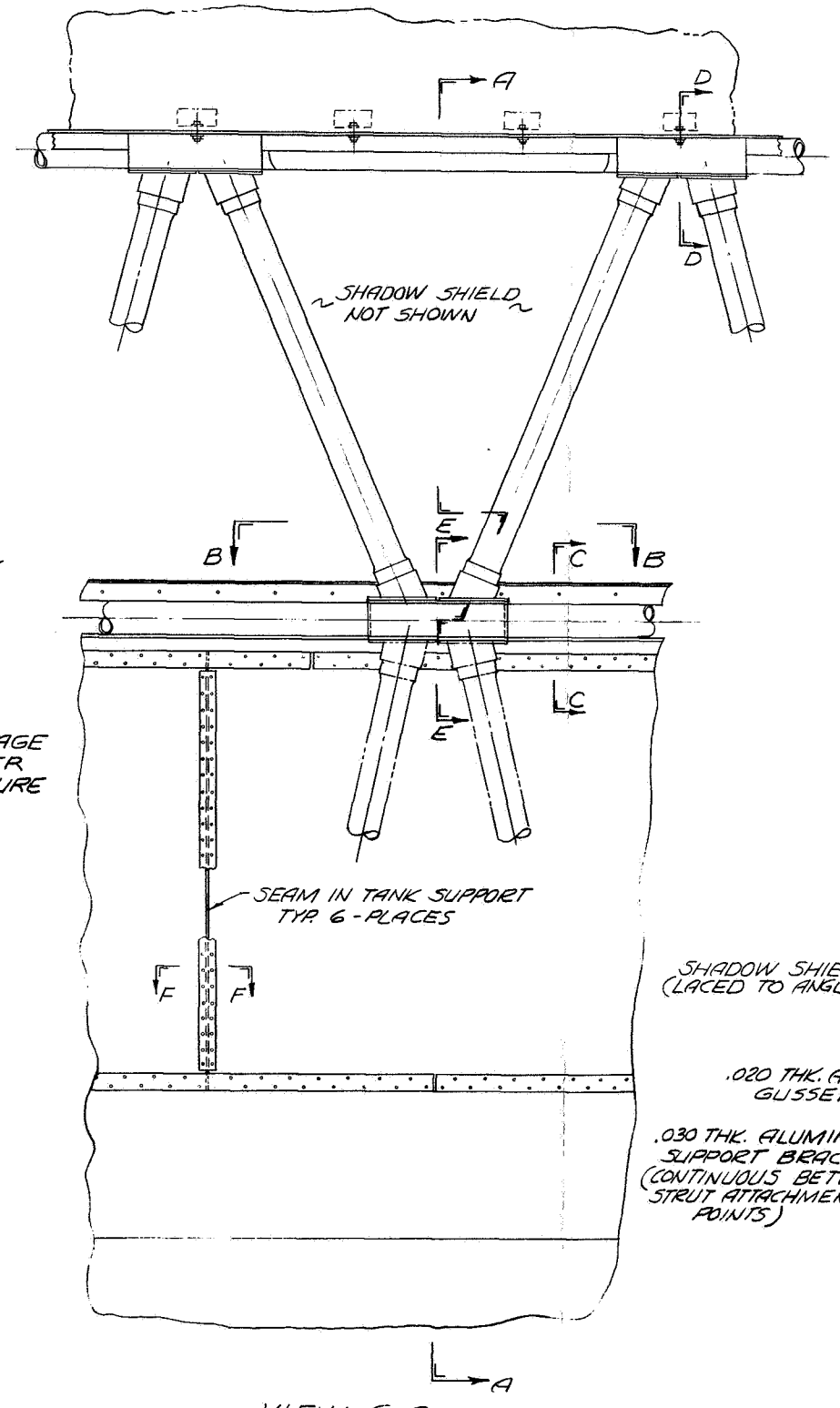

VIEW G-G

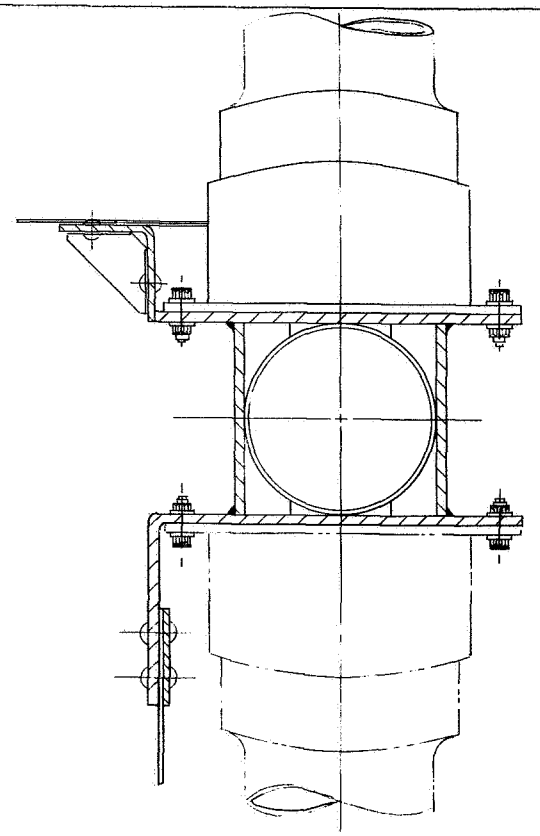

SECT. E-E

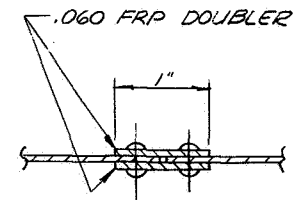

SECT. F-F

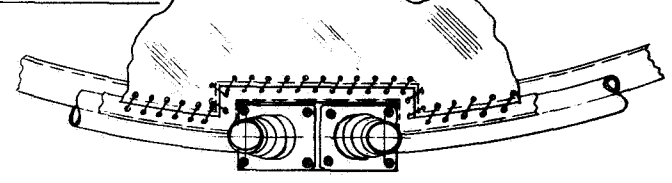

PLAN B-B

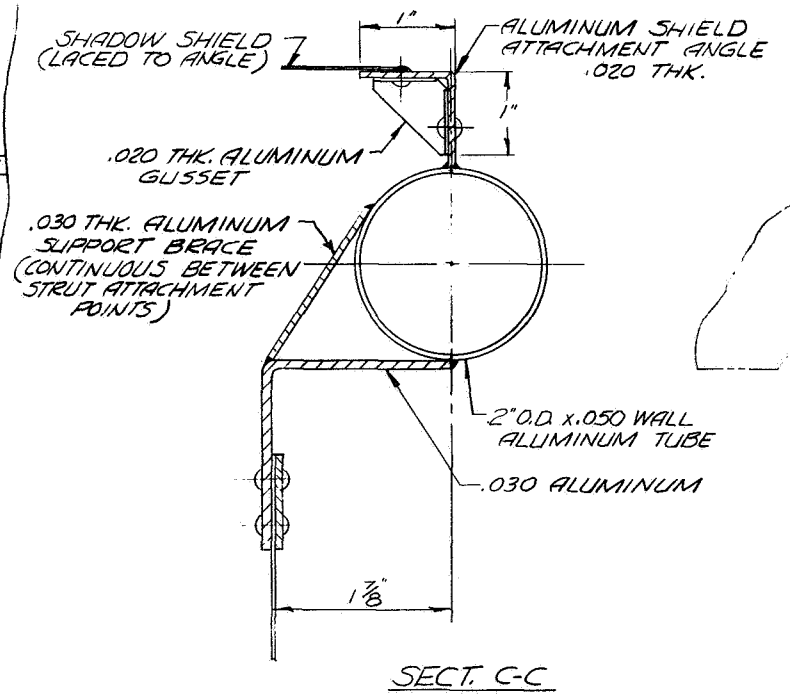

SECT. C-C

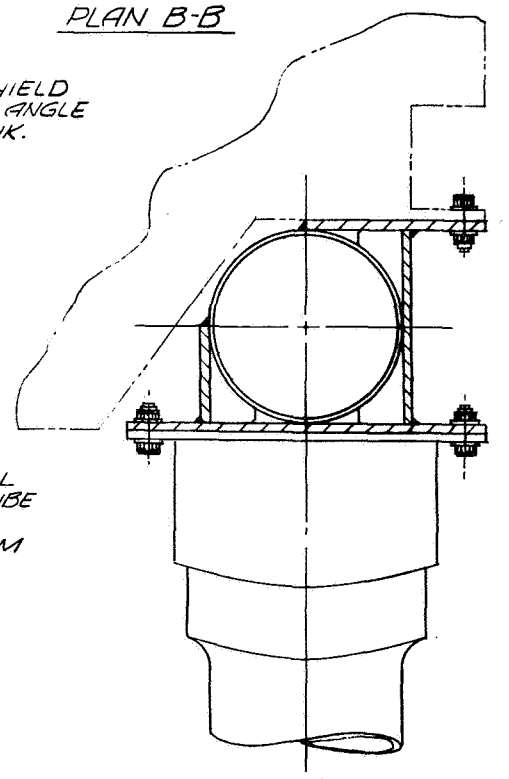

SECT. D-D

FIGURE - 50
LH_2 TANK SUPPORT DETAILS

to provide a continuous surface for lacing the aft radiation shield. The longitudinal struts, themselves, are reinforced at the ends to permit attachment of a mounting flange. For titanium truss structures, a mounting flange is welded to the strut; and for fiber glass truss structures, a flange is molded on the end of the strut itself. In the latter case, a clamping ring is required for bolting the strut to the box section on the attachment ring. The payload attachment ring is similar to the tank attachment ring. It consists of a rolled circular tube to which box sections are welded for attachments of struts. A continuous plate is welded around the top of this tube for attachment of the payload.

The structure shown in Figure 50 is intended to be indicative of typical structural details and has been used for estimating the mass of the system. The actual design of the two attachment rings and the details of the various attachments to them requires a more complete specification of the loads and the interfaces with the rest of the kick-stage vehicle.

8.4 Design Analysis

The loads imposed on the cylindrical tank support structure are those from the tank alone, since all other loads will be carried around the tank by appropriate truss work or shell sections. In the discussions which follow, we have considered that all launch forces occur at the tank attachment ring. In determining the loads on the support structure, we have used a tank mass of 200 pounds and a liquid-hydrogen mass of 1160 pounds, or a total mass of 1360 pounds. The loads imposed on the cylindrical tank support system during launch are the inertia forces required to accelerate this mass. In calculating these forces, we have taken a maximum axial acceleration of 9 g's and a maximum transverse acceleration of 1 g. Therefore, the maximum axial design force is 12,250 pounds; and a maximum transverse design force is 1360 pounds. These accelerations, and hence the design forces, are actually about 1-1/2 times the anticipated levels, so that the design loads incorporate a factor of safety. Consequently, in sizing the tank support, we have not included any further factor of safety, but have selected section thicknesses so that the structure is stressed to its ultimate limit under the most critical loading condition.

8.4.1 Aluminum Tank Skirt

The cylindrical skirt on the tank provides a transition between the tank shell and the fiber glass support cylinder, and serves the dual purpose of transferring the inertia loads from the tank to the fiber glass cylinder and accommodating changes in tank diameter with internal pressure without transferring the resulting strains into the fiber glass cylinder. Tc a first order, the former requirement

dictates the thickness of the skirt and the latter determines its length. The skirt is made out of the same aluminum alloy as the tank (2219-T81) to facilitate welding.

The critical loading condition for this skirt occurs when it is subjected to bending plus axial compression by simultaneous application of the maximum axial load and the maximum transverse load. Under this condition, the entire skirt can be considered as a catilever beam supported at the joint between the skirt and the fiber glass cylinder. A uniform axial compressive force and a transverse end force are imposed on this beam. For this situation and the geometry under consideration, the mode of failure for this skirt is local buckling. The critical area on the skirt is that point on the circumference adjacent to the aluminum-to-fiber glass joint where the maximum compressive bending stress occurs, for at that point the compressive stress in the shell is at its maximum value. In order to determine the required thickness of this skirt, the shear stresses in the skirt were neglected and an analytical model was used in which the shell is loaded with a uniform axial stress which is equal to the uniform axial stress due to the axial load plus the maximum compressive bending stress.

The required skirt thickness is given by the equation (c.f., Fung and Sechler (1967)):

$$\sigma_a = \sigma_c = E\left[9(t/R)^{1.6} + 0.16\ (t/L)^{1.3}\right]$$

where σ_a = allowable stress in the shell, psi

σ_c = stress at which local buckling occurs, psi

E = modulus of elasticity, psi

t = shell thickness, in.

R = radius of shell, in.

L = unrestrained length of shell, in.

The required skirt thickness, based on this analysis, is 0.030 inch; and the resulting skirt mass is 8.1 pounds. The maximum axial compressive stress in the skirt is 1300 psi.

This estimate of the mass of the aluminum section of the support does not take into account the stress induced by the expansion of the LH_2 tank during pressurization or the relative thermal contraction at the aluminum-fiber glass joint.

The thickness and mass of the skirt could be reduced somewhat if a more efficient design were used for the shell (i.e., a design which incorporates reinforcing elements to raise the stress level at which local buckling occurs). Examples of such designs are semi-monocoque structures incorporating longitudinal stringers, truss core structures, and honeycomb-type structures. The spacing of the

reinforcing elements in such a structure would have to be less than about 2.2 inches (the length of the buckling half wave in the present shell) in order to realize any thickness reduction from this approach. A detailed design of a semi-monocoque or truss core skirt would reduce the mass calculated above. It is estimated that the mass of a skirt of this type would be 5.0 to 5.5 pounds since, typically, the mass of a well-designed, reinforced structure will be 60 to 70% of the mass of a monocoque structure of the same load bearing capacity (c.f., Sterbentz and Baxter, (1966) page 655).

8.4.2 Fiber Glass Support Cylinder

The fiber glass support cylinder must transmit the loads from the aluminum tank skirt to the main structure of the vehicle while providing adequate thermal isolation during ground-hold and during portions of the mission when the tank attachment ring is at a temperature significantly higher than the tank temperature (for instance, during parking orbit maneuvers). Its diameter and length are fixed by the overall geometry of the vehicle, so the only variable at the discretion of the designer is the material choice and its thickness.

Since the choice of material for this cylinder is not so obvious as for the aluminum skirt, several materials were considered. The selection process consisted of designing support cylinders of a number of the candidate materials, determining the cylinder mass and the heat leak under ground-hold conditions for each design, and then choosing the least-mass structure which had an acceptable heat leak.

As with the aluminum skirt, the critical design load for this cylinder is simultaneous application of the maximum axial compressive force and the maximum transverse force. The critical area is at the junction with the tank attachment ring at the point on the circumference where the maximum compressive stress occurs, and the critical failure mode is local buckling. The design approach used is identical to that used for the aluminum skirt.

Using this approach, monocoque cylinder designs were evolved for supports of fiber glass, titanium, and stainless steel. These designs are summarized in the table below:

MONOCOQUE SUPPORT CYLINDER DESIGNS

Material	Cylinder Thickness (in.)	Axial Compressive Stress (psi)	Cylinder Mass (lb_m)
Fiber glass	.060	690	41.4
Titanium	.032	1400	45.5
Stainless Steel	.025	1750	71.1

The stainless steel cylinder was eliminated from consideration because of its high mass. The difference in mass between the fiber glass and titanium cylinders is not really significant, so the choice cannot be made on the basis of mass alone. Fiber glass was finally selected because it resulted in a lower heat leak during those portions of the mission in which the insulating capability of this cylinder is important.

The mass of the fiber glass cylinder can also be reduced by using a more efficient structure, such as semi-monocoque or truss core. It is estimated that a refined design of such a support cylinder could have a mass of about 25 to 30 lb_m. The spacing for the reinforcement in this design would have to be less than 3.1 inches, the half length of the buckling wave, in order that the thickness be reduced below that required for the monocoque cylinder.

8.4.3 Summary of Design Analysis

An analysis of the support system concept chosen for the shadow shield system has shown that the combination of an aluminum skirt section and an FRP cylindrical support will provide the required structural characteristics. The use of the FRP section will result in a small heat leak to the LH_2 tank during ground-hold and those portions of the mission where the thermal resistance of the skirt assembly is important.

A summary of the mass associated with the tank support system is presented in the following table. The range of estimated mass for the support system is from 65 to 85 lb_m depending on the type of construction used in fabricating the skirt sections.

As mentioned previously, some reduction in the overall mass of a ground-erected shadow shield system may be realized if the length of the tank support system were decreased. This may allow for the use of a shorter overall stage which would be advantageous. In the case of a space-erected shadow shield system, the length of the tank support system could not be reduced appreciably.

MASS SUMMARY FOR TANK SUPPORT SYSTEM

	"A"	"B"
Aluminum skirt	8.1	5.0
FRP cylindrical support	41.4	25.0
Aluminum doublers	1.4	1.4
Rivets	0.5	0.5
Aft support tube	10.8	10.8
FRP support-to-tube angle	8.3	8.3
Support brace for angle	2.1	2.1
Aft ring box-type support points	10.1	10.1
Hardware	2.2	2.2
TOTAL	84.9 lb_m	65.9 lb_m

"A" - mass summary based on monocoque structure selected for present analysis.

"B" - mass summary based on estimated mass of semi-monocoque or truss core support assemblies.

9.0 GROUND-HOLD AND ORBITAL INSULATION SYSTEMS

9.1 Introduction

There are a number of system concepts which have been considered for insulating an LH_2 storage tank during ground-hold conditions (pre-launch) when the external environment is at ambient temperature and pressure. Usually, the criterion for the choice of a suitable system is one in which the heat flux to the tankage is limited to between 100 and 250 Btu/hr ft^2. In addition to the normal launch environmental conditions of shock and vibration, the insulation on unshrouded vehicles must withstand the forces and heating due to aerodynamic effects.

The following discussion of ground-hold insulation systems pertains to shrouded vehicles where the ground-hold and orbital insulations are not directly exposed to the aerodynamic environment and the insulation system is not jettisoned after launch. Further, it is assumed that the LH_2 tankage will require some amount of multilayer insulation (MLI) for near-planetary orbital operation in vacuo as well as a ground-hold insulation system which will limit the heat flux at ambient conditions to between 100 and 250 Btu/hr ft^2.

A number of favorable characteristics for any ground-hold insulation system are listed below (not necessarily in order of importance):

- Lightweight
- Thermally efficient
- Low outgassing rate in vacuo
- Reliable (accept shock, vibration, handling and temperature cycling without damage)
- Repairable
- Will minimize formation of deleterious condensables (e.g., water, air) within the associated MLI system
- Will not impede venting of an MLI system during ascent
- Easily integrated with conventional MLI systems for orbital use
- May be easily applied to a wide variety of tank shapes and sizes
- Will accept or tolerate a finite amount of hydrogen tank leakage without a corresponding increase in heat flux
- If applicable, the ground-hold system will provide for preconditioning of the MLI material to minimize outgassing during orbital operation

Several basic concepts and many variations thereof have been examined for ground-hold insulation systems. The systems basically fall into three categories:

1) Gas-purged systems in which helium (or in some instances, another gas) is introduced either through the MLI contained in a purge bag or in a purged substrate attached to the tank wall.

2) Sealed-cell systems, such as a low density foam, attached to the tank or a sealed-cell honeycomb, which are cryopumped at the existing cryogenic temperatures to lower their effective conductivity.

3) Vacuum-jacketed multilayer systems in which the MLI is sealed in a vacuum-tight membrane and low pressures within the insulation are achieved by cryopumping.

A summary of various ground-hold systems including weights, thickness and measured thermal performance under ambient temperature and pressure is given in Table VIII. The system weights range from approximately 0.1 to 1.0 lbs/ft^2, and the ground-hold heat fluxes generally range

TABLE VIII

SUMMARY OF SEVERAL GROUND-HOLD INSULATION SYSTEMS

	System Wt. (psf)	System Size	Thickness (in)	Heat Flux $BTU/hr\ ft^2$	Reference
A. Gas-Purged					
1. He-purged fiberglass mat - mylar purge bag	~0.2	26 in. dia. tank	1.5	~150-200	Sterbentz, et al, (1966)
2. Saturn S-II - foam-filled honeycomb with He purge on cold side	0.9	6000 ft^2	1.6	~230	Glaser, et al, (1967)
3. Saturn IV-B - internal seal - foam	0.7	-	1.0	175	Apisa, et al, (1966)
4. He-purged MLI - 5 shields and spacers	-	40 ft^2	0.4 to 1.0	165	Black, et al, (1964)
5. He-purged MLI - 48 layers		105 in. dia. tank	~1.0	~140	Cody, et al, (1966)
6. Composite - 1/2 foam with 5 layers He-purged MLI and purge bag	0.24	40 ft^2	~1 1/2	92	Black (op. cit.)
B. Vacuum-Jacketed Multilayer					
7. Cryopumped sealed multilayer with 11 layers MLI and MAAM jacket with 2 in. of external He-purged multilayer (37 - 1/4 mil mylar shields)	0.133	30 in. dia. tank	0.40	~100	Apisa (op. cit.)
C. Sealed-Cell (Cryopumped)					
8. Mylar honeycomb sealed with 1/4 mil MAAM film with external He-purged multilayer (37 - 1/4 mil mylar shields)	0.148	30 in. dia. tank	0.40	~ 70	"
9. Urethane foam - glass fiber reinforced with MAM vapor barrier (4 lb/ft^3 foam)	0.20	40 ft^2	0.5	93	Black (op. cit.)
10. Fiber-reinforced polyurethane foam (2 lb/ft^3 foam)	0.17	26 in. dia. tank	1.0	150-200	Sterbentz

between 100 and 230 Btu/hr ft^2. Ranking these systems on a heat flux-per-unit-weight basis is usually not applicable since the LH_2 boil-off resulting from the ground-hold heat leak is replaced by topping the tank prior to launch. In other words, the weight penalty to the vehicle is only the weight of ground-hold insulation required to maintain an acceptable heat leak during pre-launch operations. Therefore, the choice of a system will be heavily influenced by considerations other than the absolute value of the heat flux.

The following discussion of the performance and merits of ground-hold insulation systems pertains to gas-purged, sealed-cell foam systems, or combinations thereof as directed by contract.

9.2 Gas-Purged Systems

The basic concepts for gas-purged systems have been evaluated by Knoll and Oglebay (1963); and tests on helium-purged systems have been reported by Sterbentz and Baxter (1966), Black, et al (1964) and Cody and Hyde (1966). Three different approaches have been considered. The first is to purge the entire MLI system (enclosed in a purge bag) with helium. The second approach is to provide a purge space (e.g., a fiber glass mat) beneath the MLI used for orbital protection, and the third is to use a low-density foam bonded directly to the cold tank wall and purge the MLI attached to the outside of the foam. In this latter case, it is possible to use gases other than helium, such as CO_2, A, Ne, N_2, etc., by selecting a foam thickness which will preclude condensation within the MLI.

Previous testing in our laboratory has been reported by Black, et al (1964) with a helium-purged multilayer insulation system using five radiation shields with netting spacers and a 2-mil polyester film, aluminum foil tri-laminate purge bag. The spacing between the cryogenic vessel and the purge bag varied over the surface from about 0.4 to 1.0 inches. The testing was accomplished with LN_2 in the inner vessel with an atmospheric pressure helium purge. The ambient air temperature (outside the purge bag) was approximately 540R. The tests showed that the average heat leak during this ground-hold simulation was approximately 165 Btu/hr ft^2. The measured average temperature of the purge bag was 327R (-133F). As a result of this low temperature, considerable frost formation occurred on the purge bag outer surface. For the same test conditions, the computed heat flux was 250 Btu/hr ft^2. The heat flux was calculated by assuming that the heat transfer between the purge bag and cryogenic tank was due to conduction through the helium gas. The effects of the transient formation of frost on the purge bag and the resulting change in external heat transfer coefficient or convection effects within the purge bag were not included in the analysis. It is expected that a similar test with LH_2 in the tank instead of LN_2 would not appreciably affect the resulting ground-hold heat flux - the heat leak would probably be larger by approximately 10-20% because of the increased temperature differential.

Test results presented by Cody and Hyde (1966) with a 48-layer, He-purged MLI system applied to an LH_2 tank with approximately a 1-in. spacing between the tank and purge bag also show that the average heat flux was of the order of 140 Btu/hr ft^2. For this 105-in. dia. tank, a helium purge rate of 2.5 scfm reduced the air concentration within the MLI to less than 5% and the moisture content to less than 50 ppm in an 8-hour purge period.

A somewhat different approach to the design of a helium-purged system was taken by Sterbentz and Baxter (1966). In their work, a porous glass fiber mat approximately 1.5 inches thick was used as a spacer and served to reduce convection effects, and an Aclar purge bag was used to contain the purge gas. The MLI system used for orbital thermal protection was mounted on the exterior surface of the 7-mil Aclar purge bag. Typical test data showed that a purge rate of 1/2 CFM of helium would reduce the air content within the system to approximately 0.1% by volume after 1 hour of purging. The ground-hold thermal tests yielded an estimated heat flux between 150 and 200 Btu/hr ft^2 - slightly higher than that which would be calculated for an equivalent thickness of helium whose conductivity was evaluated at an average temperature of 250R.

The calculated thermal performance of a simple, helium-purged MLI system is shown in Figure 51. The heat flux is plotted vs. the spacing between the purge bag and tank for external heat transfer coefficients ranging between 1.0 and 2.0 Btu/hr ft^2 F. The heat flux was calculated by assuming that the conductance between the purge bag and tank was equivalent to the conductance of helium between the two temperature limits, and taking the ambient air temperature to be 520R. From Figure 51, it may be seen that the purge bag spacing must be between 1.5 to 2 inches in order to limit the ground-hold heat leak to between 150 and 200 Btu/hr ft^2. Further, it is seen that the purge bag temperatures are below 492R (32F) indicating that frost will form on the purge bag surface if the ambient air contains water vapor.

One of the major disadvantages of a helium-purged system is the large spacing required. With a shadow shield system, the thickness of MLI required for orbital thermal protection would be about 1/4 to 1/2 inch and, therefore, would not approach the required spacing of 1.5 inches if inserted between the tank and purge bag. Thus, some method for spacing the purge bag away from the tank during ground hold is required. The spacing could possibly be maintained by use of a loose-fitting bag which is internally pressurized to have a slight ΔP or by use of a low density fiber glass mat substrate. (A fiber glass substrate roughly 1.5 inches thick, which would weigh about 0.08 lbs/ft^2 exclusive of the purge bag.) The use of a fiber glass substrate creates the problem of not providing a reasonable structural base on which to attach MLI. Attaching the MLI to the exterior of a purge bag would result in water-vapor condensation and subsequent frost formation within the MLI due to the low surface temperatures, with attendant damage to the reflective coatings and possible venting and outgassing problems.

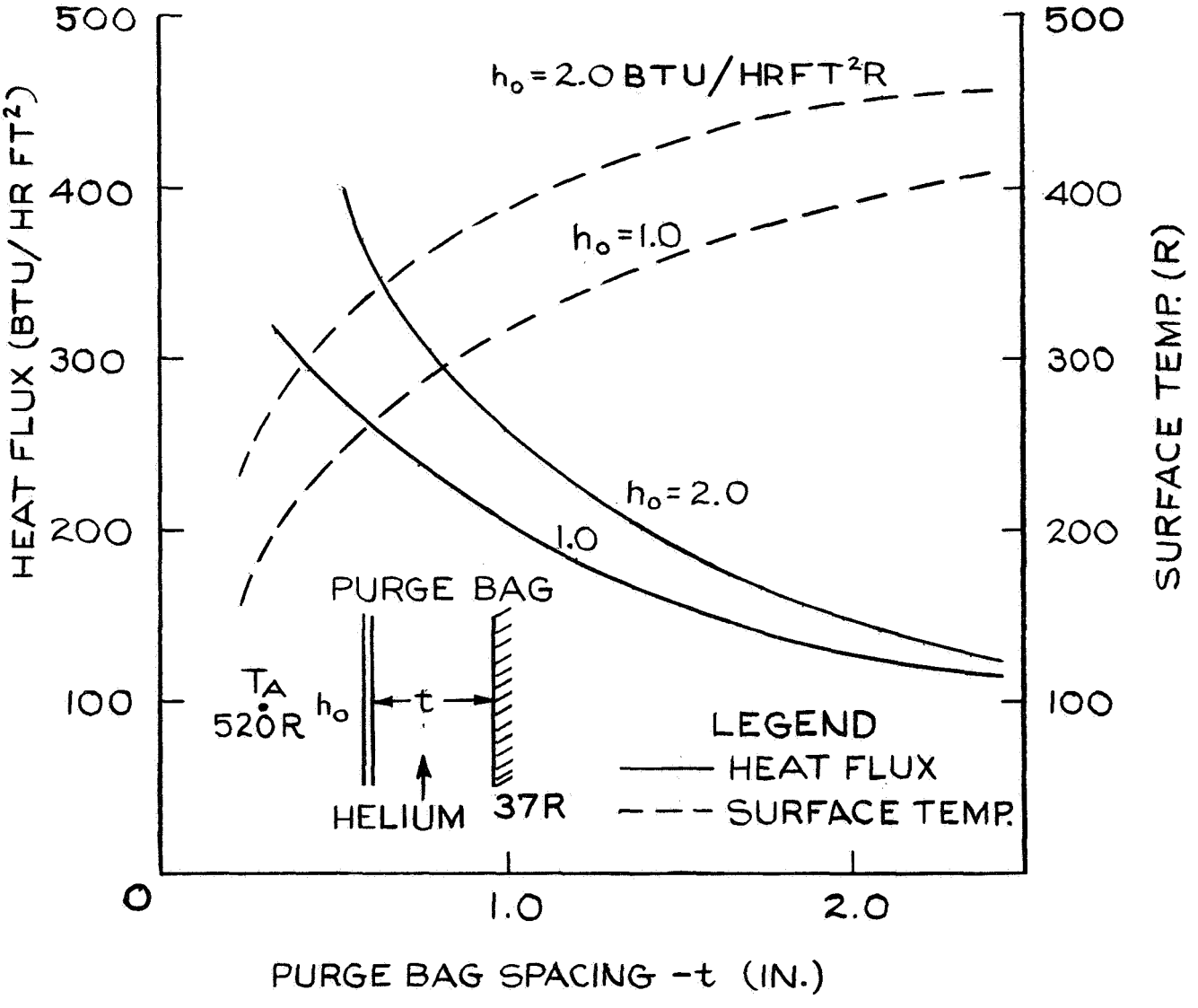

FIGURE 51 - HEAT FLUX - HELIUM PURGED INSULATION

9.3 Foam Systems

Experience with applying low-density foams directly to a cryogenic tank using foam-filled honeycomb which is bonded to the tank surface has been described in the literature. The latter method results in a reasonably large system weight, approximately 1.0 lb/ft^2 but may well have significant advantages for very large tankage because it may be applied in modular form. For this study, which is restricted to tankage approximately 9 ft. in diameter, the use of a low-density, sealed and cryopumped foam applied by foam-in-place methods as described by Black, et al (1964) or by bonding pre-cut foam sections with polyurethane resin using a vacuum cure as described by Sterbentz and Baxter (1966) can be considered technically feasible.

The calculated ground-hold thermal performance of a sealed, cryopumped, foam-insulated LH_2 tank is shown in Figure 52. The conductivity of the cryopumped foam was taken to be 0.01 Btu/hr ft F. over the temperature range of 520R to 37R. The calculated heat flux is plotted against the foam thickness for external heat transfer coefficients of 1.0 and 2.0 Btu/hr ft^2R and an ambient temperature of 520R. It can be seen that a foam thickness of approximately 1/4 inch will limit the heat flux under ground-hold conditions to below 200 Btu/hr ft^2.

The calculated performance of the foam ground-hold system presented in Figure 52 is also in good agreement with the test results obtained with an LH_2 tank using glass-fiber-reinforced, 1/2-inch-thick, rigid polyurethane foam reported by Black, et al (1964). The measurements reported for a 4-ft. dia. tank indicate a ground-hold heat flux of 93 Btu/hr ft^2 with the same ambient air temperature (520R) as assumed in the analysis.

Our experience with foam systems applied to LH_2 tanks indicates that a 1/4-inch thickness also represents a practical limit for the minimum thickness as governed by resistance to thermal shock, ease-of-application and the tolerance of external forms if the foam is "foamed-in-place." The system weight of a 1/4-inch-thick foam layer would range from approximately 0.04 to 0.092 pounds per square foot for foam densities in the range of 2 to 4.4 lbs/ft^3, respectively.

From a practical standpoint, a system weight study based on foam densities of 2 lb/ft^3 would, in our opinion, be overly optimistic. An "as-installed" system density would more likely approach 3-4 lbs/ft^3 even if a 2 lb/ft^3 foam were used because of the additional weight of reinforcing material, bonding resins, etc.

Unlike helium-purged MLI systems which can be evacuated during launch and thereby serve a dual function of providing ground-hold as well as orbital thermal protection, a foam system offers little thermal protection during space operation. Therefore, an MLI system must be provided in addition to the foam substrate. Based on our experience with MLI and the results presented by Crawford, et al (1966),

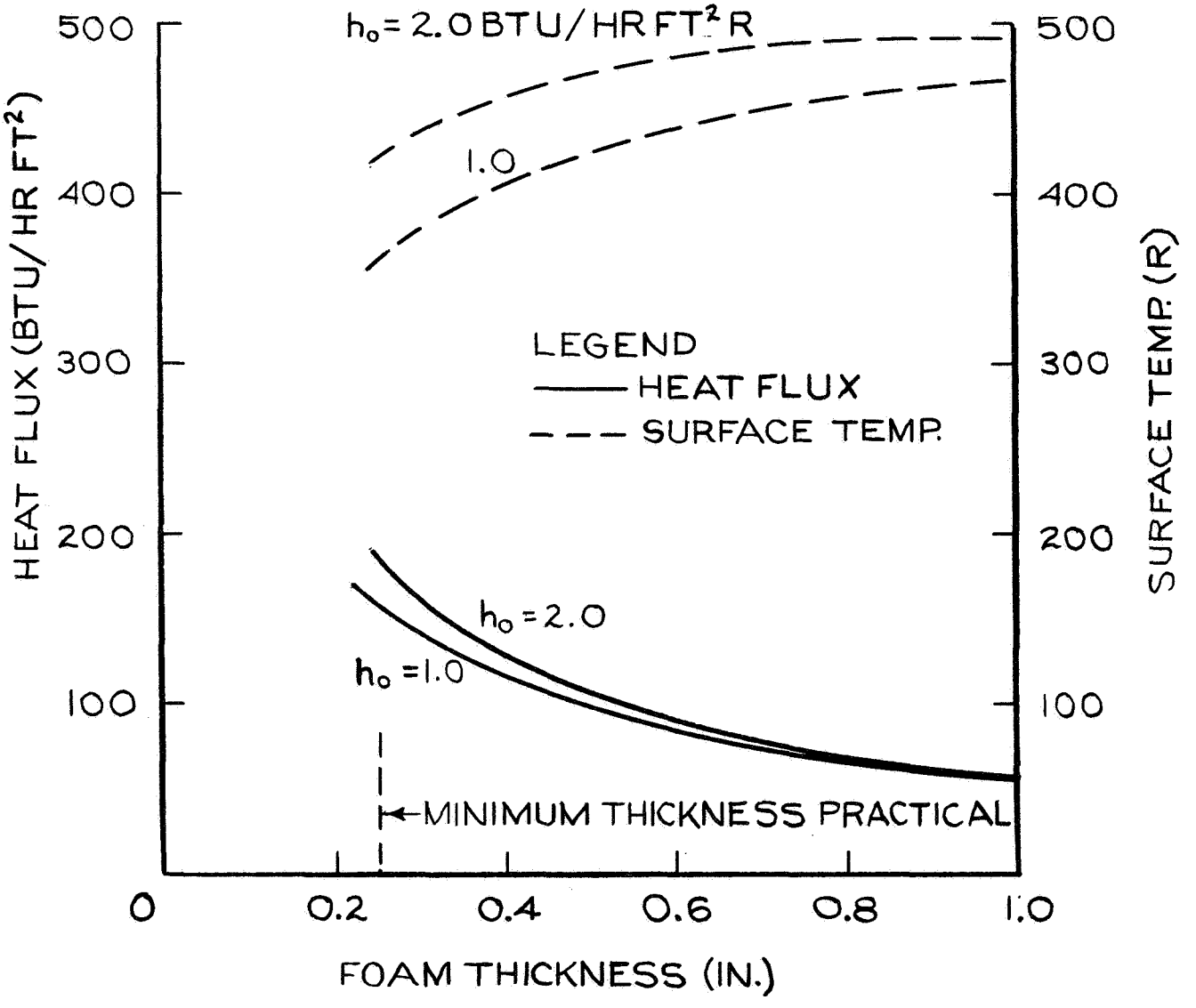

FIGURE 52- HEAT FLUX - FOAM INSULATION

the MLI applied to the foam substrate would be preconditioned prior to launch with a purge operation, using helium or nitrogen gas as a purging medium.

For the reasons presented above, the evaluation of foam insulation systems for ground-hold systems will be restricted to a concept in which the MLI is purged prior to launch for preconditioning purposes.

9.4 Evaluation of Ground-Hold Concepts

A sketch illustrating three approaches to a ground-hold insulation system is presented in Figure 53. The systems may be described as follows:

System "A" - Helium-Purged Multilayer with Purged Substrate

System "B" - Inflated Purge Bag

System "C" - Foam Substrate with External Purged Multilayer Insulation

A mass estimate (per unit area) for each of the systems is presented in Table IX. In this mass tabulation, the design of the ground-hold insulation system was based on an acceptable maximum heat leak of 200 Btu/hr ft^2 for all systems; and the tabulation includes the mass of an MLI system comprising five, 1/4-mil double-aluminized polyester or polyimide radiation shields and lightweight silk netting spacers. The effective emittance of such an MLI system (with approximately 2% of the area perforated for venting)[1] under space conditions will be approximately 0.0075 with boundary temperatures of 540R and 37R, respectively. The corresponding heat flux between these temperature limits would be approximately 0.941 Btu/hr ft^2.

The mass tabulation does not include the mass of the helium-purge plumbing, regulators, vents, etc., since it is assumed that the mass of such a system would be identical for all systems.

The mass tabulation shows that the inflated purge bag system would result in the lowest mass, while the purged fiber glass substrate and the foam substrate system have essentially the same mass.

A list of the advantages and disadvantages of the three systems is presented in Tables X through XII.

---

1. The requirements for venting are taken to be representative of a typical system. Fewer layers of MLI - approximately three radiation shields - would be required if the shields were not perforated.

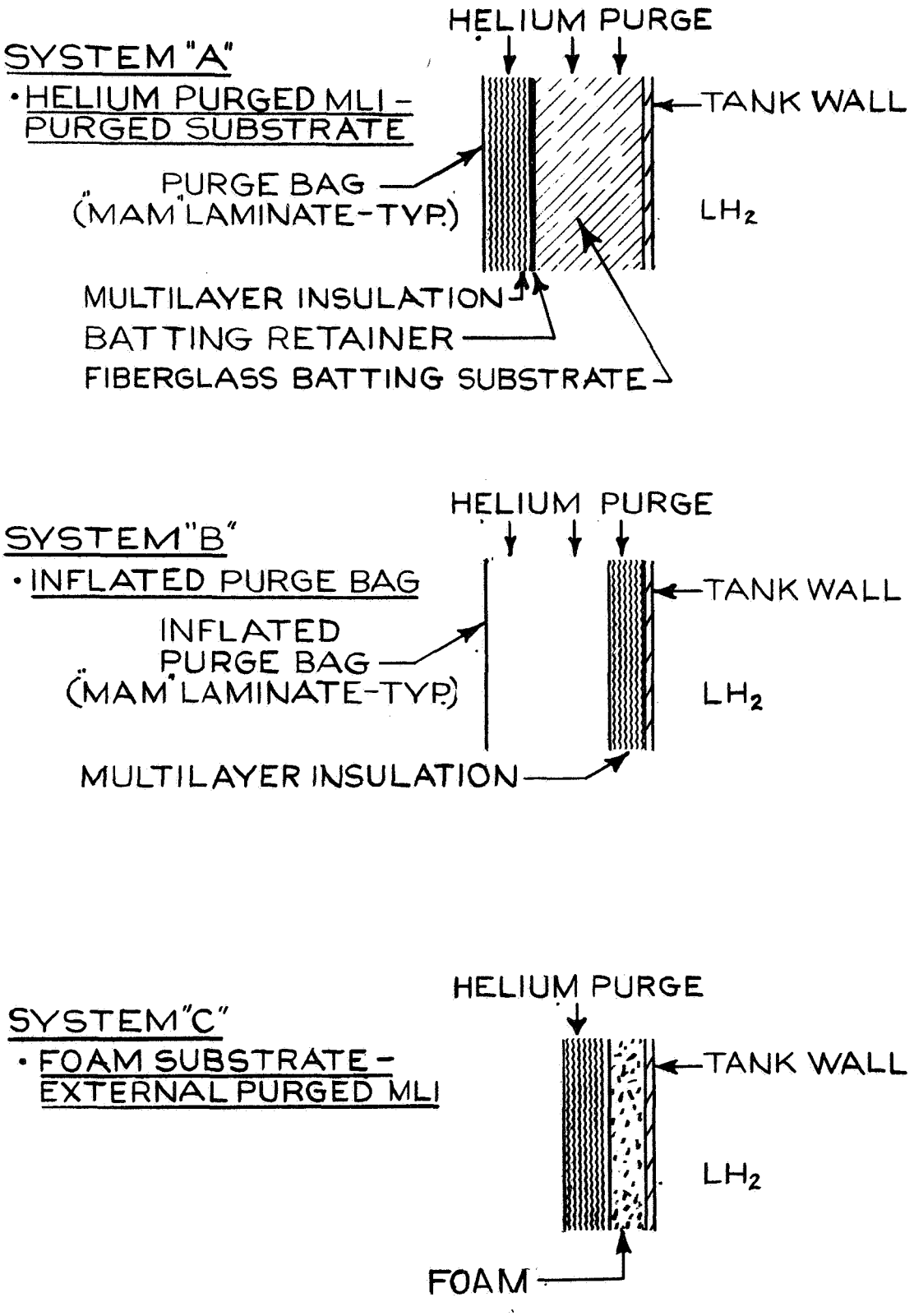

FIGURE 53 – SKETCH OF GROUND-HOLD INSULATION SYSTEMS

TABLE IX

GROUND-HOLD INSULATION SYSTEM MASS COMPARISON*

System "A"		Mass (lbs/ft^2)
1.	Fiber glass substrate, 1.5" thick, 0.5 lbs/ft^3	0.063
2.	Substrate retainer (20-mil fiber glass screen)	0.030
3.	Multilayer insulation	0.027
4.	Purge bag - MAM tri-laminate	0.021
5.	Installation factor (seams, edges, tape, reinforcing)	0.012
	Total mass per unit area***	0.153
System "B"		
1.	Multilayer insulation**	0.027
2.	Purge bag - MAM tri-laminate	0.021
3.	Installation factor	0.010
	Total	0.058
System "C"		
1.	Foam substrate - 1/4", 3.3 lbs/ft^3	0.063
2.	Foam seal - MAM tri-laminate	0.021
3.	Multilayer insulation	0.027
4.	Purge bag - MAM tri-laminate	0.021
5.	Installation factor	0.010
	Total	0.142

---

* Ground-hold heat leak of 200 Btu/hr ft^2.

** Five - 1/4-mil polyester shields, aluminized both sides and 10 netting spacers.

*** Does not include purge lines, regulator valves, etc., which are common to all systems.

TABLE X

SYSTEM "A" - HELIUM-PURGED MLI-PURGED SUBSTRATE

Advantages

- Relatively easy to install and remove.
- Fiber glass batting provides some measure of spacing to provide the proper purge space.
- Can be applied to a wide variety of tank shapes and sizes.
- Due to the compliance of the substrate, the MLI may not be subject to excessive compressive loads.

Disadvantages

- Substrate does not provide a good structural base for attaching the MLI.
- Higher weight per unit area than System "B" - Inflated Purge Bag
- Spacing control may be difficult around penetrations or highly curved surface due to compression of the substrate.
- Requires a relatively large space.
- Purge rate must be carefully controlled and properly distributed over all areas.

TABLE XI

SYSTEM "B" - INFLATED PURGE BAG

Advantages

- Lightweight

Disadvantages

- Difficult to maintain correct spacing for ground-hold insulation requirements.
- System must be sealed to have small leakage rates to permit proper inflation and spacing.
- Cannot be easily integrated with supports of piping penetrations.
- Difficult to properly restrain purge bag during launch vibration environment.
- Requires a relatively large space.
- Purging rates and ΔP must be controlled.

TABLE XII

SYSTEM "C" - FOAM SUBSTRATE WITH EXTERNAL MULTILAYER INSULATION

Advantages

- Most reliable of all systems from ground-hold insulation standpoint since the foam thickness may be accurately determined.
- Provides a good structural base on which the MLI may be mounted.
- With foam-in-place techniques, supports and piping penetrations can be easily insulated.
- Precise purge control rates are not required to minimize air and water-vapor concentration.
- Space occupied by the insulation is minimal.
- Foam substrate can be repaired.

Disadvantages

- System weight is larger than System "B".
- Foam substrate may not be easily removed.
- May be difficult to foam-in-place over very large tanks.

From a qualitative assessment of the advantages and disadvantages of the various systems, we have concluded that System "C", incorporating a foam substrate with external multilayer insulation, would be the best system - based on reliability, and weight considerations - for the 9-foot-diameter LH_2 tank considered in this study. Although the inflated purge bag concept - System "B" - would result in the lightest insulation weight, we believe that it would require considerable development effort to be a reliable system.

Discussions of the ground-hold heat and orbital heat leak to the LH_2 tank based on the use of System "C" are presented in the following sections.

9.5 Ground-Hold Heat Leak - Selected System

There are three sources of heat leak to the LH_2 tank which occur during ground-hold operation. They include heat leakage via: a) the foam insulation over the surface area of the tank, b) the support cylinder used to support the tank, and c) the piping (vent, fill, pressurization, instrumentation) penetrations.

The heat flux to the LH_2 tank over the major surface area may be obtained from Figure 52 for System "C". For a 1/4-inch thickness of foam, the resulting heat flux will be approximately 200 Btu/hr ft^2 for an ambient temperature of 520R and a surface coefficient of heat transfer of 2.0 Btu/hr ft^2 F. The surface area of the 9' dia. (oblate spheroid) tank is 406 ft^2, and the resultant heat flow is 81,200 Btu/hr. The equivalent boil-off rate of LH_2 is 418 lbs LH_2 per hour.*

The second source of heat leakage is the cylindrical skirt which supports the tankage. First, we will derive the general expressions for the heat flow and then compute the heat flux for various support materials.

A diagram of the support skirt is shown below:

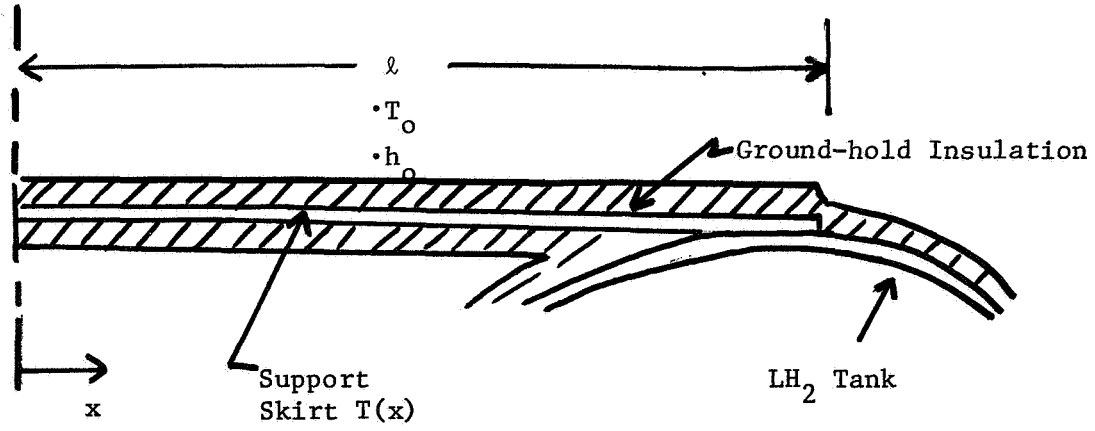

* It is noted that the small thermal resistance afforded by the multilayer insulation which is at atmospheric pressure has been neglected.

Let T_o be the ambient temperature and LH_2 be the temperature of the LH_2 tank. We assume that there is an overall heat transfer coefficient $\bar{h}$ between the ambient air temperature T_o and the support cylinder defined by the equation

$$\bar{h} = \frac{1}{\frac{1}{h_o} + t/k_i} \tag{1}$$

where h_o - surface heat transfer coefficient

t - thickness of insulation

k_i - insulation conductivity

The differential equation for the support temperature is

$$-k\delta \frac{d^2T}{dx^2} + 2\bar{h}\,(T_o - T) = 0 \tag{2}$$

where k - support conductivity

δ - support thickness

The solution, subject to the boundary conditions

$$T = T_o \quad \text{at } x = 0$$

$$T = T_{LH_2} \quad \text{at } x = \ell$$

is given by

$$\frac{T - T_o}{T_{LH_2} - T_o} = \frac{\sinh \mu x}{\sinh \mu \ell} \tag{3}$$

where

$$\mu^2 \equiv \frac{2h}{k\delta} \tag{4}$$

The heat flow to the tank over the cylinder of radius r is

$$q = -2\pi rk\delta \left.\frac{dT}{dx}\right|_{x=\ell} = \frac{2\pi rk\delta\mu\,(T_o - T_{LH_2})}{\tanh \mu \ell} \tag{5}$$

It is important to note that when $\mu \ell \geq 3$

$$\tanh \mu \ell \doteq 1$$

and the heat flow to the tank becomes

$$q = 2\pi rk\delta\mu \ (T_o - T_{LH_2}) \tag{6}$$

This limiting case applies when the thermal conductance ($k\delta$ product) of the skirt is relatively low. The heat flow to the tank is then independent of the skirt length. Another limiting case occurs when the argument $\mu \ell << 1$. Then

$$\tanh \mu \ell \doteq \mu \ell \tag{7}$$

and the heat flow to the tank becomes the usual conduction equation

$$q = \frac{2\pi rk\delta}{\ell} \ (T_o - T_{LH_2}) \tag{8}$$

This situation applies when the surfaces of the skirt are well insulated, or the skirt has a relatively high conductance.

The ground-hold heat leak was evaluated for a monocoque cylindrical support skirt (c.f., Fig. 50) for various structural materials using an external coefficient of heat transfer h_o of 2 Btu/hr ft^2 F, an ambient temperature of 520R and a ground-hold insulation comprising 1/4" of sealed cryopumped foam having an average thermal conductivity of 0.01 Btu/hr ft F. The skirt length was taken to be 38 in. although in all cases which were evaluated the heat flow was independent of the length.

The ground-hold heat leak to the LH_2 tank via the 4.5 ft radius support skirt is given in the following table.

Material	Thickness (in.)	Heat Flow (Btu/hr)	Boil-off (lbs/hr)
FRP	.060	450	2.3
Ti(5Al 2.5Sn)	.032	1156	5.9
304 SS	.025	1459	7.5
2219 Al	.031	5004	25.7

It may be seen from the table presented above that the boil-off rate attributable to the support is quite small considering that a usual guideline for maximum ground-hold heat leak is of the order of 200 Btu/hr ft^2 which, as we have seen previously, would result in a boil-off rate of LH_2 of over 400 lbs/hr. Furthermore, these calculations are conservative since the thermal resistances across the riveted joints of the support cylinder have been neglected.

In order to estimate the magnitude of the heat leak via the piping connections, we have made a number of assumptions regarding the arrangements of the piping and the dimensions. We have assumed that the engine feed and tank fill lines are located on the bottom of

the tank and that the pressurization and vent lines are located on the top of the tank. During "hold" periods, it is assumed that the fill and engine feed lines contain LH_2. The lines are assumed to be aluminum with a wall thickness of 0.037" and insulated with 1/4" of foam.

In estimating the heat flow via the vent line, it is conservatively assumed that none of the heat flowing into and along the line is intercepted by the venting hydrogen. The valves for the fill and engine feed lines are taken to be approximately 12 inches from the tank.

A summary of the heat leakage to the LH_2 tank via the piping lines is presented below.

Line	Line Size	Heat Flow (Btu/hr)	LH_2 Boil-Off (lbs/hr)
Pressurization	1/2" OD	47	.24
Vent	2" OD	186	.96
Drain and fill	1.5" OD	218	1.12
Engine feed	1.5" OD	218	1.12

Estimated total - 3.44 lbs/hr

It can be seen that the total LH_2 boil-off due to the piping connections is small, with respect to the heat leak via the major surface area of the tank.

A summary of the estimated ground-hold heat leak for the LH_2 tank insulated with 1/4"-thick foam insulation is shown below:

Summary of Ground-Hold Heat Leak

	Heat Flow (Btu/hr)	LH_2 Boil-Off (lbs/hr)
Tank surface	81,200	418
Cylindrical Support (0.060" FRP)	450	2
Piping connections	669	3
Total	82,319	423

9.6 Heat Leak during Ascent

During the ascent period, the shroud surrounding the LH_2 tank is aerodynamically heated and simultaneously the pressure in the inter-stage decreases. The driving force for heat transfer between the shroud and the ground-hold insulation (ΔT) thus increases with time, while the pressure decrease tends to reduce the overall convective heat

transfer coefficient between the gas in the shroud and the insulation surface. Until the pressure reaches a level of approximately 10^{-4} torr, the multilayer insulation on the exterior of the foam insulation is not thermally effective; and the major thermal resistance is in the foam. Upon reaching high altitudes, the shroud begins to cool off by radiation, and the multilayer insulation begins to provide an effective barrier to heat flow. The net effect is one in which the heat flowing to the foam insulation during the initial stages of the ascent, where convection effects are important, is trapped by the increasing effectiveness of the multilayer insulation as the pressure within the insulation decreases to the point where the mean-free path is of the same order as the spacing between shields. Thus, virtually all of the heat flow which goes into increasing the temperature of the foam appears as LH_2 boil-off since the thermal resistance of an evacuated multilayer insulation is much higher than the foam insulation used for ground-hold.

In order to estimate the heat flow to the LH_2 tank during ascent, a simplified, one-dimensional, finite-difference mathematical model of the insulation system was set up; and the transient temperature distributions and heat flow in the insulation were computed by use of a thermal analysis digital computer program.

During the aerodynamic heating period - from launch to the time at which the maximum shroud temperature is reached - it was assumed that the surface temperature of the foam was equal to the shroud temperature. This assumption is equivalent to stating that the combined thermal resistances associated with the convective heat transfer coefficients between the shroud and the gas and the gas and the insulation, as well as the thermal resistance of the multilayer insulation, are small with respect to the thermal resistance of the foam.

During the period associated with the cooldown of the shroud, the conservative assumption was made that the effectiveness of the multilayer insulation was equal to the effectiveness of the insulation under a fully evacuated condition. Since the thermal resistance afforded by the foam insulation is less than that of the multilayer, a major fraction of the heat stored in the foam will appear as LH_2 boil-off.

The ascent heating period was taken to be 160 seconds with shroud temperatures as presented in Table XIII. The shroud was assumed to cool exponentially to an average orbital temperature of approximately 540R in the period from 160 to 500 seconds. During this period the shroud emittance was taken to be unity, and the effective emittance $\bar{\varepsilon}$ of the multilayer insulation was assumed to be 0.0072.

The 1/4" thickness of the foam was subdivided, and the temperatures at 7 equally spaced nodes within the foam were calculated as a function of time. The heat flux to the stored cryogen q_{LH_2} was

TABLE XIII

TYPICAL INTERSTAGE SHROUD TEMPERATURE HISTORY

	Time (secs.)	Temp. °K	Temp. °R
Launch	0	290	522
↑	10	309	
	20	327	589
	40	363	
Ascent Heating	60	396	713
↓	80	424	
	100	448	806
	120	465	
	140	476	856
T_{max} - Start Cooldown	160	480	864
↑	180	446	
	200	417	751
	240	375	
Shroud Cooldown	280	346	623
↓	320	328	
	440	301	542
	500	296	

calculated from the temperature gradient history at the LH_2 tank wall. A sketch of the mathematical subdivision of the foam used in the one-dimensional heat flow model is shown below:

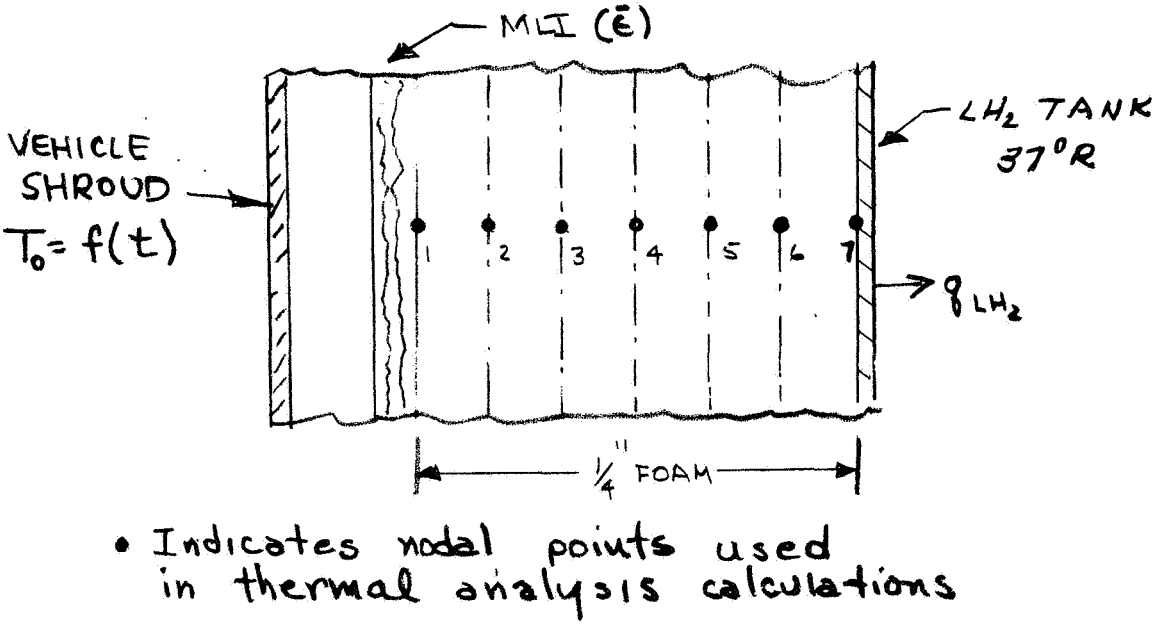

The calculated heat flows and the equivalent boil-off of LH_2 for the 9-foot-diameter LH_2 tank are presented below:

Time	Total Heat Flow (Btu)	LH_2 Boil-Off (lbs)
0-160 secs.	1544	7.9
160-500 secs.	1547	7.9
Total	3091	15.8

It can be seen that the total amount of heat entering the LH_2 tank during the ascent period and cooldown to an average orbital condition results in an equivalent boil-off of approximately 16 lb_m of LH_2. Again, it is emphasized that these calculations are approximate; however, the magnitude of the boil-off is expected to be conservative due to the nature of the assumptions made in the analysis.

9.7 Heat Leak during Orbital Operation

In order to select a reasonable mass of multilayer insulation for protection during planetary orbital operations, an analysis was made to determine the heat flow to the LH_2 tank by radiation through the multilayer insulation during earth orbital operation.

In order to estimate the heat flow through the insulation during orbital operation, a "space-equivalent" average background temperature was established for a typical earth orbit based on radiative fluxes from direct sunlight, infrared radiation emitted from the earth and earth albedo. This orbital average temperature was used as a "hot" boundary temperature for the outermost layer of the multilayer insulation. Experimental data for the heat flux through the insulation between calculated temperature of the outermost layer and the LH_2 tank was used to establish the heat flow to the stored cryogen.

The "space-equivalent" background temperature was calculated for a cylindrical control surface surrounding the LH_2 tank. The control surface was assumed to be in radiative equilibrium with the space environment (i.e., thermal mass effects were neglected). The following schematic diagram illustrates the arrangement of the LH_2 tank and the control surface.

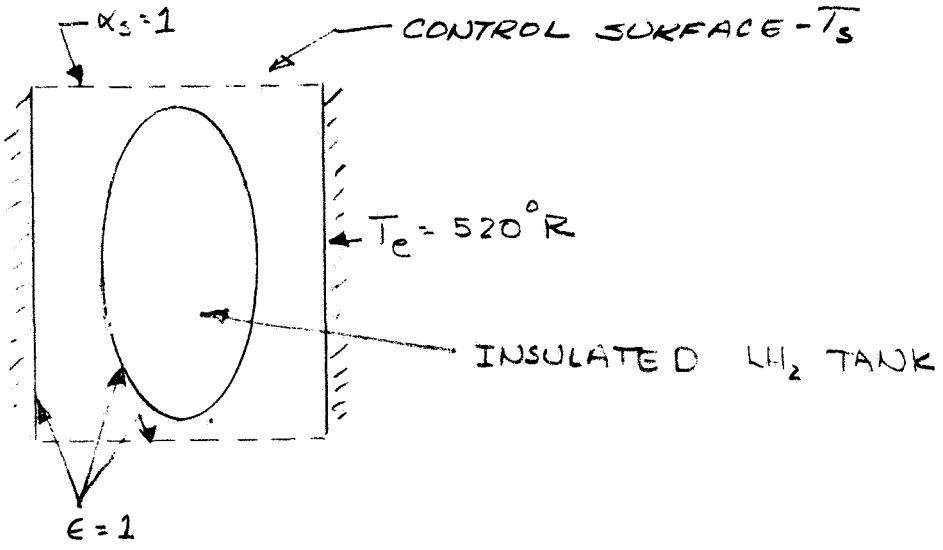

The control surface temperature, T_S, would represent the temperature of an interstage shroud of low thermal mass and low azimuthal conductance. Mathematically, the control surface temperature would also be nearly identical to the average temperature of the outermost surface on the MLI on the LH_2 tank for a non-shrouded stage. Thus, the calculations as presented herein would apply to either the case of an unshrouded stage (interstage jettisoned after launch) or a shrouded stage in which the thermal time constant of the skin was small and the azimuthal conductance was also small.

To place an upper bound on the calculated heat leak to the LH_2 tank, the presence of the LO_2 tanks, engine, structure and shadow shield system was neglected. For a shrouded system, this will be a good approximation since the outer layer of MLI on LH_2 tank will be in equilibrium with the interior of the shroud which will act like a blackbody cavity.

The cylindrical control surface surrounding the LH_2 tank and shadow shield system was subdivided to represent an octagonal prism; and the temperatures of each of the eight nodes were calculated as a function of time using an existing ADL Orbital Heat Flux Program, neglecting azimuthal conduction and internal radiation. The program calculates the flux incident on each of the subdivisions arising from direct sunlight, earth-shine and albedo over an orbit and then computes the orbital temperature of each node. The orbital parameters selected for the study are:

Inclination	- 34° to equatorial plane
Altitude	- 435 n. miles
Eccentricity	- 0°
Percent sun time	- 82.6
Orbital period	- 100.99 minutes

The solar absorptance-to-emittance ratio of the control surface was chosen to be unity.

The average temperature of the control surface over an orbit was obtained by numerically integrating the temperature-time history of each node and determining the average temperature. For the orbit cited, the average temperature was calculated to be 520R. This temperature will depend on the orbital characteristics and surface properties used for a given kick-stage design. The orbit chosen for this study with an 82.6% time-in-sunlight and the choice of a solar absorptance-to-emittance ratio of unity are conservative, and result in a somewhat elevated average shroud temperature. The average shroud temperature would be lower for orbits with a lower percent time in sunlight and a shroud exterior with a low solar absorptance-to-emittance ratio.

The heat flux to the LH_2 tank was then calculated as a function of the number of orbits for two multilayer insulation systems. The first system comprised five radiation shields (1/4-mil double aluminized polyester or polyimide film) with two silk netting spacers per shield. The second system comprised 10 radiation shields, i.e., a system with double the mass. The insulation systems were assumed to be perforated for venting and outgassing with a 2% perforation factor. Experimental data (Black, et al (1966)) for the five-shield system for a hot boundary temperature of 520R were used to establish the base-line unperforated heat flux. The heat flux was corrected for the 2% perforation factor using the theory and data also obtained in the previous cited document. The heat fluxes used in this study for the five-layer and ten-layer systems are 0.941 Btu/hr ft^2 and 0.471 Btu/hr ft^2, respectively, between the boundary temperatures of 520 and 37R. The installed mass of these MLI systems including purge bag are estimated to be 0.058 and 0.085 lb_m/ft^2, respectively.

In addition to the heat flow via the MLI, it is necessary to include the conduction heat flow via the tank support skirt during orbital operation. For the 0.060" fiber glass skirt, the LH_2 boil-off rate was calculated to be 0.04 lbs/hr.

The calculated MLI insulation mass and the resultant mass of LH_2 boil-off are shown in Table XIV for five-layer and ten-layer systems as a function of the number of orbits (101-minute period). The mass of insulation is based on a coverage of 406 ft^2 for the LH_2 tank and tank support.

From Table XIV it can be seen that the mass penalties associated with either a five-layer or ten-layer system are approximately equal for orbital operations of about 15 orbits. Since the exact number of orbits for this study are not defined, the system design cannot be optimized in the usual manner. Usually, the minimum system mass is minimized for a fixed time period. In that case, the minimum overall mass penalty occurs when the mass of insulation equals the mass of LH_2 boil-off.

For purposes of this study, it was assumed that a 15-orbit capability would be sufficient; and the five-layer MLI system was selected for protection during the earth orbital portion of the mission.

9.8 Summary of Ground-Hold and Orbital Heat Leak Calculations

The insulation system chosen for the shadow shield thermal protection concepts comprises a foam substrate for ground-hold protection with an external perforated (2%) multilayer insulation system for orbital thermal protection. For this 1160-lb_m-capacity LH_2 tank with fiber glass support skirt, the installed mass of the foam and multilayer insulation is estimated to be approximately 50 lb_m. The total ground-hold heat leak is estimated to be 82,320 Btu/hr - an LH_2 boil-off rate of 423 lb_m/hr.

A breakdown of the mass penalties and performance is presented below:

	Mass (lb_m)
Foam insulation (1/4" reinforced polyurethane)*	26.0
MLI insulation (5 double aluminized, 1/4-mil polyester films with netting spacers)	24.0
Ascent boil-off (mass of LH_2)	16.0
Orbital boil-off (mass of LH_2 for 15 orbits)	26.0
Total mass penalty	92.0 lb_m

* The area of foam coverage is 306 ft^2 which includes 206 ft^2 of tankage and 100 ft^2 of skirt - 50% of the total skirt length.

TABLE XIV

MLI MASS PENALTY FOR
ORBITAL THERMAL PROTECTION

	Number of Orbits				
	5	10	15	20	25
System 1* (Five layers)					
Insulation mass (lb_m)	23.6	23.6	23.6	23.6	23.6
LH_2 boil-off mass (lb_m)	8.7	17.4	26.0	34.8	43.5
Total (lb_m)	32.3	41.0	49.6	58.4	67.1
System 2** (Ten layers)					
Insulation mass (lb_m)	34.5	34.5	34.5	34.5	34.5
LH_2 boil-off mass (lb_m)	4.5	9.1	13.6	18.2	22.7
Total (lb_m)	39.0	43.6	48.1	52.7	57.2

* Five double-aluminized, polyester, radiation shields and two layers of netting spacer per shield.

** Ten double-aluminized shields with two layers of netting.

From this summary it can be seen that the mass penalties associated with ground-hold, ascent and orbital phases of the mission are appreciable.

10.0 THERMAL INTERACTIONS BETWEEN SHADOW SHIELDS AND SUPPORT STRUCTURES

10.1 Introduction

Due to the large number of variables affecting the overall mass and thermal performance of shadow shield systems, a number of the important parameters were screened and optimized independently to arrive at the designs which have been described above. When the shadow shields and the payload support structures were analyzed independently in the parametric studies, the calculations of the LH_2 boil-off by radiation and conduction effects were made assuming "no thermal interactions" between the shields and structure (shields and structure thermally isolated).

In order to determine the importance of thermal interactions and define guidelines for more complete mathematical models for the thermal analysis of the final designs, if required, several analytical studies were completed. A representative example was chosen for analysis, and the radiation and conduction heat leaks with interactions were compared to those calculated for the same configuration when the shields and structure were thermally isolated. In particular, this study was concerned with the influences of thermal conductance couplings at shield structure interfaces and radiation interchange between the shields and supports.

10.2 Interaction Analysis of Shadow Shields

A payload support structure arranged in cylindrical fashion near the boundaries of a shadow shield system can influence the thermal performance of shadow shields in the following ways:

- Intercept and reflect heat to the shadow shields which would be radiated to outer space if the structure was neglected.
- Radiate heat to the shadow shields.
- Influence the temperatures of the rims of the shadow shields due to the thermal-conductance couplings at the shield-support interfaces (bolted-joint conductances, mounting brackets, etc.).

The interaction analysis of the shadow shields, and structures considered a system with a spacing ratio of 0.25, a shield on the payload at 520R, two intermediate equally spaced shields, and a shield on the

tank support which was assumed to be a cold sink at 37R. The surfaces of shields were assumed to have a diffuse emittance of 0.03 and a diffuse reflectance of 0.97. The support structure was a Warren truss with 12 titanium supports, 2 inch OD x .017 wall. The support surfaces viewing the shields were assumed to have a reflectance of 0.97.

The thermal model of the shield system accounting for interactions with the support structure was formulated with the aid of the Radiant Transfer computer program described in Section 4. After the computer setup of the heat balance equations for a "thermally isolated" shield system, the equations were modified as required to describe the shield-structure interchange using the Data Insertion Routine, and the temperature distributions and radiant heat leaks were computed. The pertinent results of this investigation relating to the thermal performance of the shadow shields are summarized below:

1) The heat intercepted by the structure and reflected back to the shields produced a noticeable increase in the LH_2 boil-off. As shown in Table XV, the reflections increased the LH_2 boil-off by 20% and produced a small increase in temperatures of the intermediate shields.

2) The heat radiated from the structure to the shields did not produce a noticeable change in the radiant heat leak or the temperature distributions in the shields. This is due to two considerations: a) the structure has a small radiating area compared to the area of the shields, b) the surfaces of the structural supports and the shields which are radiatively coupled have a low emittance.

3) Conductive couplings between the rims of the shadow shields and the support structure do not increase the shield temperatures or the radiant heat leak to the LH_2 tank. Actually, the influence of conductive couplings between the structure and shields is to locally reduce the temperatures of the shield rims. (When the structure and shields are thermally isolated, the temperatures of the structure are lower than those of the shield rims at all the interconnection locations.) However, since the shields are constructed of low-thermal-conductance material, the influence of the coupling to the structure is localized in a small region near the interconnection, and the radiant heat transfer to the LH_2 tank is not affected.

Since this study demonstrated that neglecting the reflecting surfaces of the payload support structure could result in optimistic values of computed radiant heat leak, the thermal analysis of the conceptual designs was modeled to account for the reflecting structures.

TABLE XV

EFFECT OF INTERACTIONS ON THE THERMAL PERFORMANCE OF SHADOW SHIELDS

Shield System

L/D = 0.25
2 Equally Spaced Intermediate Shields, $\varepsilon = 0.03$.

Payload Support Structure

Warren truss with 12 titanium supports, 2 inch diameter, $\varepsilon = 0.03$ for surfaces viewing shadow shields.

	"NO INTERACTION"	"INTERACTION" INCLUDING REFLECTIONS FROM SUPPORT STRUCTURE
LH_2 BOIL-OFF BY RADIATION IN 10,000 HOURS (LB_M)	5.46	6.49
SHIELD TEMPERATURES (°R)		
Intermediate Shield near Payload		
Rim Temperature	204	212
Center Temperature	278	282
Intermediate Shield near Tank		
Rim Temperature	97	103
Center Temperature	143	146

10.3 Interaction Analysis of Support Structure

A payload support structure radiatively and conductively coupled to shadow shields is subject to a number of spatially variant boundary conditions in addition to constraints on the boundary temperatures and exposure to outer space. Therefore, in the interaction analysis, a thermal model of the structure was described using finite-difference techniques. (The example of the shadow shield system used for this study was identical to that described above in Section 10.2.) A mathematical model was formulated for one structural element of the truss which is connected to the payload, the tank support, and the two intermediate shadow shields. The LH_2 tank support was assumed to be at a temperature of 37R.

The support was subdivided into a number of zones, defining locations at which temperatures were to be computed; the heat balance equations were written for each temperature location including appropriate terms describing radiative and conductive interchange with the shadow shields; and the heat balance equations were solved numerically on a computer. The heat balance equations were written according to the Zone Method* of Strong and Emslie (1963) which allows the temperature to vary parabolically with the space coordinates.

Figure 54 illustrates the temperature distribution in the structure for varying degrees of thermal coupling to the shadow shields. It is evident that the radiative coupling to the shadow shields and the conductive couplings to the warmer shield rims (at X/L = .33 and .66) raise the structure temperatures and consequently the LH_2 boil-off by conduction. The effect of the shield-structure interactions on the LH_2 boil-off is shown in the following tabulation:

---

* A recent paper, Nathanson et al (1968) demonstrated that in problems involving conduction and radiation, the Zone Method can provide a more accurate description of temperature distributions than conventional nodal or "lumped parameter" techniques which allow the temperature to vary linearly between mesh points.

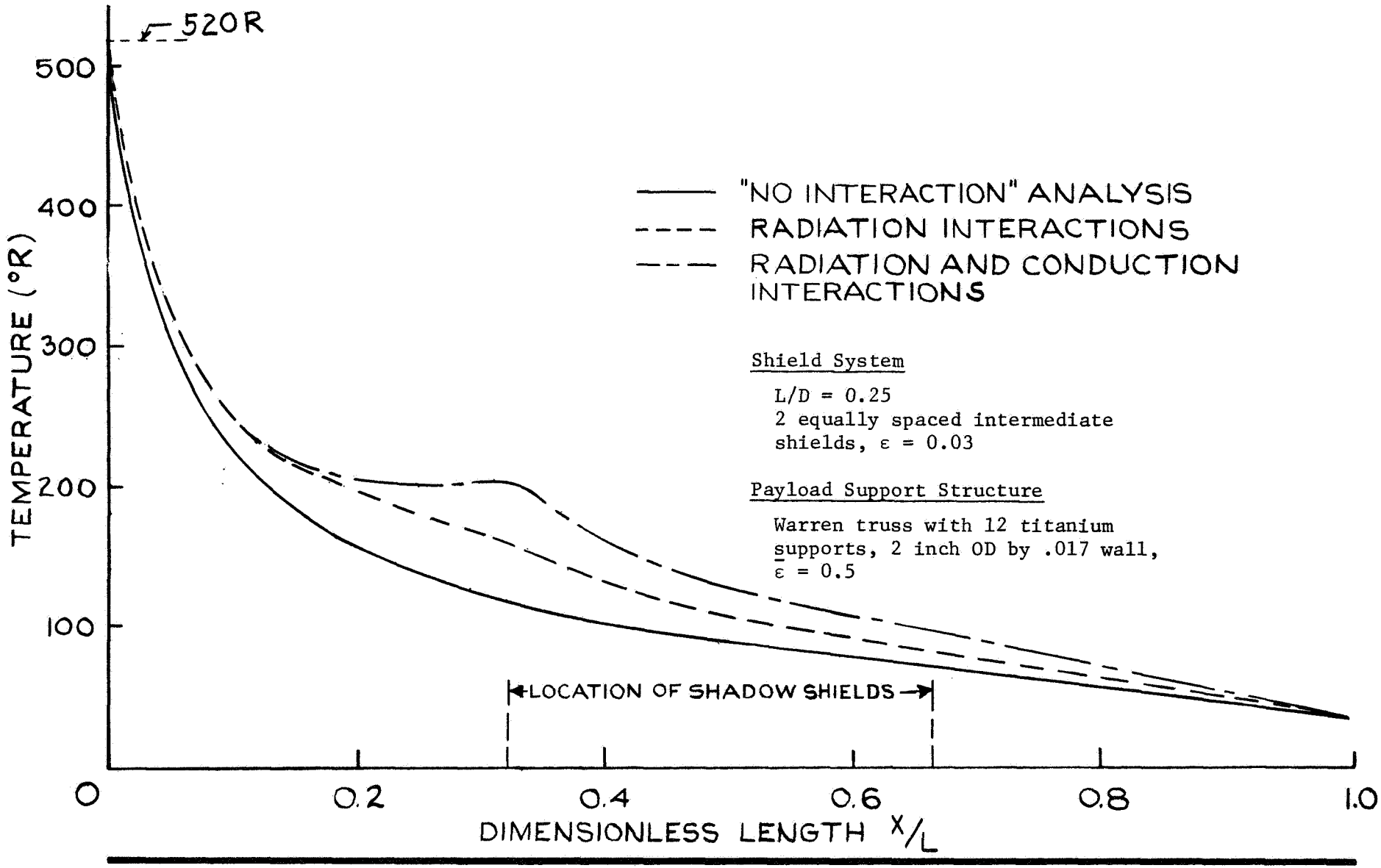

FIGURE 54- TEMPERATURE DISTRIBUTIONS IN A SUPPORT STRUCTURE THERMALLY COUPLED TO SHADOW SHIELD ASSEMBLIES

Concept No.	L/D	Number of Intermediate Shadow Shields	Payload Support Structure
1	0.15	3	Fixed Warren truss with 16 fiber glass supports, 2 in. OD x .030 wall
2	0.25	2	Fixed Warren truss with 12 titanium supports, 2 in. OD x .017 wall
3	0.25	2	Same as Concept 2 with the structural supports cooled using the sensible enthalpy of LH_2 boil-off
4	0.25	2	Same as Concept 2 with pant-leg radiators on the structural supports
5	0.25	2 (with space-erected annular shields to compensate for 15 deg. solar-vector misalignment)	Fixed Warren truss with 16 fiber glass supports, 2 in. OD x .037 wall
6	1.0 (deployed)	1 (space-erected)	Space-erected "A"-frame structure with 6 titanium supports, .88 in. OD x .011 wall

11.2 Radiant Heat Leak and Shield Temperature Distributions

The mathematical models used to determine the radiant transfer and temperature distributions in the shadow shield systems accounted for the following:

- A 520R shield located at the payload
- "n" intermediate shadow shields
- A single shield located on the conical tank support (last shield)
- A ground-hold and orbital thermal protection system between the last shield and the LH_2 tank
- Radiative interactions with the support structure

	LH_2 Boil-Off by Conduction in 10,000-Hour Coast Mission, lb_m
"No interactions" between structure and shields	20
Radiative interactions between structure and shields	29
Radiative and conductive* interactions between structure and shields	38

In summary, a "no interaction" thermal analysis is an effective means of performing independent optimization studies, obtaining measures of system performance and ranking various materials and configurations. However, since the estimates of LH_2 boil-off due to conduction and radiation can be optimistic with this procedure, thermal interactions should be accounted for in the detailed analysis of the final design configurations.

11.0 THERMAL ANALYSIS OF CONCEPTUAL DESIGNS

11.1 Conceptual Designs

The shadow shield concepts which were selected for final evaluation and were described in Section 7.0 are summarized in the following tabulation:

---

* In this calculation, the structure was coupled to the rim of the shadow shields by a thermal conductance of 0.76 Btu/Hr-°R. This value is representative of existing experimental data of bolted-joint conductances in vacuum for configurations similar to the rigid shield-structure connections.

In addition, the calculations were made according to the following assumptions:

- The total hemispherical emittance of all shields was taken as 0.03
- The shields emitted diffusely and had a specular or diffuse reflectance, depending upon which assumption led to the more conservative result
- The shields were assumed to have zero radial conductance since the preliminary analysis showed no appreciable difference in the heat transfer results comparing one-mil, aluminized, polyester shields and non-conducting shields.

The computed temperature distributions in the shields and the LH_2 boil-off due to radiation effects are shown in Figures 55 to 58. The LH_2 boil-off during a 10,000-hour coast mission was computed to be less than 4 lb_m for all systems including the closely spaced fixed-structure concepts. The maximum temperature on the tank shield was found to be less than 110R for all concepts. It is interesting to note that even if tank shield had a uniform temperature of 110R, the LH_2 boil-off in 10,000 hours would be less than 6 lbs.

11.3 Conduction Heat Leak and Structural Temperature Distributions

The fixed structures, and the space-erected structure in the deployed configuration, have a number of symmetrically positioned supports extending between the payload and the attach ring on the cylindrical tank support. The supports of each structure were selectively coated with a high-emittance paint to allow radiation to outer space, lower the support temperatures, and minimize the LH_2 boil-off by conduction.

A finite-difference mathematical model was formulated for each concept using the techniques described in Section 10.3 of the interaction analysis. That is, a support was subdivided into a number of zones, defining locations at which temperatures were to be calculated; heat-balance equations were written for each temperature location including appropriate terms for radiative interchange with the shields, conductance couplings at the connections to the shields, and the thermal resistance of the conical skirt used to distribute the loads over the LH_2 tank. Typically, the thermal model of the structural supports was formulated by subdividing the support into 44 zones, which required the preparation of input data for 93 heat-balance equations. At the appropriate spatial locations, each support was conductively coupled to the shadow shields by a thermal conductance of 0.76 Btu/Hr °R. The temperatures of the shadow shields were specified at the values calculated during the previous radiant heat transfer analysis and were assumed

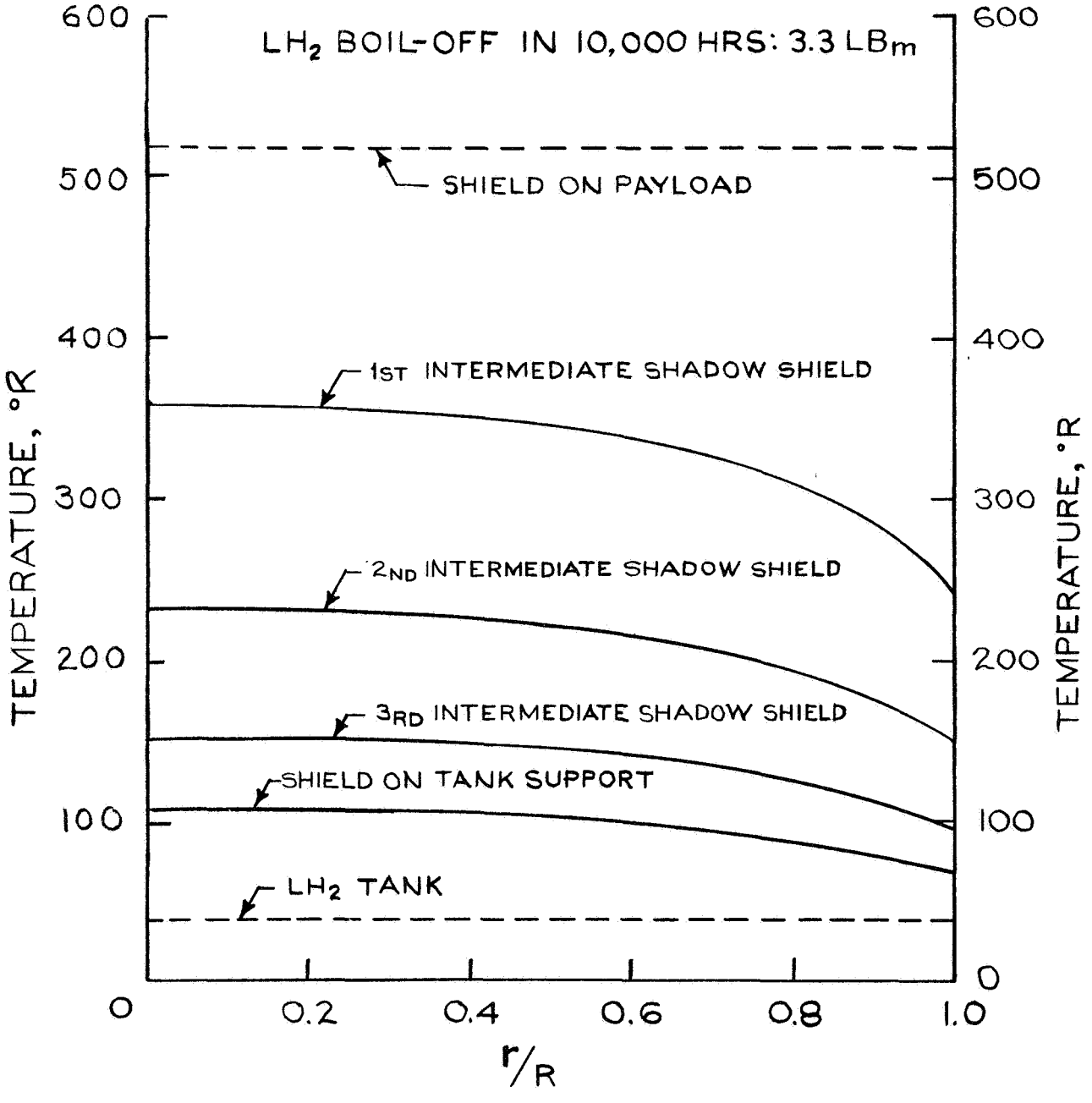

FIGURE 55 - TEMPERATURE DISTRIBUTIONS IN SHIELDS

—CONCEPT 1—

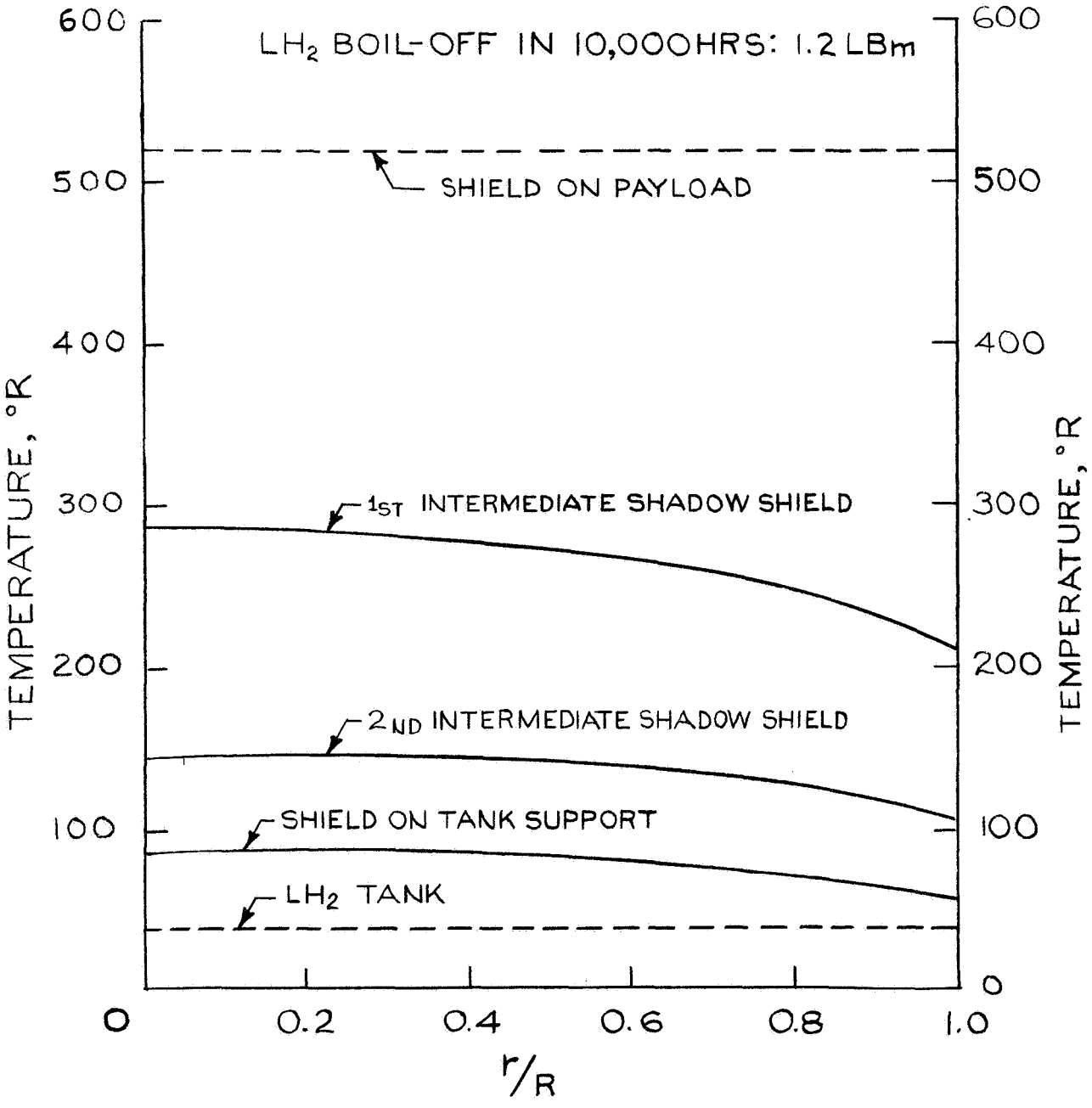

FIGURE 56 - TEMPERATURE DISTRIBUTIONS IN SHIELDS

— CONCEPTS 2, 3, AND 4 —

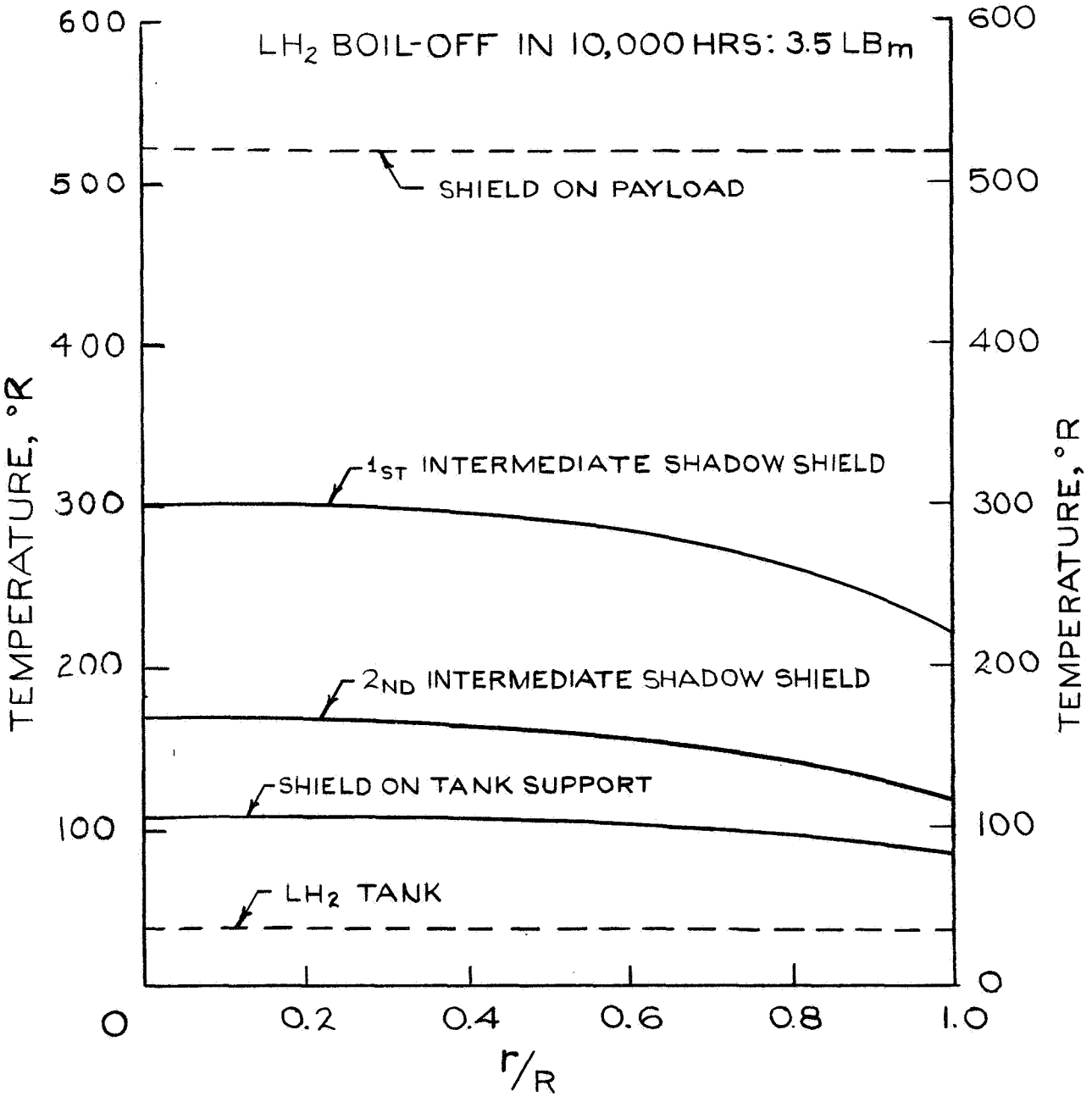

FIGURE 57 - TEMPERATURE DISTRIBUTIONS IN SHIELDS

— CONCEPT 5 —

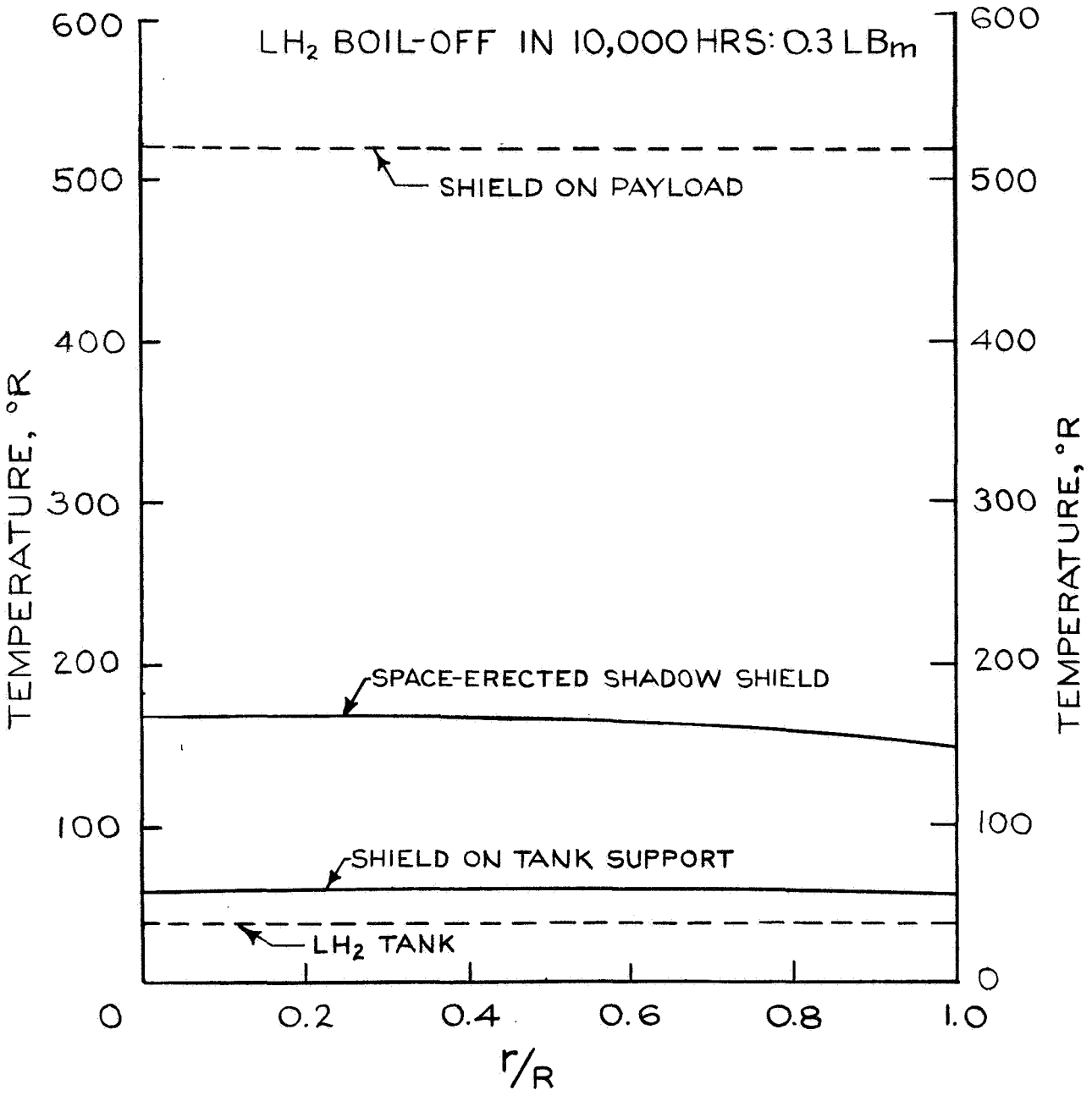

FIGURE 58 - TEMPERATURE DISTRIBUTIONS IN SHIELDS

—CONCEPT 6—

to be constant (i.e., not influenced by the support temperature distributions). It should be noted that in these calculations the assumption of a constant shield temperature leads to a conservative prediction of the support heat leak. The end of each support (connected to the attach ring on the cylindrical tank support) was coupled to the LH_2 tank via the thermal conductance of the cylindrical tank support (.00692 Btu/Hr °R divided by the number of supports).

The support structures for the six shadow shield concepts lie in three basic categories: 1) supports which were cooled by radiation to outer space, 2) supports which were radiatively cooled and also cooled by the sensible enthalpy of the LH_2 boil-off due to conduction and radiation heat transfer, and 3) supports which had additional radiating area (pant-leg radiators).

11.3.1 Radiatively Cooled Supports (Concepts 1, 2, 5 and 6)

The temperature distributions and the LH_2 boil-off by conduction in the supports of Concepts 1, 2, 5 and 6 are shown in Figures 59 through 62.

The structure temperatures are plotted as a function of dimensionless length, X/L, where X is a coordinate measured from the payload parallel to the central axis of the shadow shield system and L is the payload-to-tank spacing. It is evident from the irregular shape of the temperature distributions that the thermal couplings to the shadow shields significantly influence the support temperatures. However, the computed LH_2 boil-off by conductions were relatively low, ranging between 2 and 13 lb_m in 10,000 hours.

11.3.2 Vapor-Cooled Supports (Concept 3)

The payload support structure of Concept 3 is identical to that of Concept 2 except that there is a coolant circuit allowing the structural supports to be cooled by the sensible enthalpy of the LH_2 boil-off gas due to conduction and radiation. Each support radiates to outer space, is conductively coupled to the shadow shields, and is conductively coupled to the LH_2 tank via the tank support. A vapor-coolant line is joined to each support at ten locations approximately four inches apart.

The heat exchange between the structure and the gas is related to the gas flow rate which is, in turn, dependent upon the total boil-off due to conduction and radiation effects. The flow rate of GH_2 through each coolant tube can be defined from the following equation:

$$\dot{w} = \frac{(Q_R + Q_c)}{h_{fg}\ n}$$

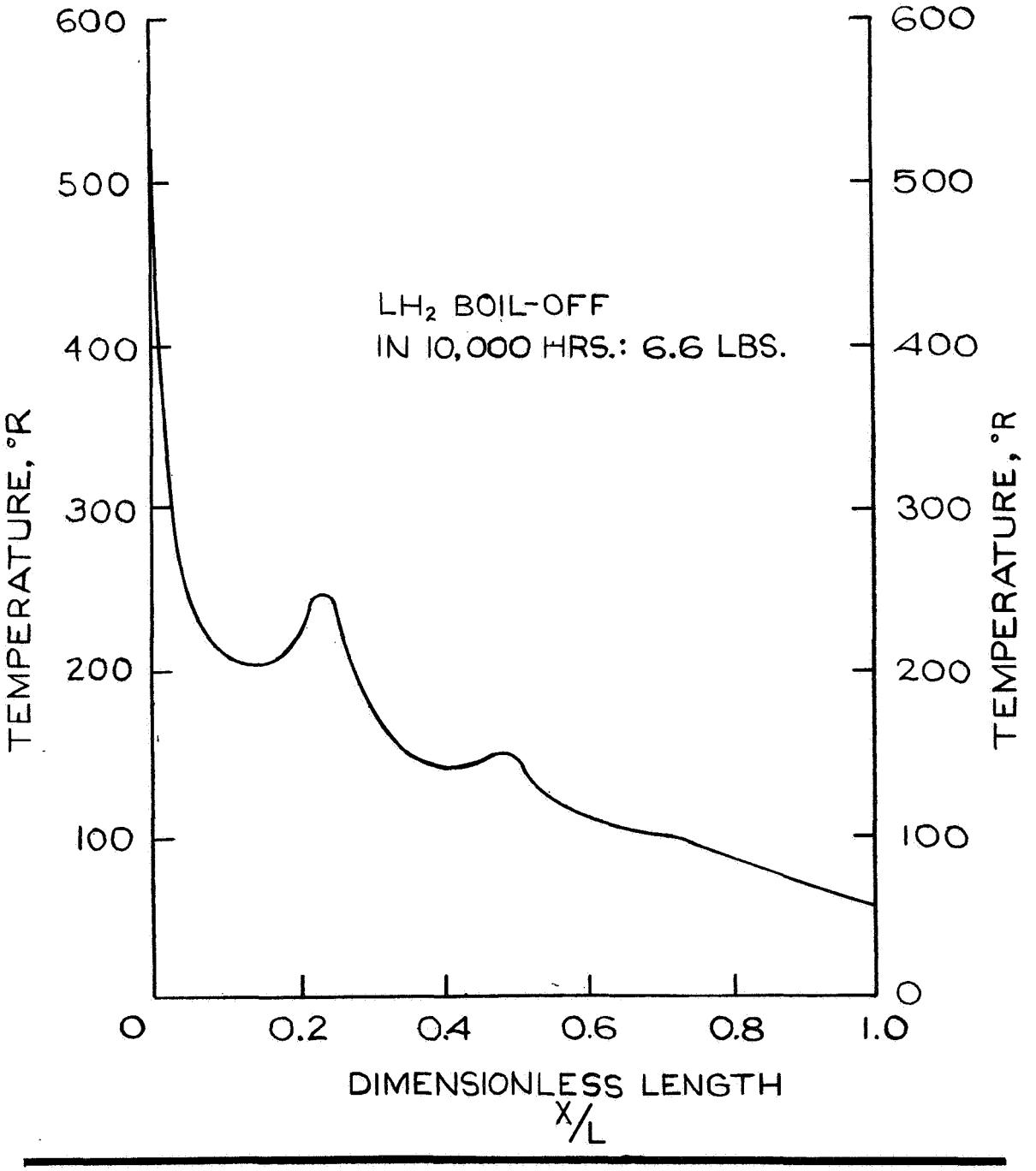

FIGURE 59 - TEMPERATURE DISTRIBUTION IN FIBERGLASS SUPPORT STRUCTURE

— CONCEPT 1 —

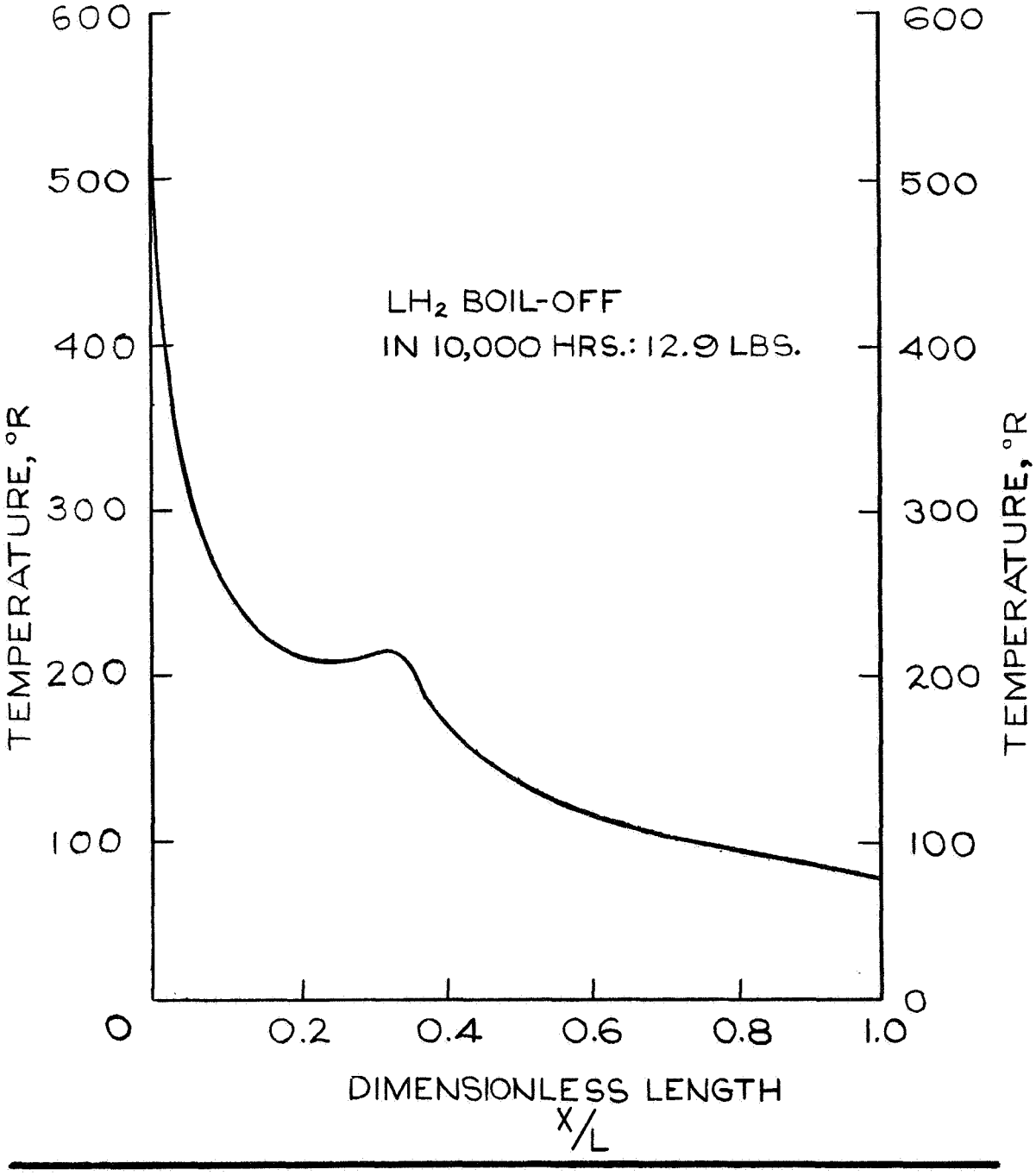

FIGURE 60 - TEMPERATURE DISTRIBUTION IN TITANIUM SUPPORT STRUCTURE

— CONCEPT 2 —

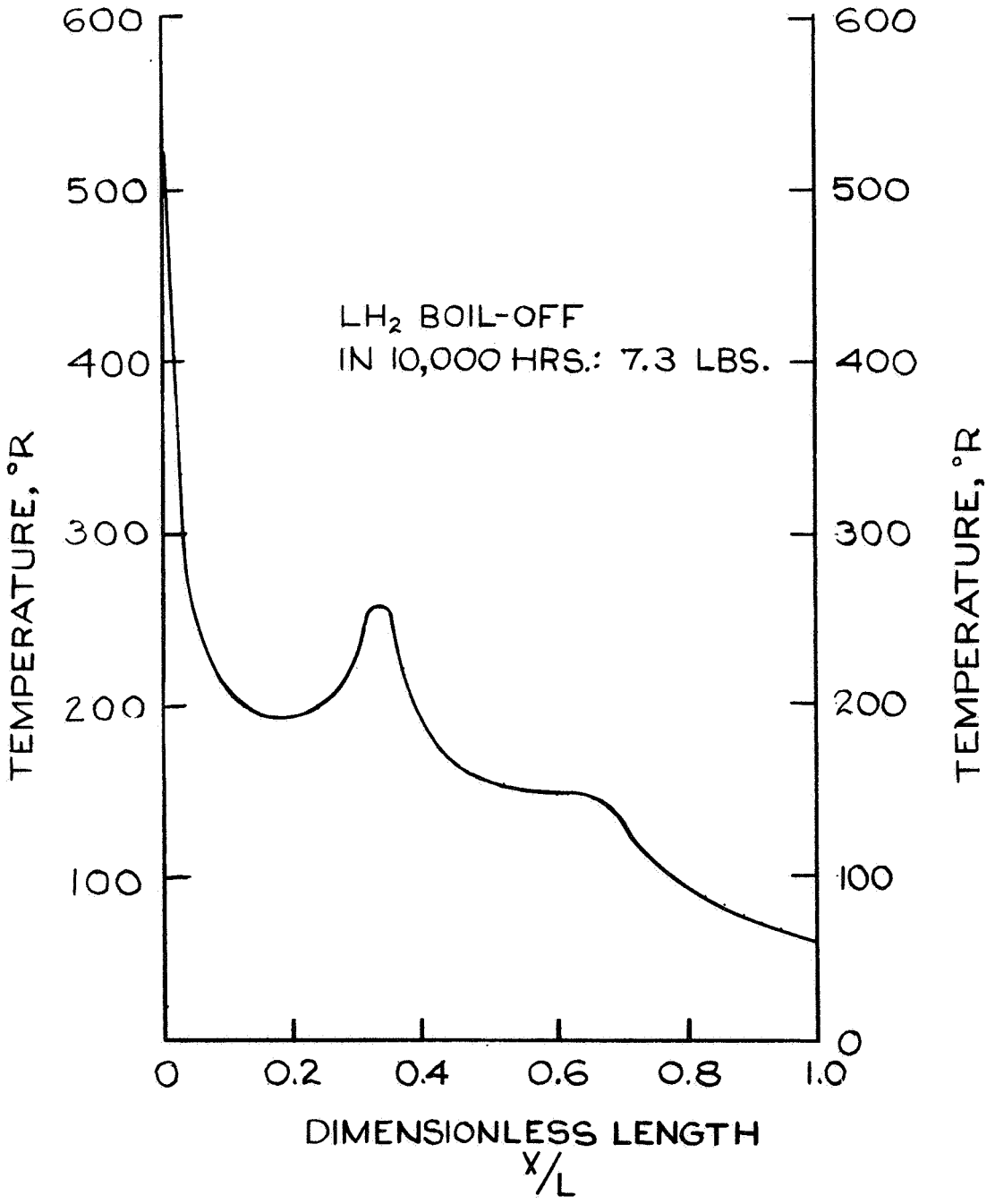

FIGURE 61-TEMPERATURE DISTRIBUTION IN FIBERGLASS SUPPORT STRUCTURE

— CONCEPT 5 —

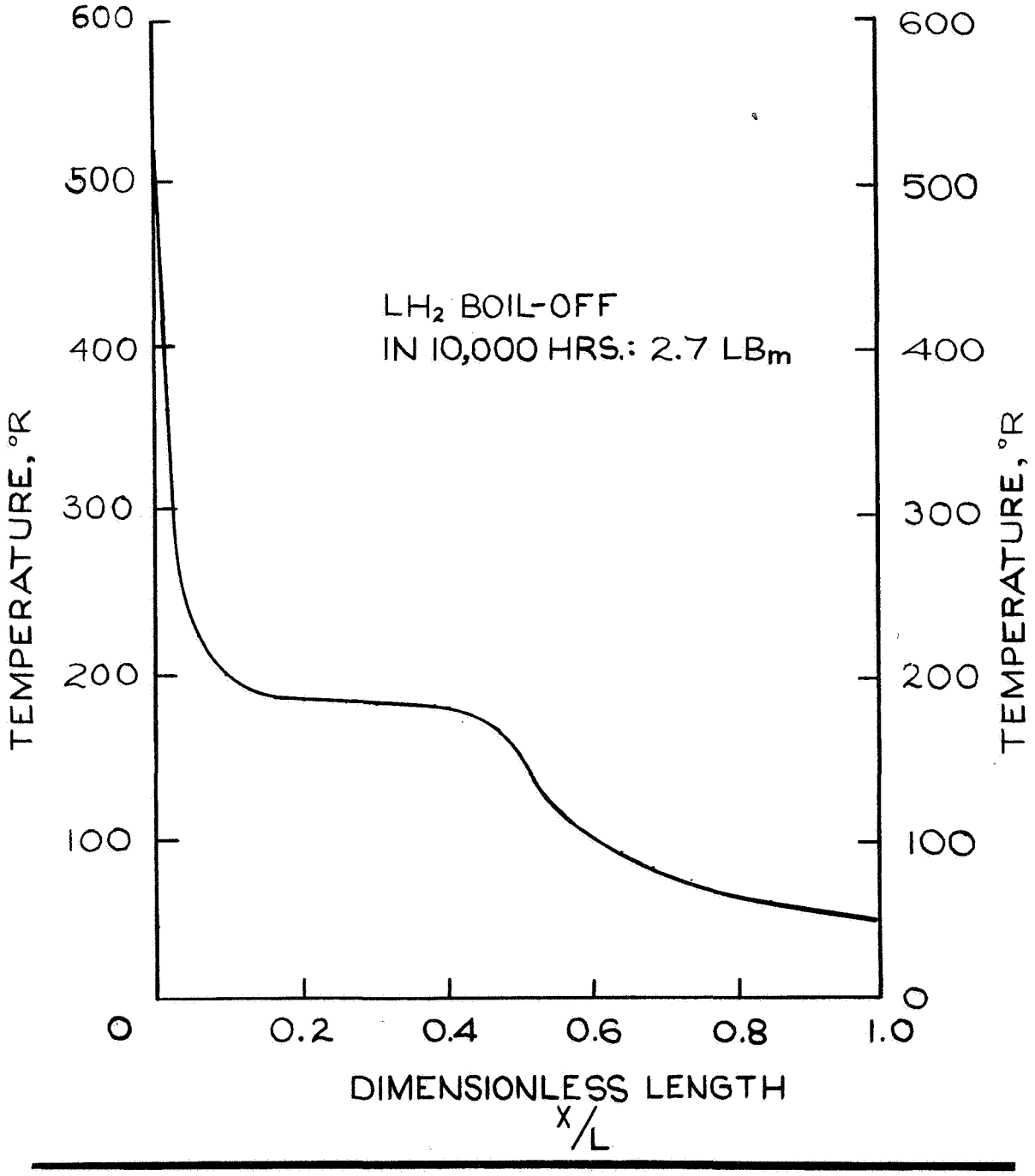

FIGURE 62 - TEMPERATURE DISTRIBUTION IN TITANIUM "A"-FRAME STRUCTURE, DEPLOYED CONFIGURATION
— CONCEPT 6 —

where Q_R = heat absorbed by the LH_2 from radiation

Q_c = heat absorbed by the LH_2 from support conduction

n = number of structural supports

$\dot{w}$ = coolant (GH_2) mass flow rate

The flow rate of GH_2 is dependent upon the conduction heat transfer to the LH_2 tank and, conversely, the conduction heat transfer is dependent upon the GH_2 flow rate. (The radiant heat transfer to the LH_2 tank for Concept 3 was already presented and resulted in an LH_2 boil-off of 1.2 lb_m in 10,000 hours.) Therefore, several calculations of the LH_2 boil-off by conduction were made with flow rate as a variable; and the solution was obtained graphically. The LH_2 boil-off due to conduction in the vapor-cooled structure vs. GH_2 flow rate is represented by the solid line in Figure 63. The relationship between the conduction boil-off and the available GH_2 flow rate due to radiation and conduction effects is also shown on this figure as a dotted line. The 1.2×10^{-4} lb_m/hr flow due to radiant heat transfer to the LH_2 tank is shown as a constant; because of the multiplication factor chosen for the abscissa, the variable flow rate due to conduction heat transfer is represented as a 45° line. Consequently, the solution for the LH_2 boil-off due to conduction in the vapor-cooled structure is indicated as 11.5 lb_m at the intersection of the two lines.

The computed temperature distribution in the vapor-cooled structure is shown in Figure 64. The influence of the vapor cooling is primarily evident near the end of the structure (X/L = 0.8 to 1.0) where the cooling reduced the structure temperatures by approximately 10R.

A simplified analysis, described in Appendix I, indicated that vapor cooling could reduce the conduction heat transfer in an insulated support ($\varepsilon = 0$) by approximately 68%. The calculations represented in Figure 63 show that vapor cooling can also reduce the heat leak in a structure which is radiatively cooled. However, since the heat leak is so low to begin with, due to the radiation cooling, the 11% improvement is not significant, especially when the mass of the tubings, fittings, etc., for the coolant circuit are considered.

Thus, for radiation-cooled structures of reasonably large spacing and low conductance, we conclude that vapor cooling is not an effective method for reducing the LH_2 boil-off.

11.3.3 Supports with Pant-Leg Radiators (Concept 4)

The support structure of Concept 4 has the same configuration and material of Concept 2, but has additional pant-leg

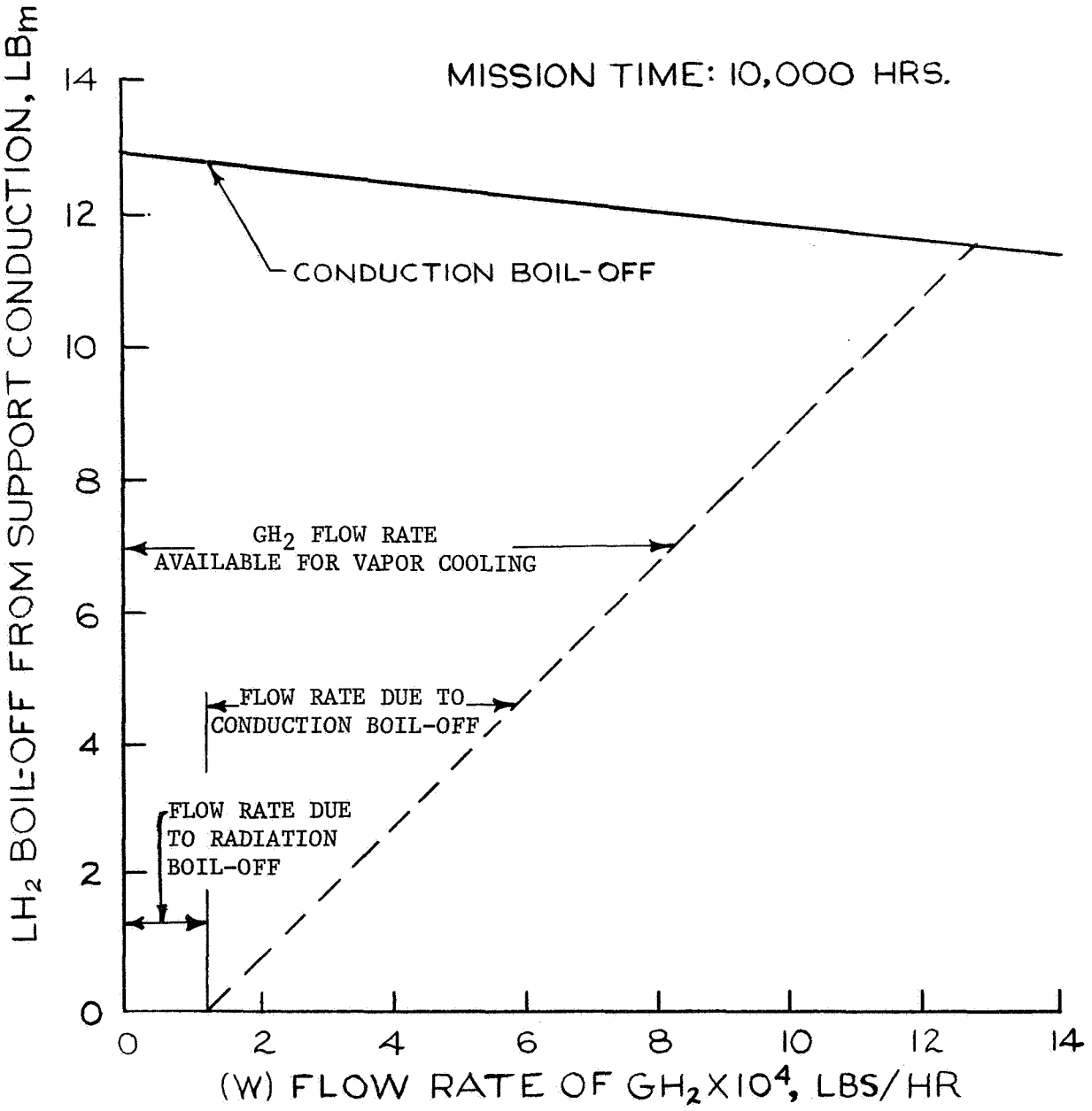

FIGURE 63 - LH_2 BOIL-OFF FROM SUPPORT CONDUCTION IN A TITANIUM VAPOR-COOLED STRUCTURE

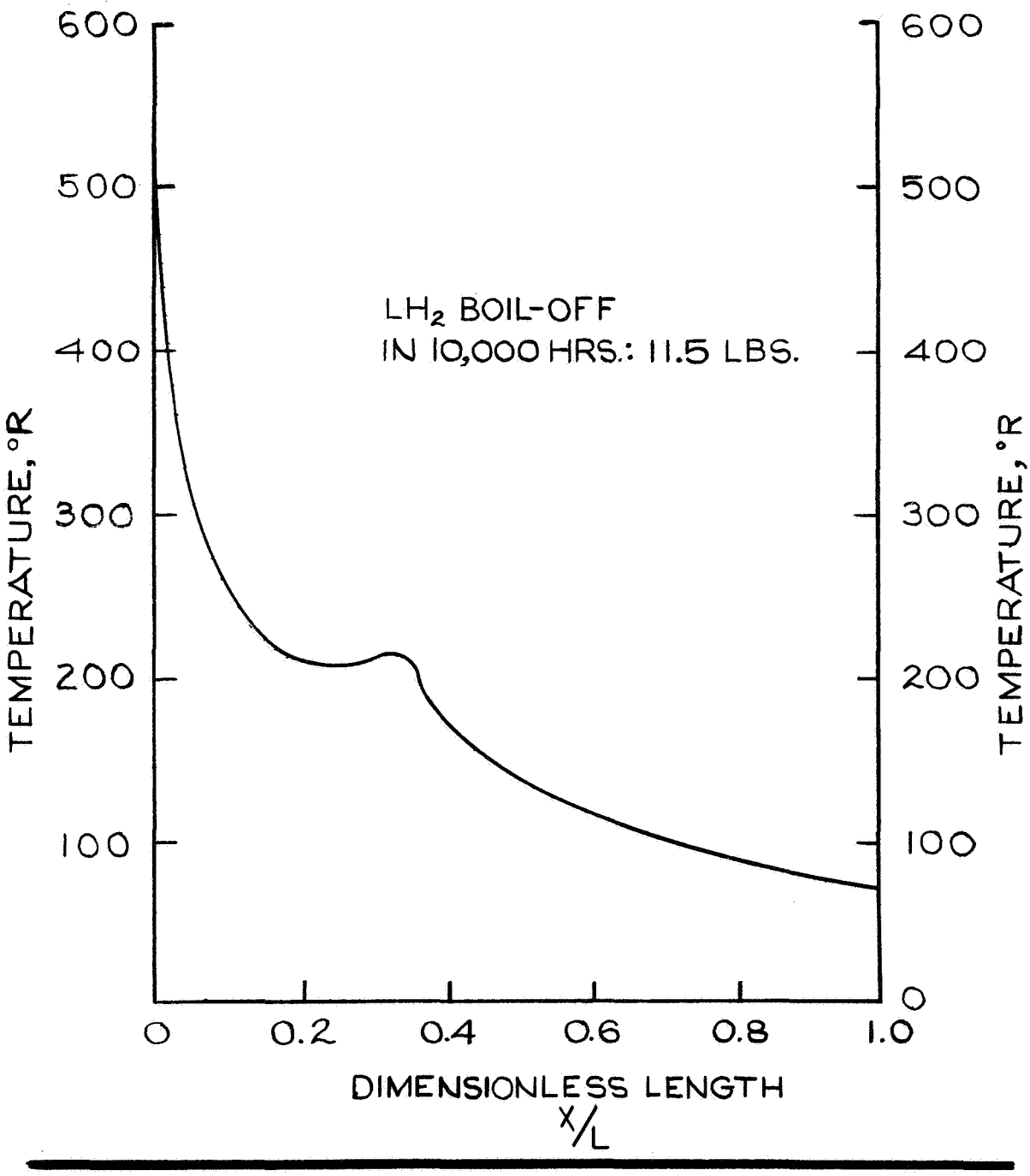

FIGURE 64 - TEMPERATURE DISTRIBUTION IN TITANIUM VAPOR-COOLED SUPPORT STRUCTURE
— CONCEPT 3 —

radiators and a different distribution of thermal control coatings. Pant-leg radiators are joined to the supports near the connection to the second intermediate shadow shield and enclose the support up to the attach ring on the tank support. The area of the support enclosed by the radiator and the internal surface of the radiator have low-emittance surfaces to minimize radiative interactions. The remainder of the support and the external surface of the radiator have an effective emittance of 0.5.

The computed temperature distribution in the structure and the LH_2 boil-off due to conduction are presented in Figure 65. By comparison with Figure 60, it can be seen that the temperature X/L = 1 and the LH_2 boil-off due to conduction are slightly higher than that for the same structure without pant-leg radiators.

The differences in the temperatures and heat flows for Concept 2 and 4 are quite small. Therefore, for the purpose of illustration, an exaggerated comparison of the temperature distributions near the ends of the structures are shown schematically in Figure 66. Although the temperature near the shield location (location 1) is higher for Concept 2, the slope and temperature at location 2 is lower because the entire support radiates to outer space. On the other hand, in Concept 4, the cooling of the pant-leg radiator lowers the temperature of the support near the shield location, but the slope and temperature are higher than that for Concept 2 at point 2 because the end of the support is shielded ($\varepsilon \cong 0$), and is not radiatively cooled.

In this analysis of the structure of Concept 4, the performance of the pant-leg radiator was influenced by the conductive coupling to the shadow shield. Other calculations with a thermal model of this structure considering "no interactions" with the shields demonstrated that the pant-leg radiators could reduce the conductive heat flow to the LH_2 tank by approximately 13%. Also, parametric studies varying the position of the radiator indicated that the location of the pant-leg radiator as shown in Concept 4 was one in which the reduction was maximized.

However, the reduction in heat flow accomplished by providing pant-leg radiators is not significant when the structure is radiatively cooled and has a low conduction heat leak (resulting in an LH_2 boil-off of 10-15 lb_m).

It is conceivable that the geometry of the shields in Concept 4 could be modified to make the radiators more effective. For example, spacing the shadow shields closer to the payload and increasing the distance between the support-shield and support-radiator interfaces might further depress the radiator temperature. However, on the basis of our studies with "no interactions" between the supports and shields, significant reductions in system mass would not be expected.

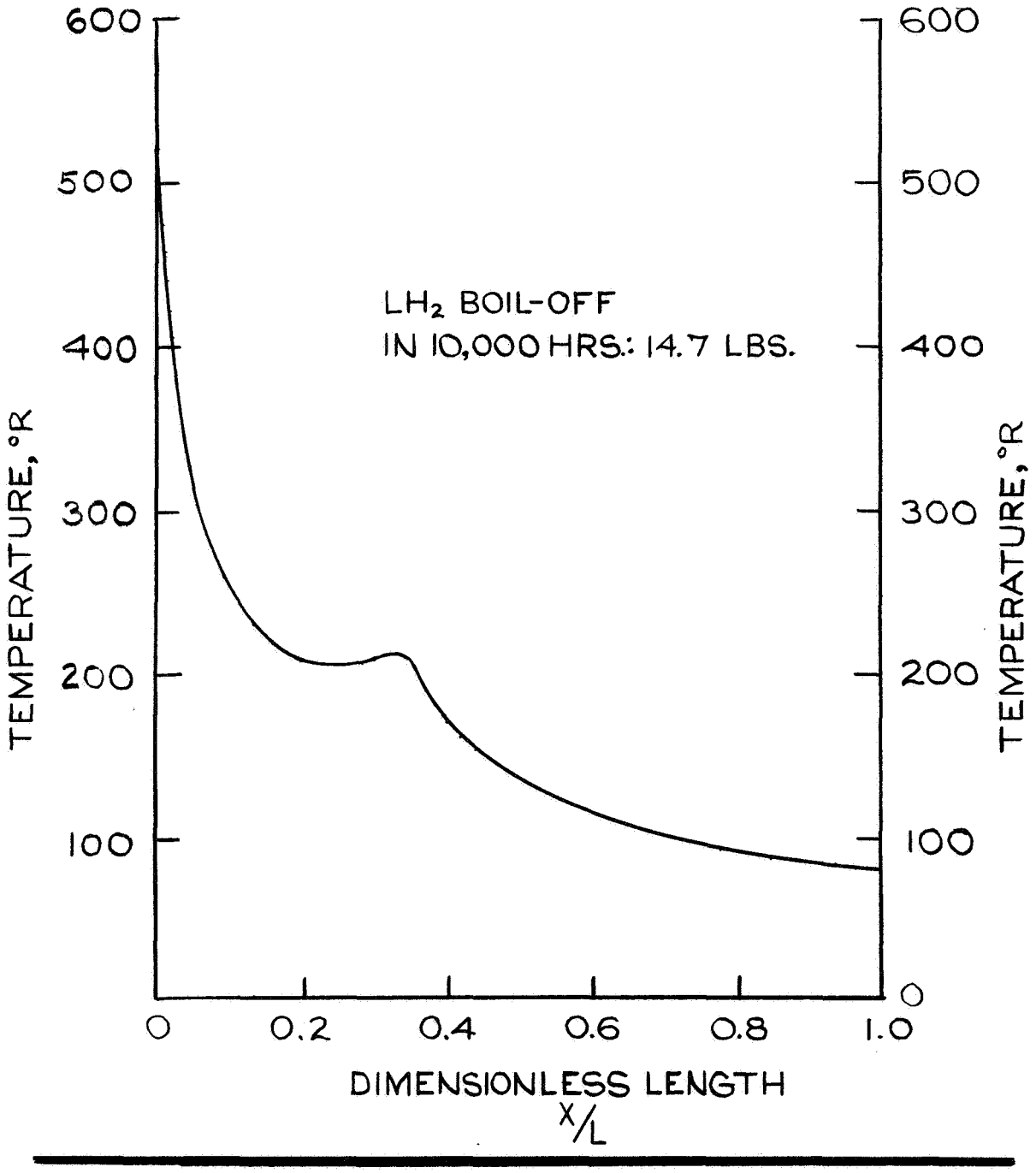

FIGURE 65 - TEMPERATURE DISTRIBUTION IN TITANIUM SUPPORT STRUCTURE WITH PANT-LEG RADIATORS
— CONCEPT 4 —

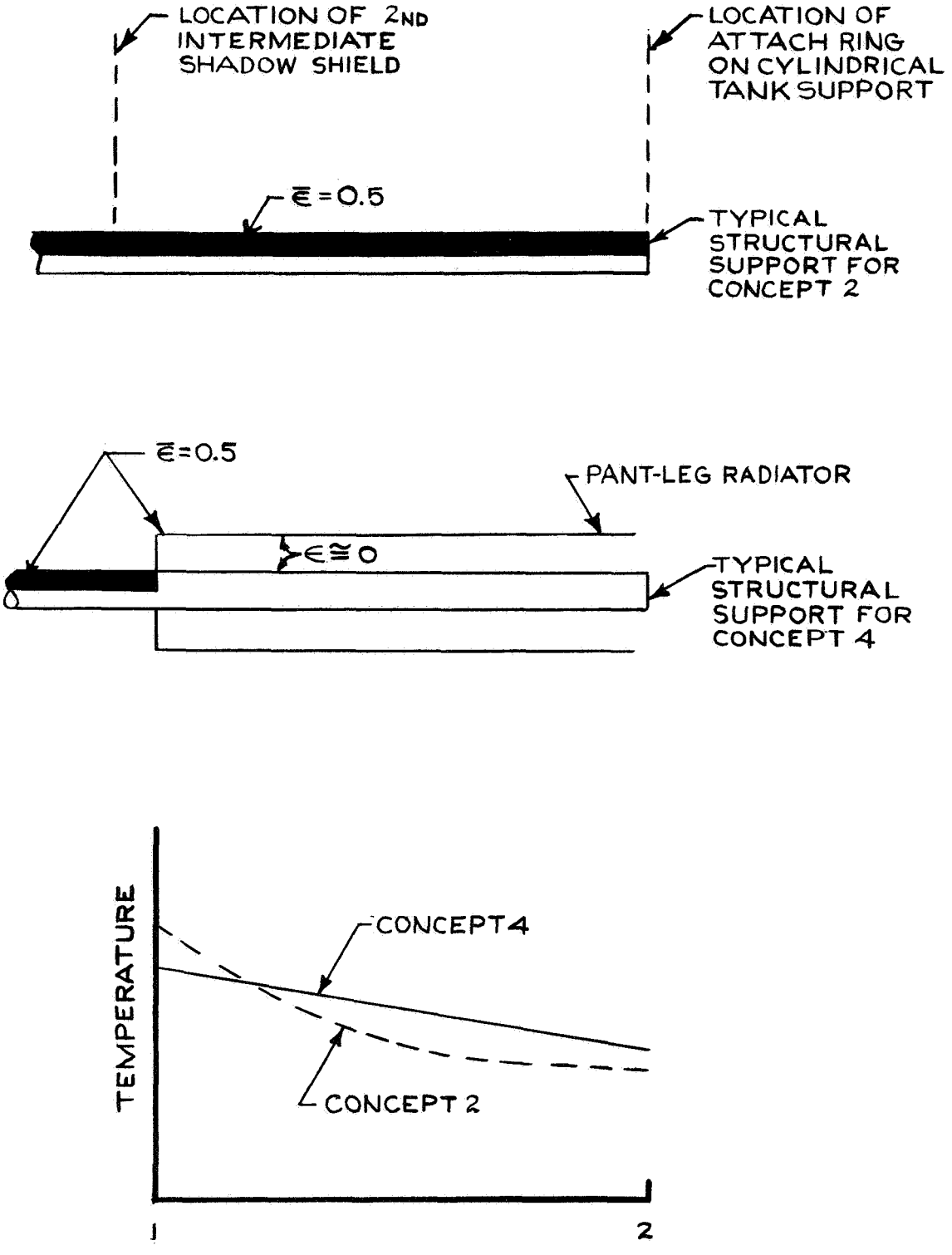

FIGURE 66 - ILLUSTRATION OF DIFFERENCE IN STRUCTURAL TEMPERATURE DISTRIBUTIONS OF CONCEPTS 2 AND 4

12.0 EVALUATION OF CONCEPTUAL DESIGNS

12.1 Mass Summary

Table XVI contains a compilation of the estimated overall masses of the six shadow shield systems described in Section 7.0 and a breakdown of the masses attributable to LH_2 boil-off during a 10,000-hour mission, insulation and shielding, and structural components.

The LH_2 boil-off during ascent and orbital operations, the insulation for ground-hold, ascent and orbital thermal protection, and the cylindrical tank support are common to all concepts; their associated mass penalties have been detailed in previous sections.

A detailed summary of the masses of the shadow shield assemblies, which consist of material (including reinforcements, eyelets, lacing, etc.) and support rings and the payload support structures, which generally include provisions for making interconnections to the shadow shields, payload and cylindrical tank support, is presented in Table XVII. In the listing of the masses for Concept 5, the mounting brackets used to interconnect the shadow shields and payload support structure are included in the tabulation of the mass of the shadow shield assemblies, since their design is related to the configuration of the rings required to support the stowed annular shields, deployment arms, etc.

The overall masses of the shadow shield systems ranged between 240 and 320 lb_m, the maximum being for Concept 5, which has space-erected shields to compensate for solar-vector misalignment.

12.1.1 Alternate Systems

It has previously been mentioned that several alternate concepts could be considered based upon the basic arrangements of the five concepts with fixed structures. For example, the design of all the shadow shield systems was based on each shadow shield assembly having a single-sheeted, reinforced, polyester shield coated on both sides to have a low emittance. It was suggested that double-sheeted shadow shields with four reflective surfaces could also be considered to improve the reliability of the system, since the interior low-emittance surfaces would not be exposed to the environment. If double-sheeted shields were considered for the shadow shield assemblies of Concept 1, the overall configuration would remain the same, but there would be five additional sheets of material adding a mass of approximately 13 lb_m.

The results of computer calculations were used to compare the thermal performance of single- and double-sheeted shields for a system with three intermediate shadow shields equally spaced

TABLE XVI

MASS SUMMARIES OF SHADOW SHIELD CONCEPTS
(All values in lb_m)

CONCEPT NO.*	1	2	3	4	5	6
• LH_2 BOIL-OFF	51.9	56.1	54.7	57.9	52.8	45.0
1) Ascent	16.0	16.0	16.0	16.0	16.0	16.0
2) Orbital Operation (15 orbits)	26.0	26.0	26.0	26.0	26.0	26.0
3) 10,000-Hour Coast Mission						
a) Radiation	3.3	1.2	1.2	1.2	3.5	0.3
b) Conduction	6.6	12.9	11.5	14.7	7.3	2.7
• INSULATION AND SHIELDING	72.9	68.6	68.6	68.6	126.4	61.7
1) Ground Hold	26.0	26.0	26.0	26.0	26.0	26.0
2) Orbital	24.0	24.0	24.0	24.0	24.0	24.0
3) Shadow Shields	22.9	18.6	18.6	18.6	76.4	11.7
• STRUCTURAL COMPONENTS	133.5	134.2	140.6	136.5	135.0	127.4
1) Cylindrical Tank Support	84.9	84.9	84.9	84.9	84.9	84.9
2) Payload Support Truss Structure	48.6	49.3	55.7	51.6	50.1	42.5
TOTAL MASS	258.3	258.9	263.9	263.0	314.2	234.1

* 1 - Fixed fiberglass structure, fixed shields.

2 - Fixed titanium structure, fixed shields.

3 - Fixed titanium structure with vapor-cooled supports, fixed shields.

4 - Fixed titanium structure with pant-leg radiators, fixed shields.

5 - Fixed fiberglass structure, fixed shields with space-erected shields to compensate for solar-vector misalignment.

6 - Space-erected structure, space-erected shield.

TABLE XVII

MASS BREAKDOWN OF SHADOW SHIELD ASSEMBLIES
AND PAYLOAD SUPPORT STRUCTURES OF SHADOW SHIELD CONCEPTS

Concept No. 1 (Fixed fiberglass structure, fixed shields)

SHADOW SHIELD ASSEMBLIES	
• Shield Material	13.0
• Shield Support Rings	11.3
	24.3 lb_m
PAYLOAD SUPPORT TRUSS STRUCTURE	
• Payload Support Tube	11.5
• Payload Attach Ring	11.0
• Box-type Support Points	4.5
• Foam-filled Structural Supports	8.3
• Shield Mounting Brackets	3.0
• End Connections	10.3
	48.6 lb_m

Concept No. 2 (Fixed titanium structure, fixed shields)

SHADOW SHIELD ASSEMBLIES	
• Shield Material	10.6
• Shield Support Rings	8.0
	18.6 lb_m
PAYLOAD SUPPORT TRUSS STRUCTURE	
• Payload Support Tube	11.5
• Payload Attach Ring	11.0
• Box-type Support Points	4.5
• Foam-filled Structural Supports	10.6
• Shield Mounting Brackets	4.0
• End Connections	7.7
	49.3

TABLE XVII (Cont'd.)

Concept No. 3 (Fixed vapor-cooled titanium structure, fixed shields)

SHADOW SHIELD ASSEMBLIES	
• Shield Material	10.6
• Shield Support Rings	8.0
	18.6 lb_m
PAYLOAD SUPPORT TRUSS STRUCTURE	
• Payload Support Tube	11.5
• Payload Attach Ring	11.0
• Box-type Support Points	4.5
• Foam-filled Structural Supports	10.0
• Shield Mounting Brackets	4.0
• End Connections	7.7
• Piping and Fittings for Vapor Cooling Circuit	7.0
	55.7 lb_m

Concept No. 4 (Fixed titanium structure with pant-leg radiators, fixed shields)

SHADOW SHIELD ASSEMBLIES	
• Shield Material	10.6
• Shield Support Rings	8.0
	18.6 lb_m
PAYLOAD SUPPORT TRUSS STRUCTURE	
• Payload Support Tube	11.5
• Payload Attach Ring	11.0
• Box-type Support Points	4.5
• Foam-filled Structural Supports	10.6
• Shield Mounting Brackets	4.0
• End Connections	7.7
• Pant-leg Radiators	3.3
	51.6 lb_m

TABLE XVII (Cont'd.)

Concept No. 5 (Fixed fiberglass structure, fixed shields with space-erected annular shields to compensate for solar-vector misalignment)

SHADOW SHIELD ASSEMBLIES		
• Material for Fixed Shields	10.6	
• Material for Annular Shields	1.8	
• Support Hardware	60.0	
Shield Support Rings		
Mounting Brackets		
• Deployment Arms, Restraining Bands and Release Mechanisms	4.0	
	76.4	lb_m
PAYLOAD SUPPORT TRUSS STRUCTURE		
• Payload Support Tube	11.5	
• Payload Attach Ring	11.0	
• Box-type Support Points	4.5	
• Foam-filled Structural Supports	12.8	
• Shield Mounting Brackets (included above)		
• End Connections	10.3	
	50.1	lb_m

Concept No. 6 (Space-erected structure and shield)

SHADOW SHIELD ASSEMBLIES		
• Shield Material	7.8	
• Shield Support Rings	3.9	
	11.7	lb_m
PAYLOAD SUPPORT "A" FRAME STRUCTURE		
• Payload Support Tube	11.5	
• Foam-filled Tubes and Fittings	11.0	
• Drive System (Motorized Winch, Cables, and Pulleys)	20.0	
	42.5	lb_m

between a 520R payload and a 37R uninsulated LH_2 tank with an L/D of 0.15. The results showed that changing from single-sheeted to double-sheeted shields reduced the LH_2 boil-off from radiation by approximately an order of magnitude. For Concept 1, the use of double-sheeted shields would increase the total system mass by approximately 10 lb_m due to the increased mass of the shields. Although there would be a reduction in the LH_2 boil-off mass due to radiation, the effect is negligible since the LH_2 boil-off from radiation with single-sheeted shields is only 3.3 lb_m. The LH_2 boil-off from support conduction, 6.6 lb_m, would be subject to a small reduction since the temperature level of the shadow shields, which interact thermally with the structure, would be reduced. Thus, for three intermediate shield assemblies (Concept 1), double-sheeted shields increase the total mass of the system; however, they may provide some measure of added reliability since any emittance degradation on the exterior surfaces will not appreciably increase the LH_2 boil-off. A detailed "failure mode" analysis would be required to determine whether or not the emittances were subject to degradation due to effects other than those considered (relative humidity, handling, etc.) in selecting a conservative value of 0.03 for the total hemispherical emittance.

However, with double-sheeted shields, the deflections during launch can be appreciable (c.f., Section 5.4), and there exists some minimum spacing allowable which will prevent the flexible shields from contacting during launch vibration and abrading the low-emittance surface coating.

It may be noted that other design configurations using double-sheeted shields could prove attractive. For example, the use of two double-sheeted intermediate shield assemblies instead of three single-sheeted shield assemblies (as described above) could result in a slightly different mass penalty due to trade-offs between shield mass, the shield supports, and boil-off due to radiation heat leak.

Another alternate concept could be considered to have the same basic configuration as Concept 5, except that no provisions would be made to increase the allowable angle of misalignment with the solar vector (no space-erected annular shields, deployment arms, release mechanisms and support hardware). The tolerance in pointing angle for this configuration would be 4.2°. The arrangement of this alternate concept would also be similar to Concept 2 (same L/D and number of shields), the differences being in the number, length and material of the structural supports. Concept 2 has a fixed structure composed of twelve 2" OD x .017 wall titanium supports, while the alternate concept has sixteen 2" OD x .037 wall fiber glass supports. The masses of the foam-filled structural supports of both systems would be nearly equal, but the LH_2 boil-off mass from support conduction in Concept 2 (12.9 lb_m) would be approximately double that for the fiber glass support structure of the alternate concept. Therefore, the system mass of an alternate shadow shield system similar to

Concept 5 but without provisions for increasing the allowable angle of misalignment would be approximately 255 lb_m.

12.1.2 Effect of Payload Mass on System Mass

The optimization, selection and design of the aforementioned shadow shield concepts were made assuming that the payload support structure supported the maximum payload mass, 4000 lb_m. The following discussion describes the effects of considering different payload masses (1500, 2500 and 4000 lb_m) on the overall mass of the shadow shield systems.

The payload mass primarily affects the size of the supports of the payload support structures since the launch loads used to size the fixed structures and the maneuvering loads used to design the space-erected structure are dependent upon the mass of the supported payload. (Since the design analysis of the tank support system, outlined in Section 8.0, was based on the inertial loads of the LH_2 tank, considering other loads around the tank to be supported by appropriate truss work or shell sections, its mass is independent of the payload mass.)

For the fixed-structure concepts, the wall thickness of the supports and the support mass (not including foam and fixtures) were computed for a variable payload mass. The results tabulated below illustrate the changes which occur in the support size and mass when the payload mass is reduced from 4000 to 1500 lb_m.

	Payload Mass lb_m	Concept 1 (Fiber glass)	Concepts 2,3,4 (Titanium)	Concept 5 (Fiber glass)
Wall thickness (inches)	4000	.030	.017	.037
	2500	.026	.014	.028
	1500	.023	.013	.022
Mass of supports (lb_m)	4000	6.6	8.7	10.6
	2500	5.7	7.5	7.9
	1500	5.1	6.8	6.4

A variable payload mass also offsets the LH_2 boil-off mass from support conduction. Considering the changes in support wall thickness tabulated above for the minimum payload mass, the overall mass of the fixed-structure concepts presented in Table XVI would decrease by less than 10 lb_m (less than 4% of system mass penalty). This is also true of the overall mass of Concept 6 where the sum of the support mass (not including fixtures) and the LH_2 boil-off from support conduction in the deployed configuration is less than 10 lb_m when the system is designed for a 4000 lb_m payload. Therefore, from the standpoint of overall mass, the performance of the selected shadow shield

systems are relatively insensitive to variations in the payload mass between 1500 and 4000 lb_m. The mass breakdowns presented in Table XVI represent upper bounds for the support mass and LH_2 boil-off from support conduction since they are based on the maximum payload mass of 4000 lb_m.

12.2 Evaluation of Shadow Shield Concepts

The subject contract on shadow shield development calls for a design evaluation establishing the merit of the conceptual designs by providing a rating of overall system mass and mechanical and operational complexity (inherent reliability). The evaluation of the system from the mass standpoint has been described and is combined with the evaluation of the systems from a mechanical and operational standpoint in Table XVIII. Two alternate concepts which are similar to the basic arrangements of other fixed structure concepts and were described above are included in the evaluation.

The major distinctions between the various shadow shield concepts are that some have payload support structures and shadow shield assemblies which remain fixed during the entire mission, while others require that portions of the shields be erected in space, or both the payload support structure and shadow shield assembly be capable of being deployed and retracted in space. Although pyrotechnic devices, release mechanisms, actuation systems and provisions for movable components are common to both manned and unmanned spacecraft, extensive tests are required to insure reliable operation. Because the deployable systems used for the shadow shield concepts in this study have not been fabricated and tested, one cannot attach any statistical significance to their inherent reliability. In ranking the various systems, the reliability ranking was based on whether or not the systems had moving parts.

13.0 REFERENCES

13.1 Cited References

Advanced Development and Evaluation Division at NASA LeRC, "An Analysis of Chemical Upper Stages for NASA Scientific Missions," NASA TMX-52127 (1965).

Apsia, J. N., et al, "Development of Materials and Materials Application Concepts for Joint Use as Cryogenic Insulation and Micrometeroid Bumpers," Conference Proceedings - Long Term Cryo-Propellant Storage in Space, NASA MSFC (October 1966).

Arthur D. Little, Inc., "Cryogenic Propellant Feed Systems for Electrothermal Engines," prepared under Contract NAS 8-2575 (January 1963).

TABLE XVIII

EVALUATION OF SHADOW SHIELD CONCEPTS

	CONCEPTS SELECTED FOR EVALUATION						ALTERNATIVE	
CONCEPT NO.*	1	2	3	4	5	6	7	8
a) SYSTEM MASS PENALTY	258	258	264	263	314	234	268(1)	255(1)
b) LH_2 BOIL-OFF MASS (10,000-HR. MISSION)	52	56	55	58	53	45	49(1)	52(1)
c) PAYLOAD-TANK SPACING (FT)	1.5	2.5	2.5	2.5	2.5	~0(2)	1.5	2.5
d) TOLERANCE TO ALIGNMENT WITH SOLAR VECTOR	adequate (± 5.1°)	adequate (± 4.2°)	adequate (± 4.2°)	adequate (± 4.2°)	large (± 15°)	small (± 1.8)	adequate (± 5.1°)	adequate (± 4.2°)
e) DEVELOPMENT EFFORT REQUIRED	moderate	small	small	small	large	large	moderate	moderate
f) SYSTEM COST	moderate	low	low	low	high	very high	moderate	moderate
g) SENSITIVITY OF SYSTEM MASS PENALTY TO CHANGE IN SHIELD EMITTANCE(3)	low	low	low	low	low	very low	very low	low
h) DEGREE OF MECHANICAL COMPLEXITY	small	small	moderate	small	large	very large	small	small
i) DEPLOYMENT ACTUATION	none	none	none	none	required	required	none	none
j) INHERENT RELIABILITY	good	excellent	good	good	acceptable	acceptable	good	good
k) RANK	2	1	4	3	5	6		

*1 - Fixed fiberglass structure, fixed shields.
2 - Fixed titanium structure, fixed shields.
3 - Fixed vapor-cooled titanium structure, fixed shields.
4 - Fixed titanium structure with pant-leg radiators.
5 - Fixed fiberglass structure, fixed shields, space-erected annular shields to compensate for solar-vector misalignment.
6 - Space-erected structure and shields.
7 - Same as 1 with double-sheeted shadow shields.
8 - Same as 5 without provisions for space-erected annular shields.

NOTES (1) Estimated values
(2) Payload tank spacing = 10 ft. when deployed.
(3) Based on an increase of 100% in shield emittance.

Black, I., et al, "Basic Investigations of Multilayer Insulation Systems," Final Report by A. D. Little, Inc., NASA CR-54191 (October 1964).

Black, I., et al, "Advanced Studies on Multilayer Systems," Final Report by A. D. Little, Inc., NASA CR-54929 (1966).

Cody, J. C. and Hyde, E. H., "Thermal Problems Associated with the Development of a Flight Configured Cryogenic Insulation System," Conference Proceedings - Long Term Cryo-Propellant Storage in Space, NASA MSFC (October 1966).

Crawford, R. F. and Hannah, R. L., Final Report Contract NAS 8-11397 (June 1966).

Fung, Y. C. and Sechler, E. E., "Buckling of Thin-Walled Circular Cylinders under Axial Compression and Internal Pressure," J. of Aeronautical Sciences, Vol. 24, No. 5 (May 1967).

Glaser, P., et al, "Thermal Insulation Systems," NASA SP-5027, A. D. Little, Inc. (1967).

Knoll, R. H., Bartoo, E. R. and Boyle, R. J., "Shadow Shield Experimental Studies," Conference Proceedings - Long-Term Cryo-Propellant Storage in Space, NASA MSFC (October 1966).

Knoll, R. H. and Oglebay, J. C., "Lightweight Thermal Protection Systems for Space Vehicle Propellant Tanks," Paper No. 746C, NASA Engineering and Manufacturing Meeting (1963).

Nathanson, D., Gabron, F. and Almgren, D. W., "The Accuracy of Zone and Nodal Methods for Computing Spacecraft Temperatures," AIAA Paper No. 68-63 (January 1968).

Rimrott, F. P. J., "Storable Tubular Extendible Member," Machine Design (December 9, 1965).

Ruccia, F. and Hinckley, R. B., "The Surface Emittance of Vacuum Metallized Polyester Film," Vol. 12, Advances in Cryogenic Engineering (1966).

Shaker, F., NASA LeRC, Personal Communication (1967).

Staley, J. A. and Leondis, A. F., "Load Factors for Kick Stage," Report by General Dynamics, Convair Div., NASA CR-72167 (February 1967).

Sterbentz, W. H. and Baxter, J. W., "Thermal Protection System for a Cryogenic Spacecraft Propulsion Module," Report by Lockheed Missiles and Space Company, NASA CR-54879 (November 1966).

Strong, P. F., and Emslie, A. G., "The Method of Zones for the Calculation of Temperature Distribution," ASME Paper 65-WA/HT-47 (1965).

Viskanta, R., Schornhorst, J. R. and Toor, J. S., "Analysis and Experiment of Radiant Heat Exchange between Simply Arranged Surfaces," Technical Report AFFDL-TR-67-94 (June 1967).

13.2 References - Properties of Materials

1. Cryogenic Materials Data Handbook, Durham, McClintock, Reed, National Bureau of Standards, Contract #AF04(647)-59-3.

2. "A Compilation of Mechanical Properties of Materials at Cryogenic Temperatures," McClintock, Gibbons, NBS Report 6064, July 1, 1959.

3. Cryogenic Material Data Handbook, 12th Progress Report, Project #7381, TASK #738103.

4. "A Compilation of Materials Research Data (Titanium for Cryogenic Propellant Tankage)," Hurlich, Hooper. General Dynamics Report MR6278, Contract AF 33(616)-7984.

5. "Mechanical Properties of Titanium at Cryogenic Temperatures," General Dynamics Report MRG-189, October 14, 1960.

6. Handbook of Chemistry & Physics (43rd Edition), Chemical Rubber Co.

7. "A Compendium of the Properties of Materials at Low Temperatures," (Phase I), WADD Technical Report #60-56, Part II. Properties of Solids, NBS Cryogenic Engineering Laboratory, October 1960.

8. "Thermophysical Properties of Plastic Materials and Composites to Liquid Hydrogen Temperatures," Technical Documentary Report #ML-TDR-64-33, Part I, June 1964.

9. "Behavior of Materials at Cryogenic Temperatures," ASTM STP 387, June 13-18, 1965. From a paper by Robert L. Powell.

10. Thermophysical Properties Research Center Data Book, Y. S. Touloukian, Ed. Volume 1, Chapter 1, Purdue University, Lafayette, Indiana, 1964.

11. Advances in Cryogenic Engineering, (Vol. 10), Proceedings of 1964 Cryogenic Engineering Conference, K. D. Timmerhause, Ed. Plenum Press, N. Y., 1965.

12. Metallic Materials and Elements for Aerospace Vehicle Structures, MIL-HDBK-5A, Project No. 1500-0064, Department of Defense, Washington 25, D. C.

13. Cryogenic Materials Data Handbook, Supplements #1, 2, 3.

14. "Report on Physical Properties of Metals & Alloys from Cryogenic to Elevated Temperatures," ASTM Spec. Tech. Pub. #296.

15. Beryllium - Its Metallurgy and Properties, Hausner, University of California Press, Berkeley and L. A., 1965.

16. Materials for Missiles and Space Craft, E. Porter, Ed., McGraw-Hill, 1963.

17. Cryogenic Materials Data Handbook, AFBMD, 1959.

18. "Filament Winding," Rosato & Groves, Interscience - 1964.

19. "Beryllium in Aero/Space Structures," The Brush Beryllium Company.

APPENDIX I

EFFECTIVENESS OF VAPOR COOLING A CONDUCTING SUPPORT

One method of reducing the conductive heat flow in a structural support between a high-temperature sink and a cryogenic container is to utilize the sensible enthalpy of the cryogen vapor boil-off gas to cool the support. The effect of cooling the support reduces the boil-off rate attributable to conduction down the support.

A simplified mathematical analysis of vapor cooling an insulated support structure is presented in this Appendix.

Consider a structural support of length L and constant cross-sectional area maintained between a high-temperature source at T_h and a sink (the cryogen container) at T_c. The coordinate x is measured from the sink and the vapor is vented at x = L.

The conductive heat flow to the cryogenic container and the flow rate of the coolant are related by:

$$q = \lambda\omega \tag{I-1}$$

where q is the conductive heat flow at x = 0

λ is latent heat of vaporization of the cryogenic field

ω is the flow rate of the cryogen boil-off

The following assumptions are made in the mathematical analysis:

1) The temperatures of the coolant and the support are equal at all locations, i.e., a perfect heat exchanger.

2) The external surface of the tube is insulated (no radiation at the surface).

3) All thermal properties are independent of temperature.

4) Conduction effects for the coolant tube and the coolant are neglected.

The differential equation for the temperature distribution in the support is

$$\frac{d^2T}{dx^2} - \frac{\omega c_p}{kA}\frac{dT}{dx} = 0 \tag{I-2}$$

where T is the temperature of the support and gas (°R)

k is the thermal conductivity of the support $\left(\frac{\text{Btu}}{\text{hr-ft°R}}\right)$

c_p is the specific heat, at constant pressure of the vapor $\left(\frac{Btu}{lb_m\ ^\circ R}\right)$

A is the cross-sectional area of the support (ft^2)

Integration of Equation (I-2) and substitution of the boundary conditions $T(0) = T_c$ and $T(L) = T_h$ yields the solution for the support temperature as a function of x:

$$T(x) = Tc + (T_h - T_c)\frac{(e^{ux} - 1)}{(e^{u\ell} - 1)} \qquad \text{(I-3)}$$

where $$u = \frac{\omega c_p}{kA}$$

The heat flow to the cryogenic container, $kA\left(\frac{dT}{dx}\right)_{x = 0}$ is given by the equation

$$q_o = \frac{\omega c_p\ (T_h - T_o)}{\ell^{u\ell} - 1} \qquad \text{(I-4)}$$

After substituting Equation (I-1) into (I-4) and rearranging terms, the heat flow to the container becomes

$$q_o = \frac{\lambda kA}{c_p \ell}\ \ell og_e\left[1 + \frac{c_p\ (T_h - T_c)}{\lambda}\right] \qquad \text{(I-5)}$$

If the support was not vapor cooled, the heat flow to the container by conduction, q_c, would be

$$q_c = \frac{kA}{L}\ (T_h - T_c) \qquad \text{(I-6)}$$

The ratio of Equation (I-5) to Equation (I-6) then yields a measure of the effectiveness of allowing the boil-off of the cryogenic fluid to cool the structural support.

$$\frac{q_o}{q_c} = \frac{\ell n\ (1 + \xi)}{\xi} \qquad \text{(I-7)}$$

where

$$\xi = \frac{c_p\ (T_h - T_c)}{\lambda}$$

Therefore, the ratio of the heat flow with vapor cooling to that for an uncooled support is independent of the thermal conductance and is a function only of the specific heat of the vapor, the heat of vaporization of the liquid cryogen and boundary temperatures of the support.

As an illustration of the reduction by vapor cooling, consider a structural support with a temperature of 520R at the warm end and 37R at the connection to a container filled with LH_2.

$$\xi = 6.21$$

and

$$\frac{q_o}{q_c} = 0.318$$

Therefore, in this example the LH_2 boil-off due to conduction in the support is reduced by 68% by utilizing the sensible enthalpy of the LH_2 vapor.

APPENDIX II

EFFECT OF MLI USED FOR ORBITAL THERMAL PROTECTION ON THE THERMAL PERFORMANCE OF A SHADOW SHIELD SYSTEM

To illustrate the magnitude of the heat flux reduction to a shadow-shielded tank by interposing additional MLI at the tank surface, consider a source at temperature T_o radiating to a sink at a temperature of 0°K. The conductive heat transfer via supports is neglected; and it is assumed that the source and sink have emittances much less than unity, that the surfaces are diffuse, and that the radiosity absorbed and emitted by the surfaces is uniformly distributed over the radius.

First, consider the heat flux between a source and sink of equal dimensions as illustrated in the diagram below.

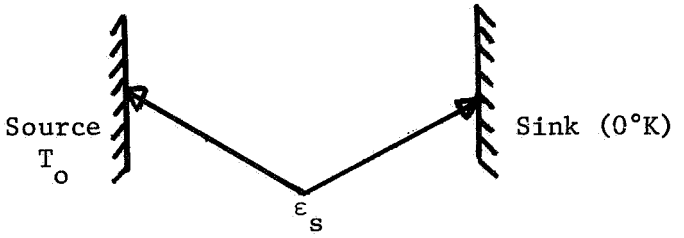

The net heat flux to the 0°K sink is given by the equation

$$(q/A)_1 \doteq \frac{\varepsilon_s^{\,2} F\sigma T_o^{\,4}}{1 - \rho^2 F^2} \qquad \text{(II-1)}$$

where F = view factor between the source and sink - a function of the diameter and spacing

$\sigma T_o^{\,4}$ = intensity of radiation leaving the source

ε_s = surface emittance of source and sink

ρ = surface reflectance $(1 - \varepsilon_s)$

$(q/A)_1$ = heat flux absorbed by the 0°K sink

Next, consider the case in which MLI is placed between the sink representing the LH_2 tank and the source. It is assumed that the thickness of the MLI is small by comparison to the spacing between the source and sink and that the outermost surface of the insulation has an emittance, ε_s. We also assume that the heat flux between the outermost surface of the insulation and the sink can be defined in terms of an effective emittance of the entire multilayer system. A diagram of this arrangement is shown below:

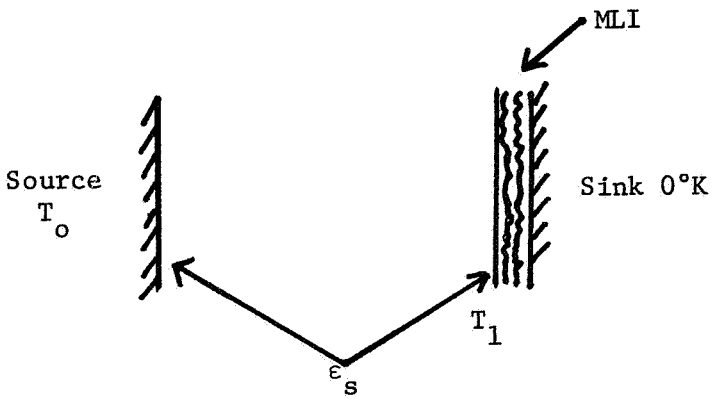

We define the effective emittance of the insulation in the conventional manner

$$\bar{\varepsilon} \equiv \frac{(q/A)_2}{\sigma T_1^4} \qquad \text{(II-2)}$$

where $\bar{\varepsilon}$ = effective emittance of the MLI

$(q/A)_2$ = heat flux through the MLI

T_1 = outer surface temperature of the MLI

The heat flux absorbed at the 0°K sink in this case is given by the equation

$$(q/A)_2 = \frac{\varepsilon_s^2 F \sigma T_o^4}{\left(\frac{\varepsilon_s}{\bar{\varepsilon}} + 1\right)\left(1 - \rho^2 F^2\right) - \frac{\varepsilon_s^2}{\bar{\varepsilon}} F^2 \rho} \qquad \text{(II-3)}$$

The ratio of the heat flux to the sink without MLI to that when MLI is used on the sink is given by the equation

$$\frac{(q/A)_1}{(q/A)_2} = 1 + \frac{\varepsilon_s}{\bar{\varepsilon}} - \frac{\varepsilon_s^2 F^2 \rho}{\bar{\varepsilon}\,(1 - \rho^2 F^2)} \qquad \text{(II-4)}$$

In most practical applications, the third term on the right side of Equation (II-4) will be negligible since both ε_s and F are usually small. Then Equation (II-4) becomes

$$\frac{(q/A)_1}{(q/A)_2} \doteq 1 + \frac{\varepsilon_s}{\bar{\varepsilon}} \quad \text{for } \varepsilon_s \text{ and } F << 1 \qquad \text{(II-5)}$$

For a typical system, the value of ε_s may be approximately 0.03 - characteristic of low-emittance vacuum-deposited aluminum (VDA) surfaces - and $\bar{\varepsilon}$ for an MLI system comprising five layers of aluminized (both sides) polyester film with a spacer will be of the order of 0.007. The resulting ratio of heat fluxes is

$$\frac{(q/A)_1}{(q/A)_2} = 1 + \frac{0.030}{0.007} = 5.3$$

For this simplified case, the reduction in heat flux due to the addition of five layers of MLI on an LH_2 tank (required for near-planetary thermal protection) will be approximately five for the same spacing between the source and sink. Since this calculation is based on a simplified mathematical model, the heat flux correction will not be exact for all conceivable arrangements when, for example, multiple shadow shields are interposed between the tank and the payload (source).

Detailed computer calculations for two equally spaced shadow shields of 0.03 emittance and an L/D (spacing-to-diameter) ratio of 0.25 with and without MLI applied to a 20.4K (37R) LH_2 tank show that the heat flux is reduced by a factor of 5.5 for an MLI system with $\bar{\varepsilon} = 0.0073$. This test would indicate that the simplified model can be used to predict the approximate reduction for any given effectiveness of the MLI applied to the tank surface.

Distribution List for Interim Report NASA CR-72369

"CONCEPTUAL DESIGN AND ANALYSIS OF SHADOW SHIELD SYSTEMS FOR THERMAL PROTECTION OF CRYOGENIC PROPELLANTS"

NAS3-10292

Arthur D. Little, Inc.

Cambridge, Massachusetts 02140

		COPIES
National Aeronautics and Space Administration Lewis Research Center 21000 Brookpark Road Cleveland, Ohio 44135		
Attention:	Contracting Officer, MS 500-210	1
	Liquid Rocket Technology Branch, MS 500-209	8
	Technical Report Control Office, MS 5-5	1
	Technology Utilization Office, MS 3-16	1
	AFSC Liaison Office, MS 4-1	2
	Library	2
	D. L. Nored, MS 500-209	1
	Office of Reliability & Quality Assurance, MS 500-203	1
	E. W. Conrad, MS 100-1	1
	W. E. Roberts, MS 3-17	1
	R. Knoll, MS 501-2	1

	COPIES
National Aeronautics and Space Administration Washington, D. C. 20546	
Attention: Code MT	1
RPX	2
RPL	2
SV	1
RV-2	1
Scientific and Technical Information Facility P. O. Box 33 College Park, Maryland 20740	
Attention: NASA Representative Code CRT	6
Office of the Director of Defense Research & Engineering Washington, D. C. 20301	
Attention: Dr. H. W. Schulz, Office of Ass't. Dir. (Chem. Technology)	1
Defense Documentation Center Cameron Station Alexandria, Virginia 22314	1
RTD (RTNP) Bolling Air Force Base Washington, D. C. 20332	1
Arnold Engineering Development Center Air Force Systems Command Tullahoma, Tennessee 37389	
Attention: AEOIM	1
Advanced Research Projects Agency Washington, D. C. 20525	
Attention: D. E. Mock	1

	COPIES
Aeronautical Systems Division Air Force Systems Command Wright-Patterson Air Force Base Dayton, Ohio 45433	
Attention: D. L. Schmidt Code ASRCNC-2	1
Air Force Missile Test Center Patrick Air Force Base Florida	
Attention: L. J. Ullian	1
Air Force Systems Command (SCLT/Capt. S. W. Bowen) Andrews Air Force Base Washington, D. C. 20332	1
Air Force FTC (FTAT-2) Edwards Air Force Base California 93523	
Attention: Col. J. M. Silk	1
Air Force Office of Scientific Research Washington, D. C. 20333	
Attention: SREP, Dr. J. F. Masi	1
National Aeronautics and Space Administration Ames Research Center Moffett Field, California 94035	
Attention: Library	1
E. R. Streed, SED	1
National Aeronautics and Space Administration Flight Research Center P. O. Box 273 Edwards, California 93523	
Attention: Library	1

	COPIES
National Aeronautics and Space Administration Goddard Space Flight Center Greenbelt, Maryland 20771	
Attention: Library	1
W. C. Lund, Code 623	1
National Aeronautics and Space Administration John F. Kennedy Space Center Cocoa Beach, Florida 32931	
Attention: Library	1
National Aeronautics and Space Administration Langley Research Center Langley Station Hampton, Virginia 23365	
Attention: Library	1
R. R. Heldenfels	1
National Aeronautics and Space Administration Manned Spacecraft Center Houston, Texas 77001	
Attention: Library	1
Merlyn Lausten (EP-2)	1
National Aeronautics and Space Administration George C. Marshall Space Flight Center Huntsville, Alabama 35812	
Attention: Library	1
Keith Chandler, R-P&VE-PA	1
Clyde Nevins	1
E. H. Hyde	1
I. C. Yates	1

	COPIES
Jet Propulsion Laboratory 4800 Oak Grove Drive Pasadena, California 91103	
Attention: Library	1
U. S. Air Force Washington, D. C. 20325	
Attention: Col. C. K. Stambaugh, Code AFRST	1
Bureau of Naval Weapons Department of the Navy Washington, D. C.	
Attention: J. Kay, Code RTMS-41	1
Commander U. S. Naval Missile Center Point Mugu, California 93041	
Attention: Technical Library	1
Commanding Officer Office of Naval Research 1030 E. Green Street Pasadena, California 91101	1
Director (Code 6180) U. S. Naval Research Laboratory Washington, D. C. 20390	
Attention: H. W. Carhart	1
Picatinny Arsenal Dover, New Jersey	
Attention: I. Forsten, Chief Liquid Propulsion Laboratory	1

	COPIES
Aerojet-General Corporation P. O. Box 296 Azusa, California 91702	
Attention: Librarian	1
Aerojet-General Corporation P. O. Box 1947 Sacramento, California 95809	
Attention: Technical Library 2484-2015A	1
Aeronutronic Division of Philco Corporation Ford Road Newport Beach, California 92600	
Attention: Library	1
Aeroprojects, Incorporated 310 East Rosedale Avenue West Chester, Pennsylvania 19380	
Attention: C. D. McKinney	1
Aerospace Corporation P. O. Box 95085 Los Angeles, California 90045	
Attention: J. G. Wilder, MS-2293	1
Library-Documents	1
Air Products and Chemicals, Inc. Allentown, Pennsylvania	
Attention: A. Lopin	1
Astrosystems, Incorporated 1275 Bloomfield Avenue Caldwell Township, New Jersey	
Attention: A. Mendenhall	1

	COPIES
Atlantic Research Corporation Shirley Highway & Edsall Road Alexandria, Virginia 22314	
Attention: Security Office for Library	1
Battelle Memorial Institute 505 King Avenue Columbus, Ohio 43201	
Attention: Report Library, Room 6A	1
Beech Aircraft Corporation Boulder Facility Box 631 Boulder, Colorado 80302	
Attention: J. H. Rodgers	1
R. L. Reed	1
Bell Aerosystems, Inc. Box 1 Buffalo, New York 14205	
Attention: T. Reinhardt	1
W. M. Smith	1
Autonetics 3370 Miralona Avenue Anaheim, California 92803	
Attention: Dr. Edward Lax Dept. 447, Bldg. 202	1
The Boeing Company Aero Space Division P. O. Box 3707 Seattle, Washington 98124	
Attention: Library	1
C. F. Tiffany	1

	COPIES
Chemical Propulsion Information Agency Applied Physics Laboratory 8621 Georgia Avenue Silver Spring, Maryland 20910	1
Curtiss-Wright Corporation Wright Aeronautical Division Woodridge, New Jersey Attention: G. Kelley	1
University of Denver Denver Research Institute P. O. Box 10127 Denver, Colorado 80210 Attention: Security Office	1
McDonnell Douglas Corporation Santa Monica Division 3000 Ocean Park Blvd. Santa Monica, California 90405 Attention: J. W. Price	1
General Dynamics/Astronautics P. O. Box 1128 San Diego, California 92112 Attention: Library & Information Services (128-00)	1
Convair Division General Dynamics Corporation P. O. Box 1128 San Diego, California 92112 Attention: Karl Leonhard	1
Paul Stevens	1

	COPIES
General Electric Company Flight Propulsion Lab. Department Cincinnati 15, Ohio	
Attention: D. Suichu	1
Grumman Aircraft Engineering Corporation Bethpage, Long Island New York	
Attention: Joseph Gavin	1
The Garrett Corporation 1625 Eye Street, N. W. Washington, D. C.	
Attention: C. Shepard	1
IIT Research Institute Technology Center Chicago, Illinois 60616	
Attention: Technical Library	1
Goodyear Aerospace Corporation 1210 Massillon Road Akron, Ohio	
Attention: Clem Shriver, Dept. 481	1
Lockheed Missiles & Space Company P. O. Box 504 Sunnyvale, California	
Attention: James Guill	1
Library	1

		COPIES
Marquardt Corporation 16555 Saticoy Street Box 2013 - South Annex Van Nuys, California 91404		
Attention:	Librarian	1
	W. D. Boardman, Jr.	1
Martin-Marietta Corporation Martin Division Baltimore 3, Maryland		
Attention:	Science-Technology Library	1
	R. Crawford	1
McDonnell Douglas Corporation P. O. Box 6101 Lambert Field, Missouri		
Attention:	R. A. Herzmark	1
North American Aviation, Inc. Space & Information Systems Division 12214 Lakewood Boulevard Downey, California 90242		
Attention:	Technical Information Center, D/096-722 (AJ01)	1
	H. Storms	1
Northrop Space Laboratories 1001 East Broadway Hawthorne, California		
Attention:	Dr. William Howard	1
Purdue University Lafayette, Indiana 47907		
Attention:	Technical Librarian	1

	COPIES
Republic Aviation Corporation Farmingdale, Long Island New York	
Attention: Dr. William O'Donnell	1
Rocketdyne Division of North American Rockwell, Inc. 6633 Canoga Avenue Canoga Park, California 91304	
Attention: Library, Department 596-306	1
Space-General Corporation Division, Aerojet 9200 East Flair Drive El Monte, California 91734	
Attention: Library	1
Stanford Research Institute 333 Ravenswood Avenue Menlo Park, California 94025	
Attention: P. R. Gillette	1
Thiokol Chemical Corporation Reaction Motors Division Denville, New Jersey 07834	
Attention: A. Sherman	1
Librarian	1
TRW Systems, Incorporated 1 Space Park Redondo Beach, California 90200	
Attention: G. W. Elverum	1
STL Tech. Lib. Doc. Acquisitions	1

	COPIES
Union Carbide Corporation Linde Division P. O. Box 44 Tonawanda, New York 14152	
Attention: C. R. Lindquist	1
United Aircraft Corporation Corporation Library 400 Main Street East Hartford, Connecticut 06118	
Attention: Dr. David Rix	1
Erle Martin	1
United Aircraft Corporation United Technology Center P. O. Box 358 Sunnyvale, California 94088	
Attention: Librarian	1
Vought Astronautics Box 5907 Dallas, Texas	
Attention: Warren C. Trent	1
Cryonetics Corporation Northwest Industrial Park Burlington, Massachusetts	
Attention: James F. Howlett	1
Martin-Marietta Corporation Denver Division Denver, Colorado	
Attention: Library	1
D. W. Murphy	1

	COPIES
National Research Corporation 70 Memorial Drive Cambridge, Massachusetts	1
New York University University Heights New York, New York Attention: P. F. Winternitz	1
Chrysler Corporation Space Division P. O. Box 29200 New Orleans, Louisiana 70129 Attention: G. L. Davis	1
General Dynamics P. O. Box 748 Fort Worth, Texas 76101 Attention: D. E. Westerheide MZ 2886	1